The Dissertation Committee for Bo Chen Certifies that this is the approved version of the following dissertation:

EXPERIMENTAL AND MODELING STUDY OF THERMAL RESPONSE OF SKIN AND CORNEA TO INFRARED WAVELENGTHS LASER IRRADIATION

Committee:

Ashley J. Welch, Supervisor

Sharon L. Thomsen

Robert J. Thomas

Thomas E. Milner

H. Grady Rylander III

James W. Tunnell

EXPERIMENTAL AND MODELING STUDY OF THERMAL RESPONSE OF SKIN AND CORNEA TO INFRARED WAVELENGTHS LASER IRRADIATION

by

BO CHEN, B.S.; M.S.

Dissertation

Presented to the Faculty of the Graduate School of

The University of Texas at Austin

in Partial Fulfillment

of the Requirements

for the Degree of

Doctor of Philosophy

The University of Texas at Austin

December 2007

Dedicated to my dear parents Mr. Suwei Chen and Mrs. Yuexia Zhang,

and brother Mr. Lin Zhang

Acknowledgements

I would like to thank my supervisor, Professor Ashley J. Welch. I found that it was too difficult to find words to fully express my appreciation and gratitude for his continuous support and encouragement throughout my whole PhD life. It is him who introduced me into this research area, left me the freedom to express my ideas and explore my interest without a restricted path, and provided insightful advices and suggestions to help me pursuit my goals. Dr. Welch is a kind and patient person, with whom I feel very lucky to be associated.

However, none of this work would have been accomplished without support and advices from numerous other people. Professor Sharon L. Thomsen is one such person to whom I want to express my appreciation. Dr. Thomsen has given a lot of valuable advice and ideas throughout my whole PhD study. Her help on histology and pathology has made my PhD research much easier and faster.

My gratitude also goes to Professor Robert J. Thomas for his valuable advice and collaboration on computer modeling work. I also appreciate Dr. Thomas for reviewing many of my manuscripts for publication and giving very detail and thoughtful comments.

I would like to thank Professor H. Grady Rylander III for his kind help and important suggestions on my cornea damage study. Professors Thomas E. Milner and James W. Tunnell were also very supportive and helpful for my research especially with

ragards to questions relating to optical properties measurements. Another person who helped me a lot in my research is Dr. Jeffrey Oliver. He has provided tremendous help on my study of skin and cornea damage.

My appreciation goes to the people from Air Force Research Laboratory, Dr. Ben Rockwell and Victor Villavicencio for allowing me to borrow equipment and optical components for my experimental setup; to Dr Randolph D. Glickman and Peggy Miller from the Lions Eye Pathology Laboratory, UTHSCSA, for their preparation of histological tissue sections; to nurses in animal research center, Jennifer Cassaday and Kathryn Starr, for taking care of animals in my *in vivo* experiments.

Additionally, I wish to thank Jinze Qiu, Amit Paranjape, Junghwan Oh, Hyun Wook Kang, Jihoon Kim, Rebecca Vincelette, Badr Elmaanaoui, Raiyan Zaman and many other friends from biomedical engineering laser lab. The days and nights I spent with them in the past 4 years have been a joyful and wonderful memory for me.

Last but not least, my appreciation is extended to Chris Humphrey for her language corrections and invaluable help on my tuition bills and other miscellaneous administrative needs. My research funding is from Northrop Grumman Information Technology, The Air Force Research Laboratory, and the Albert and Clemmie Caster Foundation.

EXPERIMENTAL AND MODELING STUDY OF THERMAL RESPONSE OF SKIN AND CORNEA TO INFRARED WAVELENGTHS LASER IRRADIATION

Publication No._____

Bo Chen, Ph.D.

The University of Texas at Austin, 2007

Supervisor: Ashley J. Welch

Lasers pose a safety hazards both to skin and particularly to something you value highly - your vision. The increasingly widespread use of IR wavelengths laser systems requires awareness with the potential hazards associated with the misuse of these valuable products. The principal goal of this research is to integrate experimental and theoretical descriptions of thermal response of skin and cornea to IR wavelength laser irradiation to yield a basis for the dosimetry of laser-tissue interaction.

The threshold radiant exposures for various spot sizes and exposure durations were investigated on *in vivo* skin and cornea for 2.0 μm laser irradiation. Similar study was also conducted on *in vivo* skin using 1.214 μm laser and compared with 2.0 μm results. This PhD study has, for the first time, linked temperature response, histopathology, and the more common "minimal visible lesion (MVL)" endpoint into what can be a meaningful comparison of rate process models for injury.

Based on experimental data, a finite-element optical-thermal-damage model was developed. Histological damage was measured and modeled using sub-threshold, threshold, and super-threshold 2.0 μm laser powers. The data provided experimental evidence of the correlation of sub-threshold histological change to visible threshold lesion for the irradiation condition of this study. Moreover, the computer model, supported by experimental validation, ensured that rate process models were used correctly in the prediction of "MVL" thresholds which were based upon a finite damage extent and not necessarily central surface layer damage.

Thermal image method was employed to measure the absorption coefficient of *in vivo* skin at 2.0 μm, at which wavelength scattering can be ignored. At laser wavelengths below 1.4 μm where scattering cannot be ignored, an ameliorative method was explored to measure absorption and reduce scattering of *in vivo* tissue by combining pulse photothermal radiometry (PPTR) and diffuse reflectance (DR) measurements.

Table of Contents

List of Tables

List of Figures

Chapter 1. Introduction

1.1. MOTIVATION

Laser systems operating in the middle-infrared region (MIR), wavelengths from approximately 1.4 to 5 μm, are becoming increasingly important tools in areas such as optical telecommunications, atmospheric pollution monitoring, industrial process control, leak detection, automotive engineer exhaust analysis, drug detection, and medical diagnosis and surgery (Niemz 1996; Sorokina and Vodopyanov 2007). For instance, the Q switch and long pulse Ho:YAG lasers ($\lambda = 2.1$ μm) are used to ablate bone and cartilage, with many arthroscopy applications in orthopedics (Trauner, Nishioka et al. 1990; Trauner, Nishioka et al. 1995), endoscopic sinus surgery in otolaryngology (Shapshay, Rebeiz et al. 1991; Oswal and Bingham 1992; Shapshay, Rebeiz et al. 1992), and endoscopic disc removal in spine surgery (Min, Leu et al. 1996). Another sample is the detection of polluting gases and combustion products that have strong absorption lines at wavelengths from 2 to 5 μm (Rothman, Gamache et al. 1992). These chemical components and associated absorption wavelengths are: NH_3 (2.1 μm), HF (2.5 μm), CH_4 (2.35 μm and 3.3 μm), HCHO (3.5 μm), HCl (3.5 μm), N_2O (3.9 μm and 4.5 μm), SO_2 (4 μm), CO_2 (4.25 μm), and CO (2.3 μm and 4.6 μm).

The increasingly widespread use of lasers requires awareness with the potential hazards associated with the misuse of this valuable product of modern science. Lasers pose a safety hazards both to skin and particularly to something you value highly - your vision. While the dangers of firearms and explosives are obvious to most sane people, the possibility that a stream of massless photons even from a low power laser can cause instant severe and irreversible damage to skin and vision or even total blindness is something that often needs to be stressed and restressed.

Maximum Permissible Exposure (MPE) is the level of radiation to which a person may be exposed without hazardous effect or adverse biological changes in the eyes and skin (ANSI 2007). The MPEs for various wavelengths and pulse widths are defined by the American National Standards Institute (ANSI). This determination is done by the experts on the bioeffects subcommittee upon evaluation of minimum visible lesion threshold data, modeling and understanding of the mechanisms for damage. The ANSI Z136.1-2000, American National Standard for Safe Use of Lasers for skin and eye at MIR wavelengths is based on very little experimental data. With the recent development of laser systems at MIR wavelengths, it is necessary to evaluate and refine the existing MPE laser safety standards for these systems. Moreover, an understanding of biological tissues (such as skin and eye) response to MIR wavelengths irradiation provides important information for the use of these laser systems in medicine and surgery.

This research investigated the thermal response of *in vivo* skin and cornea to IR laser irradiation. Two laser systems were employed (a rack mountable fiber optic 1.214 μm laser system and mainly a 2.0 μm thulium laser system) to gain the dosimetry of the interaction between biological tissue and these IR wavelength lasers. Experiments were directed to improve understanding of the mechanisms of laser-induced thermal injury, and this data led to simulations of tissue thermal response and injury.

1.2. AIM OF THE RESEARCH

The principal goal of my research is to integrate experimental and theoretical descriptions of thermal response of skin and cornea to IR wavelength laser irradiation to yield a basis for laser-tissue interaction.

The objective of experimental study is to determine laser-induced damage thresholds for skin and eye and develop or utilize various imaging techniques, such as

infrared thermal imaging, microscopy, optical coherence tomography (OCT), and diffuse reflectance measurement, to investigate thermal, optical and histopathologic changes of skin and cornea to IR laser irradiation. Qualitative and quantitative histopathologic study of skin and corneal damage was performed to determine the mechanisms of laser effects in skin and cornea, map the extent and severity of the lesions for comparisons with surface temperature measurements and damage predictions with a mathematical model.

Based on the experimental data, a finite element computer model simulated light propagation, blood perfusion, heat generation, storage, and diffusion in biological tissues. Validation of the computer model provided a system for predicting thermal response with a minimum number of animal experiments. The information rendered by the model allowed me to 1) predict temperature and the occurrence and size of thermal lesions in the tissue, 2) evaluate the applicability of the standard rate process model for different thermal lesion end point definitions, 3) guide experiments by providing trends and pinpointing experimental data that does not follow experimental trends, and 4) predict and test the ANSI MPE laser safety standard.

Objectives are achieved through the following specific aims:

Experimental study of the thermal response and damage threshold of skin and cornea to infrared wavelength laser irradiation, specifically focusing on the study of using lasers at wavelengths of 2.0 and 1.214 μm.

Based on the skin experimental data, formulate an optical-thermal-damage computer model to simulate the temperature response of skin to laser irradiation and predict thermal damage in skin.

Evaluate laser-induced thermal damage in skin. Study the histological section of the lesion, determine the mechanism of laser effects in the skin, identify the minimal damage dose laser parameters at the microscopic level and map the extent and severity of

the lesions for comparison with the temperature measurement and my optical-thermal-damage model.

Measure *in vivo* skin optical properties by combining IR signal with diffuse reflectance measurements.

1.3. DISSERTATION OVERVIEW

The dissertation could be structurally divided into three major parts. The first part describes experimental and modeling studies on thermal response of porcine skin to IR laser irradiation (Chapter 3 to 7). The second part presents the experimental results of 2.0 μm laser thermal response and injury on *in vivo* rabbit cornea (Chapter 8). The third part of the dissertation explains the theory and experimental design for *in vivo* optical properties measurement, which recorded signals from both diffuse reflected light and IR emission on the tissue surface (chapter 9).

In detail, Chapter 3 introduces the experimental procedures of *in vivo* porcine skin damage study and discusses minimal visible lesion thresholds for skin at 2.0 μm laser irradiation. The threshold study shows that consideration for lowering the MPE standards should be explored as the laser beam diameter becomes larger than 3.5 mm. Based on the limited experimental data, an empirical equation is proposed to describe the correlation between laser duration/spot size and damage thresholds (published in *Lasers Surg. Med*. (Chen, O'Dell et al. 2005)).

Chapter 4 examines the effect of pigmentation density upon 2.0 μm laser irradiation thermal response. It is found that dark and light skin have similar thermal responses to laser irradiation owing to similar optical and thermal properties at 2.0 μm wavelength. In terms of laser safety limits, both threshold powers and histological study of threshold lesions confirm that the damage threshold data of dark mini-pig skin with

heavy melanin density can be extrapolated to various colored skin with sufficient accuracy. On the other hand, the light mini-pig skin is more suitable for damage threshold evaluation because the visual determination of redness on light skin is much easier and therefore has less observational error than dark skin (accepted by *Health Physics,* In Press).

In chapter 5, an finite-element optical-thermal-damage model is presented. The model simulates light propagation, heat generation, transient temperature response, and thermal damage produced by a radially symmetric laser beam of normal incidence. This optical-thermal-damage model, supported by experimental validation, provides a system for predicting the thermal response of skin to laser irradiation and the damage caused by MIR wavelengths laser irradiations (published in *J. Biomed. Opt.* (Chen, Thomsen et al. 2006*)*).

Qualitative and quantitative histopathlogical study of skin thermal lesions by 2.0 μm laser irradiation is described thoroughly in chapter 6. A sequence of damage endpoints is defined in the skin as irradiated power increases. The quantitative measurements of laser-induced thermal injury sizes are compared with our optical-thermal-damage model and the results show that: by choosing rate process coefficients to match specific mechanisms of lethal thermal damage, the optical-thermal-damage model is capable of predicting various types of thermal injury in the skin, such as epidermal necrosis, vascular thrombosis, and dermal collagen coagulation.

Chapter 7 portrays the study of skin injury to 1.214 μm wavelength laser irradiation and compares the threshold damage results with the study at 2.0 μm. The difference of skin optical properties (i.e. scattering and absorption) at these two wavelengths results a distinct power for threshold damage.

Chapter 8 explains the experiments and results of 2.0 μm laser thermal damage to *in vivo* rabbit cornea. A power law relation between threshold radiant exposure and exposure duration is evaluated for different spot diameters. Corneal thermal response to various laser duration and spot size is measured and discussed (accepted by *JOSA A,* In press).

The aim of chapter 9 is to give details of the theory and experimental design for *in vivo* optical properties measurement. The proposed method combines the measurements of diffuse reflected light by using a integrating sphere and IR signal emitted from *in vivo* tissue surface. Measurements on tissue phantoms are made to validate the theory and detection system. Tests are also conducted on *in vivo* human skin with various pigmentations.

1.4. REFERENCES

ANSI (2007). ANSI Z136.1-2007, American National Standard for Safe Use of Lasers. Orlando, FL, Laser Institute of America, American National Standards Institute.

Chen, B., D. C. O'Dell, et al. (2005). "Porcine skin ED50 damage thresholds for 2,000 nm laser irradiation." Lasers Surg Med **37**(5): 373-81.

Chen, B., S. L. Thomsen, et al. (2006). "Modeling thermal damage in skin from 2000-nm laser irradiation." J Biomed Opt **11**(6): 064028.

Min, K., H. Leu, et al. (1996). "Quantitative determination of ablation in weight of lumbar intervertebral discs with holmium: YAG laser." Lasers Surg Med **18**(2): 187-90.

Niemz, M. H. (1996). Laser-Tissue Interactions. Berlin, Germany, Springer-Verlag Berlin Heidelberg.

Oswal, V. H. and B. J. Bingham (1992). "A pilot study of the holmium YAG laser in nasal turbinate and tonsil surgery." J Clin Laser Med Surg **10**(3): 211-6.

Rothman, L. S., R. R. Gamache, et al. (1992). "The Hitran Molecular Database - Editions of 1991 and 1992." Journal of Quantitative Spectroscopy & Radiative Transfer **48**(5-6): 469-507.

Shapshay, S. M., E. E. Rebeiz, et al. (1991). "Holmium: yttrium aluminum garnet laser-assisted endoscopic sinus surgery: laboratory experience." Laryngoscope **101**(2): 142-9.

Shapshay, S. M., E. E. Rebeiz, et al. (1992). "Holmium:yttrium aluminum garnet laser-assisted endoscopic sinus surgery: clinical experience." Laryngoscope **102**(10): 1177-80.

Sorokina, I. T. and K. L. Vodopyanov, Eds. (2007). Solid-State Mid-Infrared Laser Sources (Topics in Applied Physics Vol. 89) Springer Verlag GmbH.

Trauner, K., N. Nishioka, et al. (1990). "Pulsed holmium:yttrium-aluminum-garnet (Ho:YAG) laser ablation of fibrocartilage and articular cartilage." Am J Sports Med **18**(3): 316-20.

Trauner, K. B., N. S. Nishioka, et al. (1995). "Acute and chronic response of articular cartilage to holmium:YAG laser irradiation." Clin Orthop Relat Res(310): 52-7.

Chapter 2. Background

This chapter provides a brief overview of the injury response of biological tissue to supraphysiological heating. A history of experimental observations as well as quantitative analysis of thermal injury in biological tissue is introduced. Subsequently, the latter part of this chapter summarizes laser hazards to human skin and eye and laser safety concern for various wavelengths laser systems.

2.1. EXPERIMENTAL STUDY OF THERMAL RESPONSE OF BIOLOGICAL TISSUES

High temperature has been used for treatment of various disease dating back to as early as 5000 years ago by early civilizations in China, Egypt, the Indus valley and Mesopotamia, and Greece (Hornback 1989; Dahl and Overgaard 1995). Heating sources such as hot fluids, burning sticks, hot coals or heated metal rods were the tools used to control of bleeding and treat wounds, ulcers and tumors since Neolithic times (Majno 1975). With the rapid development of modern techniques, various electromagnetic energy sources have been exploited to produce heat for thermal medical treatment (Ryan and Wong 1999). These sources includes lasers, radiofrequency, microwave frequency and ultrasound generators. However, a handicap to the widespread use of thermal therapy technique is the lack of understanding of thermal and injury behavior during and after the heating procedure. The knowledge of the mechanisms associated with this technique is still limited, although considerable research has been conducted over the last four decades.

The study of tissue thermal response is an interdisciplinary research field involving both biology and engineering. Studies from the perspective of biology mainly focus on determining the thermally induced injury mechanisms at the macromolecular, cellular and tissue (*in vitro* and *in vivo*) levels. Studies from the engineering perspective

emphasize how to measure and predict thermal and injury behavior using engineering tools. This chapter gives a brief overview of studies relevant to biological tissue thermal response from both the biological and engineering points of view. This includes experimental observations of cellular and vascular alteration during and after thermal therapy and the quantification of thermal histories and corresponding injuries using mathematical models.

2.1.1. Heat-induced Injury in Biological Tissues

Cells, extracellular matrix, and vasculature are the main constituents of tissue. The possible mechanisms of heat-induced injury in these constituents is briefly introduced in the following paragraphs.

At the molecular level, lipid, protein, DNA, and RNA are the major structural and functional macromolecules inside a cell. Most living cells and tissues can tolerate and survive modest temperature elevations for limited time periods depending on the species and the metabolic status of the individual cell. This phenomenon is termed thermotolerance and is related to the constitutive and inducible expression of heat shock proteins such as HSP70 and HSP60, as a result of thermal denaturation of cellular proteins (Tropea and Lee 1992; Kim, Hwang et al. 2007). Most nonlethal thermal injuries of individual cells are secondary either to heat-induced acceleration of metabolism or to thermal inactivation of particular enzymes and rupture of cellular membranes (Alexander and Moylan 1986; Mizuno 1986). Cell death and subsequent necrosis result when damage is so severe that the usual repair mechanisms cannot cope and/or the mediator of the repair mechanisms themselves are thermally destroyed. Various macromolecules have different injury response to heating. It has been found that DNA and structured RNA will not undergo conformational change below about 85-90 ^{o}C (Dewey 1989; Lepock 2003).

Therefore, their disruption does not play an important role in the cell killing at moderate temperatures ranging from 37 to 85 ^{o}C. On the other hand, other RNAs (e.g., tRNA and rRNA) which perform enzymatic functions and form protein/RNA complexes such as ribosomes are frangible at certain moderate temperature ranges (Wimberly, Brodersen et al. 2000; Lepock 2003). Lepock claimed that possible RNA thermal targets are tRNA and other forms of compact RNA such a rRNA and the small, nuclear ribonucleoprotein (snRNP) complexes. With the recent discoveries of the large number of enzymatic functions performed by RNA and its important role in many protein-RNA complexes such as ribosomes, it must be considered as a potential target much like protein. The remaining and most likely rate-limiting molecular targets are cellular protein. In situ thermal denaturation of cellular proteins has shown that detectable protein denaturation by differential scanning calorimetry starts at about 40 ^{o}C and has also been implicated as a mechanism of heat shock response and thermotolerance (Freeman, Borrelli et al. 1995). Another study of the thermally induced protein denaturation in human erythrocytes has shown that a protein/protein group transition around 60 ^{o}C is the rate-limiting step of thermally induced hemolysis (Lepock, Frey et al. 1989). However, lipids can still play a important role in hyperthermic cell injury, because many cellular proteins are embedded in lipids, and their stability is strongly affected by the lipids surrounding them (Cress and Gerner 1980; Quinn 1989).

At the subcellular organelle level, many studies have shown that: the highly selective plasma membrane containing both protein and lipid has been implicated as the primary target during heating (Cress and Gerner 1980; Yatvin and Cramp 1993; Bischof, Padanilam et al. 1995). Besides the cell membrane, some other systems/organelles (includes constitutive system, mitochondria, ribosome, Golgi apparatus, cytoskeleton, lysosome, centrosome, and endoplasmic reticulum) are possible leading targets of cell

injury (Rakow and Hochmuth 1975; Clark, Robins et al. 1983; Borrelli, Thompson et al. 1990). One thing need to be emphasized is that: Usually, supraphysiological thermal insult is a complex matter with thermal morphological and functional alterations of multiple organelles, and always has a pleotropic effect (i.e., multitarget) on cells.

Thermal denaturation of ubiquitous extracellular fibrous structural proteins, the collagens, is marked histologically by swelling and an amorphous, glassy (hyalinization) transformation of the fibers (Schober, Ulrich et al. 1986; Thomsen 1991). When heated the complex Type I collagen macromolecules and fibrils undergo several configuration changes depending upon the tissue temperature and time at temperature. Thermally-associated swelling of the collagen fibers seen at the light microscopic level is associated with an expansion of the collagen fibril diameters due to radial dissociation of the collagen macromolecules detected in transmission electron micrographs. This swelling seen at lower temperatures as shown in *in vitro* experiments of rat skin heated at 50 ^{o}C for 1000s is not associated with another heat induced alteration of type I collagen birefringence image intensity loss. Total birefringence loss occurs at 60 - 65 ^{o}C under the same experimental conditions (Pearce, Thomsen et al. 1993).

It has been found by many researchers that most normal *in vivo* tissues response to heat by an initial increase followed by a drop in blood perfusion until vascular stasis occurs (Song 1984; Brown, Hunt et al. 1992). The initial increase in blood perfusion can be attributed to the thermoregulatory control system of the host, and the latter drop is associated with heat-induced vascular injury. Regarding to the mechanisms of heat-induced vascular injury, damage to the endothelium is the first concern. Alteration of the endothelial monolayer may cause a loss of osmotic pressure difference across the vascular wall, which eventually leads to edema and vascular stasis. Another possible mechanism of vascular injury is related to thermal coagulation of red blood cells (RBC).

Damage of RBC can lead to thrombosis and vascular stasis. When vascular stasis occurs, cells suffer ischemia-induced effects such as hypoxia, malnutrition, and decrease pH, which can both thermally sensitize the cells and lead to cell death and finally tissue necrosis. This may explain why the thermal threshold of cellular injury *in vivo* is often suggested to be lower than its *in vitro* counterpart (Kang, Song et al. 1980).

Studies of the relation of temperature to injury are at not only cellular level, but also tissue level. Several biological tissues, such as cornea, retina, muscle, aorta and skin have been investigated. As temperature increases, denaturation of vital mitochondrial enzyme proteins and rupture of the cellular membranes can lead to death and necrosis of tissues and cells. Thermal coagulation of structural cellular and extracellular proteins including cell shrinkage, collagen hyalinization, collagen and muscle birefringence changes and tissue whitening, occur at higher temperatures. As temperatures reach 100 ^{o}C or more, water-vaporization causes tissue desiccation, the formation and expansion of steam vacuoles and explosive fragmentation. Tissue carbonization and ablation occur when temperatures are higher than the pressure dependent boiling point of tissue water (Thomsen 1991; Niemz 1996; Thomsen 2000; Thomsen and Coad 2007).

2.1.2. Wound Healing

Wound healing involves a series of steps that can be divided into three general categories: 1) organization of the necrotic debris, 2) tissue regeneration and 3) scar formation and contraction (Cohen, Diegelmann et al. 1992; Thomsen 2000).

The necrotic tissue must be removed before wound healing can be completed. The bottom line of organization is that the necrotic tissue has to be broken into manageable components to be removed before healing takes place. Initially, infiltrates of inflammatory cells, particularly polymorphonuclear white blood cells, rally to the injured

tissue not only to contribute to the necrosis process but also to continue the lytic breakdown of the necrotic debris. Depending on the species and organ, thermal lesion organization begins from one day (rat skin), to two to three days (pig skin and goat breast) to three to five days (pig lung) after treatment. The organization originates from the peripheral viable tissues and progresses into the lesion (Thomsen 2000).

After lethal injury, some tissue such as the epidermis of skin can totally regenerate. Tissue regeneration is initiated by production of various growth factors. Vascular and fibroblast growth factors stimulate new blood vessel growth, fibroblast proliferation and collagen formation to feed and support the functioning regenerated tissue (Thomsen 2000), On the other hand, tissues such as liver and breast ducts only partially regenerate and tissues such as heart and nerve never regenerate..

Depending on the size of the thermal lesions and the general physiology of the tissue/organ, the rate of vascular and fibroblast proliferation can be greater than the rate of tissue regeneration. This proliferation leads to the formation of vascular and fibrous granulation, the early forms of scar tissue. Scar tissue is usually pale tan reflecting its collagen content and is readily distinguished from surrounding tissues (Thomsen 2000).

2.1.3. Time Window for Lesion Assessment

The final thermal lesion is the composition of both primary thermal injury and secondary non-thermal injury due to vascular thrombosis/stasis, toxins, nutrient depletion, inflammation, wound healing reactions and other mechanisms. Depending on the time window in which the lesion is assessed, the contribution of primary and secondary injury to the lesion's size and composition will vary. The histological assessment of *in vitro* lesion and *in vivo* lesion at times less than 3 hours will primarily provide information related to cell death and injury related to the direct thermal damage.

The histological assessment of 3-5 day *in vivo* lesions will provide information related to cell death and injury from both direct thermal and secondary pathways of injury. At these and subsequent time points, the overall cell injury magnitude and death can be assessed; however, assigning a percentage to direct and secondary injury is difficult without comparative information from the same acute lesions (<3 hours) or similar acute lesions produced under exactly the same conditions. By day 7 early wound healing will begin, at this and subsequent time points the lesion will represent the sum total effects of the initial primary injury plus all secondary changes including the wound healing response. As a result, thermal models based on lesion sizes at later time points (> 3 hours) reflect the net effects of both the direct and secondary cell injury pathways (Thomsen and Coad 2007).

2.2. QUANTITATIVE MEASUREMENT ON THERMAL DAMAGE

As discussed above, the mechanisms of supraphysiological temperature injury are directly related to the thermal histories experienced by the tissue/cells. From an engineering point of view, a principle goal for study thermal injury or therapy is to understand and predict the final outcome of cell/tissue response for a given thermal history. Therefore, thermal damage models have been proposed based upon the biological response to temperature rise. The first order rate process model proposed by Henriques and Moritz is well accepted and widely used for thermal damage predictions.

2.2.1. Kinetic Model of Reaction Product Formation Rate

Thermal damage in tissue is typically described as a unimolecular process --- tissue constituents transition from the native state to the damaged state. Absolute reaction rate theory can explain the rate of formation assuming a time lag exists between molecular activation and denaturization. During this time lag, the molecules may either denature or relax back to the native state. However, the probability of denatured tissue

relaxing back to native state tissue is near enough to zero that it may be regarded as the impossible event in the absence of an energy-consuming healing process. Therefore, the rate of damage formation is proportional to only those molecules which remain activated. For a unimolecular process in the native state, C, the rate of disappearance of native state molecules, d[C] is given by:

$$-\frac{d[C]}{dt} = k[C] \tag{2.1}$$

where k is an overall reaction velocity constant and the bracket is used to indicate molar concentration. Therefore, the remaining native tissue at time τ is:

$$C(\tau) = C(0)e^{-\left(\int_0^\tau k dt\right)} \tag{2.2}$$

The basis for this rate process model of thermal damage may be obtained from chemical reaction kinetics. In a typical reaction process, thermally active reactants jump over an energy barrier (E_0) [J/mole] to form products. The reaction velocity, k [s^{-1}] determines the rate of formation of product and is related to the equilibrium constant for formation of activated complex, K^*, by

$$k = \frac{RT}{Nh}K^* \; and \; K^* = e^{-\Delta G^*/RT} \tag{2.3}$$

where N is Avogadro's number [6.023×10^{23}], h is Planck's constant [6.627×10^{-34} J·s], R is the universal gas constant [8.314472 J · K^{-1} · mol^{-1}], T is temperature in Kelvin, and ΔG^* is Gibbs free energy of formation of activated complex. In turn, the free energy of formation is given by

$$\Delta G^* = -T\Delta S^* + \Delta H^* \quad and \quad \Delta H^* = E_0 - iRT \tag{2.4}$$

where ΔH^* is the enthalpy of activation, ΔS^* is the entropy of activation, and i is 1 for first-order reactions in solution and gases which is a proper assumption in thermal denaturation process. In practice, ($\Delta H^* \approx 5\times10^5$)>>($RT\approx3\times10^3$), so that $E_0 \approx \Delta H^*$. Therefore, the reaction velocity, k is approximately equal to

$$k = \frac{RT}{Nh}e^{-\Delta G^*/RT} = \left(\frac{RT}{Nh}\right)e^{\frac{\Delta S^*}{R}}e^{-\frac{\Delta H^*}{RT}} = Ae^{-\Delta H^*/RT} \approx Ae^{-E_0/RT} \tag{2.5}$$

The temperature dependence of the sampling frequency (*A*) is not strong because the modest range of temperature variation in most experiments results in only a moderate change in temperature on the Kelvin scale (usually 273 to 373 K). Therefore, the linear dependence of *A* on T is extremely weak and its effect is negligible for all practical purposes (Welch and vanGemert 1995).

2.2.2. Damage Model: First Order Rate Process Model

The standard rate process model of tissue damage was introduced by Henriques and Moritz in the 1940's. In 1947, Henriques and Moritz exposed the skin of pigs, *in vivo*, to flowing water at a controlled temperature for exposure times varying over several orders of magnitude and derived a set of coefficients to match the experimental data corresponding to a "second degree" burn or trans-epidermal necrosis (Henriques 1947; Moritz and Henriques 1947). The damage parameter Ω, which indicates the level of damage, is computed using the Arrhenius equation:

$$\Omega(r,z,t) = \ln\{\frac{C(0)}{C(\tau)}\} = A\int_0^t e^{-\frac{E_0}{RT(r,z,t')}}dt' \tag{2.6}$$

where *A* is the molecular collision frequency factor, E_0 is denaturation activation energy, and *R* is the universal gas constant, and *t* is the heating time. Henriques and Moritz assigned $\Omega = 0.53$ corresponded to a threshold of first-degree burn (persistent but reversible erythema), $\Omega = 1$ to the threshold of second degree-burn (irreversible partial-thickness injury), and $\Omega = 10000$ corresponded to a threshold of third-degree burn (irreversible full-thickness injury). The original values for *A* and *E* calculated by Henriques and Moritz were:

$$A = 3.1\times10^{98}\ \ [1/s],\ \ E = 628000\,[\text{J/mole}] \tag{2.7}$$

2.2.3. Rate Process Coefficients Study on Biological Tissue

Thus far, several studies have been conducted to derive rate process coefficients of biological tissue using different heating sources. The usual experimental method is to expose tissue to constant temperature using either a water bath, a heated metallic plate or laser irradiation for selected time intervals. Several biological tissues, such as retina, muscle, aorta, cornea and skin have been investigated with identification of various defined thermal damage end points and their rate process coefficients. The following three paragraphs give a brief review of studies on skin, cornea and retina.

The original study conducted by Henriques and Moritz obtained a good match of model to their experimental results for long burn times, but there was a significantly greater discrepancy for shorter burns. Subsequent researchers applied greater sophistication to obtain different coefficients. Considering the experimental results from Henriques, Fugitt in 1955 (Fugitt 1955) and Wu in 1982 (Wu 1982) attempted to improve the method by introducing a two-stage temperature activation model. In 1974, Takata (Takata 1974) and in 1967 Weaver and Stoll (Weaver and Stoll 1967) suggested different values of A and E that best fit their own data and injury criteria. These models were analyzed and compared by Diller and associates in 1991 (Diller, Hayes et al. 1991) for different types of thermal insults on skin. In 1989, Gaylor and Rocchio measured the stability of mammalian skeletal muscle cell membranes in isolated cell culture to supraphysiologic temperature by determining the kinetics of onset of altered membrane permeability to intracellular carboxyfluorescein dye and proposed a set of coefficients for cell membrane rupture (Gaylor 1989). They defined $\Omega=1$ to represent the point when 5 percent of the dye had leaked across the membrane in the average experiment. They found that the supraphysiologic temperatures damaged membranes at a rate which was temperature-dependent and that cell membrane lysis was probably the initial destructive

event of tissue damage. This set of rate process coefficients has been used in several mathematic models to predict skin injury. In 1993, Pearce et al. wrapped freshly excised rat skin pieces in water-tight aluminum foil packets that were immersed in a controlled temperature water bath for times between 120 and 6000 s over the temperature range of 45 to 90 °C (Pearce, Thomsen et al. 1993). Based on the histopathologic results, they proposed a set of coefficients for birefringence loss in skin collagen.

In 2000, Kampmeier et al. determined the time dependence of the first phase transition of corneal collagen by measuring the transmission of visible probe laser light through an excised cornea in a temperature-controlled water bath (Kampmeier, Radt et al. 2000). The detected reduction in transmission and the scattering of the probe light during denaturation were used to characterize the process. They proposed corneal damage rate process coefficients associated with the end point defined at 50% loss of optical transmission of 632 nm light at temperatures ranging from 60 to 95 ^{o}C.

In 1984, Welch and Polhamus derived a set of rate process coefficient for visible lesion in bovine retina under argon laser irradiation (Welch and Polhamus 1984). The temperatures were not measured directly, but were determined in separate experiments on retinas in which a correlation between temperature and radius was established using microthermocouples advanced from the posterior surface of the eye to a point just below the retina. The correlates were used to estimate the retinal temperature given laser-beam power and duration. Previous study done by Takata et al. in 1974 proposed a two-stage temperature activation model with similar decision criterion for retinal damage at short exposure times (Takata, Goldfinch et al. 1974). Another estimation on rate process coefficients of retinal damage takes into account of the thermodynamics of protein and enzyme denaturation processes (Birngruber, Hillenkamp et al. 1985).

All the rate process coefficients described above are listed in Table 2.1.

Table 2.1. Published damage rate process coefficients of skin, cornea and retina.

Damage Endpoint	Model	Temperature Range (°C)	E_0 [J/mole]	A [1/s]
Skin				
Trans-epidermal necrosis, (pig skin)	Henriques	All T	6.27×10^5	3.1×10^{98}
Threshold Blister formation, (Human skin)	Weaver and Stoll	T≤50	7.82×10^5	2.185×10^{124}
		T>50	3.27×10^5	1.823×10^{51}
In-depth skin burn, (pig skin)	Takata	T≤50	4.18×10^5	4.322×10^{64}
		T>50	6.69×10^5	9.389×10^{104}
Trans-epidermal necrosis, (Human skin)	Wu	T≤53	6.27×10^5	3.1×10^{98}
		T>53	$(6.27 - 0.0051 \times (T-53)) \times 10^5$	3.1×10^{98}
Trans-epidermal necrosis, (Human skin)	Fugitt	T≤55	6.27×10^5	3.1×10^{98}
		T>55	2.96×10^5	5.0×10^{45}
Membrane permeability change, (mammalian skeletal muscle cell)	Gaylor	All T	2.4×10^5	2.9×10^{37}
Birefringence loss in skin collagen, (rat skin)	Pearce	All T	3.06×10^5	1.606×10^{45}
Cornea				
Optical attenuation in cornea, (porcine cornea)	Kampmeier	All T	1.5×10^5	1.5×10^{103}
Retina				
Visible lesion on retina (Bovine retina)	Welch and Polhamus	All T	6.28×10^5	3.1×10^{99}
Visible lesion on retina (Retina)	Takata	T≤50	4.18×10^5	4.322×10^{64}
		T>50	6.69×10^5	9.389×10^{104}
Protein and enzyme denaturization	Birngruber	All T	2.93×10^5	10^{44}

2.3. LASER HAZARDS AND SAFETY STANDARDS

2.3.1. Ocular Hazards

The ocular hazards associated with UV, visible and IR wavelengths represent a potential for injury to several different structures of the eye. This is generally dependent on which structure absorbs the most radiant energy per volume of tissue and the fluence rate at this structure. Retinal effects are possible when the laser emission wavelength

occurs in the visible and near-infrared spectral regions (0.4 μm - 1.2 μm). Light directly from the laser or from a specular reflection entering the eye at these wavelengths can be focused to an extremely small image on the retina. The incidental corneal irradiance and radiant exposure will be increased approximately 100,000 times at the retina due to the focusing effect of the cornea and lens (Niemz 1996; ANSI 2007; ANSI 2007).

Laser emission in the UV and Far-IR spectral regions (outside 0.4 μm - 1.4 μm) produce ocular effects primarily at the cornea. However, laser radiation at certain wavelengths may reach the lens and cause damage to that structure. Heating of the cornea by laser irradiation can cause severe white lesions when the tissue protein are denatured by the absorption of middle infrared wavelengths, such as 2.0 μm irradiation.

2.3.2. Skin Hazard

Although compared to ocular hazards skin effects are considered of secondary importance from a safety point of view, however, skin effects are becoming more and more important concern since the widespread use of lasers emitting in the ultraviolet spectral region as well as high power visible and IR lasers is becoming more common in medicine, industry and military.

UV radiation can cause skin damage including wrinkles, lower immunity against infection, produce aging skin disorders, and cancer (Morison 1988; Madronich and Degruijl 1993). However, the process producing these effects are still not fully understand. Some of the possible mechanisms for UV skin damage are collagen breakdown, the formation of free radicals, interference with DNA repair, and inhibiting the immune system. In the dermis, UV radiation causes collagen to break down at a higher rate than that due to just chronologic aging. UV damages collagen fibers and causes the accumulation of abnormal collagen that stains like elastin. When this UV-

induced elastin accumulates, enzymes scalled metalloproteinases are produced in large quantities. Normally, metalloproteinases remodel UV-injured skin by manufacturing and reforming collagen. However, this process does not always work well and some of the metalloproteinases actually break down collagen. This results in the formation of disorganized collagen fibers known as solar scars. When the skin repeats this imperfect rebuilding process over and over wrinkles develop (Takema, Nishijima et al. 1997). The laser at visible wavelengths can cause skin photo-aging and skin cancer. At laser wavelengths beyond 1.4 microns, the radiated energy is mainly absorbed in the epidermis and superficial dermis and usually cause thermal coagulation, desiccation and ablation.

2.3.3. Laser Safety Standards

The ANSI scheme has four hazard classifications. The classification is based upon the beam output power or energy from the laser (emission) if it is used by itself. If the laser is a component with a laser system where the raw beam does not leave the enclosure, but instead a modified beam is emitted, the modified beam is normally used for classification. The higher the classification number, the greater is the potential hazard. Brief descriptions of each class are given as follows (ANSI 2007):

Class I lasers - Lasers that are not hazardous for continuous viewing or are designed in such a way that prevent human access to laser radiation. These consist of low power lasers or higher power embedded lasers (i.e., laser printers).

Class II visible lasers (400 to 700 nm) - Lasers emitting visible light which because of normal human aversion responses, do not normally present a hazard, but would if viewed directly for extended periods of time.

Class IIa visible lasers (400 to 700 nm) - Lasers emitting visible light not intended for viewing, and under normal operating conditions would not produce a injury to the eye if viewed directly for less than 1,000 seconds (i.e. bar code scanners).

Class IIIa lasers - Lasers that normally would not cause injury to the eye if viewed momentarily but would present a hazard if viewed using collecting optics (fiber optics loupe or telescope).

Class IIIb lasers - Lasers that present an eye and skin hazard if viewed directly. This includes both intrabeam viewing and specular reflections. Class IIIb lasers do not produce a hazardous diffuse reflection except when viewed at close proximity.

Class IV lasers - Lasers that present an eye hazard from direct, specular, and diffuse reflections. In addition such lasers may be fire hazards and produce skin burns.

Very important is the so-called MPE value which denotes maximum permissible exposure to which a person may be exposed without hazards effect or adverse biological changes in the eyes and skin. The MPE value depends on both exposure time and wavelength.

This PhD study is related to the study of MPE limits for class IV lasers at wavelengths 1.2 and 2.0 μm. The exposure durations and spot sizes investigated are larger than those published previous work. ANSI Z136.1 2007 defined MPE standards for skin at wavelengths below 100 μm with a limiting aperture of 3.5 mm. Moreover, the MPE values defined for the whole spectra are not functions of spot size. However, it is more realistic to consider spot size-effects when large beams are accidently exposed on human body. Thus, it is necessary to estimate the relation between lesion threshold and exposure spot size.

2.4. REFERENCES

Alexander, G. A. and D. J. Moylan, 3rd (1986). "Hyperthermia in cancer treatment." Pa Med **89**(9): 64-5.

ANSI (2007). ANSI Z136.1-2007, American National Standard for Safe Use of Lasers. Orlando, FL, Laser Institute of America, American National Standards Institute.

Birngruber, R., F. Hillenkamp, et al. (1985). "Theoretical Investigations of Laser Thermal Retinal Injury." Health Physics **48**(6): 781-796.

Bischof, J. C., J. Padanilam, et al. (1995). "Dynamics of Cell-Membrane Permeability Changes at Supraphysiological Temperatures." Biophysical Journal **68**(6): 2608-2614.

Borrelli, M. J., L. L. Thompson, et al. (1990). "Time-Temperature Analysis of Cell Killing of Bhk Cells Heated at Temperatures in the Range of 43.5-Degrees-C to 57.0-Degrees-C." International Journal of Radiation Oncology Biology Physics **19**(2): 389-399.

Brown, S. L., J. W. Hunt, et al. (1992). "Differential Thermal Sensitivity of Tumor and Normal Tissue Microvascular Response during Hyperthermia." International Journal of Hyperthermia **8**(4): 501-514.

Clark, A. W., H. I. Robins, et al. (1983). "Structural-Changes in Murine Cancer Associated with Hyperthermia and Lidocaine." Cancer Research **43**(4): 1716-1723.

Cohen, I. K., R. F. Diegelmann, et al. (1992). Wound Healing: Biochemical and Clinical Aspects. Philadelphia, W.B.Saunders, Co.

Cress, A. E. and E. W. Gerner (1980). "Cholesterol Levels Inversely Reflect the Thermal Sensitivity of Mammalian-Cells in Culture." Nature **283**(5748): 677-679.

Dahl, O. and J. Overgaard (1995). "A century with hyperthermic oncology in Scandinavia." Acta Oncol **34**(8): 1075-83.

Dewey, W. C. (1989). "Failla memorial lecture. The search for critical cellular targets damaged by heat." Radiat Res **120**(2): 191-204.

Diller, K. R., L. J. Hayes, et al. (1991). "Analysis of alternate models for simulating thermal burns." J Burn Care Rehabil **12**(2): 177-89.

Freeman, M. L., M. J. Borrelli, et al. (1995). "Characterization of a Signal Generated by Oxidation of Protein Thiols That Activates the Heat-Shock Transcription Factor." Journal of Cellular Physiology **164**(2): 356-366.

Fugitt, C. E. (1955). A rate process of thermal injury. Armed Forces Special Weapons Project No. AFSWP-606.

Gaylor, D. C. (1989). Physical mechanism of celluar injury in electrical trauma Massachusetts Institute of Technology. **Ph. D. Dissertation**.

Henriques, F. F. (1947). "Studies of thermal injury V: The predictability and the significance of thermally induced rate processes leading to irreversible epidermal injury." Arch. of Pathol. **43**: 489-502.

Hornback, N. B. (1989). "Historical aspects of hyperthermia in cancer therapy." Radiol Clin North Am **27**(3): 481-8.

Kampmeier, J., B. Radt, et al. (2000). "Thermal and biomechanical parameters of porcine cornea." Cornea **19**(3): 355-363.

Kang, M. S., C. W. Song, et al. (1980). "Role of Vascular Function in Response of Tumors Invivo to Hyperthermia." Cancer Research **40**(4): 1130-1135.

Kim, H. J., N. R. Hwang, et al. (2007). "Heat shock responses for understanding diseases of protein denaturation." Mol Cells **23**(2): 123-31.

Lepock, J. R. (2003). "Cellular effects of hyperthermia: relevance to the minimum dose for thermal damage." Int J Hyperthermia **19**(3): 252-66.

Lepock, J. R., H. E. Frey, et al. (1989). "Relationship of Hyperthermia-Induced Hemolysis of Human-Erythrocytes to the Thermal-Denaturation of Membrane-Proteins." Biochimica Et Biophysica Acta **980**(2): 191-201.

Madronich, S. and F. R. Degruijl (1993). "Skin-Cancer and Uv-Radiation." Nature **366**(6450): 23-23.

Majno, G. (1975). The healing hand. Cambridge, MA, Harvard University Press.

Mizuno, S. (1986). "[Biological bases of cancer treatment by hyperthermia]." Gan To Kagaku Ryoho **13**(4 Pt 2): 1336-42.

Morison, W. L. (1988). "Skin-Cancer and Artificial Sources of Uv-Radiation." Journal of Dermatologic Surgery and Oncology **14**(8): 893-896.

Moritz, A. R. and F. C. Henriques, Jr. (1947). "Studies of thermal injury: II. The relative importance of time and surface temperature in the causation of cutaneous burns." Am J Pathol **23**: 695-720.

Niemz, M. H. (1996). Laser-Tissue Interactions. Berlin, Germany, Springer-Verlag Berlin Heidelberg.

Pearce, J. A., S. Thomsen, et al. (1993). Kinetics for birefringence changes in thermally coagulated rat skin collagen, Proc. SPIE 1876:180-185.

Quinn, P. J. (1989). "Principles of Membrane Stability and Phase-Behavior under Extreme Conditions." Journal of Bioenergetics and Biomembranes **21**(1): 3-19.

Rakow, A. L. and R. M. Hochmuth (1975). "Effect of Heat-Treatment on Elasticity of Human Erythrocyte-Membrane." Biophysical Journal **15**(11): 1095-1100.

Ryan, T. P. and T. Z. Wong (1999). Thermal Treatment of Tissue with Image Guidance. Proc. SPIE 3594:1-234.

Schober, R., F. Ulrich, et al. (1986). "Laser-induced alteration of collagen substructure allows microsurgical tissue welding." Science **232**(4756): 1421-2.

Song, C. W. (1984). "Effect of Local Hyperthermia on Blood-Flow and Microenvironment - a Review." Cancer Research **44**(10): 4721-4730.

Takata, A. N. (1974). "Development of criterion for skin burns." Aerosp. Med. **45**: 634-637.

Takata, A. N., L. Goldfinch, et al. (1974). Thermal Model of Laser-Induced Eye Damage. USAF School of Aerospace Medicine Report IITRI J-TR-74-6324.

Takema, Y., A. Nishijima, et al. (1997). "Skin morphology at the time of UV irradiation is important for wrinkle formation." Journal of the Society of Cosmetic Chemists **48**(6): 297-306.

Thomsen, S. (1991). "Pathologic analysis of photothermal and photomechanical effects of laser-tissue interactions." Photochem Photobiol **53**(6): 825-35.

Thomsen, S. L. (2000). "Qualitative and quantitative pathology of clinically relevant thermal lesions " Crit. Rev. Opt. Sci. Technol. **75** 425-58.

Thomsen, S. L. and J. E. Coad (2007). Developing clinically successful biomedical devices by understanding the pathophysiology of the target tissue: insights from over 25 years at the microscope. Proceedings of SPIE

Tropea, B. I. and R. C. Lee (1992). "Thermal injury kinetics in electrical trauma." J Biomech Eng **114**(2): 241-50.

Weaver, J. A. and A. M. Stoll (1967). NADC Memo Report 6708. Johnsville, Pennsylvania, United Stated Naval Air Development Center.

Welch, A. J. and G. D. Polhamus (1984). "Measurement and prediction of thermal injury in the retina of the rhesus monkey." IEEE Trans Biomed Eng **31**(10): 633-43.

Welch, A. J. and M. J. C. vanGemert (1995). Optical-thermal response of laser-irradiated tissue. Chapter 17: Rate processs analysis of thermal damage. New York and London, Plenum Press.

Wimberly, B. T., D. E. Brodersen, et al. (2000). "Structure of the 30S ribosomal subunit." Nature **407**(6802): 327-39.

Wu, Y. C. (1982). A Modified Criterion for predicting thermal injury. Nat. Bur. Stand. Washington, District of Columbia.

Yatvin, M. B. and W. A. Cramp (1993). "Role of Cellular Membranes in Hyperthermia - Some Observations and Theories Reviewed." International Journal of Hyperthermia **9**(2): 165-185.

Chapter 3. ED50 Damage Thresholds of Porcine Skin from 2.0 μm Laser Irradiation[1]

3.1. ABSTRACT

Background and Objective: To gain refinement in safe-exposure limits, indicated by the Maximum Permissible Exposure (MPE) limits, the minimum visible lesion thresholds for three spot sizes (5 mm - 15 mm) and four exposure durations (0.25 s - 2.5 s) were determined for the skin at 2000 nm continuous wave laser irradiation.

Study Design/Materials and Methods: A series of experiments were conducted *in vivo* on female Yucatan mini-pigs to determine the ED50 damage thresholds for 2000 nm continuous wave laser irradiation. The study employed Gaussian laser beam exposures with nominal spot diameters ($1/e^2$) of 5 mm, 10 mm and 15 mm and exposure durations of 0.25 s, 0.5 s, 1.0 s and 2.5 seconds as a function of laser power. The effect of each irradiation was evaluated within one minute after irradiation and the final determination was made at 48 hours post exposure. Probit analysis was conducted to estimate the dose for 50% probability of laser-induced damage (ED50) defined as persistent redness at the site of irradiation for the mini-pig skin after 48 hours.

Results: The MPE spot size and exposure duration trends for 2000 nm laser exposure are consistent for exposure diameters less than 3.5 mm. However, for larger exposure diameters of 5 mm, 10 mm and 15 mm and exposure duration longer than 0.25 s, the current MPEs are bigger than one tenth of our damage thresholds. For Gaussian laser profile, which is common for many laser output irradiance distributions, lower energy is required to generate a lesion on skin for smaller spot sizes and shorter exposure duration. On the other hand, for spot sizes greater than 5 mm and exposure duration over 0.25 s,

[1] Significant portions of this chapter have been previously published in *Lasers Surg. Med.*, 37:373-381, 2005

the average radiant exposure at threshold is inversely proportional to spot size. The irradiance-time and temperature-time power law at the threshold were investigated as well and showed that the irradiance-time power law was a close approximation to estimate laser irradiance at ED50 damage threshold.

Conclusions: The thresholds study shows that consideration for lowering the MPE standards should be explored as the laser beam diameter becomes larger than 3.5 mm. Based on the limited experimental data, the duration and size dependences of the ED50 damage thresholds could be described by an empirical equation: $\textit{Irradiance at the threshold} = (5.669 - 1.81 \times \textit{spot diameter}) \times \textit{exposure duration}^{-0.794}$.

Key words: Gaussian laser irradiation; laser injury; laser safety; Maximum Permissible Exposure (MPE); skin damage; visible lesion; Yucatan mini-pig

3.2. INTRODUCTION

Laser systems operating in the wavelength around 2000 nm are in widespread use in military, medical, and industrial applications. Being relatively new to the medical fields, the Q switch and long pulse Ho:YAG lasers (λ=2.1 μm) are principally used to precisely ablate bone and cartilage, with many applications in orthopedics for arthroscopy (Trauner, Nishioka et al. 1990; Trauner, Nishioka et al. 1995), urology for lithotripsy (removal of kidney stones) (Razvi, Denstedt et al. 1997; Takema, Nishijima et al. 1997), otolaryngology for endoscopic sinus surgery (Shapshay, Rebeiz et al. 1991; Oswal and Bingham 1992), and spine surgery for endoscopic disc removal (Min, Leu et al. 1996). With the recent development of continuous-wave systems at 2000 nm, it may be necessary to evaluate the need to refine the existing laser safety limiting exposure limits for these systems.

Maximum Permissible Exposure (MPE) is the level of radiation to which a person may be exposed without hazardous effect or adverse biological changes in the eyes and skin (ANSI 2007). The MPEs for various wavelengths and pulse widths are defined by the American National Standards Institute (ANSI). This determination is done by the experts on the bioeffects subcommittee upon evaluation of minimum visible lesion threshold data, modeling and understanding of the mechanisms for damage. The ANSI Z136.1-2000, American National Standard for Safe Use of Lasers (ANSI 2007) for skin at wavelengths between 1.8 μm and 2.6 μm and laser exposures from 1.0 ms to 10.0 s (see Table 3.1) is based on very little experimental data (Lund, Beatrice et al. 1981; McCally, Farrell et al. 1992). In this wavelength regime, the limited experiments have investigated cornea epithelial damage thresholds for exposure duration less than 0.25 s and laser spot size smaller than 1.8 mm.

Table 3.1. Maximum permissible exposure (MPE) for skin exposure to a laser beam (From ANSI Z136.1-2000) (ANSI 2007)

Wavelength (μm)	Exposure Duration, t (s)	MPE (J cm^{-2})	Limit Aperture Diameter (mm)
1.800 to 2.600	10^{-3} to 10	0.56 $t^{0.25}$	3.5

t is the laser exposure duration.

Studies on laser safety evaluate the MPE of the eye and the skin to laser irradiations. It is typically a factor of ten below the ED50 damage threshold. Exposure to levels at the published MPE values for the eye and skin may be “uncomfortable” (ANSI 2007). Thus, it is good practice to maintain exposure levels sufficiently below the MPE to avoid discomfort (ANSI 2007). In an effort to provide additional data for 2000 nm laser safety standards, a series of experiments and tests were conducted on Yucatan mini-pigs to determine various parameters that inflict threshold damage on skin at 2000 nm for

large spot sizes (5 mm - 15 mm). Thresholds were determined in terms of the minimum visible lesion for exposure durations from 0.25 second to 2.5 seconds.

The formation of thermally induced lesions in skin is a temperature-time rate process that is associated with the thermal denaturation of proteins (Henriques 1947). The process begins with the local absorption of laser light in skin that is converted to heat. The localized heat source S [W/cm^3] at position $\boldsymbol{r}$(x,y,z) and time t is a function of the local wavelength dependent absorption coefficient μ_a[1/cm] of the laser light

$$S(\boldsymbol{r},t) = \mu_a(\boldsymbol{r})\phi(\boldsymbol{r},t), \tag{3.1}$$

where $\phi(\boldsymbol{r},t)$ [W/cm^2] is the fluence rate at position $\boldsymbol{r}$(x,y,z) and time t. The primary absorbers, chromophores, for visible light and near IR radiation in skin are blood and melanin in the pigment epithelium. At 2000 nm, water becomes the primary chromophore. Temperature $T(\boldsymbol{r},t)$ resulting from the absorbed laser light is governed by heat generation, storage, diffusion and perhaps blood perfusion for long laser exposures. The actual pattern of light absorption is governed by light scattering at visible and near IR wavelengths; However at wavelength above 1.4 μm where scattering is insignificant, light propagation can be described by Beer's law. When $\mu_a(r) = \mu_a$:

$$S(\boldsymbol{r},t) = \mu_a(1-r_s)E(x,y,t)e^{-\mu_a z}, \tag{3.2}$$

where $E(x,y,t)$ [W/cm^2] is the irradiance and r_s is the specular reflectance from the skin surface (Takata 1977).

The animal model that best represents black human skin is the Yucatan mini-pig. It is anatomically similar to all human skin than the commonly used Yorkshire model (Eggleston, Roach et al. 2000). The skin of the Yucatan mini-pig has less hair and increased density of melanin granules relative to the Yorkshire pig. The Yucatan mini-pig has dark skin color and statistically, the flank skin thickness is approximately close to that of human face, arm, and neck skin, which have high probability of accidental

exposure. By using this model, the properties of the human skin can be more closely approximated to gain a better understanding of human laser-tissue interaction for the wavelength of interest.

3.3. MATERIAL AND METHODS

3.3.1. Animal Preparation

The animal use protocol was approved by the Institutional Animal Care and Use Committee at the University of Texas at Austin. Six female Yucatan mini-pigs, weighing between 24.3 to 34.8 kg, were used in this study. Before beginning each of the experiments, the mini-pig was anesthetized initially with IM Telazol-Ketamine-Xylazine(TKX) and intubated. Isoflurane (1-3%) was administered for anesthesia maintenance throughout the procedure by a certified registered laboratory animal technologist. Heart rate, SpO_2 and respiration were monitored throughout the experiment. In addition, Rimadyl (Carprofen) was given at the end of procedure to alleviate possible post surgical pain. After the mini-pig was anesthetized, its hair was removed using Nair® depilatory. Nair® was removed five minutes after application and the mini-pig skin was bathed with Betadine and then water. The mini-pig was marked with a metallic-silver permanent marker to make grids for identification and location of the numerous irradiation sites. The dimensions of the grids depended upon the laser spot size.

3.3.2. Experimental Setup

A rack mountable fiber optic CW laser (IPG Photonics Corporation) with a maximum 20 W output at a wavelength 2000 nm was used to create an array of irradiations. The output power was adjusted by changing the current on the front panel display. A power meter EPM2000 (Molectron Detector Inc., Portland, OR) with air-cooled power meter probes PM30 or PM150 (Molectron Detector Inc., Portland, OR) was

used to measure the output power corresponding to each current setting. Telescopes were employed to generate a collimated laser beam with desired spot diameters. A pulse generator (DG535, Stanford Research Systems) was used to trigger laser output and control the exposure durations. The pulse generator also triggered a function generator (HP 33120A, Hewlett-Packard Company), which controlled the imaging rate of an IR array detector thermal camera (Phoenix^{TM} DAS camera system, Indigo, CA). The IR camera began capturing infrared images 0.1 second before the laser irradiation on the mini-pig skin, and continued recording for 4 - 9 seconds after the laser was turned off. The IR camera imaging rate was set at 100 frames per second. The measurement system was arranged as depicted in Figure 3.1. Temperature calibration for the IR camera was done by using a blackbody heat source after laser irradiations on pig skin. The telescope and IR mirror were both mounted on the IR camera to ensure all burn sites were located at a fixed distance from the laser for the same spot size.

Three different laser spot sizes were produced by various telescopes. The laser beam profiles were measured using the knife-edge method (Siegman, Sasnett et al. 1991) before conducting the mini-pig experiment, and were confirmed by temperature distribution taken by IR camera prior to heat conduction. Both the knife-edge method and the measured temperature distribution indicated that the laser beam profiles were nominally Gaussian with $1/e^2$ diameters of 5 mm, 10 mm and 15 mm for the three telescope settings. The exact values of the nominal 5, 10 and 15 mm spot diameters were measured using the knife-edge method as 4.83, 9.65 and 14.65 mm respectively. The experimental uncertainty for spot diameter measurement by knife-edge method is 0.01 mm. An example of the measured skin surface temperature distribution after 30ms laser irradiation is illustrated in Figure 3.2 for a laser power of 3.23 W and spot diameter of 5 mm. The heat conduction in skin within 30 ms is quite small and can be neglected.

Therefore, the temperature rise on the surface is linearly proportional to the irradiance and therefore can be used to represent the incident laser beam irradiance distribution.

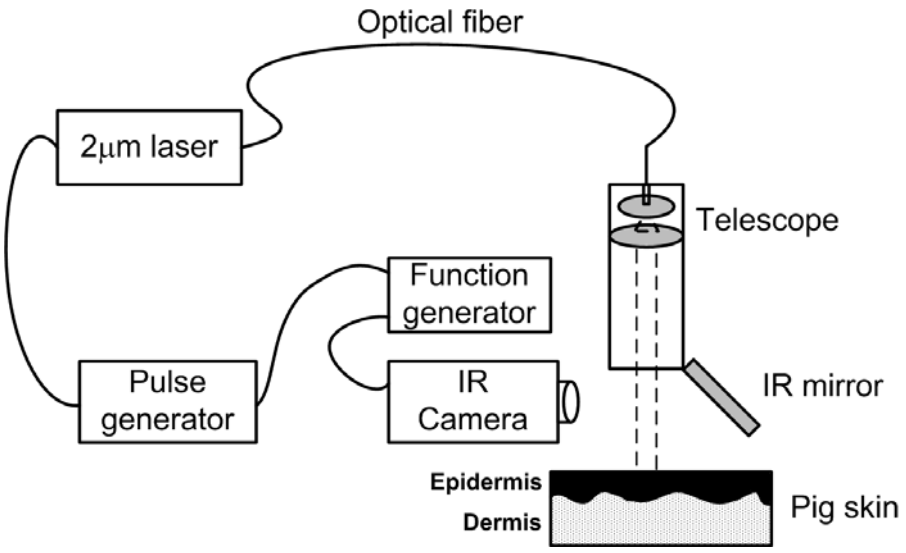

Figure 3.1. Laser irradiation system with an IR camera.

3.3.3. Experimental Procedures

Radiant exposures were made at specified exposure durations of 0.25 sec, 0.5 sec, 1 sec, and 2.5 seconds for spot diameters of 5 mm, 10 mm, and 15 mm. The number of irradiations for each of the 12 spot size-exposure conditions was 19 - 37 with an average of 27 per condition. The variation in laser power provided sufficient data points for probit analysis of damage/no damage response as a function of power. Forty-eight hours after laser irradiation, the size and type of lesions were observed and photographed by a digital camera (C-3040, Olympus Optical Co., Ltd., Japan) in order to find the ED50 damage threshold for the spot size-exposure conditions.

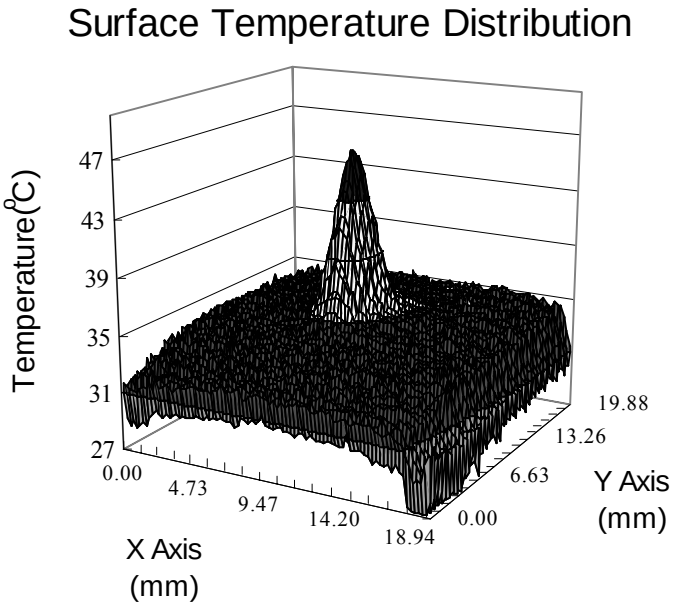

Figure 3.2. Skin surface temperature distribution after 30 ms laser irradiation. Laser power: 3.23 W, beam diameter: 5 mm.

3.3.4. ED50 Damage Threshold Determination

To determine different degrees of damage and to choose a reliable and reproducible threshold of minimal visual laser-induced damage, a pilot study was conducted on a Yucatan mini-pig to generate damages from no visible lesion to tissue ablation and charring. Based on the 48-hours post exposure reading, we defined the threshold thermal damage as grossly apparent persistent redness of the skin at the irradiation site at 48 hours. This kind of lesion was characterized as second-degree burn. More severe damage included epidermal roughening, blistering and whitening coagulation of the underlying dermis. Based on visible skin damage/no damage (i.e. persistent redness), probit analysis was used to determine the ED50 damage threshold. Probit analysis (Finney 1971; Cain and Noojin 1996) provided a statistically-estimated

dose for 50% probability of minimal visual laser-induced damage (ED50) for the mini-pig skin. Data points (damage/no damage for each condition) were entered into the probit statistical analysis package (Lund, B., Probit Fit Dose-Response Data Analysis Program, Version 1.02, U.S. Army Medical Research and Material Command, Hazards Research Branch) and the ED50 was calculated along with fiducial limits at the 95% confidence level.

In order to truly evaluate laser damage thresholds, average irradiance [W/cm^2] or radiant exposure [J/cm^2] reported in this paper was calculated as the applied laser power or energy divided by the $1/e^2$ spot area rather than 1/e spot area which is used in the laser safety classification. In fact, the peak irradiance or radiant exposure for our near Gaussian profile was twice the average value. Peak values were not reported.

3.4. RESULTS

3.4.1. ED50 Damage Threshold

Lesions around damage threshold initially appeared as red, flat spots on the skin at the site of irradiation. Most of the lesions appeared instantly during laser irradiation on the skin. However, at some specific power level near the estimated threshold, redness developed on the skin several seconds after the laser irradiation took place and persisted in the 48-hours post reading. Several red spots recorded immediately after irradiations were not observed at the 48-hours post reading. However, the more common occurrence was that after 48 hours, near the threshold, thermal lesion formed flat red papules concomitantly with the shrinking of the epidermis at the center of irradiation sites. As laser power went higher than threshold, the size of red papules increased and superficial ulcers occurred. Dark scabs were observed at 48 hours post-exposure when power was about 1.5 - 2 times the thresholds. In this case, coagulation and dehydration of the

epidermis occurred. When the power was higher than four times of the thresholds, an audible pop accompanied with the abrupt temperature drop (the maximum skin temperature before drop reached around $160\,°C$) was found. For this darkly pigmented skin, skin whitening, which was the usual symptom of third-degree burn, was not observed. Therefore, instead of whitening, persistent erythema (skin reddening) was the criterion on which the visible skin damage was based (Figure 3.3).

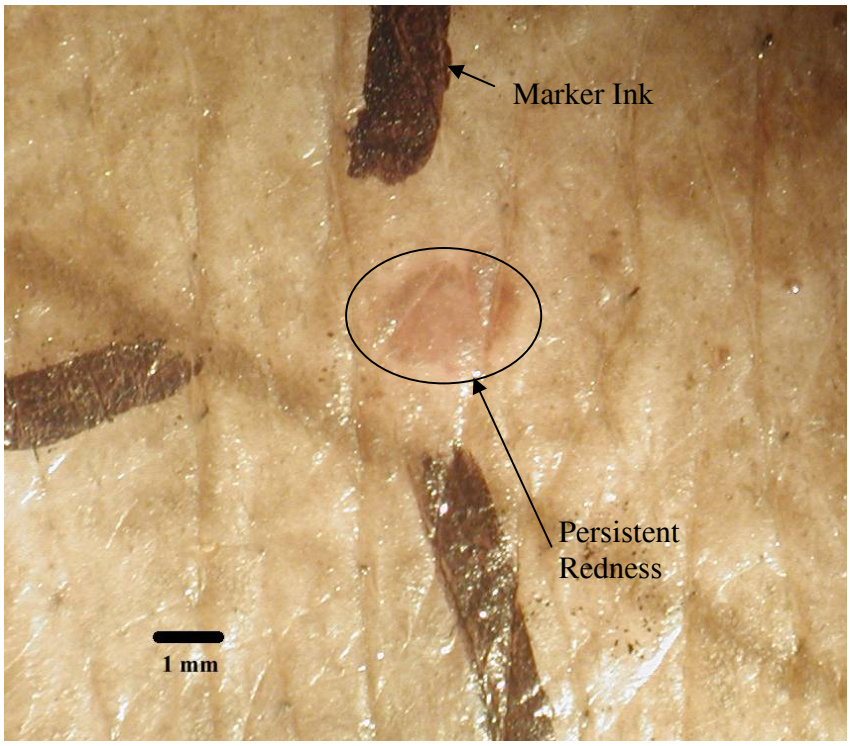

Figure 3.3. A gross image of thermal lesion at the threshold. Laser condition: beam diameter 5 mm, exposure duration 0.25 s, laser power 2.84 W.

The laser power for ED50 thresholds at 48-hours post exposure readings are listed in Table 3.2. Standard deviation (σ) was derived from the probit fit curve by the definition:

$$\sigma = (ED_{84} - ED_{16})/2, \quad (3.3)$$

where ED_{84} represented the dose for 84% probability of laser-induced damage, and similarly for ED_{16}. An example of probit fit analysis for damage/no damage as a function of power is illustrated in Figure 3.4.

At some irradiation conditions, direct estimations were made without using probit analysis, because the data was quite consistent and there was insufficient scatter for the probit program. In other words, there was consistently damage or no damage above or below a specific exposure level (respectively). For instance, at 2.5 s exposure time and 10 mm diameter, there were constant damages at 1.57 W but no damage at the next lower possible power level of 1.25 W.

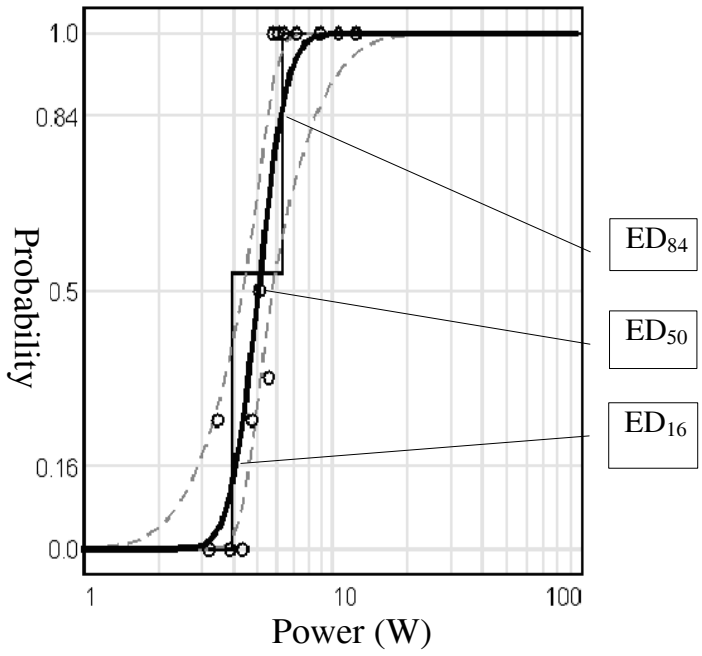

Figure 3.4. Probit fit analysis to estimate ED50 damage threshold for 15 mm diameter laser spot and 1 s duration. The circles are the experimental data (the probabilities to find damage after irradiations) and the solid curve is the probit fit curve. Zero represents no damage and one represents damage. Some circles are not zero or one due to the variation of multiple measurements at the same power.

Table 3.2. The ED50 power and standard deviation at damage thresholds* followed by lower and upper 95% confidence limits.

Diameter(mm) / Duration(s)	5	10	15
0.25	2.62 ± 0.28 W**	8.46 ± 1.04 W (8.46~8.46 W)	16.09 ± 0.43 W (15.18~16.65 W)
0.5	1.49 ± 0.48 W (0.08~1.91 W)	4.94 ± 0.27 W (4.94~4.94 W)	8.46 ± 0.80 W (8.08~9.48 W)
1.0	0.93 ± 0.29 W**	2.88 ± 0.35W**	5.02 ± 1.06 W (4.30~5.72 W)
2.5	0.41 ± 0.12 W (0.30~0.68 W)	1.41 ± 0.11 W**	2.46 ± 0.30 W (2.04~2.74 W)

*: Thresholds of apparent persistent redness of the skin visible at 48 hours.
**: Estimated without using probit fit.

Even though the Yucatan mini-pig skin best represents human skin, the dark pigmentation of the skin hindered the visual determination of threshold damage, and therefore could have contributed to inflation in the ED50 value due to observational threshold differences. Other experimental uncertainties are mainly from the power measurements. The air-cooled power meter probes PM30 and PM150 have 3% uncertainties, and the power meter EPM2000 has 1% read-out error. However, these instrumental errors are relatively small to the uncertainty from visual damage determination.

3.4.2. Peak Temperature at ED50 Power

Peak temperature associated with ED50 power levels of Table 3.2 are presented in Table 3.3. Base line temperatures were approximately $33\,^{\circ}C$. Peak temperature rise is defined as the maximum temperature rise at the irradiation center on the skin relative to the initial skin temperature at the start of radiation. Because of the Gaussian shape of the laser beam, peak temperature represents the temperature rise at the irradiation center.

3.4.3. Peak Temperature Rise with respect to Power

Peak temperature rise as a function of laser power are presented in Figures 3.5a, 3.5b and 3.5c for spot diameters of 5 mm, 10 mm and 15 mm respectively. Linear fits were computed for peak temperature rises less than $70\,°C$. (Note: scales are different between Figure 3.5a and Figure 3.5b/3.5c)

Table 3.3. The peak temperature rise at ED50 damage thresholds

Diameter(mm) / Duration(s)	5	10	15
0.25	$42.5\,°C$	$32.3\,°C$	$33.9\,°C$
0.5	$39.6\,°C$	$30.3\,°C$	$29.0\,°C$
1.0	$38.5\,°C$	$27.9\,°C$	$26.8\,°C$
2.5	$31.4\,°C$	$25.4\,°C$	$22.9\,°C$

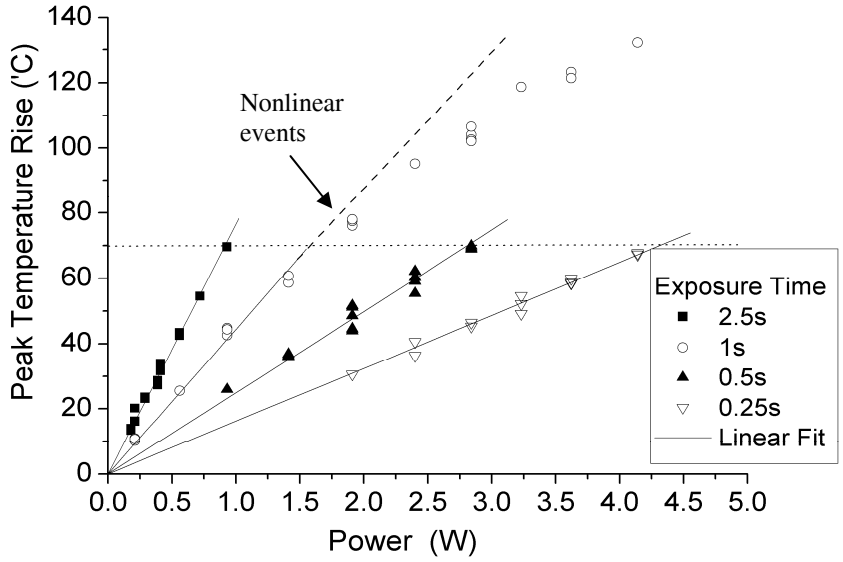

Figure 3.5a. Peak Temperature Rise vs. Power. Laser beam diameter 5 mm. Linear fits were computed for peak temperature rises less than $70\,°C$.

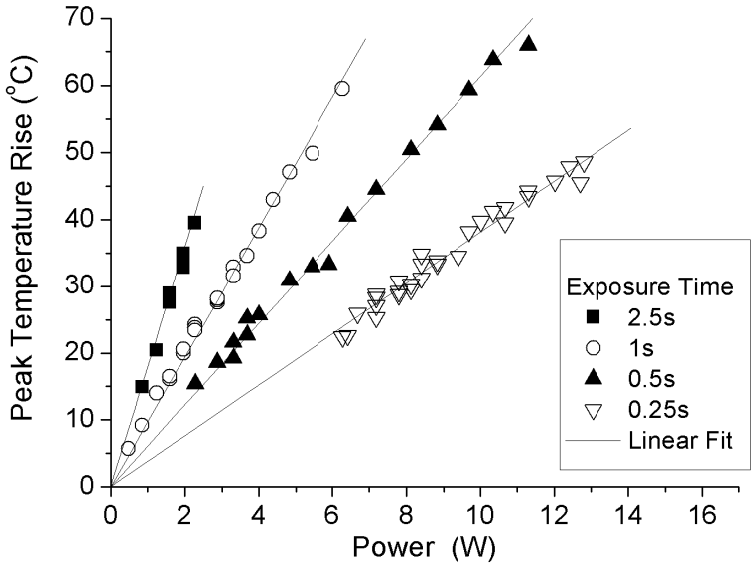

Figure 3.5b. Peak Temperature Rise vs. Power. Laser beam diameter 10 mm. Note: scales are different between Figure 3.5a and Figure 3.5b/3.5c.

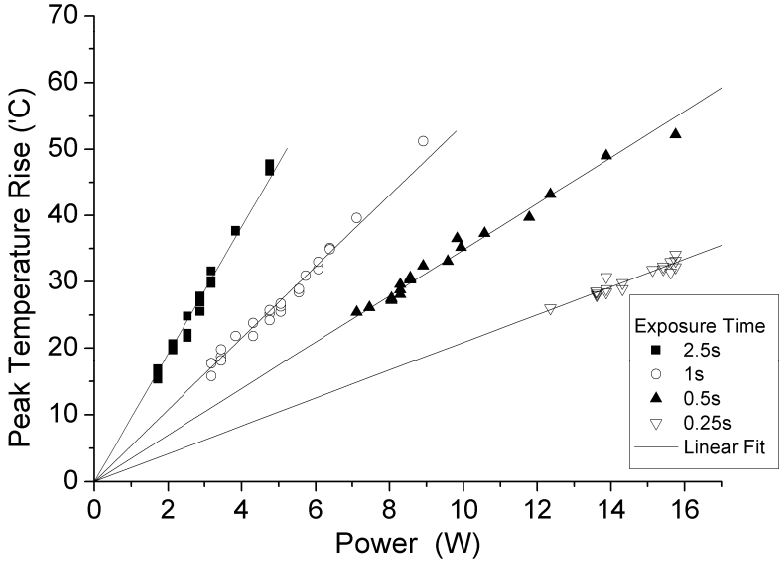

Figure 3.5c. Peak Temperature Rise vs. Power. Laser beam diameter 15 mm.

3.5. DISCUSSION

It is usually assumed that infrared radiations at wavelengths above 1.4 μm are absorbed in a thin surface layer of the skin, thereby heating the tissue, and inducing an injury as the temperature increases. The conversion of radiant energy to thermal energy can produce damage which can be predicted using the standard rate process model:

$$\Omega = \int_0^t A e^{-[\frac{E_0}{RT(t')}]} dt', \tag{3.4}$$

where Ω is a dimensionless damage parameter, t is the exposure time, A is the pre-exponential frequency factor, E_0 is an energy barrier molecules surmount in changing from native state to denatured, R is the gas constant and T is the temperature (Henriques 1947). The damage parameter Ω indicates the serious level of thermal injury on the skin, and, in this experiment, is set to be 1 for a second degree burn indicated by a persistent red papule at 48 hours.

The total exposure energy at the ED50 damage threshold (Table 3.4) is the product of the power and exposure time. Because the skin absorbs the irradiated energy linearly, the energy deposited into the skin is linearly proportional to the radiated energy. Table 3.4 shows that more energy is required to generate a visible lesion for longer laser exposure durations. This can be explained by the energy lost due to the heat conduction from hot to cool regions during the irradiation. Additionally, convection on the skin-air surface consumes some of the absorbed energy. Furthermore, blood under the heated skin surface will flow quicker than usual to cool down the higher temperature area. The longer the exposure time, the more energy is lost to the surrounding area. In other words, more energy is needed to raise skin temperature to the critical level that could generate lesions.

The ANSI standard of MPE for skin exposure to 2000 nm laser and the experimental results of average energy fluence at ED50 damage threshold at various

durations and beam sizes are compared in Table 3.5. Since the MPE level is established for a limiting aperture of 3.5 mm at this wavelength and these exposure durations, the larger spot sizes of our experiment provided additional data for the specification of safety standards for large spots. Table 3.5 displays the threshold energy divided by the laser spot area. The ED50 values for the four exposure times are slightly less than 10 times the corresponding MPEs but not inconsistent considering the inversely proportional size-dependence of ED50 values. Based on the experimental data, we can predict that the average energy fluence at ED50 damage thresholds for 3.5 mm diameter laser is about ten times larger than MPE standard. Secondly, over the range of exposures, the MPE is larger than one tenth of the damage threshold. It means this MPE standard must be considered carefully and could be decreased as the beam diameter becomes larger than 3.5 mm. In conclusion, this experiment supports the need to reduce the MPE standard for NIR laser beams with 5 mm - 15 mm diameter.

One thing to be noted is that the laser beam diameter for non uniform beam profile are typically quoted at 1/e rather than $1/e^2$ to give more conservative radiant exposures to compare to published MPE values in the laser safety classification. The radiant exposure based on 1/e diameter is just twice as large as the $1/e^2$ diameter radiant exposure, and indicates the peak radiant exposure for Gaussian shape laser beam. Although 1/e diameter is a conservative estimation of the laser hazard classification, $1/e^2$ diameter must be used to truly evaluate laser damage thresholds which require average irradiance.

Another feature evident from Table 3.5 is that the ED50 radiant exposure decreases with increasing spot size. This is due to the Gaussian shape of the laser beam and spot diameter dependent heat conduction that takes place during irradiation. Theoretically, if there is no heat transfer during laser irradiation, the temperature rise on

the skin is linearly proportional to the local radiant exposure. However, the heat conduction cannot be ignored for durations longer than the characteristic diffusion time (actually longer than a tenth of the characteristic diffusion time), which is applicable to our experiments. The light 1/e penetration depth at 2000 nm is approximately 200 μm and the associated characteristic diffusion time for a large spot diameter is about 300 ms (Jacques 1993). Heat conduction is described by

$$\frac{dT}{dt} = \frac{K}{\rho c_p}\nabla^2 T + \frac{Q}{\rho c_p}, \tag{3.5}$$

where Q is the heat source term due to the laser irradiation in our experiments, T is the temperature, K is the thermal conductivity, ρ is the density and C_p is the specific heat of tissue. The equation indicates that the temperature change with respect to time is directly proportional to $\nabla^2 T$. In this case, a laser spot with larger diameter have a flatter radiant exposure distribution so that smaller $\nabla^2 T$ is generated on the skin. Therefore, the temperature at the irradiation center increases quicker (less heat loss due to conduction) for larger beam sizes with the same radiant exposure, in other words, smaller radiant exposure is needed to generate ED50 lesions.

Although more energy is needed to generate a lesion on skin for longer laser exposure time, at the ED50 damage threshold, the peak temperature rise just after laser irradiation is in inverse proportion to exposure time (Table 3.3) Since thermal damage follows a rate process, a lower temperature rise is needed to generate a burn on skin for longer exposure time. Although the peak temperature provides an important aspect of the temperature trait on mini-pig skin, it does not necessarily represent the actual threshold temperature that is associated with the boundary between normal and significant thermal damaged tissue.

Table 3.4. The energy irradiated on the mini-pig skins at ED50 damage thresholds

Diameter(mm) / Duration(s)	5	10	15
0.25	0.66 ± 0.07 J	2.12 ± 0.26 J	4.02 ± 0.11 J
0.5	0.75 ± 0.24 J	2.47 ± 0.14 J	4.23 ± 0.40 J
1.0	0.93 ± 0.29 J	2.88 ± 0.35 J	5.02 ± 1.06 J
2.5	1.03 ± 0.30 J	3.53 ± 0.28 J	6.15 ± 0.75 J

Table 3.5. The average radiant exposure [J/cm^2] at ED50 damage thresholds

Diameter(mm) / Duration(s)	5	10	15	3.5 (MPE from ANSI)
0.25	3.57 ± 0.38 J/cm^2	2.89 ± 0.36 J/cm^2	2.39 ± 0.06 J/cm^2	0.396 J/cm^2
0.5	4.07 ± 1.31 J/cm^2	3.38 ± 0.18 J/cm^2	2.51 ± 0.24 J/cm^2	0.471 J/cm^2
1.0	5.08 ± 1.58 J/cm^2	3.94 ± 0.48 J/cm^2	2.98 ± 0.63 J/cm^2	0.560 J/cm^2
2.5	5.59 ± 1.64 J/cm^2	4.82 ± 0.38 J/cm^2	3.65 ± 0.44 J/cm^2	0.704 J/cm^2

The average irradiance, exposure time and surface peak temperature rise at ED50 damage threshold were investigated based on the power law relation postulated by Stoll and Greene in 1959 (Stoll and Greene 1959). They investigated the relationship between pain and tissue damage due to white light irradiation using three human subjects. Based on the data they acquired a simple irradiance-time power law and a temperature-time power law:

$$E = \mathrm{A}\, t^{-\mathrm{B}}, \tag{3.6}$$

$$\Delta T = \mathrm{C}\, t^{-\mathrm{D}}, \tag{3.7}$$

were found, where A,B,C,D are positive constants, E is the irradiance at the threshold, ΔT is the temperature rise on skin at the threshold and t is the exposure time. Figure 3.6a clearly shows that the irradiance-time power law can precisely describe our experimental results of irradiance at ED50 damage thresholds. Although coefficient A varies with

respect to beam size, the power coefficient B is constant around 0.8, which is close to the Stoll's finding-----B=0.74 for thresholds of pain with burning. For a spot diameter around 15 mm, which is used in Stoll's experiment as well, the power law for laser induced lesion is given by $E = (3.07\ \mathrm{W/cm^2})t^{-0.81}$. This is close to Stoll's finding when the skin tissue was irradiated by a white light projection lamp yielding an irradiance-time power law of $E = (2.82\ \mathrm{W/cm^2})\ t^{-0.74}$**.** Power law coefficient A for various spot diameters are examined in Figure 3.7. A least square linear fit indicates there is a simple relationship between coefficient *A* and spot diameter *d*(cm) ------ A =5.669 -1.81*d* (Figure 3.7). In conclusion, the irradiation at the ED50 damage threshold could be predicted by this empirical equation $E = (5.669 - 1.81d)t^{-0.794}$ ($\mathrm{W/cm^2}$). Recalling the MPE standard and that the standard is a factor of ten lower than threshold, the MPE radiant exposure is $H = 0.56t^{0.25}$ ($\mathrm{J/cm^2}$). For spot diameter equals 0.35 cm, the empirical power law gives a close estimation $H = 0.50t^{0.206}$ ($\mathrm{J/cm^2}$) (define the MPE radiant exposure as one tenth of the radiant exposure at the ED50 damage threshold.). For d=1.465 cm, the MPE radiant exposure from our estimation should be $0.302t^{0.206}$ ($\mathrm{J/cm^2}$). Although the empirical equation $E = (5.669 - 1.81d)t^{-0.794}$ ($\mathrm{W/cm^2}$) fits our threshold results quite well, it is obviously not suitable for much smaller or larger spot sizes. For spot diameters much larger than 15 mm, the irradiance at threshold should be independent of the spot size. On the other hand, for smaller spot diameters much less than 5 mm, the threshold irradiance will increase faster than this linear prediction (Tan, Motemedi et al. 1988; Keijzer, Pickering et al. 1991). For instance, McCally *et al.* (McCally, Farrell et al. 1992) measured the cornea epithelial damage thresholds for 0.235 s exposure and 1.33 mm $1/e^2$ spot diameter at wavelength 2.02 μm. The measured threshold radiant exposure was 8.46 $\mathrm{J/cm^2}$ which is higher than the predicted value 4.03 $\mathrm{J/cm^2}$ from our linear empirical equation.

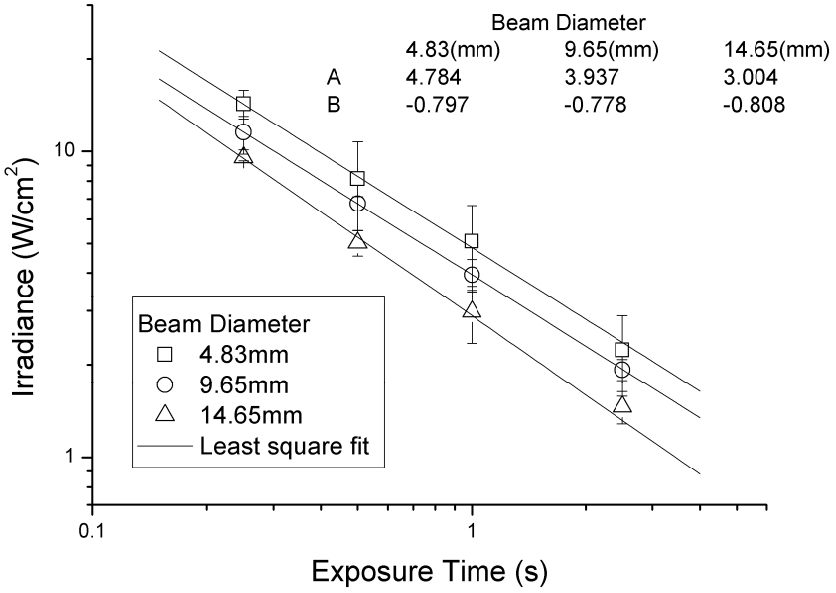

Figure 3.6a. The least square fit line of exposure time and irradiance, $\boldsymbol{E_T}$=A $\boldsymbol{t}^{B}$.

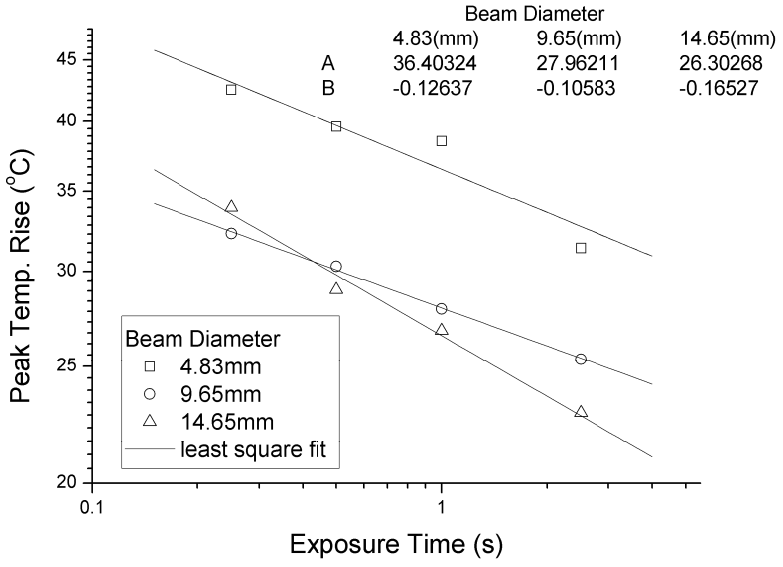

Figure 3.6b. The least square fit line of exposure time and peak temperature rise, $\boldsymbol{T}$=C $\boldsymbol{t}^{D}$.

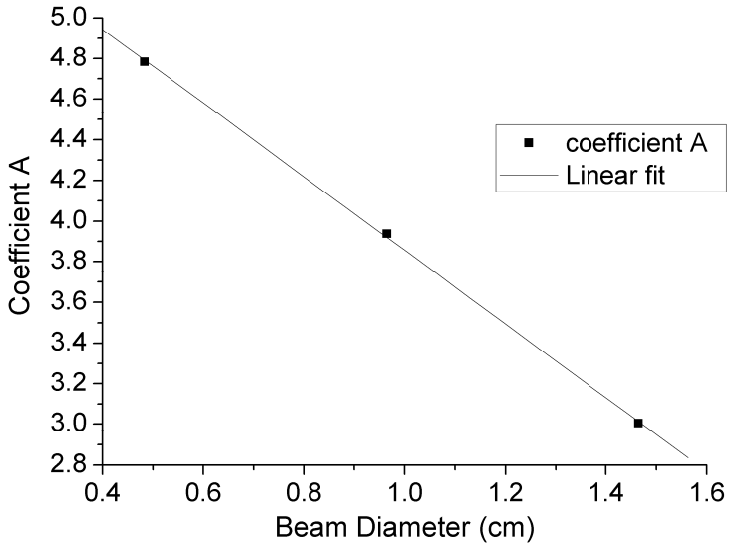

Figure 3.7. Coefficient A for various diameters (d(cm)). Linear fit shows $A = 5.669 - 1.81d$

It is difficult to compare our results to data at other wavelengths and spot sizes since ED50 thresholds are functions of optical properties and spot sizes. Even when scattering can be neglected, differences in the absorption coefficient affect threshold. For example, the classical data of human skin laser damage thresholds (Rockwell and Goldman 1974) support a threshold for CO_2 irradiation for 1.05 cm diameter spot and 1 s exposure duration of 2.8 J/cm^2 where as our results report a value of 3.9 J/cm^2 at 2.0 μm. The difference is due to penetration depths of the radiation for the two wavelengths. Radiation will penetrate deeper into skin at wavelength 2.0 μm rather than 10.6 μm; that is, more energy is needed for 2.0 μm radiation to increase skin temperature to the critical level that generates thermal damage.

Although irradiance and exposure time nearly fit the power law relation, peak temperature and exposure time have a much more complicated relationship. Figure 3.6b

shows the linear fit line of the logarithmic exposure time and peak temperature rise. Neither coefficient C nor the exponential coefficient D remains constant for the different beam sizes. The main reason for these differences is that the laser beam used in this experiment was a Gaussian profile whereas uniform radiation on skin is reported in Stoll's experiment. Due to the non-uniform laser beam profile (i.e. Gaussian profile) on skin, the temperature changes with position and the peak temperature does not represent the actual threshold temperature that is associated with the boundary between normal and significant thermal damaged tissue.

Linear fits of the peak temperature rise with respect to power (Figure 3.5a, 3.5b and 3.5c) show that the peak temperature response is linearly proportional to the laser power when peak temperature rise is below $70\,°C$. This indicates that the optical and thermal properties of the skin tissue, such as absorption, scattering and thermal conduction, do not significantly vary during heating. Furthermore, even though the redness caused by stepped-up blood flow has been discovered during irradiation, the conduction of heat energy away from the skin surface by way of the blood perfusion is insignificant compared to thermal conduction in the tissue. In other words, the increased blood flow does not significantly cool the skin surface during the laser irradiations in these experiments. The linear heat conduction equation predicts that temperature rise is proportional to absorbed energy. That is, the temperature response at T(x,y,z,t) scales with power. The surface temperature of the mini-pig skin is about $33\,°C$, so the turning point of this linear trend is around $100\,°C$, the boiling point of water. The vaporization of water from the tissue surface is probably the reason for the discontinuation of linearity. As water diffuses from tissue, local thermal properties of conductivity, heat capacity and density are altered (Takata 1977). Moreover, the optical properties of the skin undoubtedly changes around $100\,°C$, and contributes to the discontinuation of linearity as

well. Visual observations notes that irradiated mini-pig skin which is heated to $100\,°C$ or higher temperature becomes much darker and brittle on the surface. Even above $100\,°C$, tissue may not be ablated but remains in a super heated state owing to the strength of the epidermis preventing the escape of water vapor.

3.6. CONCLUSION

We have measured the minimum visible lesion thresholds in Yucatan mini-pig skin for three different laser spot sizes at four various pulse durations. For a CW 2000 nm wavelength laser, the irradiance exposure-time power-law has been evaluated based on the experimental results of the average irradiance values at the thresholds. It shows that the average irradiance at the ED50 damage threshold has a simple power law relation to exposure time $E = (5.669 - 1.81d)t^{-0.794}$ (W/cm^2). This simple empirical equation reveals the duration and size dependences of the ED50 damage thresholds. For Gaussian shape laser irradiation, which is common in many laser medical applications, lower energy is needed to generate a lesion on skin for smaller spot sizes and shorter exposure durations. On the other hand, the average radiant exposure at threshold is inversely proportional to spot size. These effects occur due to the Gaussian shape of the laser beam and the heat transfer during irradiation. The peak temperature rise at threshold and the corresponding exposure time may have a more complicated relationship that is not explained by simple power law relation.

We calculate the MPE from ANSI standards for 2000 nm wavelength at the exposure duration used in the experiments and conclude that the MPE standard is reasonable for the original 3.5mm spot diameter, but larger than necessary for 5 mm, 10 mm and 15 mm spot sizes and exposure durations of 0.25 second and longer. For our criterion of damage, the MPEs are bigger than one tenth of ED50 damage thresholds,

therefore the MPE standard should be considered carefully and could be decreased as the laser beam diameter becomes larger than 3.5 mm.

3.7. ACKNOWLEDGMENTS

Opinions, interpretations, conclusions, and recommendations are those of the authors and are not necessarily endorsed by the University of Texas, the United States Air Force or the Department of Defense.

The authors wish to thank Dr. Darrell Tata, Dr. Robert J. Thomas, Dr. Sergey Telenkov, Victor Villavicencio, Dan Polhamus and Jennifer Cassaday for their kind help.

3.8. REFERENCES

ANSI (2007). ANSI Z136.1-2007, American National Standard for Safe Use of Lasers. Orlando, FL, Laser Institute of America, American National Standards Institute.

Cain, C. P. and G. D. Noojin (1996). A Comparison of Various Probit Methods for Analyzing Yes/No Data on a Log Scale, Brooks AFB, TX: USAF Armstrong Laboratory; AL/OE-TR-1996-0102.

Eggleston, T. A., W. P. Roach, et al. (2000). "Comparison of two porcine (Sus scrofa domestica) skin models for in vivo near-infrared laser exposure." Comp Med **50**(4): 391-7.

Finney, D. J. (1971). Probit Analysis 3rd ed. New York, Cambridge University Press.

Henriques, F. F. (1947). "Studies of thermal injury V: The predictability and the significance of thermally induced rate processes leading to irreversible epidermal injury." Arch. of Pathol. **43**: 489-502.

Jacques, S. L. (1993). "Role of tissue optics and pulse duration on tissue effects during high-power laser irradiation." Applied Optics **32**(13): 2447-2454.

Keijzer, M., J. W. Pickering, et al. (1991). "Laser beam diameter for port wine stain treatment." Lasers Surg Med **11**(6): 601-5.

Lund, D. J., E. S. Beatrice, et al. (1981). Biological Research in Support of Project MILES, Letterman Army Institute of Research Report- Institute Report No. 96.

McCally, R. L., R. A. Farrell, et al. (1992). "Cornea epithelial damage thresholds in rabbits exposed to Tm:YAG laser radiation at 2.02 microns." Lasers Surg Med **12**(6): 598-603.

Min, K., H. Leu, et al. (1996). "Quantitative determination of ablation in weight of lumbar intervertebral discs with holmium: YAG laser." Lasers Surg Med **18**(2): 187-90.

Oswal, V. H. and B. J. Bingham (1992). "A pilot study of the holmium YAG laser in nasal turbinate and tonsil surgery." J Clin Laser Med Surg **10**(3): 211-6.

Razvi, H. A., J. D. Denstedt, et al. (1997). "Intracorporeal lithotripsy with the holmium:YAG laser - Reply." Journal of Urology **158**(1): 187-187.

Rockwell, R. J., Jr and L. Goldman (1974). Research on human skin laser damage threshold. Final report, Conract F41609-72-C-0007. Brooks Air Force Base, TX., USAF School of Aerospace medicine.

Shapshay, S. M., E. E. Rebeiz, et al. (1991). "Holmium: yttrium aluminum garnet laser-assisted endoscopic sinus surgery: laboratory experience." Laryngoscope **101**(2): 142-9.

Siegman, A. E., M. W. Sasnett, et al. (1991). "Choice of Clip Levels for Beam Width Measurements Using Knife-Edge Techniques." Ieee Journal of Quantum Electronics **27**(4): 1098-1104.

Stoll, A. M. and L. C. Greene (1959). "Relationship between pain and tissue damage due to thermal irradiation." J App. Physiology **14**(3): 372-382.

Takata, A. N. (1977). Laser-induced thermal damage of skin. USAF School of Aerospace Medicine. Brooks Air Force Base, TX.

Takema, Y., A. Nishijima, et al. (1997). "Skin morphology at the time of UV irradiation is important for wrinkle formation." Journal of the Society of Cosmetic Chemists **48**(6): 297-306.

Tan, O. T., M. Motemedi, et al. (1988). "Spotsize effects on guinea pig skin following pulsed irradiation." J Invest Dermatol **90**(6): 877-81.

Trauner, K., N. Nishioka, et al. (1990). "Pulsed holmium:yttrium-aluminum-garnet (Ho:YAG) laser ablation of fibrocartilage and articular cartilage." Am J Sports Med **18**(3): 316-20.

Trauner, K. B., N. S. Nishioka, et al. (1995). "Acute and chronic response of articular cartilage to holmium:YAG laser irradiation." Clin Orthop Relat Res(310): 52-7.

Chapter 4. Effect of pigmentation density upon 2.0 μm laser irradiation thermal response

4.1. ABSTRACT

Yucatan mini-pigs with predominantly dark skin have been used to determine skin safety standard for IR wavelength irradiation due to its anatomical similarity to all human skin. It has generally been argued that water is the principle absorber in the IR-B band and melanin has relatively low absorbance (Wolbarsht, Walsh et al. 1981). To accept dark pigmented damage thresholds for skin with various melanin densities, it is necessary to investigate the potential role of melanin in producing skin injury as characterized by an erythermal response. A spotted Yucatan mini-pig covered with lightly pigmented pink and darkly pigmented brown skin was used in this study. The significance of skin pigmentation was investigated by comparing the transient thermal response, absorption coefficient and the threshold damage of instant redness with in 1 minute and persistent redness at 48 hours post exposure for dark and light skin areas at 2.0 μm wavelength. The density of melanin granules did not significantly alter the thermal and optical properties of in vivo skin exposed to 2.0 μm laser irradiation. For Gaussian shape beam radiation at 1 second exposure duration and 4.83 mm $1/e^2$ spot diameter, the average radiant exposures at instant and persistent redness threshold were 3.88 J/cm^2 and 5.08 J/cm^2 for dark skin respectively, as well as 4.09 J/cm^2 and 4.09 J/cm^2 for light colored skin. Subjectively speaking, however, lightly pigmented mini-pig skin was more suitable for damage threshold estimation because of the increased contrast for visual determination of redness on light skin.

Key words: 2.0 μm laser; damage threshold; melanin; skin color;

4.2. INTRODUCTION

Yucatan mini-pigs with predominantly dark skin are commonly used to evaluate safety standards for laser irradiation of skin because of their anatomical similarity to human skin. The flank and dorsal neck of the Yucatan mini-pig are better suited than are the Yorkshire pig models because of epidermal skin thickness and melanin assessment (Eggleston, Roach et al. 2000). In 2004, female Yucatan mini-pigs with dark skin were used to determine damage thresholds for 2.0 μm laser irradiation (Chen, O'Dell et al. 2005). At this wavelength, water is the primary absorber of the laser radiation. The resulting generation and conduction of heat denature the tissue. However, we question the role of melanin density upon the thermal response and determination of laser induced damage thresholds at 2.0 μm wavelength, and examine the suitability of dark skin experimental results as applied to various skin colors of human skin.

Rockwell et al have studied the threshold lesions on the skin of human forearm (both Caucasian and Black) at several wavelengths. At some wavelengths such as 694.3 nm produced by a long pulse (2.5 ms) ruby laser, laser induced thermal injury is strongly dependent upon skin pigmentation. However, threshold reactions with the argon (wavelength 488-514 nm) and Nd:YAG laser (wavelength 1064 nm) at 1 s exposure are only slightly higher for Caucasian skin (4.0-8.2 J/cm^2 and 48-78 J/cm^2 respectively) than Negro skin (4.5-6.0 J/cm^2 and 46-60 J/cm^2 respectively) and are somewhat pigment related (Rockwell and Goldman 1974). The minimal reaction dose to CO_2 laser (wavelength 10600 nm) irradiation is exactly the same for the different colors of human skin (Rockwell and Goldman 1974). Unfortunately, definition of threshold end point in all the above studies varied, and included erythema, papules, blanching, ashen char, etc (Rockwell and Goldman 1974; Borrelli, Thompson et al. 1990; Eggleston, Roach et al. 2000).

In this report, the significance of the absorption and scattering effects of melanin granules are studied by comparing the transient thermal response and absorption coefficients of different colored skin to 2.0 μm wavelength laser irradiation. The power and gross observation of threshold lesions for dark and light skin are compared with respect to the effect of skin pigmentation upon the visual determination of the occurrence of a minimal visible lesion.

4.3. MATERIAL AND METHODS

4.3.1. Apparatus

The experimental setup for laser irradiation and measurement of surface temperature was described in detail in chapter 3. Briefly, the laser source was a rack mountable thulium fiber optic CW laser (IPG Photonics Corporation) with a maximum output power of 20 W at a wavelength 2.0 μm. Output power was adjusted by changing the current on the laser front panel display and duration was controlled by a pulse generator (DG535, Stanford Research Systems). An IR array detector thermal camera (Phoenix^{TM} DAS camera system, Indigo, CA) was used to record IR images on skin surface during laser irradiation. The IR images were converted to temperature according to the calibration of a blackbody heat source.

4.3.2. Animal Preparation

A dark skin Yucatan mini-pig spotted with relatively large lightly pigmented areas was used in this study. Skin color was determined by the density of melanin pigment in the skin (Eggleston, Roach et al. 2000). In comparison, light color skin had much less melanin and appeared pinkish due to visible light scattering in the underlying dermis. We assumed that light and dark skin of the mini-pig had identical constituents

and structure except for the density of the melanin granules. Animal care, anesthesia and skin preparation were described in chapter 3.

4.3.3. Absorption Coefficient Measurement

For mild millisecond IR laser irradiation of skin, all of the absorbed radiation is converted to thermal energy which increases skin temperature. If the exposure time is much less than the characteristic thermal diffusion time, then the temperature increase on the surface is proportional to the absorption coefficient of skin. The diffusion time for our large spot irradiation is determined by the optical radiation penetration depth and is approximately 300 ms for these experiments (Jacques 1993). The temperature increase is given by:

$$\Delta T = \mu_a \frac{\phi\left(z = 0^+\right)t}{\rho c}, \tag{4.1}$$

where $\phi\left(z = 0^+\right)$ is the fluence rate just below the surface. ϕ is approximately equal to the incident flux $(1-r_s)E(r,t)$ since the scattering of infrared radiation is insignificant at 2.0 μm wavelength. r_s is the specular reflectance and $E(r,t)$ is the irradiance on skin surface.

The absorption coefficient was estimated using the slope of the temperature response curve during the laser exposure time. The temperature responses during the first 100 ms laser irradiation were recorded by a thermal camera with an imaging rate 800 frames per second.

4.3.4. ED50 Damage Threshold Determination

At least 2 trained lesion readers were used to evaluate the presence or absence of skin lesions. A lesion was recorded as a “yes” if both readers identified it as positive. The third reader was used to give final decision when the two readers gave inconsistent

readings. Probit analysis (Finney 1971) was conducted to estimate ED50 damage thresholds according to two different end points of thermal lesions: 1) instant redness observed on skin within 1 minute after laser irradiation and 2) persistent redness at the site 48 hours after irradiation. Data points (damage/no damage for each condition) were entered into the probit statistical analysis package (Lund, B., Probit Fit Dose-Response Data Analysis Program, Version 1.02, U.S. Army Medical Research and Material Command, Hazards Research Branch) to calculate the ED50 values. For light colored skin, direct estimations were made without using probit analysis, because the data was quite consistent and there was insufficient scatter for the probit program. In other words, there was consistently damage or no damage above or below a specific exposure level (P_{yes} and P_{no} respectively). In these cases, the ED50 values were estimated as the middle point between the minimum measured consistent positive (consistent damage) dose (P_{yes}) and maximum measured consistent negative (consistent no-damage) dose (P_{no}).

4.4. RESULTS

Peak temperature responses of dark and light skin to various laser power irradiations with a 4.83 mm $1/e^2$ spot diameter and 1.0 s exposure duration are compared in Figure 4.1. Peak temperature rise is defined as the maximum temperature rise at the irradiation site relative to the initial skin temperature at the start of radiation. Base line temperatures are approximately 33 $^{\circ}C$. Because of the Gaussian shape of the laser beam, the temperature at the irradiation center is the peak temperature.

Absorption coefficients of dark and light colored skin were measured in vivo at two different skin locations (seven different power levels were employed at each location) on the mini-pig flank, location 1 (above belly, middle of the pig) and location 2

(back flank, front of rear legs), which were the commonly used skin areas for damage threshold study. (Table 4.1)

Table 4.1. Absorption coefficients (cm^{-1}) of dark and light skin at two different skin locations.

	Location 1	Location 2
Dark Skin	21.6 ± 1.0	22.7 ± 0.6
Light Skin	20.7 ± 1.2	22.0 ± 0.9

Visual instant redness and persistent redness thresholds for dark and light skin to 4.83 mm spot size and 1.0 s exposure duration laser irradiation are compared in Table 4.2 along with their maximum measured consistent negative dose (P_{no}) and minimum measured consistent positive dose (P_{yes}). Irradiations were repeated at least 3 times for each exposure level, and the total numbers of irradiation sites for dark skin and light skin at this laser condition were 36 and 20 respectively. The variation in laser power (0.21-1.91 W for light skin and 0.21-4.83 W for dark skin) provided sufficient data points for evaluation of damage/no damage response as a function of power. Threshold radiant exposures were calculated from the incident power divided by the area defined by the $1/e^2$ beam diameter. In the laser safety classification, non uniform beam profile were quoted at 1/e rather than $1/e^2$ to give more conservative radiant exposures to compare to published MPE values. The radiant exposure based on 1/e diameter was just twice as large as the $1/e^2$ diameter radiant exposure, and indicates the peak radiant exposure for Gaussian shape laser beam. Although 1/e diameter was a conservative estimation of the laser hazard classification, $1/e^2$ diameter must be used to truly evaluate laser damage thresholds which require average radiant exposure.

Representative gross images of persistent redness lesions on dark and light mini-pig skin 48 hours after irradiation and their corresponding microscopic H&E stained biopsies are shown in Figure 4.2.

Table 4.2. Instant redness and persistent redness thresholds for dark and light skin to laser irradiation with 5 mm spot size and 1.0 s exposure duration along with their maximum measured consistent negative dose (P_{no}) and minimum measured consistent positive dose (P_{yes}).

	Instant Redness		Persistent Redness	
	Power (W)	Radiant Exposure (J/cm^2)	Power (W)	Radiant Exposure (J/cm^2)
Dark Skin	0.71 (0.21-1.41)	3.88 (1.15-7.70)	0.93 (0.56-1.41)	5.08 (3.06-7.70)
Light Skin	0.75 (0.56-0.93)	4.09 (3.06-5.08)	0.75 (0.56-0.93)	4.09 (3.06-5.08)

4.5. DISCUSSION

Table 4.1 shows that the dark and light colored skin have similar absorption coefficients as determined by the thermal response in the first 100ms. Two sample t-tests were conducted on absorption coefficients at each location. The observed significances (P values are 0.054 and 0.138 at location 1 and 2 respectively) were larger than the 0.05 significance level. The results indicated no significant statistical differences between light and dark skin, at the 95% confidence level. At 2.0 μm wavelength, water was the major absorber; melanin had insignificant absorption and scattering which could induce higher fluence rates below the surface (Jacquez, Huss et al. 1955). When water is the primary absorber, the absorption coefficient of epidermis at 2.0 μm could be estimated by the product of absorption coefficient of water and the water content in epidermis.

$$\mu_a = \mu_{water} \times w \,, \tag{4.2}$$

where μ_{water} is the absorption coefficient of water which is 69.12 cm^{-1} at 2000 nm wavelength (Hale and Querry 1973), w is the water content in tissue, and is about 30% in

epidermis (Jacquez, Huss et al. 1955; Takata 1977; Duck 1990). The calculated absorption coefficient of epidermis using equation 4.2 is 20.74 cm^{-1} which is in good agreement with the measured skin absorption coefficients for both skin colors. These results also confirm that the melanin granules have much less absorption than water at this wavelength.

Since both dark and light skin have similar absorption capacity to 2.0 μm wavelength, we hypothesize that at this wavelength melanin density does not affect the transient thermal response to laser irradiation. Transient thermal responses measured with a thermal camera of dark and light skin to 2.0 μm laser irradiation are compared in Figure 4.1. The good match of the thermal response curves validates this hypothesis. The similarity of the thermal response curves also proves that the thermal conductivity and heat capacity of different colored skin have no significant differences. It has been recognized that the most important parameter affecting the thermal properties is the amount of water in the skin. By comparison, the effect of melanin density is of secondary importance at 2 μm and does not contribute to bulk thermal properties (Poppendick, Randall et al. 1966; Takata 1977; Duck 1990).

In this report, the damage threshold of light skin was investigated at one specific laser condition. The damage thresholds were sharply defined for light skin at this laser condition, i.e., there was consistent damage or no damage above or below a specific exposure level respectively. Table 4.2 compares the instant redness and persistent redness thresholds to laser irradiation for dark and light skin. The instant redness thresholds are very similar. However, the persistent redness threshold of light skin is slightly less than the dark skin threshold. The previous discussion has demonstrated that both skin colors have a very similar thermal response to 2.0 μm laser irradiation. Consequently, we believed that the laser irradiation had the same thermal effect on skin regardless of skin

color and therefore the persistent redness thresholds should be the identical for both skin colors. We believe that threshold differences are an observational artifact due to the visual determination of minimal visible lesions.

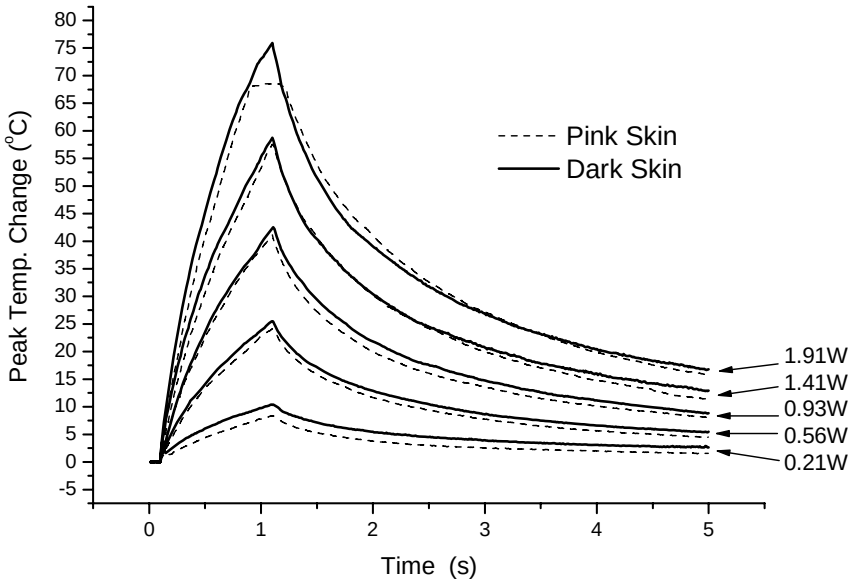

Figure 4.1. Dark and light skin peak temperature rises as a function of time. (laser spot size: 4.83 mm, exposure duration 1.0 s). The flat top on the 1.91 W curve is due to saturation of the thermal camera.

Since the contrast of redness on dark skin is much less compared to light skin (samples of gross pictures of redness lesions on dark and light skin are shown in Figure 4.2), the power which generates the minimal visible lesion is harder to determine on dark skin. In contrast, it is much easier to observe redness on light color skin. Furthermore, the "uncertain-damage" range of dark skin from the maximum measured consistent negative dose to minimum measured consistent positive dose is much broader than that of light skin. In other words, the dark skin threshold results have larger uncertainties than light

skin. Therefore, it is possible that the dark pigmentation of the skin hindered the visual determination of threshold damage, and therefore could have contributed to inflation in the ED50 value due to observational threshold differences. Therefore, from an observation point of view, light colored skin is more suitable for studying visible lesions than dark skin. The visual determination of redness on light color skin is much easier to see and therefore has much less observational error. Although the persistent redness thresholds are slightly different in the light and dark skin, the divergence of ED50 thresholds is in the range of the uncertainties of threshold measurement. Since the maximum permissible exposure (MPE) of skin to laser irradiations is roughly a factor of ten below the ED50 damage threshold, the small divergence of ED50 thresholds for different colored skin does not significantly affect the MPE values. Thus, the previous dark skin mini-pig damage threshold data are sufficiently accurate for the evaluation of MPE limits and can be extrapolated to all types of skin regardless of skin color for IR wavelengths where scattering of optical radiation is not significant and water is the primary absorber.

Histologically, light and dark skin support similar mechanisms of laser induced damage. Vascular dilation and thrombosis in dermal blood vessels, perivascular inflammation, regenerated epidermal cells growing under necrotic epidermis, and transmural necrosis of epidermis are observed in skin of both light and dark skin (figure 4.2).

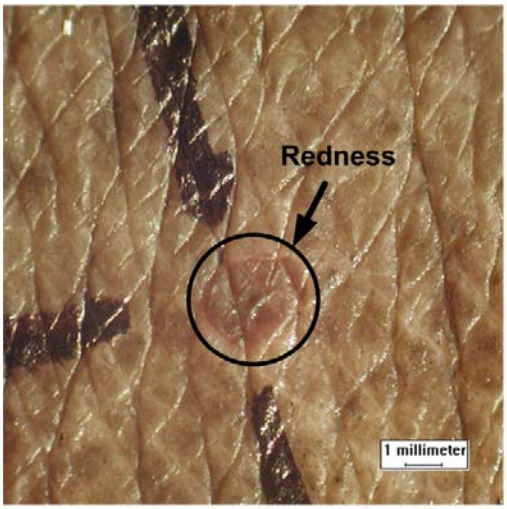

a1

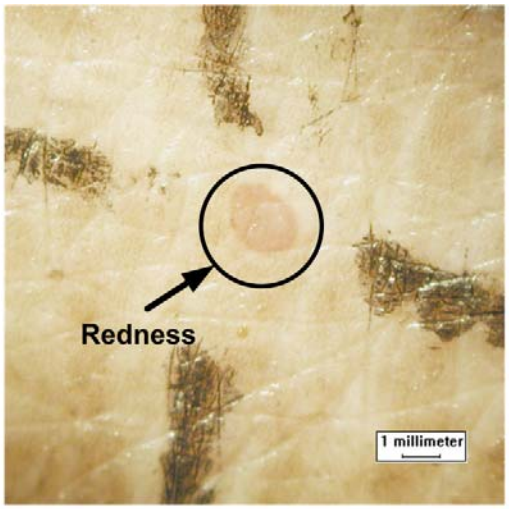

b1

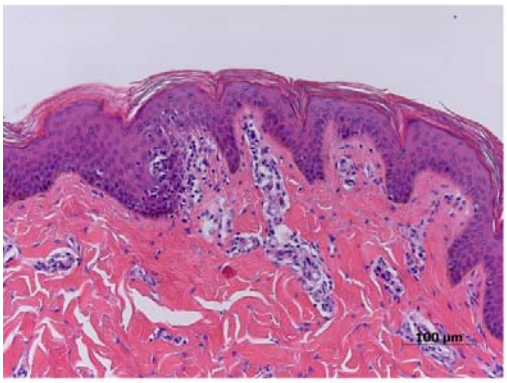

a2

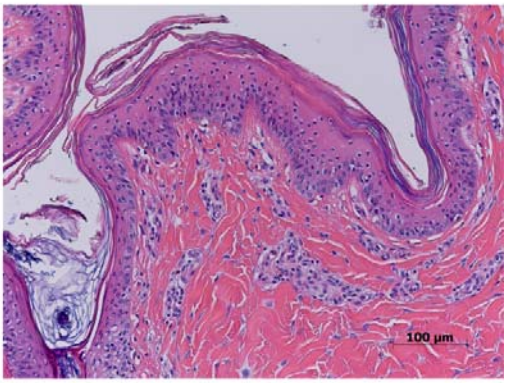

b2

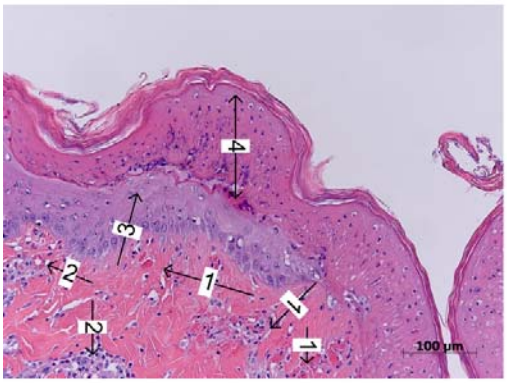

a3

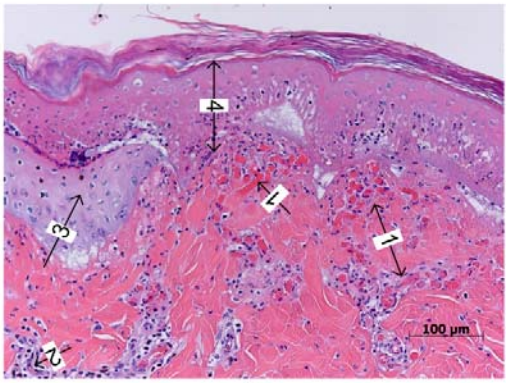

b3

Figure 4.2. The gross images of dark and light mini-pig skin surface 48 hours after threshold irradiation and their corresponding microscopic biopsies (H&E stain. Original Mag. 200X). a1-a3:dark colored skin; b1-b3: light colored skin. a1,b1: Gross image of skin lesions; a2,b2: Histological section of normal skin; a3,b3: Histological section of threshold lesions, Vascular dilation and thrombosis in dermal blood vessels (arrow 1), perivascular inflammation (arrow 2), regenerated epidermal cells growing under necrotic epidermis (arrow 3), transmural necrosis of epidermis (arrow 4).

4.6. CONCLUSION

Dark and light skin have similar thermal responses to laser irradiation owing to similar optical and thermal properties at 2.0 μm wavelength. In terms of laser safety limits, both threshold powers and histological study of threshold lesions confirm that the damage threshold data of dark mini-pig skin with heavy melanin density can be extrapolated to various colored skin with sufficient accuracy. On the other hand, the light mini-pig skin is more suitable for damage threshold evaluation because the visual determination of redness on light skin is much easier and therefore has less observational error than dark skin.

4.7. ACKNOWLEDGMENT

Opinions, interpretations, conclusions, and recommendations are those of the authors and are not necessarily endorsed by the University of Texas, the United States Air Force or the Department of Defense.

The authors wish to thank Dr. Sergey Telenkov, Victor Villavicencio, Dan Polhamus and Jennifer Cassaday for their kind help.

4.8. REFERENCES

Chen, B., D. C. O'Dell, et al. (2005). "Porcine skin ED50 damage thresholds for 2,000 nm laser irradiation." Lasers Surg Med **37**(5): 373-81.

Duck, F. A. (1990). Physical properties of tissue London, Academic Press. pp 9-42.

Eggleston, T. A., W. P. Roach, et al. (2000). "Comparison of two porcine (Sus scrofa domestica) skin models for in vivo near-infrared laser exposure." Comp Med **50**(4): 391-7.

Finney, D. J. (1971). Probit Analysis 3rd ed. New York, Cambridge University Press.

Hale, G. M. and M. R. Querry (1973). "Optical constants of water in the 200nm to 200μm wavelength region." Appl. Opt. **12**: 555--563.

Jacques, S. L. (1993). "Role of tissue optics and pulse duration on tissue effects during high-power laser irradiation." Applied Optics **32**(13): 2447-2454.

Jacquez, J. A., J. Huss, et al. (1955). "Spectral reflectance of human skin in the region 0.7-2.6mu." J Appl Physiol **8**(3): 297-9.

Poppendick, H. F., R. Randall, et al. (1966). "Thermal conductivity measurements and predictions for biological fluids and tissues." Cryobiology(3): 318-27.

Rockwell, R. J., Jr and L. Goldman (1974). Research on human skin laser damage threshold. Final report, Conract F41609-72-C-0007. Brooks Air Force Base, TX., USAF School of Aerospace medicine.

Takata, A. N. (1977). Laser-induced thermal damage of skin. USAF School of Aerospace Medicine. Brooks Air Force Base, TX.

Thompson, C. R., B. S. Gerstman, et al. (1996). "Melanin granule model for laser-induced thermal damage in the retina." Bulletin of Mathematical Biology **58**(3): 513-553.

Wolbarsht, M. L., A. W. Walsh, et al. (1981). "Melanin, a Unique Biological Absorber." Applied Optics **20**(13): 2184-2186.

Chapter 5. Modeling Skin Thermal Damage from 2.0 μm Laser Irradiation[2]

5.1. ABSTRACT

An optical-thermal-damage model of the skin under laser irradiation was developed by using finite-element modeling software (FEMLAB 3.1). The general model simulated light propagation, heat generation, transient temperature response, and thermal damage produced by a radially symmetric laser beam of normal incidence. Predictions from the model were made of transient surface temperatures and the thermal damage on a pigskin surface generated by 2000 nm laser irradiation, and those predictions were compared to experimental measurements. The comparisons validated the model predictions, boundary conditions, and optical, thermal, and rate process parameters. The model enabled the authors to verify the suitability of the ANSI maximum permissible exposure (MPE) standard for a wavelength of 2000 nm with exposure duration from 0.1 to 1 s and 3.5 mm beam diameter. Compared with the ANSI MPE standard, however, the MPE values predicted by the model were higher for exposure durations less than 0.1 s. The model indicated that it may be necessary to modify the ANSI MPE standard for cases in which the laser-beam diameter is larger than 3.5 mm when a "safety-factor" of ten is used. A histopathological analysis of the skin damage was performed to determine the mechanisms of laser-induced damage in the skin.

Key words: damage threshold; finite element modeling; laser injury; laser safety; maximum permissible exposure (MPE); skin damage.

[2] Significant portions of this chapter have been previously published in *J. Biomed. Opt.*, 11(6):064028, 2006.

5.2. INTRODUCTION

High-power laser systems operating at wavelengths of approximately 2000 nm, such as the Ho:YAG laser (λ=2.1 μm), are becoming increasingly important tools in the military, medicine, and industry. With the recent development of continuous-wave systems operating at 2000 nm, it may be necessary to refine the existing laser safety guideline limiting the exposure limits for these systems. Currently, the ANSI Z136.1-2007 guideline, *American National Standard for Safe Use of Lasers* (ANSI 2007), gives the maximum permissible exposure (MPE) limits for far-IR wavelengths between 1.8 and 2.6 μm as a function of the duration of laser exposure. Because the MPE level for a wavelength of 2.0 μm was based on minimal experimental data, several damage threshold experiments have recently been conducted to refine the safe-exposure limits. In 2005 Zuclich *et al*. investigated the wavelength dependence of ocular thresholds in the near-IR and far-IR transition regions and noted that the exposure limits in some cases were above the measured damage thresholds in the band between 1.3 and 4.0 μm (Zuclich, Lund et al. 2007).

In the present study, we conducted a series of experiments and tests on Yucatan mini-pigs to determine the effects of irradiated spot size and exposure duration on the threshold damage to skin from a laser beam with a wavelength of 2000 nm (Chen, O'Dell et al. 2005). Instead of the more commonly used Yorkshire pigs, Yucatan mini-pigs were used in this study because their skin has an anatomical similarity to human skin (Eggleston, Roach et al. 2000; Chen, O'Dell et al. 2005). During the experiments, 48-hour damage thresholds were determined by probit analysis as functions of exposure time and spot sizes. The associated transient temperatures were measured with a thermal camera, and histological sections were taken for later analysis of the relationships among temperature, time, and damage. In this study, we validated an optical-thermal-damage

model so that limited experimental data could be extrapolated to a wider range of laser conditions. The model, coupled with the 2.0 μm experimental data, provided a technique for evaluating laser safety standards.

The biological and physical changes in laser-irradiated skin depend on the temperature-time response of the tissue. The formation of a thermally induced lesion in the skin begins with the local absorption of laser light, which is converted into heat. The first mechanism by which the tissue is thermally affected can be attributed to alterations of physiological equilibria in response to the heat. As temperature increases, denaturation of proteins occurs, which leads to death and necrosis of tissue and cells. Thermal coagulation including collagen hyalinization, collagen and muscle birefringence changes, tissue whitening and cell shrinkage occurs at higher temperature (Niemz 1996).

Several published computer models have predicted heat generation, transient temperatures, and thermal damage in tissues, but few have compared predictions to measured temperatures. In the 1970's, Mainster *et al*. used the finite-difference method to solve the heat conduction equation for cylindrical symmetrical, and thermal homogeneous media (Mainster, White et al. 1970; Mainster, White et al. 1970). In 1971, Vassiliadis *et al*. developed a Green's function solution for symmetrical noncoherent sources (Vassiliadis, Christian et al. 1971). Later, Welch *et al*. combined a rate process model with the finite-difference model (Welch 1975), and Takata *et al*. expanded the model to include multiple layers, blood perfusion, blister formation, and damage (Takata, Goldfinch et al. 1974; Takata 1977). Cain and Welch tested the temperature predictions of the model for argon laser irradiation in a rabbit's eye and determined that the model was quite accurate in predicting measured retinal temperature and damage for laser-pulse durations exceeding 10 ms. In those models, the highly absorbing pigment epithelium was represented as a thin layer in a continuous medium with Beer's law absorption (Cain

and Welch 1974). Torres *et al.* modified the Takata skin model to predict the temperature response of an *in vitro* aorta irradiated with an argon laser. In that study, the Beer's law heat source of the Takata model was replaced by a Monte Carlo model of photon propagation to account for light scattering. Even with that modification, however, Torres *et al.* found that the computed steady state and relaxation temperatures were much higher than the measured results. A second set of experiments demonstrated the existence of temperature-dependent surface cooling associated with the evaporation of water at the surface of the skin (Torres and Motamedi 1993).

The study of the key factors associated with thermal injury and the evaluation of a wider range of exposure parameters are possible by modeling light propagation, heat generation, heat conduction, and temperature-dependent rate reactions and then validating the predictions with experimental data. In this paper, we compare the results of our finite-element modeling of thermal damage to results obtained from our previous experiments (see chapter 3) (Chen, O'Dell et al. 2005). Temperature distributions and damage are computed as a function of power, exposure duration, and spot size for the optical properties associated with 2000 nm irradiation of pigskin.

The extent of the damage to the surface was evaluated by visual inspection. In addition, for comparisons with the temperature and damage predicted by our thermal model, a qualitative histopathological study of the skin damage was performed to determine the mechanisms of laser-induced damage in the skin and to map the extent and severity of the lesions.

5.3. MATERIAL AND METHODS

In our previous study, a series of experiments were conducted *in vivo* on female Yucatan mini-pigs with dark skin to determine the damage thresholds for 2000 nm laser

irradiation (Chen, O'Dell et al. 2005). That limited study employed Gaussian-shaped beam diameters of approximately 5, 10, and 15 mm and exposure durations of 0.25, 0.5, 1.0, and 2.5 seconds as a function of laser power. The effects of each irradiation were evaluated shortly after exposure and 48 hours later. The transient temperature distribution on the skin surface was measured with an IR-array thermal-detector camera for each combination of spot size and exposure duration (Chen, O'Dell et al. 2005).

5.3.1. Preparation of Tissue Specimens

The mini-pigs were euthanized 48 hours after irradiation, at which time tissue specimens of each lesion were taken and fixed in 10% neutral buffered formalin, embedded with paraffin, sectioned, and stained with hematoxylin and eosin (H&E). To determine the maximum histological diameter of the lesion in the skin, serial consecutive sections were cut through the sample blocks to locate the center of the thermal lesion at the microscopic level.

5.3.2. Beam-Profile Measurement

The laser beam spatial profile, which was critical for temperature modeling, was obtained by two methods: knife-edge measurement and spatial IR imaging of the skin by a 30 ms laser irradiation. The 1/e light penetration depth into the skin at 2000 nm was approximately 200 μm, and the associated characteristic thermal diffusion time for a large spot diameter was about 300 ms (Jacques 1993). Compared to the characteristic diffusion time for skin, the heat conduction within the 30 ms pulse duration was insignificantly small. The temperature rise was directly proportional to the irradiance [W/cm^2] for the case of no heat transfer during the laser pulse. Therefore, the measured surface temperature distribution (Figure 5.1) obtained from the thermal camera represented the spatial intensity profile of the nominally Gaussian-shaped laser beam.

The spatial profile was elliptical rather than circular, with the major axis about 10% longer than the minor axis. The radial profiles along the two axes of the elliptic laser beam (see Figure 5.2) were essentially Gaussian in shape with $1/e^2$ radii of 2.55 mm and 2.33 mm. The arithmetic average of the two radii was 2.44 mm, which was close to the knife-edge measurement value of 2.42 mm for this example. To simplify calculations, the model assumed that the spatial profile was a circular, symmetric, Gaussian beam with a $1/e^2$ radius of 2.44 mm.

The spatial profiles of two larger laser beams created with various telescopes were measured by using the spatial IR imaging as well as the knife-edge method. For the radii, the model used arithmetical averages of 5.04 mm and 6.92 mm derived from IR imaging. These two radii values were close to the knife-edge measurement values of 4.83 mm and 7.33 mm, respectively, values deviating by about 5% from the averaged radii. The differences in the values from these two methods were due to the elliptical, rather than circular, spatial profile assumed by the knife-edge measurement and the slight curvature of the mini-pig skin surface.

5.4. OPTICAL-THERMAL-DAMAGE MODEL

An optical-thermal-damage model was developed by using FEMLAB finite-element modeling software (FEMLAB 3.1, Comsol Inc., Burlington, MA) to simulate the transient temperatures and thermal damage produced in skin by a radially symmetric laser beam at a normal angle of incidence. The skin was represented by two homogenous regions (epidermis and dermis) with a nonlinear air-tissue boundary condition. Because the radially symmetric beam was perpendicular to the skin surface, the skin model was simplified to 2-D (radial r and axial z) and deployed using cylindrical coordinates. The

FEMLAB model provided a time-dependent simulation that was capable of incorporating nonlinear boundary conditions and heterogeneous thermal and optical properties in tissue.

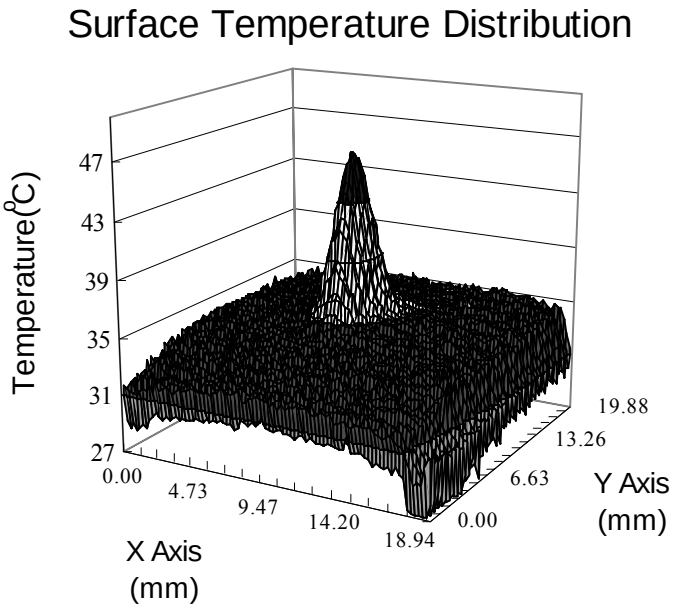

Figure 5.1. Skin surface temperature distribution after 30 ms laser irradiation. Laser power: 3.23 W, beam radius: 2.44 mm.

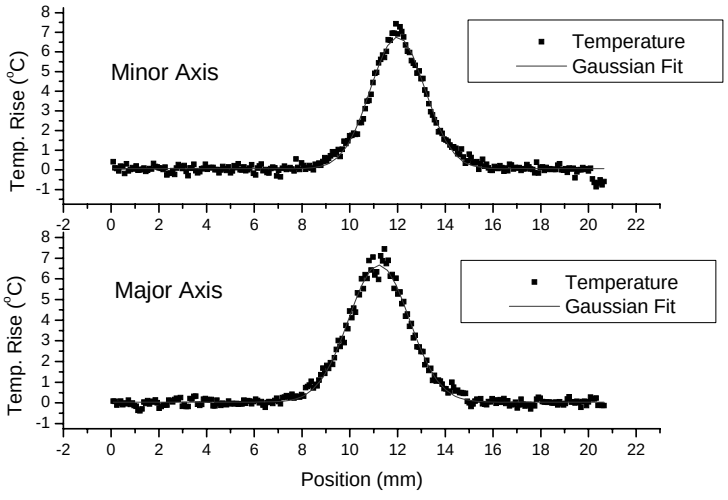

Figure 5.2. Surface temperature distribution along major and minor axes after 30 ms laser irradiation.

5.4.1. Optical Propagation

The formation of a thermally induced lesion in the skin was modeled as a temperature-time rate process associated with the thermal denaturation of proteins. The process began with the local absorption of the laser light by the skin and the conversion of the light into heat. The localized heat source S [W/cm^3] at position (r,z) and time t was a function of the local wavelength dependent absorption coefficient $\mu_a(z)$ [1/cm], as follows:

$$S(r,z,t) = \mu_a(z)\phi(r,z,t), \tag{5.1}$$

where $\phi(r,z,t)$ [W/cm^2] is the fluence rate at position (r,z) and time t. At 2000 nm, water was the primary chromophore in the skin. Because light scattering was insignificant at this wavelength, the model ignored scattering in the skin, and light propagation in the skin was described by Beer's law

$$S(\boldsymbol{r},z,t) = \mu_a(1-r_s)E(r,t)e^{-\mu_a z}, \tag{5.2}$$

where $E(r,t)$ [W/cm^2] was the irradiance and r_s was the specular reflectance on the skin surface. The specular reflectance of *in vitro* mini-pig skin at the air/epidermis interface was measured as 4.75% by use of a spectrophotometer. Gaussian distributed irradiance was used in the model to approximate the laser profile emitted from the 2000 nm laser system used in the experiments. The irradiance $E(r)$ was expressed as follows:

$$E(r) = \frac{2P}{\pi\omega^2}e^{-\frac{2r^2}{\omega^2}}, \tag{5.3}$$

where P is the radiant power [W] and ω is the 1/e^2 radius of the laser beam.

5.4.2. Heat Conduction

It was assumed that there was no heat loss/gain because of blood flow and metabolism. The assumption was reasonable for our experimental conditions with exposure durations less than several seconds (Takata 1977; Svaasand, Boerslid et al. 1985; Niemz 1996). Therefore, the temperature response of the skin to laser irradiation was governed by the heat conduction equation:

$$\rho C \frac{\partial T}{\partial t} = \frac{k}{r}\frac{\partial T}{\partial r} + \frac{\partial}{\partial r}(k\frac{\partial T}{\partial r}) + \frac{\partial}{\partial z}(k\frac{\partial T}{\partial z}) + S \qquad (5.4)$$

where $T(r,z,t)$ [K] was the temperature in the skin, $\rho(z)$ [kg/m^3] was the skin density, $C(z)$ [J/kg K] was the specific heat, and $k(z)$ [W/m K] was the thermal conductivity.

Water loss from evaporation was considered in the model boundary conditions. The evaporation occurred when water molecules near the surface experienced collisions that increased their energy above that needed to overcome the surface binding energy. The energy associated with the phase change was the latent heat of water evaporation. The energy required to sustain the evaporation came from the internal energy of the water, which experienced a reduction in temperature (the cooling effect) (Incropera and Dewitt 2001). Water evaporation was diffusion limited and highly dependent on the relative humidity of the air and temperature-dependent mass diffusion coefficients (Incropera and Dewitt 2001). This approach for estimating the rate of free-water surface vaporization loss was based on the heat and mass transfer boundary layer analogy for evaporative cooling (Torres and Motamedi 1993; Diaz, Aguilar et al. 2001; Incropera and Dewitt 2001):

$$Q_{vap} = h_{fg} h_m(T_s)[\rho_{v,sat}(T_s) - \rho_{v,\infty}], \qquad (5.5)$$

where $Q_{vap}(r, z = 0)$ is the vaporization loss term [W/m^2], $\rho_{v,sat}(T_s)$ is the mass density of saturated water vapor [kg/m^3] at the temperature of the tissue surface T_s, $\rho_{v,\infty}$ is the density of water vapor in the air [kg/m^3] at room temperature, h_{fg} is the phase-change

enthalpy [J/kg] at T_s, and h_m is the convection mass transfer coefficient [m/s]. Based on analogous heat and mass transfer mechanisms, this coefficient was obtained by applying the Lewis number (Torres and Motamedi 1993; Incropera and Dewitt 2001):

$$h_m(T_s) = h_e / (\rho_a(T_s) c_a(T_s) \mathrm{Le}^{2/3}), \tag{5.6}$$

where h_e is the heat-convection coefficient [W/m^2 K], which in this case is free convection; $\rho_a(T_s)$ is the density of the air [kg/m^3]; $c_a(T_s)$ is the specific heat of the air [J/kg K]; and Le is the Lewis number for the diffusion of water vapor into air. The value h_{fg} was approximated as a constant. value 2.35×10^6 J/kg . The value $\rho_{v,sat}(T_s)$ which is a function of temperature on the skin surface was estimated during the simulation using a fourth-order polynomial non-linear fit of the published water-vapor thermal properties (Incropera and Dewitt 2001).

$$\rho_{v,sat}(T_s) = 4\times10^{-9}\times T^4 - 6\times10^{-8}\times T^3 + 1.96\times10^{-5}\times T^2 + 1.534\times10^{-4}\times T + 6.1098\times10^{-3} \text{ kg/m}^3$$

Because radiative loss on the surface is insignificant compared to the heat losses by convection and evaporation, the surface boundary condition was described by free convection and water evaporation:

$$-k\frac{\partial T}{\partial z} = h_e(T - T_\infty) + Q_{vap}, \tag{5.7}$$

The model prediction of temperature rise as a function of time in response to laser irradiation agreed well with the experimental results when the value for h_e was 15 [W/m^2 K]. This value was in good agreement with typical values of h_e for free convection in air, which ranges between 5 to 25 [W/m^2 K] (Incropera and Dewitt 2001).

The thermal properties of the epidermis and dermis were derived from the following equations (Takata 1977) and the assumption of 80% water content in the dermis and 30% in the epidermis (Takata 1977):

$$\rho = (1.3 - 0.3w) \times 10^3 \text{ [kg/m}^3\text{]}$$
$$C = (1.55 + 2800\frac{w}{\rho}) \times 10^3 \text{ [J/kg K]}, \quad (5.8)$$
$$k = (0.06 + 570\frac{w}{\rho}) \text{ [W/m K]}$$

where w is the water content (Takata 1977).

5.4.3. Rate Process

The standard rate process model of tissue damage was introduced by Henriques and Moritz in the 1940's. The damage parameter Ω, which indicates the level of damage, was computed using the Arrhenius equation (Henriques 1947; Moritz and Henriques 1947):

$$\Omega(r,z) = A\int_0^\infty e^{-\frac{E_0}{RT(r,z,t)}} dt, \quad (5.9)$$

where A is the molecular collision frequency factor, E_0 is denaturation activation energy, and R is the universal gas constant. Henriques and Moritz assigned $\Omega = 0.53$ corresponded to a threshold of first-degree burn (persistent but reversible erythema), $\Omega = 1$ to the threshold of second degree-burn (irreversible partial-thickness injury), and $\Omega = 10000$ corresponded to a threshold of third-degree burn (irreversible full-thickness injury). The original values for A and E calculated by Henriques and Moritz (Henriques 1947; Moritz and Henriques 1947) were used in the model as follows:

$$A = 3.1 \times 10^{98}, \; E = 628000 \text{ J/mole} \quad (5.10)$$

5.4.4. Optical Property Measurements

A method that used a transient temperature measurement was developed for measuring the *in vivo* optical properties of the skin. Under conditions of insignificant heat conduction (exposure time, t_0 << characteristic thermal diffusion time τ), the slope of

peak temperature response to very short pulses *vs.* time provided a measure of the absorption coefficient μ_a:

$$\Delta T(r,t) = \frac{\phi\left(r, z = 0^+, t\right)\mu_a t}{\rho C}, \tag{5.11}$$

where $\phi\left(r, z = 0^+, t\right)$ was the fluence rate just below the surface and t is the exposure time. The value ϕ was approximately equal to the incident flux $(1-r_s)E(r,t)$, since light scattering was insignificant (r_s was the specular reflectance). Because the irradiance used in this measurement was constant during the laser pulse and had a Gaussian shape, the irradiance at $r = 0$ ($E(r=0,t)$) was equal to $\frac{2P}{\pi\omega^2}$ (see Equation 5.3). P was the input power and ω was $1/e^2$ radius. Therefore, the absorption coefficient was estimated according to the slope of the peak temperature response curve during the first 100 ms of irradiation.

The thermal and optical properties of the epidermis and dermis used in the optical-thermal-damage model are summarized in Table 5.1.

Table 5.1. Summary of thermal and optical properties used in the model.

Thickness [mm]	Epidermis	0.068
	Dermis	1.432
Water content, w	Epidermis	0.3
	Dermis	0.8
Density, ρ [kg/m^3]	Epidermis	1210
	Dermis	1060
Thermal conductivity, k [W/m ^{o}C]	Epidermis	0.20
	Dermis	0.49
Specific heat, C [J/kg ^{o}C]	Epidermis	2244
	Dermis	3663
Absorption coefficient, μ_a [1/cm]	Epidermis	21.76
	Dermis	58.02
Molecular collision frequency factor, A		3.1×10^{98}
Denaturation activation energy, E_0 [J/mole]		628000
Heat-convection coefficient, he [W/m^2 K]		15
Density of water vapor in the air at room temperature, $\rho_{v,\infty}$ [kg/m^3]		0.00865
Room temperature, T_∞ [^{o}C]		20

5.5. RESULTS

5.5.1. ED50 Thresholds for 1-Minute and 48-Hour Observations

A probit analysis (Finney 1971) was conducted to estimate the ED50 thresholds according to two different end points of the thermal lesions: 1) instant redness observed on the skin within 1 minute after laser irradiation and 2) persistent redness at the site 48 hours after irradiation.

Most of the lesions appeared immediately, that is, within 1 minute of the onset of laser irradiation, and remained on the skin after 48 hours. At some irradiation levels, which are close to the instant redness thresholds radiant exposure, however, several instant red spots recorded immediately after irradiations were not observed at the 48-hour post-exposure reading. At persistent redness thresholds, the redness at most of the

irradiated spots had appeared within 1 minute after irradiation. However, at some specific radiant exposure levels near the estimated persistent redness threshold, the redness developed on the skin several minutes after the laser irradiation ceased and persisted past the 48-hour post-exposure reading.

Table 5.2. The ED50 average radiant exposure and standard deviation at damage thresholds defined as instant redness within one minute or persistent redness after 48 hours.

Radius(mm)	2.44		5.04		6.92	
Duration(s)	Instant (J/cm^2) *	Persistent (J/cm^2) **	Instant (J/cm^2)	Persistent (J/cm^2)	Instant (J/cm^2)	Persistent (J/cm^2)
0.25	2.83 ± 1.23	$3.50 \pm 0.37^{\#}$	2.42 ± 0.19	2.65 ± 0.33	1.96 ± 0.26	2.67 ± 0.07
0.5	4.60 ± 1.02 ☆	3.98 ± 1.28	1.84 ± 1.37	3.10 ± 0.17	2.50 ± 0.14	2.81 ± 0.27
1.0	3.80 ± 1.23	$4.97 \pm 1.55^{\#}$	2.64 ± 0.03	$3.61 \pm 0.44^{\#}$	2.65 ± 0.60	3.34 ± 0.70
2.5	3.07 ± 1.07	5.48 ± 1.60	4.14 ± 0.28	$4.42 \pm 0.34^{\#}$	3.46 ± 0.55	4.09 ± 0.50

* : Thresholds of instant redness by observation within 1 min of irradiation.
** : Thresholds of apparent persistent redness of the skin visible at 48 hours after irradiation.
$^{\#}$: Estimated without using probit fit.
☆: Did not fit trend.

The average radiant exposure for the ED50 thresholds at the 1-minute and 48-hour post exposure readings are compared in Table 5.2. The radii used in the radiant exposure calculation were derived from the thermal image instead of the knife-edge measurement, therefore the average radiant exposure listed in Table 5.2 are slightly different from the values presented in our previous paper (Chen, O'Dell et al. 2005). The standard deviation (σ) was derived from the probit fit curve by the following definition:

$$\sigma = (ED_{84} - ED_{16})/2, \quad (5.12)$$

where ED_{84} represents the dose for an 84% probability of laser-induced damage, and similarly for ED_{16}. At some irradiation conditions, direct estimations were made without

a probit analysis, because the data was quite consistent and there was insufficient scatter for the probit program. In other words, there was consistent damage or no damage above or below the specific exposure levels (H_{yes} and H_{no}, respectively). In those limited cases, the ED50 value was estimated as the middle point between the lowest value of damage (H_{yes}) and largest value of no damage (H_{no}). The standard deviation of the ED50 value equaled 32% of the border width (H_{yes}- H_{no}) (Chen, O'Dell et al. 2005).

5.5.2. Microscopic Observations of the Skin

Figure 5.3 shows representative gross images of the mini-pig skin surface 48 hours after various irradiations and their corresponding microscopic H&E stained biopsies. Figures. 5.3a, b, and c correspond to mini-pig skins without irradiation, irradiation at the radiant exposure level near the instant redness threshold, and radiant exposure at the persistent redness threshold, respectively. At the instant redness threshold, no redness was observed after 48 hours (Figure 5.3b(1)), although redness had appeared immediately after irradiation. Mild perivascular edema and focal hyperkeratosis was found at some suspicious sites (Figure 5.3b(2)); however, it was doubtful whether the lesion was caused by laser irradiation or mechanical trauma (scratching).

Figure 5.3c(1) shows a gross image of the persistent redness. The thermal lesion formed flat red papules concomitantly with the shrinking of the epidermis at the center of the irradiation sites. The microscopic image of the injury is illustrated in Figure 5.3c(2). There was coagulative necrosis of varying depths at the burn site, with a loss of epidermis over some of the more severe burns. The pattern of necrosis had roughly the shape of a flattened cone. The necrotic epidermis cells had pyknotic or shrunken dense nuclei or occasionally fragmented nuclei. Regenerated epidermis cells formed underneath the dead epidermis cells at the lesion boundary. Vascular dilation and thrombosis in the dermal

blood vessels was observed, and perivascular inflammation appeared in deeper blood vessels.

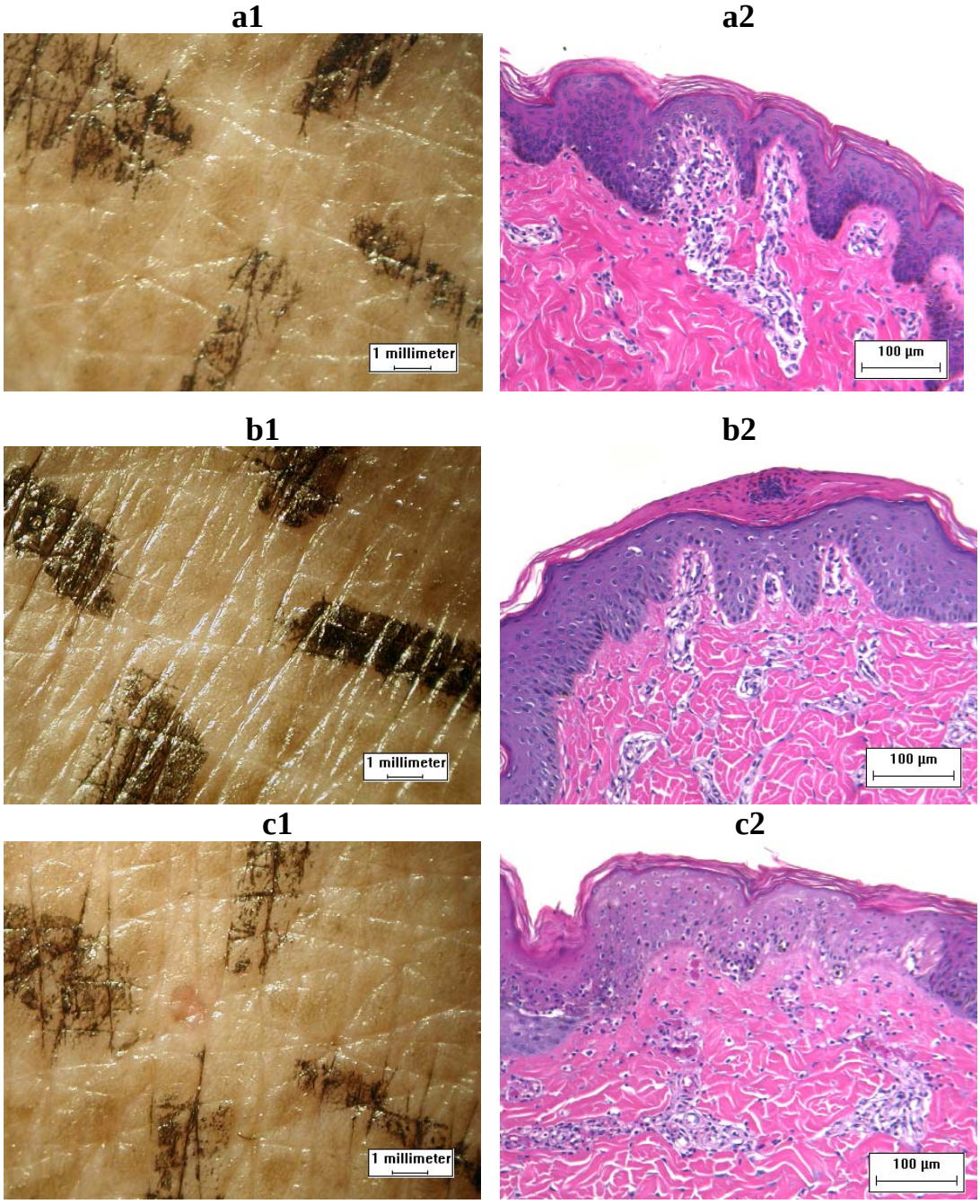

Figure 5.3. The gross pictures of mini-pig skin surface 48 hours after various irradiation and their corresponding microscopic biopsies (H&E stain. Original Mag. 20X). a1,a2: no irradiation. b1,b2: Irradiation at the radiant exposure level close to the instant redness threshold (exposure time 2.5 s, beam radius 2.44 mm, laser power 0.29 W). c1,c2: Irradiation at persistent redness threshold (exposure time 2.5 s, beam radius 2.44 mm, laser power 0.41 W). In a2 note: normal dermal blood vessels (arrow 1), edema and inflammation (arrow 2). In b2 note: edema and inflammation (arrow 2), focal hyperkeratosis (arrow 3). In c2 note: Vascular dilation and thrombosis in dermal blood vessels (arrow 4), Regenerated epidermal cells growing under necrotic epidermis (arrow 5), transmural necrosis of epidermis (arrow 6), and perivascular inflammation (arrow 7). In conclusion: All blood vessels show edema and inflammation, however, thrombosis, transmural epidermal necrosis and dermal vascular dilation were not observed in figure 5.a2 and 5.b2. .

5.5.3. Absorption Coefficient of the Epidermis and the Dermis

A dark mini-pig skin spotted with white areas was used to measure the *in vivo* absorption coefficient. The peak temperature responses during the first 100 ms of laser irradiation were recorded with an IR camera with an imaging rate 800 frames per second. The 1/e light penetration depth at 2000 nm was reported to be approximately 200 μm, and the associated characteristic thermal diffusion time for a large spot diameter was about 300 ms (Jacques 1993).

Measurements (n = 10) were conducted at two different locations on the mini-pig flank and at five different power levels. The absorption coefficient of the epidermis (μ_{a_epi}) for dark skin was 21.76 ± 0.99 cm^{-1}, which was derived from the slope of the linear fit lines of the peak temperature response curve using Equation 5.11 (linear correlation coefficient $R \approx 0.99$) (Figure 5.4).

Because water was the primary absorber at the 2000 nm wavelength, another way to estimate the absorption coefficient of the epidermis was based on the product of absorption coefficient of water and the water content in the epidermis.

$$\mu_a = \mu_{water} \times w, \tag{5.13}$$

where μ_{water} is the absorption coefficient of water, which is 69.12 cm^{-1} at 2000 nm wavelength (Hale and Querry 1973) and *w* is the water content in tissue. Values of 80% for the water content in the dermis and 30% in the epidermis were used in the model. With those estimations, the calculated absorption coefficient of the epidermis was 20.74 cm^{-1}, which was in good agreement with the measured μ_{a_epi} (21.76 ± 0.99 cm^{-1}).

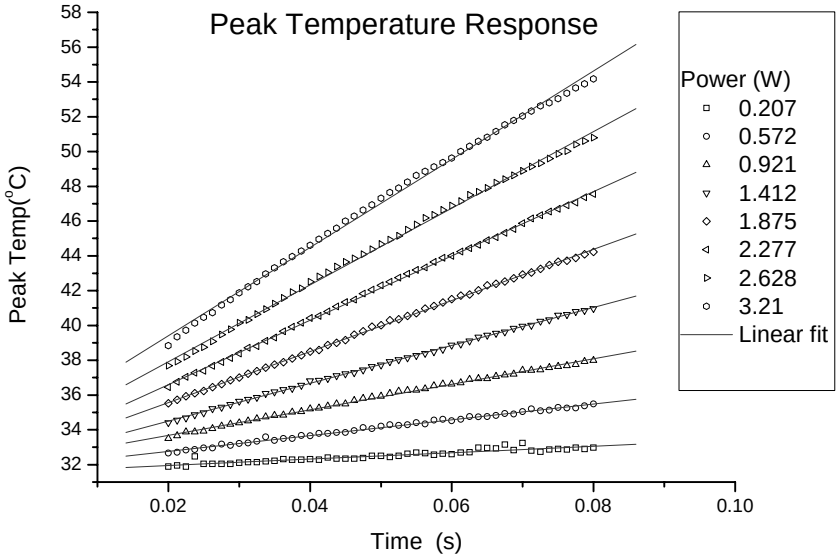

Figure 5.4. linear fits of peak temperature response curve during the period of no heat conduction.

Absorption coefficients were also measured at two white areas on the spotted mini-pig skin. Those areas had less melanin density than the dark skin used more commonly in damage experiments. The measured absorption coefficient of the white skin was 21.03 cm^{-1}, which was close to dark-skin absorption coefficient of 21.76 cm^{-1}. This similarity indicated that melanin granules played an insignificant role in absorbing the far-IR 2000 nm wavelength.

From those results, a good assumption is that the absorption coefficient for the 2000 nm wavelength was directly proportional to the water content in the tissue. Consequently, the absorption coefficient of the dermis was estimated to be 58.02 cm^{-1}, according to the water content ratio of the dermis and epidermis as well as the measured absorption coefficient of the epidermis (μ_{a_epi}).

5.5.4. Temperature Measurements *vs.* the Model Predictions

To validate the optical-thermal-damage model, model predictions of the temperature response at the skin surface were compared to the experimental results. The peak temperature was defined as the maximum temperature at the irradiation site on the skin. Because of the Gaussian shape of the laser beam, the peak temperature represented the temperature at the irradiation center.

In Figures 5.5a, b, and c, the predicted peak temperatures after laser irradiation at various laser power levels are compared with the experimental results measured by the thermal camera. The predicted values for all exposure-duration and spot-size conditions agreed well with the experimental measurements within a 10% error.

Figure 5.6 is a comparison of the experimental and predicted peak transient temperature curves for the laser radiant exposures close to the persistent redness thresholds for various exposure durations. The predicted peak temperature rise followed the measured heating (with the laser on) curve quite well. After the laser was turned off, the predicted and experimental temperatures were in good agreement for the first 1 to 2 seconds. After that period, the computed curves deviated from the experimental results. We believe this deviation was due to our over-predicted cooling rate at temperature below 50 ^{o}C.

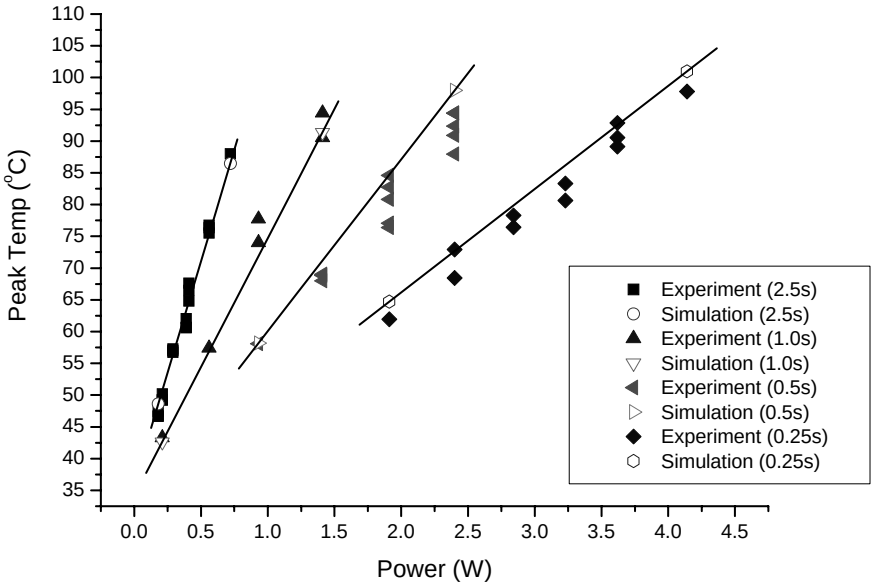

Figure 5.5a. The predicted and experimental peak temperatures after laser irradiation for various exposure durations and 2.44 mm spot radius.

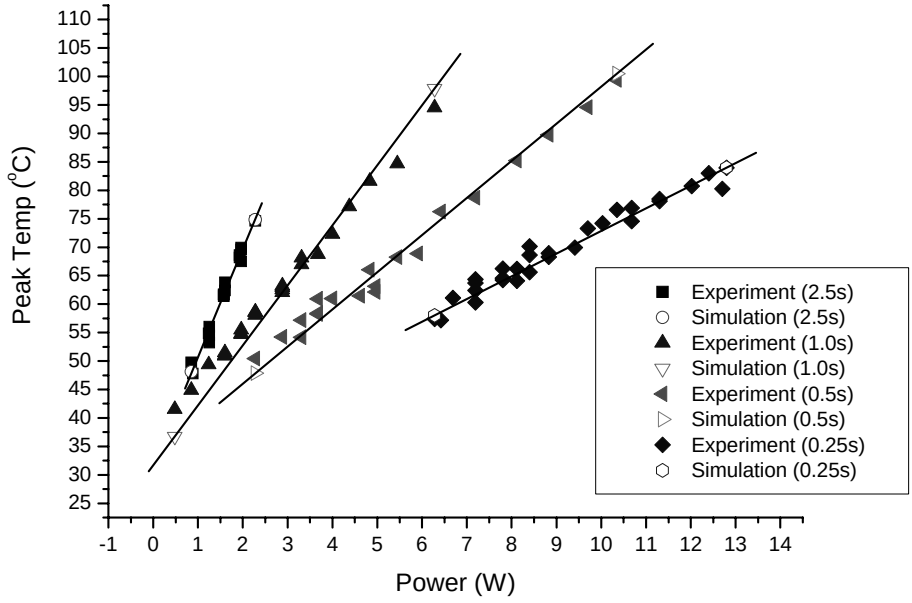

Figure 5.5b. The predicted and experimental peak temperatures after laser irradiation for various exposure durations and 5.04 mm spot radius.

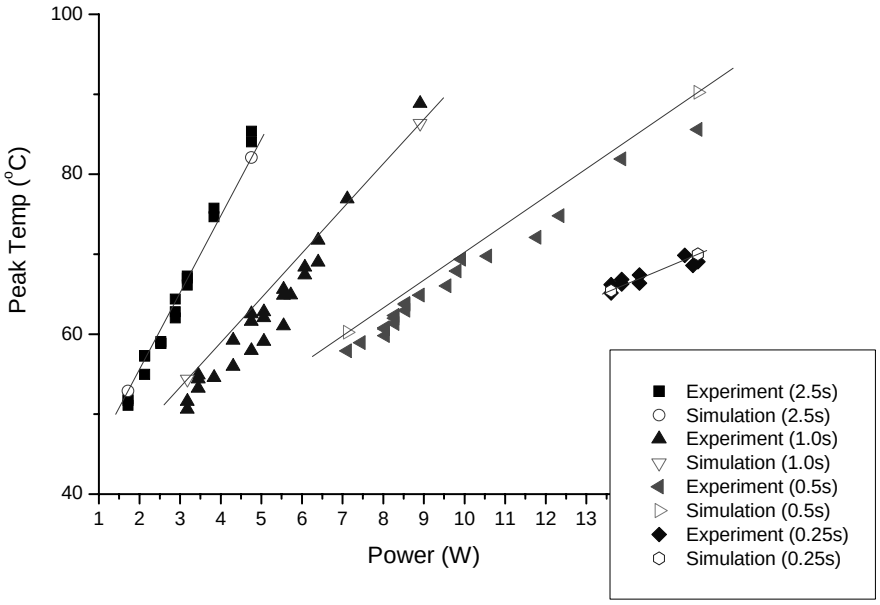

Figure 5.5c. The predicted and experimental peak temperatures after laser irradiation for various exposure durations and 6.92 mm spot radius.

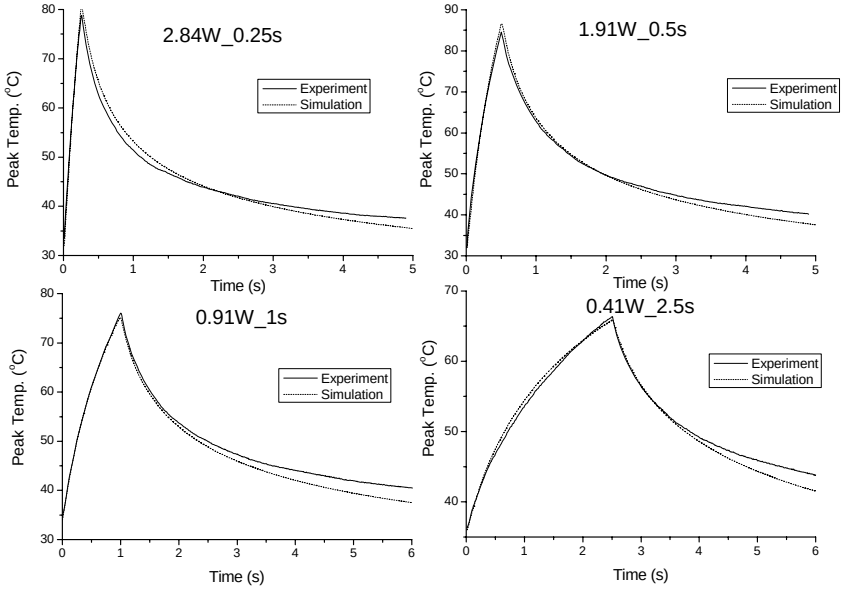

Figure 5.6. The experimental and predicted peak temperature responses by laser irradiation of various durations. Beam radius: 2.44 mm.

5.5.5. Damage Predictions by the Model

In the standard rate process model, threshold damage was associated with a "second degree" burn (irreversible partial-thickness injury), and parameters were selected so that $\Omega = 1$ at the boundary of damage and normal tissue. In our experiments, this definition corresponded to the threshold occurrence of a persistent redness lesion on the skin. Therefore, the model calculated Ω values and defined a contour line of $\Omega = 1$ as the persistent redness lesion boundary. Within this boundary, Ω was greater than 1. Thus, there was a region of super threshold damage according to the damage integral. Experimentally determined threshold energy levels do not correspond to $\Omega = 1$ at the center of the laser spot (r = 0). In practice, a finite area and a boundary of damage are necessary for an observer to determine that damage has occurred. Therefore, threshold damage becomes a function of the method of observation and the observer's ability to see a thermally induced change in natural skin. The following results were based on that definition.

The model predicted thermal lesion boundaries that were bowl-shaped. A comparison of the computed surface radii with experimental measurements is given in Table 5.3, and the computed depths are listed in Table 5.4. Because the ED50 damage threshold power levels usually did not correspond exactly to power levels used in the experiments, a corresponding experimental radius did not exist. The experimental damage radii were estimated using the measurements at the first lower and the first higher experimental power levels near the thresholds. A sample of the measured radii of redness vs. power levels is shown in Figure 5.7. An example of a probit fit analysis for damage/no damage as a function of power is illustrated in Figure 5.7 as well. The predicted temperatures at the thermal lesion boundaries after laser irradiation were compared for various spot sizes and exposure durations (Figures 5.8a and 5.8b).

Table 5.3. Radii of persistent redness on surface by experimental observations and model predictions using the threshold radiant exposure for persistent damage given in Table 5.2.

R(mm)	2.44		5.04		6.92	
T (s)	Simulation (mm)	Experiment (mm)	Simulation (mm)	Experiment (mm)	Simulation (mm)	Experiment (mm)
0.25	1.03	0.75-2.5	1.04	0.5-1.0	2.29	0.5-2.0
0.5	0.99	0.5-2.5	1.06	0.75-1.5	1.20	0.5-1.0
1.0	1.09 *	0.75-1.0	0.77	0.5-1.5	1.51 *	1.0-1.5
2.5	0.71 *	0.5-0.75	0.58	0. 5-1.25	0.58	0.5-2.0

*: Computed radii from threshold radiant exposure did not follow expected trend.

Table 5.4. Predicted maximum depths of thermal lesions at threshold radiant exposure computed for $\Omega = 1$.

Radius(mm) / Duration(s)	2.44	5.04	6.92
0.25	0.26 mm	0.16 mm	0.22 mm
0.5	0.28 mm	0.18 mm	0.17 mm
1.0	0.36 mm	0.18 mm	0.22 mm
2.5	0.32 mm	0.20 mm	0.14 mm

Table 5.5. Predicted maximum Ω values at instant damage threshold radiant exposure (at r = 0, z = 0).

Radius(mm) / Duration(s)	2.44	5.04	6.92
0.25	32.65	1.15	0.280
0.5	1.27×10^{5} ☆	8.4×10^{-4}	5.048
1.0	14.1	0.013	0.183
2.5	0.004	6.01	0.088

☆ : Experimental threshold radiant exposure did not fit the trend.

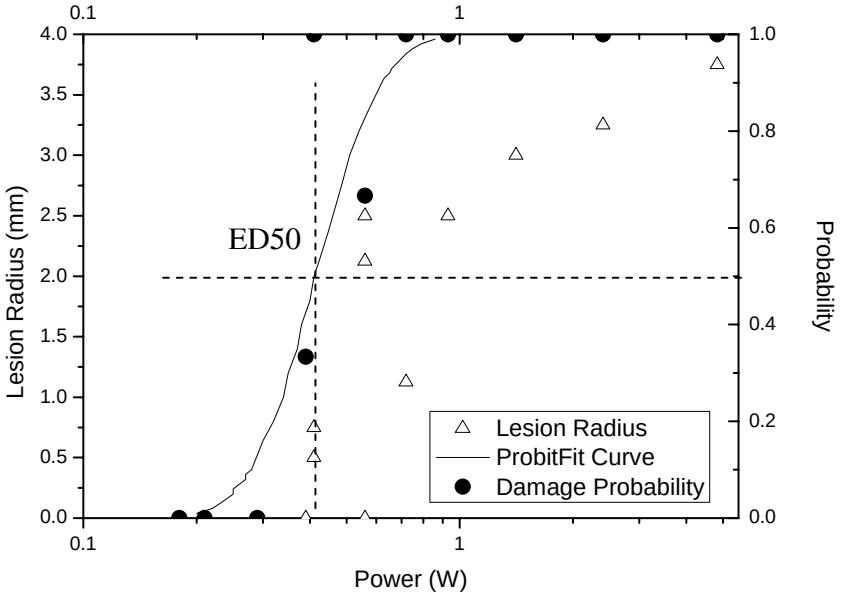

Figure 5.7. Radii of redness lesions and the probabilities of thermal damage vs. power levels. The triangles are the radii of the redness lesions that appeared on the skin after 48 hours. The circles are the experimental data (the probabilities to find damage after irradiations) and the solid curve is the probit fit curve of the no lesion-lesion observation as a function of laser power. Zero represents no damage and one represents damage. Some circles are not zero or one due to the variation of multiple measurements at the same power. Laser condition: Exposure time: 2.5 s, beam radius: 2.44 mm.

Another end point of the damage threshold, namely, the instant redness at the 1-minute observation point, was analyzed using the optical-thermal-damage model. The maximum computed Ω values at both r and z equal to zero for the radiant exposure at the instant-redness thresholds are given in Table 5.5.

In the far-IR wavelength range of 1.800 to 2.600 μm, the ANSI Z136.1-2000 defined MPE as follows:

$$H_{\max} = 0.56\, t^{0.25} \tag{5.14}$$

where H_{max} is the max radiant exposure and t is exposure duration. The standard is specified for a limited spot diameter of 3.5 mm and exposure durations between 10^{-3} to 10 seconds (ANSI 2007).

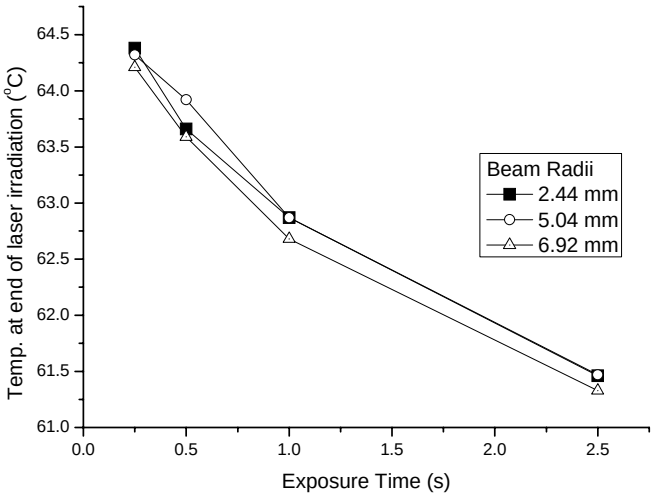

Figure 5.8a. Predicted surface temperature at the end of the laser irradiation at the lesion-no lesion boundary ($\Omega = 1$). Lesion radii are given in Table 5.3.

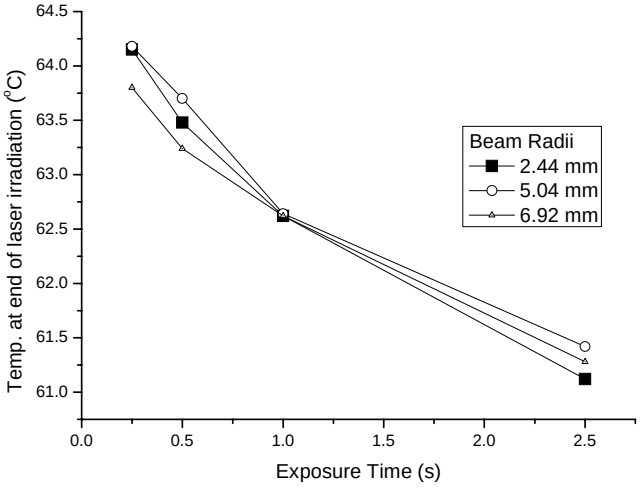

Figure 5.8b. Predicted temperature at the end of the laser irradiation at $r = 0$, z = max predicted lesion depth at $\Omega = 1$. Maximum lesion depths are given in Table 5.4.

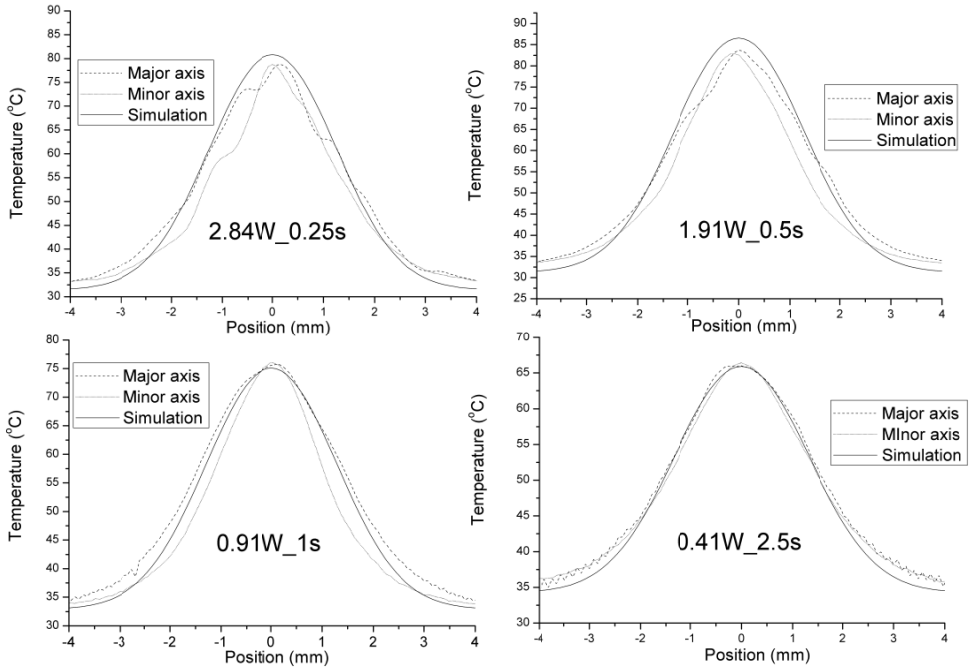

Figure 5.9. The predicted radial temperature and experimental temperature distributions along major and minor axes after laser irradiation. Beam radius: 2.44 mm.

MPE values have usually been assumed to be a factor of 10 below the radiant exposures at damage thresholds. Inversely, the threshold radiant exposures for various exposure durations were estimated to be ten times the current ANSI MPE values. Using the optical-thermal-damage model, this study examined the damage for those radiant exposures. The radii and depths of damage boundaries (Ω=1) that were simulated are listed in Table 5.6.

Table 5.6. Predicted radii and depths of thermal lesions ($\Omega = 1$) with radiant exposures (Ten times ANSI MPE values $H_{max}= 0.56\ t^{0.25}$) and 3.5 mm laser spot diameter.

Duration(s)	10	1	0.1	0.01	0.001
Radius(mm)	$\Omega_{max} < 1$	0.93	0.88	0.36	$\Omega_{max} < 1$
Depth (mm)	$\Omega_{max} < 1$	0.45	0.27	0.13	$\Omega_{max} < 1$

The optical-thermal-damage model was modified to predict CO_2 laser (10.6 μm wavelength) damage thresholds. The absorption coefficients of the epidermis and the dermis were estimated as 256.44 cm^{-1} and 683.84 cm^{-1}, respectively, based on the product of the water absorption coefficient (854.8 cm^{-1} at 10.6 μm wavelength (Hale and Querry 1973)) and water content in the epidermis and the dermis. Instead of using Gaussian beam irradiance, a 1.9 cm flattop laser beam was employed in the model to simulate the laser profile used in the published pigskin laser threshold damage experiments (Brownell, Parr et al. 1969). Simulation determined the threshold radiant exposure which produced Ω=1 within 9 mm of the beam center. Figure 5.12 is a comparison of the simulated damage thresholds and the pigskin damage threshold data (Brownell, Parr et al. 1969). The predicted damage thresholds for 10.6 μm (CO_2 laser) and 2.0 μm laser irradiation as a function of exposure duration are compared in Figure 5.13. The corresponding ANSI MPE limits for these wavelengths are drawn in Figure 5.13 as well.

5.6. DISCUSSION

5.6.1. Histological Analysis of Instant and Persistent Redness in Skin

The average radiant exposures for the ED50 thresholds for instant and persistent redness at the sites of irradiation are compared in Table 5.2. Overall, the average radiant exposures for the instant redness thresholds were lower than for the persistent redness thresholds. Gross observations also found that at some of the sites irradiated with radiant exposures near the instant redness thresholds, redness developed on the skin immediately after the irradiation but gradually disappeared after several hours.

Histologically, the instant and persistent redness observed on the skin suggests different damage mechanisms are at work. The laser-induced temperature rise in the skin causes a dilation of the blood vessels and an increase in the number of open vessels in the

dermis. The resulting increase in blood perfusion transfers more heat out of the high-temperature region to cool the skin to normal temperature.

Instant redness from hyperthermia is a reversible injury, and in this study the skin with instant redness reverted to its normal state after only a few hours without any persistent damage. The H&E stained biopsies of the skin sites where redness appeared immediately after irradiation but not after 48 hours did not present evidence of specific persistent injury (Figures 5.3 b(1) and b(2)). At some higher input of radiant exposure, the temperature reached a critical point where irreversible redness damage was generated. In other words, a site where a persistent redness was observed 48 hours after the irradiation represented a more serious thermal injury to the skin. At persistent redness thresholds, the 2000 nm wavelength laser irradiation produced death and necrosis of the epidermal cells and lethal thermal damage to superficial blood vessels. These results were the outcomes of a complex series of physiological vascular responses to heat, including the following: 1) hemostasis (blood flow stasis), 2) thrombosis, and 3) vascular dilation (see Figures 5.3 c(1) and c(2)). In the dermis, some cellular elements were more sensitive to injury than others, and they were necrotic at a greater depth than the resistant tissues. Thus, there were no sharp edges to the burn lesions. The endothelia of the blood vessels and supporting tissues were more sensitive than other tissues. The collagen bundles below the epidermis were swollen but there was no change in birefringence image intensity. When heated the complex Type I collagen macromolecules and fibrils undergo several configuration changes depending upon the tissue temperature and time at temperature. Thermally-associated swelling of the collagen fibers seen at the light microscopic level is associated with an expansion of the collagen fibril diameters due to radial dissociation of the collagen macromolecules detected in transmission electron micrographs. This swelling seen at lower temperatures as shown in *in vitro* experiments

of rat skin heated at 50 ^{o}C for 1000s is not associated with birefringence image intensity loss. Total birefringence loss occurs at 60 - 65 ^{o}C under the same experimental conditions (Pearce, Thomsen et al. 1993).

5.6.2. Predicted Thermal Damage

Good agreement between the results from the optical-thermal-damage model and the experimental results indicated that the model had included the major parameters contributing to the thermal response of the skin to 2000 nm laser irradiation. The discrepancy between the predicted and measured temperatures a few seconds after the laser was turned off is hypothesized to be attributable to surface drying which reduces the evaporative cooling effect (Figure 5.6). The difference between measured and computed temperature appeared several seconds into the relaxation phase, typically, when temperatures were less than $50\,°C$, at which point the damage term $e^{-\frac{E_0}{RT(t)}}$ of equation 5.9 did not significantly impact the damage integral. In other words, for exposure duration of less than 2.5 seconds, the predicted temperature transient and the rate process algorithm were sufficient to predict thermal damage with negligible error. However for longer exposure durations, the boundary condition must be adjusted to reflect the reduced heat loss as the skin surface dries.

The predicted radial temperature distribution was compared to the experimental temperature distributions along the major and minor axes of the experimental irradiance profile at the end of laser irradiation exposure durations of 0.25, 0.5, 1.0, and 2.5 seconds (Figure 5.9). The circular beam profile simplification did not cause the simulated temperature distributions to significantly deviate from experimental temperature distributions. Near the center of the beam where temperatures are maximum, a couple of degrees difference between computed and measured temperature would produce a

significant error in the value of the damage integral, Ω. However at the boundary of threshold damage (typically 1 mm radius in our experiments), the difference between computed and measured temperature is smaller, moreover, at this lower temperature range, the contribution to the damage integral is more time dependent.

The predicted radii of surface lesions and their experimental counterparts were compared in Table 5.3. The radii of surface spots with persistent redness were measured by an experienced clinical pathologist 48 hours after irradiation. Because of the uncertainty of the redness determination and the diversity of mini-pig skins, the measured radii near thresholds varied over a relatively large range. (A sample of measured radii of redness vs. power levels is shown in Figure 5.7). Typically, predictions were within the range of experimental results. The experimental data indicated that the lesion sizes at thresholds had approximately 1 mm radii but with a rather large range of values. Overall, the trend of the computed radii in Table 5.3 showed that damage radius (at $\Omega = 1$) was directly proportional to spot size and inversely proportional to exposure duration. Exceptions to this trend are marked by * in Table 5.3. At those points, the threshold radiant exposures may have been overestimated; that is, the computed lesion radius using the experimental threshold radiant exposures did not conform to the expected trends. The probit analysis of the experimental data indicated that the relative errors (the ratio of standard deviation and mean value given in Table 5.2) of these three threshold radiant exposures were over 20%. For our largest spot size (radius = 6.92 mm), the range of radii for experimental lesions was the largest. As spot size increased, the radial gradient of the temperature decreased. Thus, measurement uncertainty was amplified by the nonuniformity of the native tissue; that is, the tissue was not homogenous. Owing to this nonhomogenous nature of the skin, we did not have circularly symmetrical lesions. Even though the Yucatan mini-pig skin best approximates the properties of human skin, the

dark pigmentation of the skin hindered the gross visual determination of threshold damage and therefore may have contributed to an uncertainty in the threshold value because of observational threshold differences, especially for large laser spots and short exposure durations.

The predicted depths of the lesions at thresholds are listed in Table 5.4. The predicted values indicated that damage from 2000 nm wavelength laser irradiation would be confined to a very thin layer with a thickness less than 360 μm. The H&E stained skin biopsies (Figure 5.3) revealed coagulative necrosis in the epidermis and blood-vessel damage with thrombosis and stasis of blood in dilated blood vessels at the burn sites. The pattern of necrosis was roughly the shape of a flattened cone. Epidermis cells had pyknotic or shrunken dense nuclei or occasionally fragmented nuclei, which were morphological evidence of cell death and necrosis.

The predicted temperatures at the end of the laser irradiation at the predicted damage boundary (Table 5.3) were computed for the threshold radiant exposure of each spot size-exposure duration condition (Figures 5.8a and 5.8b). As expected, a smaller temperature rise was needed to generate thermal damage for longer exposure durations. Temperatures after irradiation at the damage boundary decreased concavely from 64.3 ^{o}C to 61.4 ^{o}C, whereas exposure duration increased from 0.25 s to 2.5 s, respectively. Only a 3-degree change in temperature occurred for a change in irradiation time by a factor of 10. For each exposure duration, however, there was little change in the associated threshold temperature. For our large spot sizes of irradiation, 4.88 mm to 13.84 mm diameter, most of the heat was transferred along the axial direction rather than the radial direction (Jacques 1993). Therefore, the shape of the temperature response curve depended less on the surface irradiance profile than axial light distribution, which was

governed by Beer's law of absorption. This trend is not true for small spot sizes relative to optical penetration where radial heat conduction becomes significant.

The other end point of the damage threshold was defined as instant redness, that is, redness within 1 minute of observation. Radiant exposures at the instant redness thresholds are compared with radiant exposures at the persistent redness thresholds in Table 5.2. The standard rate process model was used to compute Ω for the instant redness thresholds. The maximum Ω values at the center of the laser beam simulated by the model are presented in Table 5.5. When the exponential dependence of the damage integral on temperature (Eq. 9) is considered, the values of Ω in Table 5.5 are not unreasonable. The point marked with a ☆ represents a large threshold for instant damage that exceeded the threshold for persistent damage. Nevertheless, the analysis for instant damage did not predict a finite damage radius. The standard rate process model described the irreversible damage process associated with the thermal denaturation of cells in the tissue. Furthermore, two parameters, A and E_0, were obtained from experiments that studied the persistent damage to skin. The primary mechanism of instant redness to the skin was the increase of blood flow in the dermis, which was a reversible process without any cell denaturation. In conclusion, the standard rate process was not a good model for estimating the instant redness lesion on the skin, because the damage mechanisms for instant and persistent redness were different.

The ANSI Z136.1-2000 gives MPE limits for far-IR wavelengths between 1.8 and 2.6 μm as a function of laser exposure duration for a spot diameter of 3.5 mm and exposure durations between 10^{-3} and 10 s. Experimental results (Chen, O'Dell et al. 2005) revealed that the ANSI MPE standard was reasonable for the original 3.5 mm spot diameter and exposure durations from 0.25 s to 2.5 s. Our model, however, was used to evaluate the ANSI MPE standard for a broader range of exposure durations. Table 5.6

shows the predicted radii and depths of thermal lesions ($\Omega = 1$) with estimated threshold radiant exposures (ten times the ANSI MPE value H_{max}= 0.56 $t^{0.25}$) and a 3.5 mm laser spot diameter. For exposure durations from 1 s to 10^{-2} s, thermal lesions were less than 1 mm in radius, which was comparable to the values for the experimental sizes of skin thermal lesions at threshold (listed in Table 5.3). Most computed lesion depths at ten times the standard were less than the predicted depths at the measured persistent redness thresholds (listed in Table 5.4). Computed maximum Ωs were less than 1 for 10 s and 10^{-3} s exposure durations, indicating that no thermal damage occurred with the estimated threshold radiant exposures at those exposure conditions.

It should be noted that the value of the "safety factor" was based on considerations of the overall level of uncertainty in the data, the experimental detail, the sources of potential error, the differences between animal and humans, and the state of knowledge of the injury mechanism and the biological sequelae. Although a safety factor of less than ten has been used at times when experimental uncertainty was small, the value of ten for the safety factor has been adequate and is most frequently considered (Sliney, Mellerio et al. 2002). Therefore, the "safety factor" was chosen to be ten in this paper.

Furthermore, we used the model to obtain a rough estimate of the MPE values. Based on the discussion above and the simulated and measured radii of the persistent redness lesions at threshold (see in Table 5.3), we assumed the following: 1) the second-degree burn threshold occurred when the radius of the surface lesion ($\Omega = 1$) was equal to 1.0 mm, and 2) the estimation of MPE value was a factor of 10, which is called the "safety factor" below the radiant exposure at the second-degree burn threshold. The 1.0 mm damage radius was selected as a typical value from the range of experimental values given in Table 5.3. In Figure 5.10, the simulated threshold radiant exposure values were

compared with "10× ANSI MPE limits" as a function of time for a laser spot of 3.5 mm diameter. The comparison showed that the ANSI MPE values were close to or less than the corresponding estimations of MPE produced by the model.

In conclusion, as shown by the data in Table 5.6 and Figure 5.10, the current ANSI MPE standard matches the model predictions for exposure durations from 10^{-1} s to 1 s; however, the differences for exposure duration less than 0.1 s or longer than 10 s need to be examined. For exposure durations less than 0.1 s, the model predicts a nearly constant MPE. Generally, the damage that occurs at a point in the tissue is not only a function of the temperature increase, but it also depends on the rise time and decay characteristics of temperature. The characteristic thermal diffusion time in the skin is about 300 ms for 2000 nm laser irradiation and a large spot diameter. Therefore, for exposure durations less than 0.1 s, heat conduction during the laser irradiation is negligible, and the threshold damage according to the damage integral is a function only of peak temperature at a point and its decay transient at the end of the short exposure (Priebe and Welch 1978). In other words, the threshold radiant exposure, which is directly proportional to the temperature increase, is not a function of exposure duration in this range. Consequently, Figure 5.10 shows that the ANSI MPE limits may be underestimations for laser pulses less than 0.1 s. Furthermore, Figure 5.10 predicts a constant radiant exposure level for times between 0.001 s to 0.1 s, and potentially for even shorter times. Currently, the ANSI MPE value is constant for exposure durations from 10^{-3} to 10^{-9} s. Our modeling results indicate that the range of a constant MPE could be extended to 10^{-1} s. The ANSI plateau level for exposure durations less than 0.001 s is 0.1 J/cm^2, whereas the model predicts a plateau level of about 0.34 J/cm^2 starting at 0.1 s. Although it has been suggested that the ANSI MPE level may be too low for exposure durations less than 0.1 s, caution should be exercised until further pigskin experimental

data are available for this exposure duration range. For exposure time larger than 4 seconds (see figure 5.6), the model may underestimate temperatures due to its overestimation of evaporative cooling rate. Thus the temperature rise from a 10 s laser irradiation may be lower than the actual temperature and overestimate the MPE values.

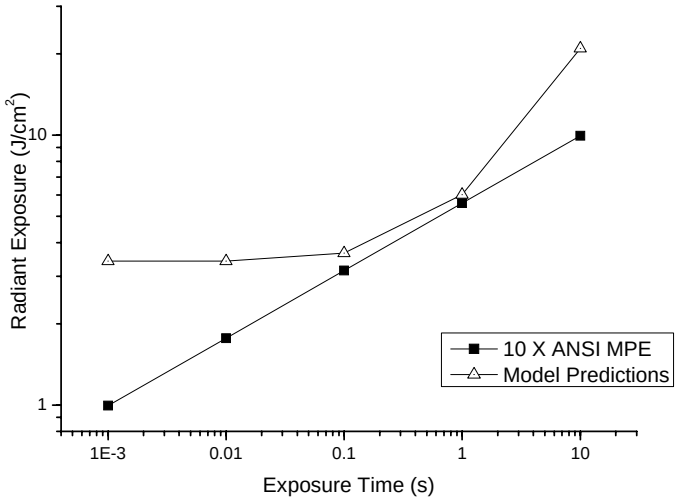

Figure 5.10. The simulated threshold radiant exposure values compared with "10× ANSI MPE limits" as a function of laser exposure time.(Spot diameter = 3.5 mm)

The spot-size-dependent threshold radiant exposure values were simulated by the model, and in Figure 5.11 they are compared with the experimental results. The experimental study of the *in vivo* pigskin damage threshold for beam diameters larger than 3.5 mm and exposure durations of 0.25 second and longer revealed that it may be necessary to revise the ANSI MPE standard to a lower value (Chen, O'Dell et al. 2005). Both experimental values (threshold average radiant exposure) and the model simulation for a lesion radius of 1.0 mm imply that the predicted MPE values are less than the ANSI standard for the large beam diameters. Our data supports the position that the MPE should be decreased as the beam diameter becomes larger than 3.5 mm. In summary, both

experiment and simulation support the need to revise the MPE standard for far-IR laser beams with large diameters (> 3.5 mm). Clearly, the model provides a system for studying the relationships between MPE value and spot size, exposure duration, and wavelength.

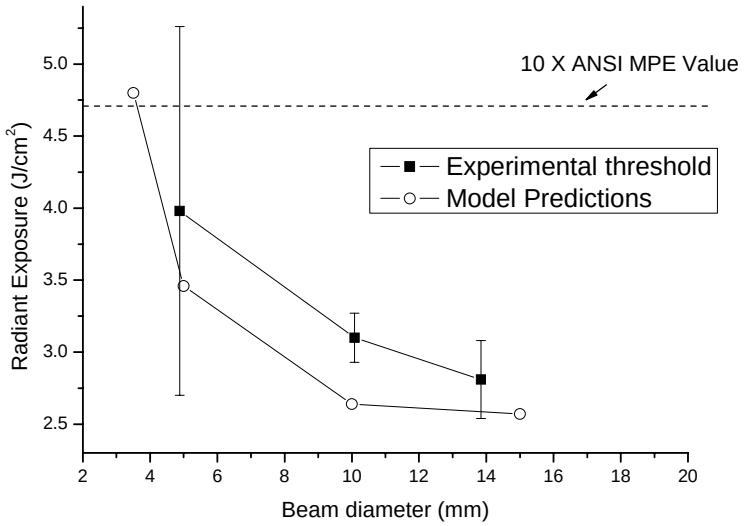

Figure 5.11. The simulated threshold radiant exposure values (damage radius = 1.0 mm) and experimental values (threshold average radiant exposure) compared to "10 × ANSI MPE" as a function of spot size. (Exposure duration = 0.5 s)

In Figure 5.12, the simulated damage threshold radiant exposures for CO_2 (10.6 μm) laser irradiation are compared with the published pigskin damage threshold data (Brownell, Parr et al. 1969). The higher prediction of threshold radiant exposure at 20 s was due to the overestimation of evaporative cooling rate. Excluding that point, good agreement was observed between the optical-thermal-damage model and experimental results. By adjustment of optical parameters as a function of wavelength, predictions are possible as a function of exposure duration and spot size at exposure duration less than 10

seconds and at laser wavelengths where water is the primary absorber and scattering is insignificant.

The predicted damage thresholds to 10.6 μm (CO_2 laser) and 2.0 μm laser irradiation as a function of exposure duration are compared in Figure 5.13. For 10.6 μm wavelength irradiation, Figure 5.13 predicts a constant radiant exposure level for time between 0.0001 s to 0.001 s, assuming linear heat conduction. Because the characteristic thermal diffusion time in the skin for 10.6 μm wavelength irradiation is approximately 100 times less than that for 2.0 μm wavelength (Priebe and Welch 1978), the time range of constant radiant exposure level for 10.6 μm wavelength ends at 0.001 s instead of 0.1 s for 2.0 μm wavelength. At 10.6 μm wavelength, the safety factors of the predicted threshold radiant exposure with respect to ANSI MPE level are less than 10 at exposure time from 10^{-4} s to 3 s. Further damage experiments may be necessary to exam the suitability of the ANSI MPE limits for the 10.6 μm wavelength.

Figure 5.14 shows the experimental threshold irradiance for both 2.0 μm and 10.6 μm wavelengths laser irradiation and their corresponding model predictions of threshold irradiance. Both experimental and simulated data indicate that a simple power law could be used to describe the relation between threshold irradiance and exposure time:

$$E = \mathrm{A}\, t^{-\mathrm{B}}\ , \tag{5.15}$$

where E is the threshold irradiance, t is the exposure time, A and B are two constant coefficients. The irradiance-time power law has been discussed in chapter 3 (Chen, O'Dell et al. 2005).

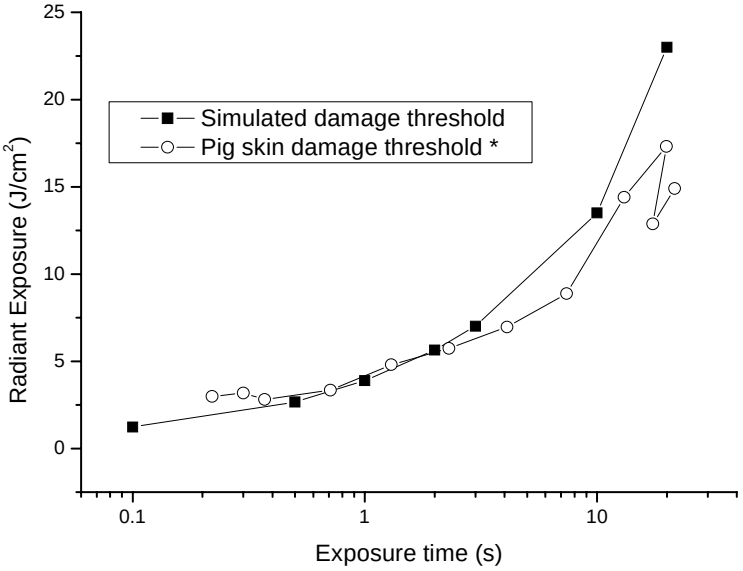

Figure 5.12. The simulated damage threshold radiant exposures to CO_2 laser irradiation compared to published pig skin damage thresholds data as a function of exposure duration. *: refer to (Brownell, Parr et al. 1969).

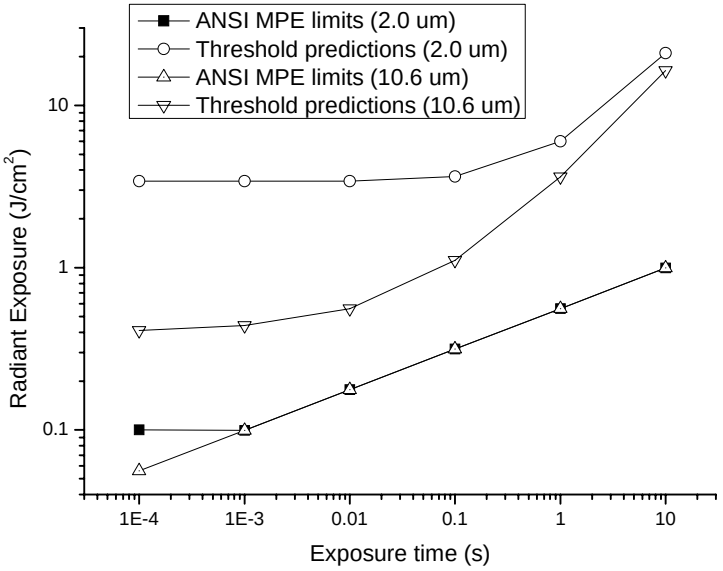

Figure 5.13. The predicted damage threshold radiant exposures to 10.6 μm (CO_2 laser) and 2.0 μm laser irradiation and their corresponding ANSI MPE limits as a function of exposure duration. (Prediction of Gaussian shape irradiance, spot diameter = 3.5 mm)

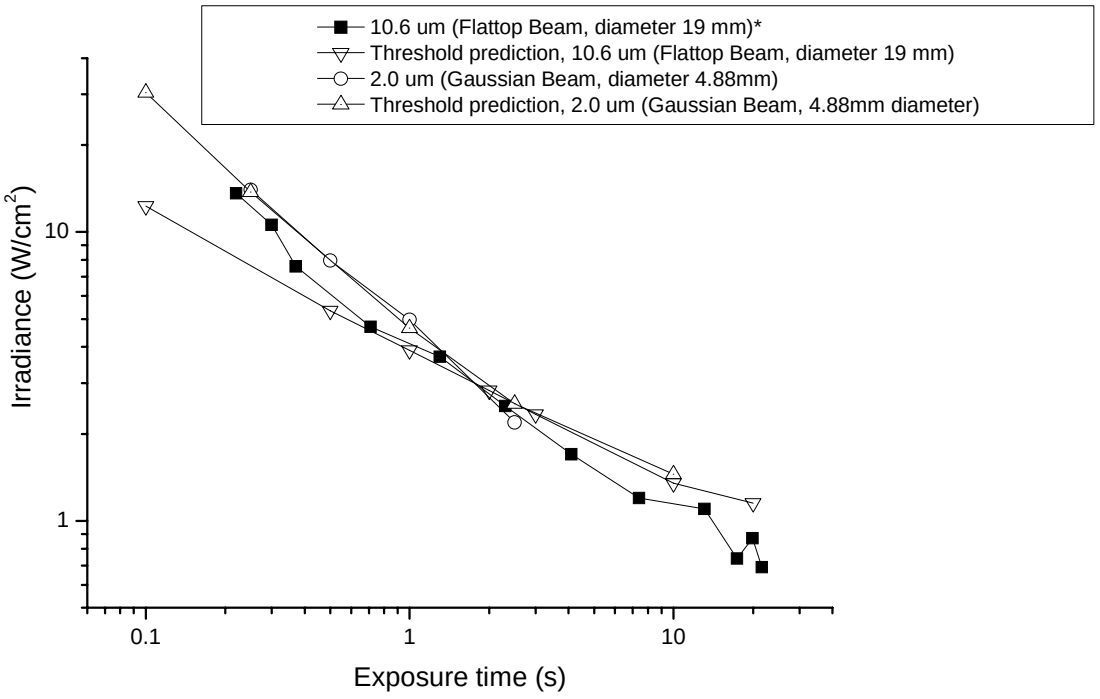

Figure 5.14. The experimental threshold irradiance levels for both 2.0 μm and 10.6 μm wavelengths laser irradiation and their corresponding model predictions. *: refer to (Brownell, Parr et al. 1969).

We were aware of the limitations of our model in that several physical processes were excluded from the model analysis. For instance, the model used for the 2000 nm wavelength did not incorporate photon scattering in skin, nor did it address changes in the optical and thermal properties of the tissue due to the temperature increase. Furthermore, the temperature gradients in skin induced water transport in the tissue from deeper layers to the surface, which may in turn have had a significant effect on the heat and mass transfer and light absorption coefficients; in other words, the heat deposition rate and surface evaporation kinetics may need more consideration in respect to the temperature

change. Another important source of uncertainty will always be human judgment in estimating lesion radii for large spot sizes (see Table 5.3).

Perhaps new technology will provide a method for replacing our qualitative visualization of damage with a more quantitative way. For example, polarization-sensitive optical coherence tomography measurements may provide an *in vivo* method for measuring birefringence loss owing to thermal denaturation in tissue. Moreover, if it is possible to quantitatively and separately record thermal damage of each constituent in tissue, a multiple damage process model which includes several standard Arrhenius integrals could be developed. Each integral would predict damage of one specific constituent in tissue.

5.7. CONCLUSION

An optical-thermal-damage model precisely predicted the temperature and thermal damage in pigskin for 2000 nm laser irradiation. The information provided by the model allowed us to 1) predict temperatures and the occurrence and size of thermal lesions in the skin, 2) evaluate the applicability of the standard rate process model for different thermal lesion end-point definitions, 3) provide trends and identify experimental data that do not follow experimental trends, and 4) predict and test the ANSI MPE laser safety standard for a 2000 nm wavelength, exposure durations between 10^{-3} to 10 s, and various spot sizes.

The model has verified the suitability of the ANSI MPE standard for a wavelength of 2000 nm with a 3.5 mm spot size and exposure durations from 0.1 s to 1 s. Compared to the published ANSI MPE standard, however, the model predictions give higher MPE values for exposure durations less than 0.1 s. The model suggests that the

ANSI MPE exposure duration range for short pulses should be extended to a larger range of 10^{-1} to 10^{-9} s at a constant or plateau level of radiant exposure.

According to the model predictions, when the laser beam diameter is larger than 3.5 mm, it may be necessary to lower the values of the ANSI MPE standard if a safety factor of ten is used to derived MPE values. This conclusion is consistent with the *in vivo* pigskin experimental results.

In conclusion, the optical-thermal-damage model, supported by experimental validation, provides a system for predicting the thermal response of skin to laser irradiation and the damage caused by such irradiation. By adjustment of the optical parameters as a function of wavelength, predictions are possible as functions of exposure duration and spot size at the laser wavelength where water is the primary absorber and scattering is insignificant.

5.8. ACKNOWLEDGMENT

Opinions, interpretations, conclusions, and recommendations are those of the authors and are not necessarily endorsed by the University of Texas at Austin, the United States Air Force, or the U.S. Department of Defense.

The authors wish to thank Dr. Karl Schulmeister, Junghwan Oh, and Daniel C. O'Dell for their kind help.

Contract grant sponsor: Northrop Grumman Information Technology; Contract grant sponsor: The Albert and Clemmie Caster Foundation.

5.9. REFERENCES

ANSI (2007). ANSI Z136.1-2007, American National Standard for Safe Use of Lasers. Orlando, FL, Laser Institute of America, American National Standards Institute.

Brownell, A. S., W. H. Parr, et al. (1969). "Skin and carbon dioxide laser radiation." Arch Environ Health **18**(3): 437-42.

Cain, C. P. and A. J. Welch (1974). "Measured and predicted laser-induced temperature rises in the rabbit fundus." Invest Ophthalmol **13**(1): 60-70.

Chen, B., D. C. O'Dell, et al. (2005). "Porcine skin ED50 damage thresholds for 2,000 nm laser irradiation." Lasers Surg Med **37**(5): 373-81.

Diaz, S. H., G. Aguilar, et al. (2001). "Modeling the thermal response of porcine cartilage to laser irradiation." Ieee Journal of Selected Topics in Quantum Electronics **7**(6): 944-951.

Eggleston, T. A., W. P. Roach, et al. (2000). "Comparison of two porcine (Sus scrofa domestica) skin models for in vivo near-infrared laser exposure." Comp Med **50**(4): 391-7.

Finney, D. J. (1971). Probit Analysis 3rd ed. New York, Cambridge University Press.

Hale, G. M. and M. R. Querry (1973). "Optical constants of water in the 200nm to 200μm wavelength region." Appl. Opt. **12**: 555--563.

Henriques, F. F. (1947). "Studies of thermal injury V: The predictability and the significance of thermally induced rate processes leading to irreversible epidermal injury." Arch. of Pathol. **43**: 489-502.

Incropera, F. P. and D. P. Dewitt (2001). Fundamentals of Heat and Mass Transfer, Fifth Edition. New York, John Wiley and Sons.

Jacques, S. L. (1993). "Role of tissue optics and pulse duration on tissue effects during high-power laser irradiation." Applied Optics **32**(13): 2447-2454.

Mainster, M. A., T. J. White, et al. (1970). "Spectral dependence of retinal damage produced by intense light sources." J Opt Soc Am **60**(6): 848-55.

Mainster, M. A., T. J. White, et al. (1970). "Transient thermal behavior in biological systems." Bull.Math. Biophys.(32): 303-314.

Moritz, A. R. and F. C. Henriques, Jr. (1947). "Studies of thermal injury: II. The relative importance of time and surface temperature in the causation of cutaneous burns." Am J Pathol **23**: 695-720.

Niemz, M. H. (1996). Laser-Tissue Interactions. Berlin, Germany, Springer-Verlag Berlin Heidelberg.

Pearce, J. A., S. Thomsen, et al. (1993). Kinetics for birefringence changes in thermally coagulated rat skin collagen, Proc. SPIE 1876:180-185.

Priebe, L. A. and A. J. Welch (1978). "Asymptotic Rate Process Calculations of Thermal Injury to Retina Following Laser Irradiation." Journal of Biomechanical Engineering-Transactions of the Asme **100**(1): 49-54.

Sliney, D. H., J. Mellerio, et al. (2002). "What is the meaning of threshold in laser injury experiments? Implications for human exposure limits." Health Physics **82**(3): 335-347.

Svaasand, L. O., T. Boerslid, et al. (1985). "Thermal and Optical-Properties of Living Tissue - Application to Laser-Induced Hyperthermia." Lasers in Surgery and Medicine **5**(6): 589-602.

Takata, A. N. (1977). Laser-induced thermal damage of skin. USAF School of Aerospace Medicine. Brooks Air Force Base, TX.

Takata, A. N., L. Goldfinch, et al. (1974). Thermal Model of Laser-Induced Eye Damage. USAF School of Aerospace Medicine Report IITRI J-TR-74-6324.

Torres, J. H. and M. Motamedi (1993). "Experimental evaluation of mathematical-models for predicting the thermal response of tissue to laser irradiation " Appl. Opt **32**(4): 597-606.

Vassiliadis, A., H. C. Christian, et al. (1971). Ocular laser threshold investigations. Brooks Air Force Base,TX., USAF School of Aerospace Medicine, Standford Research Institute.

Welch, A. J. (1975). Model of thermal injury based on temperature rise in fundus exposed to laser radiation. Brooks Air Force Base, TX., USAF School of Aerospace Medicine.

Zuclich, J. A., D. J. Lund, et al. (2007). "Wavelength dependence of ocular damage thresholds in the near-ir to far-ir transition region: Proposed revisions to MPEs." Health Physics **92**(1): 15-23.

Chapter 6. Histological and Modeling Study of Skin Thermal Injury to 2.0 μm Laser Irradiation

6.1. ABSTRACT

Background and Objective: Qualitative and quantitative gross histopathologic studies of skin damage were performed at 48 hours after irradiation with a 2.0 micron thulium CW laser to determine the mechanisms of laser effects in the skin under various exposure conditions.

Study Design/Materials and Methods: Pig skin lesions were created at, below and beyond the threshold irradiation conditions for grossly apparent thermal lesions. Histological sections of these lesions were studied. For each threshold lesion, four quantitative histopathlogical parameters were measured: the widths of 1) epidermal necrosis at the surface and 2) the outer boundary of the thrombosis zone, 3) the depth of vascular thrombosis, and 4) the depth of perivascular inflammation (increased infiltrates of inflammatory cells) and edema. The quantitative histopathologic data were compared with predictions using an optical-thermal-damage model.

Results: Histologically, the thermal damage mechanisms for grossly apparent threshold lesions of persistent redness at 48 hours included necrosis of the epidermal cells, intravascular thrombosis and perivascular inflammation and edema in dermal blood vessels. At irradiation levels just below 'gross threshold', non-lethal thermal effects, such as perivascular inflammation and edema were found in the histological sections. When the radiation reached about 1.5-2.5 times beyond the threshold, decrease of dermal collagen birefringence was observed.

Conclusions: A sequence of damage endpoints was defined in the skin as power increased. By choosing rate process coefficients to match specific mechanisms of lethal thermal damage, the optical-thermal-damage model is capable of predicting various types

of thermal injury in the skin, such as epidermal necrosis, vascular thrombosis, and dermal collagen coagulation.

Key words: Birefringence; collagen coagulation; damage model; epidermal necrosis; laser injury; laser safety; skin damage; vascular thrombosis; Yucatan mini-pig

6.2. INTRODUCTION

High-power laser systems with wavelengths above 1.4 μm are finding widespread use in the military, medicine, and industry (Sorokina and Vodopyanov 2007). One area where 2 μm laser system will play an important role is in infrared-guided missile countermeasure applications. The amplitude-modulated lasers with multiple lines throughout the 2–5-μm spectral region are desirable due to their spectral overlap with the thermal signature of aircraft. The native 2-μm output of thulium fiber lasers gives direct access to an atmospheric transmission window (Jackson, Sabella et al. 2007). Other emerging applications for 2 μm fiber lasers are in medicine and surgery (Jackson and Lauto 2002). For instance, thulium fiber lasers ($\lambda \approx 2.0$ μm) are being investigated as a replacement for holmium solid state lasers for the ablation of urinary tissues (Fried 2005; Fried 2005; Fried and Murray 2005). With many advantages such as smaller size, higher efficiency, better beam quality, and the ability to operate in either pulsed or continuous-wave mode, 2 μm fiber lasers are set to replace a number of medical lasers and open up a range of new medical applications requiring very high power and absorption characteristics. Another advantage of these wavelengths is that they are considered to be in the "eye-safe" region of the optical spectrum where radiation is primarily absorbed in the cornea and aqueous humor with insignificant energy reaching the retina (Maher 1978; ANSI 2007). The current laser safety standard for IR wavelengths between 1.8 and 2.6 μm is defined by the ANSI Z136.1-2007 guideline, *American National Standard for Safe*

Use of Lasers (ANSI 2007); this standard is based on sparse experimental data and mainly on the extrapolation of CO_2 threshold data. McCally *et al.* has reported corneal epithelial damage thresholds for a CW Tm:YAG laser radiation (2.02 μm) on New Zealand white rabbits (McCally, Farrell et al. 1992) for a laser spot diameter of approximately 1 mm and exposure durations of 0.082 sec, 0.235 sec and 4.28 seconds. The associated threshold radiant exposures were 5.26 J/cm^2, 8.46 J/cm^2 and 49.2 J/cm^2, respectively. The criteria they used for minimal epithelial damage was the presence of a superficial gray-white spot on the cornea that developed within half an hour after exposure. In 2007 Zuclich *et al*. investigated the wavelength dependence of ocular thresholds in the near-IR and far-IR transition regions and noted that the exposure limits in some cases were above the measured damage thresholds in the band between 1.3 and 4.0 μm (Zuclich, Lund et al. 2007).

With the recent development of high power CW laser systems with wavelengths around 2.0 μm, there is a need to clarify 1.8 – 2.6 μm laser effects on skin for spot sizes above 3.5 mm and achieve quantitative laser injury threshold data to validate or support refinement of the current safety standards. Recent experiments by our group have defined minimum visible threshold lesions as transient and persistent redness at 1 minute and 48 hours post exposure respectively for 2.0 μm laser irradiation of *in vivo* Yucatan mini-pigs skin (Chen, O'Dell et al. 2005). Based on the experimental data, an optical-thermal-damage model of skin damage under laser irradiation has been formulated by using a finite-element analysis program (FEMLAB 3.1, Comsol Inc.). The general model simulates light propagation, heat generation, transient temperature response, and thermal damage produced by a radially symmetric laser beam at a normal angle of incidence. Predictions of transient surface temperatures have been validated by thermal camera measurements of the *in vivo* pigskin surface during and after 2.0 μm laser irradiation

(Chen, Thomsen et al. 2006). Both the experimental and the modeling studies suggest that the ANSI maximum permissible exposure (MPE) limits should be decreased when the laser spot diameter is larger than 3.5 mm. Thus our studies indicate that damage thresholds are a function of spot size. However, the current safety standards are specified for a beam diameter limit of 3.5 mm in the 1.8 to 2.6 μm wavelength range. Current safety standards are limited to spot sizes no larger than 3.5 mm; However, the far field military applications could result in irradiation of large areas. Previous 2.0 μm threshold data was limited to spot sizes below 3.5 mm and sub-second exposure durations.

Although many studies have been conducted over a 30 years period to measure and model thermal damage in skin, there are few example that compare multiple histological end points with corresponding measurements of laser induced transient temperatures. To our knowledge, this is the first paper to integrate a) visual surface damage, b) histological end points, c) surface temperature transients, and d) rate process damage modeling in a single study. The correlation between histology, visual surface damage and modeling of threshold conditions of surface and subsurface end points ties together the many threads of the thermal damage story. Histological damage is measured and modeled using sub-threshold, threshold and super-threshold 2.0 μm laser powers. The data provides experimental evidence of the correlation of sub-threshold histological change to visible threshold lesions for the irradiation condition of this study.

We now report the next step in the process of understanding the mechanisms for thermal skin damage at 48 hours by associating the grossly visible threshold lesions to specific histopathologic lesions, determining their mechanisms of formation and identifying their temperature-time response thresholds.

The biological and physical changes in laser-irradiated skin depend on the temperature-time response. The formation of a thermally induced lesion in skin begins

with the local absorption of laser radiation, which is converted into heat. At 2.0 μm wavelength, water is the primary absorber of the laser radiation and the laser radiation is mainly deposited within a 300 μm depth in the dermis (Jacques 1993; Chen, O'Dell et al. 2005). During irradiation, both the epidermis and dermis are heated according to

$$S(r,z) = E(r,z)\mu_a(z) \quad [\mathrm{W/cm^3}], \tag{6.1a}$$

where $E(r,z)$ [W/cm^2] is the fluence rate of the laser beam, $\mu_a(z)$ [1/cm] is the local absorption coefficient, and S(r,z) [W/cm^3] is the resulting heat source term and

$$E(r,z) = E_0(1-R)e^{-\mu_a z} \quad [\mathrm{W/cm^2}], \tag{6.1b}$$

where E_0 is the surface irradiance and R is the specular reflection.

As temperature increases, denaturation of vital mitochondrial enzyme proteins and rupture of the cellular membranes can lead to death and necrosis of tissues and cells. Thermal coagulation of structural cellular and extracellular proteins including cell shrinkage, collagen hyalinization, collagen and muscle birefringence changes and tissue whitening, occurs at higher temperatures. As temperatures reach 100^{o}C or more, water-vaporization causes tissue desiccation, the formation and expansion of steam vacuoles and explosive fragmentation. Tissue carbonization and ablation occur when temperatures are higher than the pressure dependent boiling point of tissue water (Welch and vanGemert 1995; Niemz 1996).

Mathematically, the occurrence of relatively low temperature thermal-induced coagulation injury is typically modeled as a rate process and a dimensionless damage parameter Ω:

$$\Omega(r,z,\tau) = \int_0^{\tau} Ae^{-\left[\frac{\Delta E}{RT(r,z,t)}\right]} dt, \tag{6.2}$$

where τ [s] is the total time of evaluated temperature, A [1/s] is the pre-exponential frequency factor, ΔE [J/mole] is an energy barrier molecules surmount in changing from native state to denatured, R [J/K mole] is the gas constant and $T(t)$ [K] is the temporal temperature (Henriques 1947; Moritz and Henriques 1947). The damage parameter Ω indicates the level of thermal injury. The rate process coefficients A and ΔE are usually estimated experimentally and are defined for specific, measurable thermal injury end points.

Thus far, several studies have been conducted to derive rate process coefficients using different heating sources. The usual experimental method is to expose tissue to constant temperature using either a water bath, a heated metallic plate or laser irradiation for selected time intervals (Welch and vanGemert 1995). Several biological tissues, such as retina, muscle, aorta, skin, and various cultured cells have been investigated with identification of various defined thermal damage end points and their rate process coefficients (Henriques 1947; Moritz and Henriques 1947; Fugitt 1955; Weaver and Stoll 1967; Takata 1974; Wu 1982; Gaylor 1989; Diller, Hayes et al. 1991; Welch and vanGemert 1995).

In 1947, Henriques and Moritz exposed the skin of pigs, *in vivo*, to flowing water at a controlled temperature for exposure times varying over several orders of magnitude and derived a set of coefficients to match the experimental data corresponding to a "second degree" or trans-epidermal necrosis (Henriques 1947; Moritz and Henriques 1947). Henriques obtained a good match of model to his experimental results for long burn times, but there was a significantly greater discrepancy for shorter burns. Subsequent researchers applied greater sophistication to obtain different coefficients. Considering the experimental results from Henriques, Fugitt in 1955 (Fugitt 1955) and Wu in 1982 (Wu 1982) attempted to improve the method by introducing a two-stage

temperature activation model. In 1974, Takata (Takata 1974) and in 1967 Weaver and Stoll (Weaver and Stoll 1967) suggested different values of A and ΔE that best fit their own data and injury criteria. These models were analyzed and compared by Diller and associates in 1991 for different types of thermal insults on skin (Diller, Hayes et al. 1991). In 1989, Gaylor and Rocchio measured the stability of mammalian skeletal muscle cell membranes in isolated cell culture to supraphysiologic temperature by determining the kinetics of onset of altered membrane permeability to intracellular carboxyfluorescein dye and proposed a set of coefficients for cell membrane rupture. They defined $\Omega=1$ to represent the point when 5 percent of the dye had leaked across the membrane in the average experiment (Gaylor 1989; Tropea and Lee 1992; Diller 1994; Gowrishankar, Stewart et al. 2004). They found that the supraphysiologic temperatures damaged membranes at a rate which was temperature-dependent and that cell membrane lysis was probably the initial destructive event of tissue damage. This set of rate process coefficients was used in several mathematic models to predict skin injury (Tropea and Lee 1992; Gowrishankar, Stewart et al. 2004). In 1993, Pearce et al. wrapped freshly excised rat skin pieces in water-tight aluminum foil packets that were immersed in a controlled temperature water bath for times between 120 and 6000 s over the temperature range of 45 to 90 °C. Based on the histopathologic results, they proposed a set of coefficients for birefringence loss in skin collagen (Pearce, Thomsen et al. 1993). All the rate process coefficients described above are listed in Table 6.1.

Table 6.1. Published rate process coefficients of thermal tissue damage.

Model	Temperature Range (^{o}C)	ΔE [J/mole]	A [1/s]	Damage Endpoint
(Gaylor 1989)	All T	2.4×10^{5}	2.9×10^{37}	Membrane permeability change, (mammalian skeletal muscle cell)
(Henriques 1947)	All T	6.27×10^{5}	3.1×10^{98}	Trans-epidermal necrosis, (pig skin)
(Weaver and Stoll 1967)	T≤50	7.82×10^{5}	2.185×10^{124}	Threshold Blister formation, (Human skin)
	T>50	3.27×10^{5}	1.823×10^{51}	
(Takata 1974)	T≤50	4.18×10^{5}	4.322×10^{64}	In-depth skin burn, (pig skin)
	T>50	6.69×10^{5}	9.389×10^{104}	
(Wu 1982)	T≤53	6.27×10^{5}	3.1×10^{98}	Trans-epidermal necrosis, (Human skin)
	T>53	$(6.27 - 0.0051 \times (T-53)) \times 10^{5}$	3.1×10^{98}	
(Fugitt 1955)	T≤55	6.27×10^{5}	3.1×10^{98}	Trans-epidermal necrosis, (Human skin)
	T>55	2.96×10^{5}	5.0×10^{45}	
(Pearce, Thomsen et al. 1993; Pearce and Thomsen 2003)	All T	3.06×10^{5}	1.606×10^{45}	Birefringence loss in skin collagen, (rat skin)

6.3. MATERIAL AND METHODS

6.3.1. Laser Irradiation

Yucatan mini-pig skin is an established animal model for studying laser damage with infrared radiation. Six female Yucatan mini-pigs, weighing between 24.3 to 34.8 kg, were used in this study. A series of experiments were conducted *in vivo* on Yucatan pig skins to induce thermal damage lesions using 2.0 μm laser irradiation. A rack mountable thulium fiber optic CW laser (IPG Photonics Corporation; Oxford, MA; Model: TLR-20-

2000-LP) with a maximum 20 W output at a wavelength 2.0 μm provided the source of irradiation. This limited study employed Gaussian shaped spot sizes ($1/e^2$ diameters) of approximately 5, 10 and 15 mm and exposure durations of 0.25, 0.5, 1.0 and 2.5 seconds as a function of laser power. The exact values of the nominal 5, 10 and 15 mm spot diameters were measured using the knife-edge method as 4.83, 9.65 and 14.65 mm respectively. The diameter measurements had about 5% uncertainties (Chen, O'Dell et al. 2005; Chen, Thomsen et al. 2006). The gross effect of each irradiation was evaluated instantly and at 48 hours post exposure. The number of irradiations for each of the 12 spot size-exposure conditions was 19 - 37 with an average of 27 per condition. An IR camera (Phoenix^{TM} DAS camera system, Indigo, CA. detective wavelengths 3-5μm) was used to record IR images on skin surface during laser irradiation. The IR images were converted to temperature according to the calibration of a blackbody heat source. Before laser radiation, the mini-pig was marked with a metallic-silver permanent marker to make grids for identification and location of the numerous irradiation sites. The dimensions of the grids depended upon the laser spot size. A cross pattern was drawn around each irradiated location to locate the center of irradiation after each laser exposure. The details of animal preparation and experimental setup for laser irradiation were described in our recent publication (Chen, O'Dell et al. 2005).

6.3.2. Preparation for Microscopy

Forty-eight hours after irradiation, the mini-pigs were euthanized. Tissue specimens for each irradiation site were taken and fixed in 10% neutral buffered formalin, embedded with paraffin, serially sectioned, and the sections stained with hematoxylin and eosin (H&E). The cross pattern drawn after laser exposure guaranteed that the irradiation center was included in each tissue specimen even without any

apparent lesion on the surface after 48 hours. Serial consecutive histologic sections were cut through selected sample blocks and examined to locate the center of the thermal lesion at the microscopic level to determine the maximum histological diameter of the lesion in the skin. Typically, around one hundred 6-μm thickness sections were obtained from each block. A total of 49 blocks were processed including: twenty-four blocks of skin samples of threshold lesions defined as persistent redness on skin surface 48 hours post exposure (n = 2 blocks/radiation combination for a total of 12 different combinations), twelve samples of skin samples irradiated at powers below thresholds and 13 specimens produced at powers above threshold. All the skin specimens for the histological study were taken 48 hrs post exposure.

6.3.3. Skin Optical-thermal-damage Model

An optical-thermal-damage model of the skin under laser irradiation was formulated using finite-element modeling software (Femlab 3.1, Comsol Inc). The general model simulated light propagation, heat generation, transient temperature response, and thermal damage produced by a radially symmetric laser beam of normal incidence. Skin was represented by two homogenous regions (epidermis and dermis) with a nonlinear air-tissue boundary condition including free convection and water evaporation (Torres and Motamedi 1993). The optical-thermal-damage model and its validation with surface temperature measurements were described in detail in our recent publication (Chen, Thomsen et al. 2006). For the present study, this model was expanded to include blood perfusion defined as the nonvectorial volumetric blood flow per tissue volume in the dermis that contained sufficient capillaries that an average flow description was considered reasonable. Therefore, the contributions of heat conduction and perfusion were combined in the Pennes bioheat equation (Pennes 1948):

$$\rho c \frac{\partial T}{\partial t} = \nabla \cdot (k \nabla T) - \rho_b c_b w_m (T - T_a) + S(r, z, t), \quad (6.3)$$

where $T(r,z,t)$ [K] was the local tissue temperature; $T_a(r,z,t)$, [K] was the reference temperature (arterial blood); $S(r, z, t)$ [W/cm^3] was the localized heat source; ρ [kg/m^3], c [J/kg K], $k(z)$ [W/m K] were the skin density, specific heat, and thermal conductivity, respectively; c_b [J/kg K], was the specific heat of blood; ρ_b [kg/m^3] was the density of blood, and w_m [1/s] was the blood perfusion rate set as a constant of 5×10^{-3} [1/s] in the model. This value was in good agreement with the typical physiologic values for normal skin, that range between 4×10^{-3} and 6×10^{-3} [1/s] (Li, Zhang et al. 2002). Since there is no blood perfusion in the epidermis, heat lost due to blood flow was not considered in the epidermis.

Although blood flow may increase due to physiologic thermoregulation responses during the skin heating, the flow change occurs with a time lag of minutes and therefore does not affect the prediction in this case where direct thermal injury occurs within 10 seconds (Rendell, Kelly et al. 1993).

6.4. RESULTS

6.4.1. Gross and Microscopic Features of Skin Irradiated Below Threshold

By gross observation, the effect of each irradiation was evaluated acutely and 48 hours post exposure. The transient redness was defined as the presence of redness observed on the skin surface within 1 minute after laser irradiation. However, many of the transient redness lesions faded and were not visible 48 hours later. The threshold radiant exposures for transient redness and persistent redness at all tested laser combinations were compared in Figure 6.1.

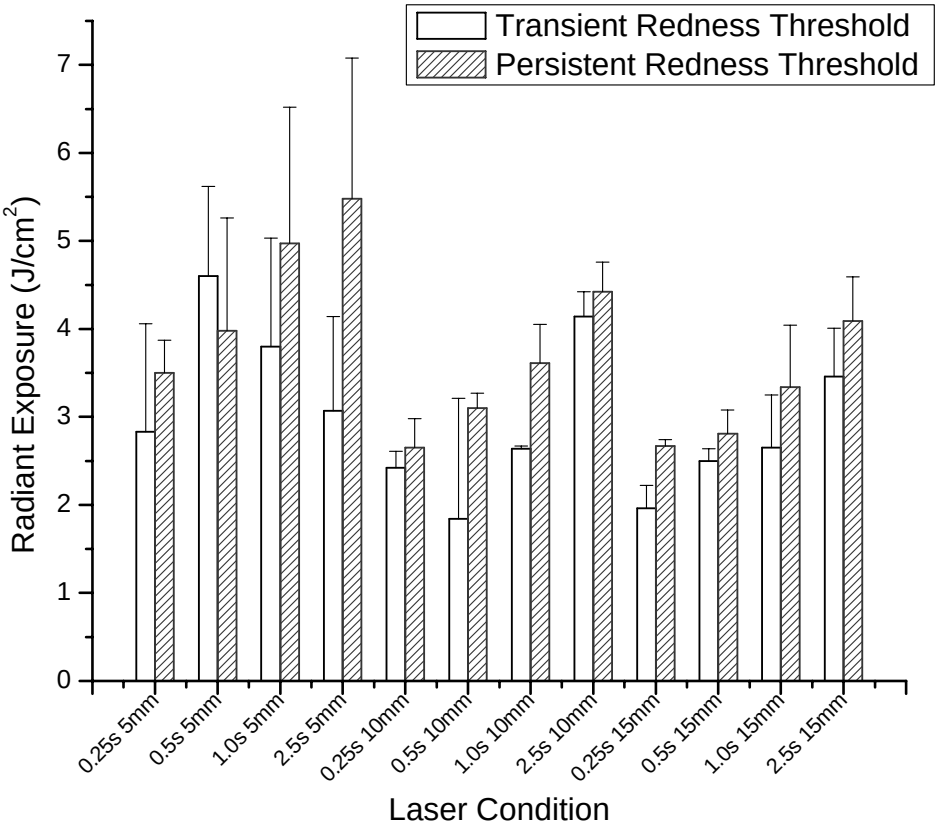

Figure 6.1. Comparison of threshold radiant exposure for transient redness at 1 min and persistent redness 48 hours post exposure.

Average of 27 irradiations with various powers were conducted on the pig skin for each spot size-exposure duration combination, including approximately 13 irradiations that did not produce any persistent redness on the skin 48 hours after exposure. Twelve representative skin samples, in which transient redness disappeared 48 hours after irradiation, were subjected to histopathlogical analyses. Eight skin samples were irradiated at 2.5-s exposure duration and 5-mm spot size with various powers from

0.18 to 0.39 W. Four samples were irradiated at 1.0-s and 5-mm with powers at 0.56 or 0.93 W. The respective thresholds for persistent redness at the above two laser conditions were 0.41 W and 0.93 W. The thresholds were estimated using probit analysis, and represented the dose for 50% probability of laser-induced damage.

Some skin samples irradiated at threshold powers did not show any gross redness 48 hours post exposure. In all of these selected skin samples, mild perivascular inflammation and edema were observed in the superficial dermis extending beyond the laser irradiation site (Figure 6.2a(H)). In these 12 selected samples, skin irradiated with relatively higher powers (two skin samples at 0.39 W- 2.5 s - 5 mm, and two at 0.93 W- 1.0 s - 5 mm) had more perivascular inflammatory cells infiltrated into the papillary dermis within the irradiation sites than those at lower powers. Focal hyperkeratosis in the epidermis was found at the irradiation site in one of the twelve skin samples. However, The focal hyperkeratosis was not associated with any markers of thermal damage suggesting that the hyperkeratosis was just as likely caused by mechanical trauma (scratching). No other injury specifically attributed to thermal injury was seen in these light microscopic sections.

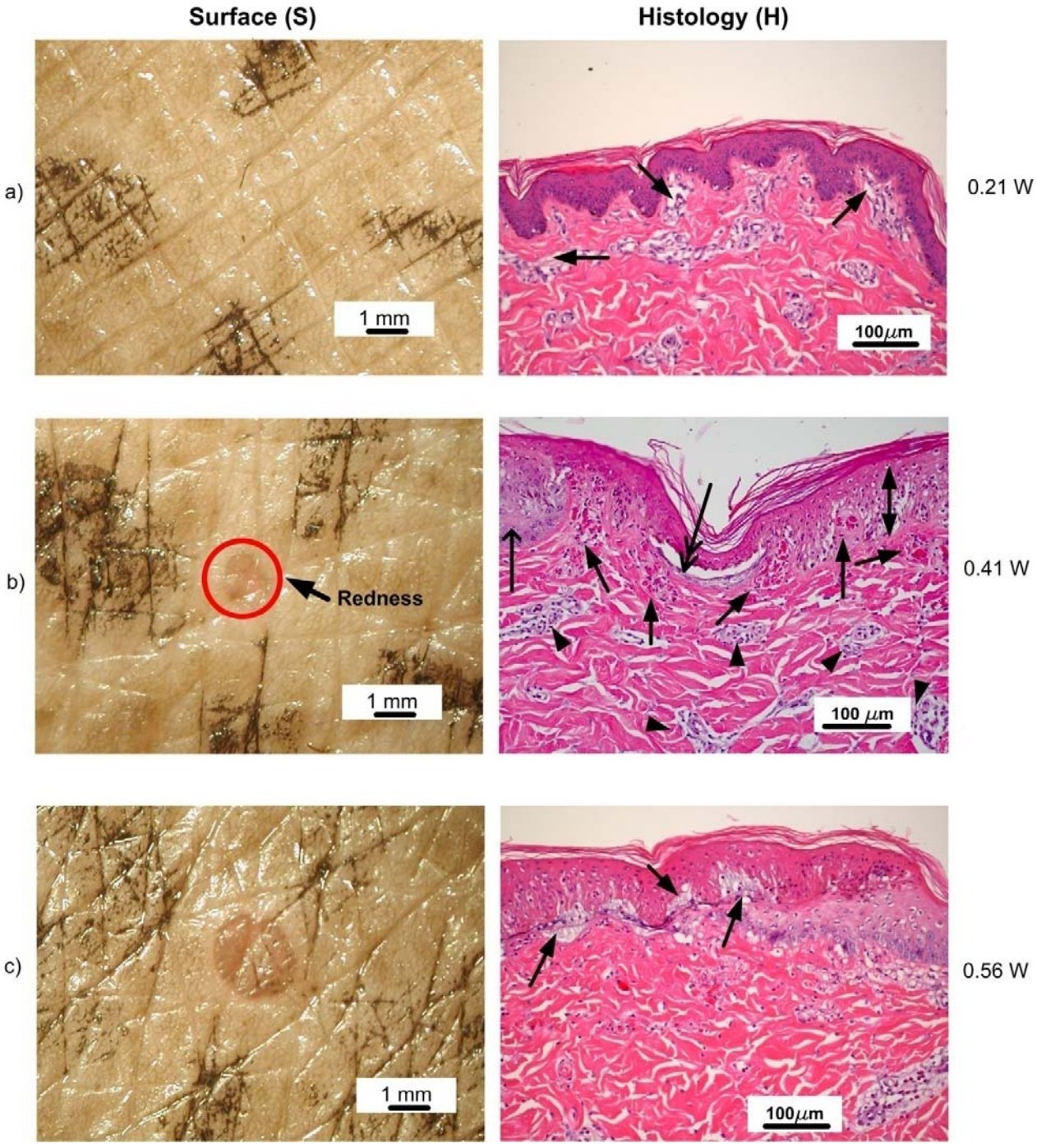
Surface (S)
Histology (H)
a)
1 mm
100 μm
0.21 W
b)
Redness
1 mm
100 μm
0.41 W
c)
1 mm
100 μm
0.56 W

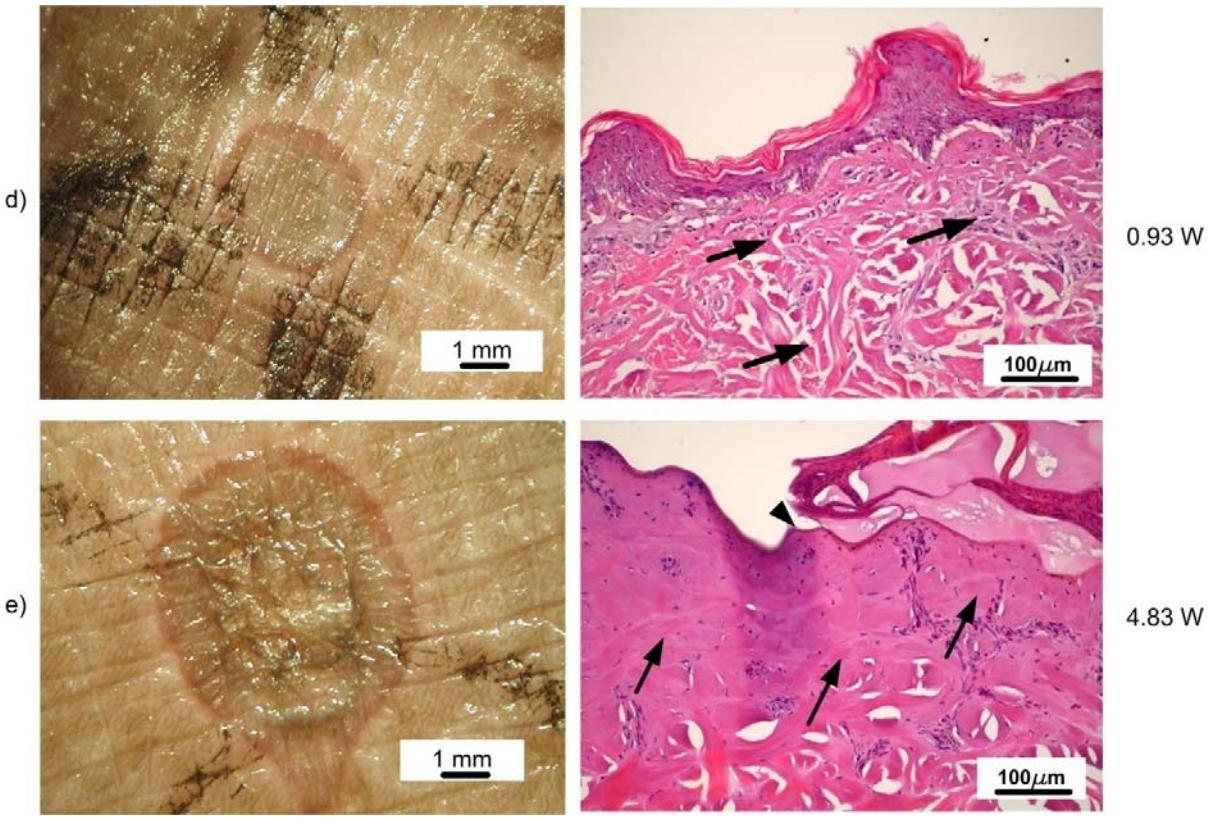

Figure 6.2. Images of thermal injuries created at, below and beyond persistent redness threshold and their corresponding microscopic sections. Laser condition: 5 mm spot size and 2.5 s exposure duration. By row: laser power: a) 0.21 W; b) 0.41 W, c) 0.56 W; d) 0.93 W; e) 4.83 W. Note: threshold power for transient redness = 0.23 W, and for persistent redness = 0.41 W. By column: (S): Gross lesions appeared on the skin 48 hours post exposure; (H): The corresponding microscopic sections (H&E stain. Original Mag. 200X). a) Mild edema (arrows); in b):Transmural necrosis of epidermis (double headed arrow), vascular dilation and thrombosis in dermal blood vessels (arrows), perivascular inflammation and edema (arrow heads), regenerated epidermal cells growing under necrotic epidermis (thin arrow), and epidermolysis generated at epidermal/dermal junction (double headed thin arrow); c) epidermolysis and epidermal necrosis (arrows), endothelial and cellular necrosis of superficial dermis and hyalinization of dermal collagen; d) swollen, hyalinized dermal collagen (arrows), epidermal necrosis, thermal coagulation (heat fixation) of endothelium and dermal cells, e) slough of epidermis with exposure of dermis (arrow head), and severe, homogenous hyalinization of dermal collagen with heat fixation of all cells in dermis. (arrows).

6.4.2. Gross and Microscopic Features of Thermal Lesions at Threshold

The first visible persistent erythema (skin reddening) seen at 48 hours was identified as the gross threshold lesion (Figure 6.2b(S)) (Chen, O'Dell et al. 2005). The peak temperatures at the spot center for threshold irradiations, ranged from 58^{o}C at 15 mm-2.5 s to 74 ^{o}C at 5 mm-0.25 s, were inversely proportional with spot size and exposure duration. The threshold lesions were formed of flat red papules (persistent erythema) covered by shrunken epidermis at the center surface of irradiation sites. The threshold lesions at each laser condition were similar in appearance.

Two representative threshold lesions for each tested laser condition were selected for detailed histological analysis. In general, all of the histological sections of persistent redness lesions showed coagulative necrosis of the epidermis. The threshold lesion surfaces showed central trans-epidermal necrosis with scattered areas of epidermolysis (early blistering) and epidermal regeneration at the lesion edges. Epidermolysis (detachment of the epidermal cells from each other) was seen at the epidermal-dermal junction or within the epidermis (Figure 6.2b(H)). The necrotic epidermal cells and their nuclei were hyperchromatic, shrunken and dense. In many of the histological sections, focal microscopic perivascular hemorrhages, vascular dilation and thrombosis appeared in papillary dermis, while perivascular inflammation and edema occurred in deeper dermal blood vessels. These concentric distinct zones of vascular thermal damage extended into the dermis away from the central heated volume at the irradiation site forming a lesion roughly the shape of a flattened cone. The vascular damage responsible for the persistent redness included the following: 1) hemostasis (blood flow stasis), 2) thrombosis (intravascular blood clotting), 3) focal microscopic perivascular hemorrhages and 4) vascular dilation. Vascular thrombosis occurred within the very superficial dermis at less than 0.3 mm in depth. Beyond this zone of vascular damage, located

predominantly in the papillary dermis, was a zone of perivascular inflammation with infiltrates of inflammatory cells and varying degrees of edema. The collagen bundles just below the necrotic epidermis were slightly swollen and glassy but there was no change in birefringence image intensity. An example of H&E stained microscopic section of persistent redness threshold lesion with the schematic drawing of the lesion boundaries is demonstrated in Figure 6.3.

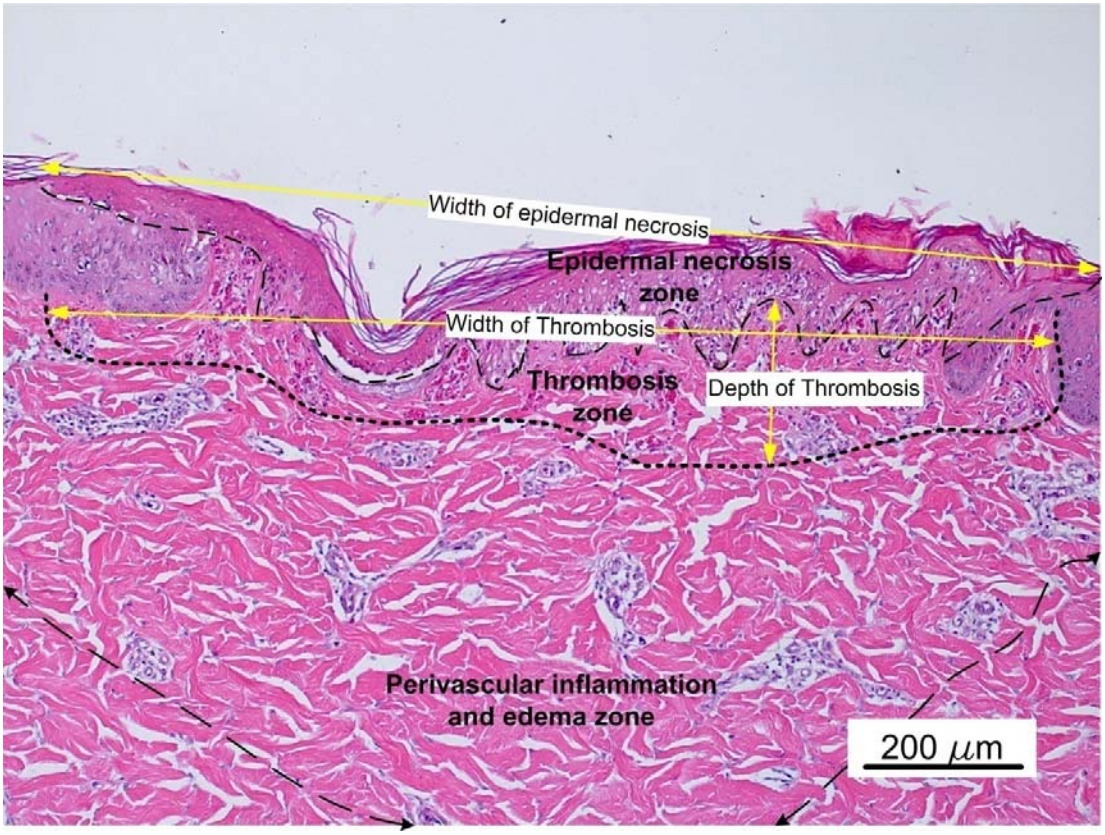

Figure 6.3. An example of various laser injury zones in skin for a threshold lesion (H&E stain. Original Mag. 100X). Laser condition: $\lambda = 2.0$ microns, 5 mm spot size, 2.5 s exposure duration and 0.41 W power.

In detail, there were some diverse features present in the total of 24 selected skin samples of persistent redness. At two laser irradiation conditions (5 mm - 0.25 s and 15 mm – 2.5 s), thrombosis was not found in the processed threshold lesion samples. Perivascular inflammation with infiltrates of inflammatory cells and varying degrees of edema were still present in the dermis even without the occurrence of thrombosis. On the other hand, ten selected histological sections of threshold lesions (threshold irradiations at 5mm-2.5s, 5mm-1.0s, 5mm-0.5s, 10mm-1.0s, and 15mm-0.5s) showed relatively more severe thermal damage to superficial papillary blood vessels, where intravascular epithelial detachment was found and occasionally the vascular endothelium was lost.

For each threshold lesion, four quantitative histopathlogical parameters were measured to map the extent of thermal damage: the widths of 1) epidermal necrosis at the surface and 2) the outer boundary of the thrombosis zone, 3) the depth of vascular thrombosis (measured from the epidermal/dermal junction to the deepest extent of thrombosis), and 4) the depth of perivascular inflammation (increased infiltrates of inflammatory cells) and edema (measured from the epidermal/dermal junction to the deepest extent of perivascular inflammation and edema) (Figure 6.3). These results were listed and compared with the lesion diameter measured *in vivo* in the living anesthetized pig in Table 6.2. The surface measurements and corresponding histological blocks came from to closest irradiated samples to the persistent redness threshold. The histological results in Table 6.2 were the average of 3 measurements in the histological section which was determined to be located at the center of the lesion. The surface widths of the gross lesion were roughly similar to the microscopic widths of the zones of epidermal necrosis and thrombosis for all lesions at the threshold. The thrombosis zone was mainly underneath the region of epidermal necrosis, with slightly smaller widths than the necrotic epidermal zone (Figure 6.3). Due to the release of tension of the

collagen bundles and the effects of formalin fixation, the skin specimens were slightly shrunken after fixation. By comparing the lengths of specimen before and after fixation, the shrinkage ratio of the skin specimen was 1.14±0.02. Therefore, all the results measured on skin histological sections were multiplied by this shrinkage factor, 1.14, to estimate the original sizes. The quantitative histological data listed in this paper were corrected for shrinkage.

Table 6.2. The extent of histological damage of the 48 hour gross threshold lesions (n = 2 for each test condition).

D(mm) / t (s)	5					10					15				
	W1 (mm)[1]	W2 (mm)[2]	W3 (mm)[3]	D1 (mm)[4]	D2 (mm)[5]	W1 (mm)	W2 (mm)	W3 (mm)	D1 (mm)	D2 (mm)	W1 (mm)	W2 (mm)	W3 (mm)	D1 (mm)	D2 (mm)
0.25	1.5	1.35	0.00	0.00	0.73	1.0	0.92	0.88	0.09	0.80	2.0	1.60	1.49	0.06	1.14
0.5	2.5	2.28	1.88	0.16	1.13	1.5	0.63	0.60	0.04	0.51	1.5	1.56	1.48	0.17	1.15
1.0	2.0	2.26	2.07	0.27	1.05	2.0	1.88	1.80	0.21	1.09	2.5	2.18	1.89	0.08	0.87
2.5	1.3	1.32	1.08	0.15	0.83	2.3	2.17	2.00	0.15	1.19	2.0	1.40	0.00	0.00	0.65

[1]: The width of gross lesion.
[2]: The surface width of epidermal necrosis (n=3 for each measured skin section).
[3]: The width of thrombosis zone (n=3 for each measured skin section)
[4]: Depth of thrombosis measured from the epidermal/dermal junction to the deepest extent of thrombosis (n=3 for each measured skin section).
[5]: Depth of perivascular inflammation and edema measured from the epidermal/dermal junction to the deepest extent of perivascular inflammation and edema (n=3 for each measured skin section).

6.4.3. Lesions Created above Threshold Irradiances

The pathological effects of increasing laser power above threshold at 5-mm spot size and 2.5-s exposure duration continue to be illustrated in Figure 6.2. The threshold power for persistent redness was 0.41 W at this laser condition, and the peak temperature at the spot center for threshold irradiation was about 66 ^{o}C. At 0.56 W, a flat, slightly indented red papule larger than the threshold redness displayed in Figure 6.2c(S). The peak temperature at the irradiation center was about 76 ^{o}C. Microscopically, the center of

the lesion showed more severe thermal damage to the epidermis and dermis than was seen in the threshold lesion. Epidermolysis at the epidermal/dermal junction was more prominent (Figure 6.2c(H)). The thermal damage zones extended deeper into the dermis. When the power was increased to 0.93 W, a darker scab-like central area on the skin surface grossly corresponded to a central shrunken, desiccated epidermis that was focally detached from the underlying dermis as revealed in the histological sections (Figure 6.2d(H)). The peak temperature at the center reached 100 ^{o}C. The underlying collagen fibers of the papillary and upper reticular dermis were swollen and hyalinized. In addition, the cells and lumens of the small blood vessels within this hyalinized area were shrunken and filled with smudged, thermally coagulated blood or thrombi characteristic of direct heat coagulation of the red blood cells. More peripherally, the concentric damage zones of thrombosis and perivascular inflammation extended further into the dermis. Increasing the power to 4.83 W produced an audible pop as superheated superficial dermis water was vaporized and the desiccated epithelium layers ruptured (Figure 6.1e). This lesion showed the characteristic histologic pattern of "popcorn" thermal damage with fragmented epidermis exposing the underlying severely thermally damaged hyalinized dermal collagen. Thermal camera measurements of surface temperature of this lesion reached 160 ^{o}C prior to the pop and then fell to 100^{o}C.

Also, these stained skin sections were examined using transmission polarization microscopic optics (TPM). At 5-mm spot size and 2.5-s exposure duration, superficial dermal collagen started to lose its birefringence intensity at 0.93 W, and there was a total loss of dermal collagen birefringence for the 4.83-W exposure (Figure 6.4).

The measurements of the extent of injury in thermal lesions produced by various power irradiations at 2.5-s exposure duration and 5-mm spot size are shown in Figure 6.5. The measured parameters included: 1) diameter of the grossly visible lesion measured on

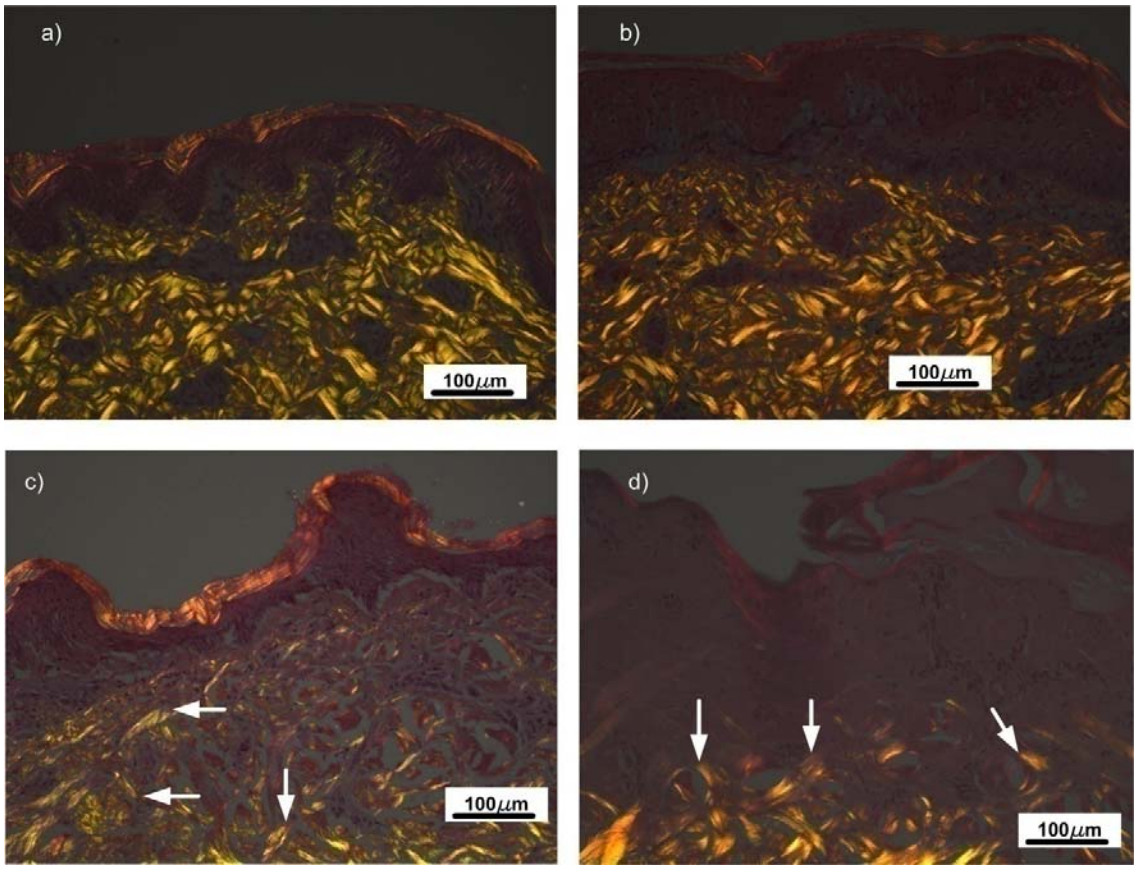

Figure 6.4. Birefringence images of skin samples using a transmission polarization microscope. Laser conditions: 5 mm spot size and 2.5 s exposure duration. Original Mag. 200X. a) same imaging field as Figure 6.1a, laser power 0.21 W. The individual strands of the dermal collagen are brightly birefringent; no birefringence change. b) Same imaging field as Figure 6.1c, laser power 0.56 W. No birefrigence change. c) Same imaging field as Figure 6.1d, laser power 0.93 W, scattered collagen strands are partially birefringent with more loss of birefringence close to the thermal lesion surface: partial birefringence loss of dermal collagen (arrows). d) Same imaging field as Figure 6.1e, laser power 4.83 W, boundary of total birefrigence loss in upper dermal collagen (arrows).

the skin surface, and, histologically, the widths of 2) epidermal necrosis at the surface, 3) the outer boundary of thrombosis, 4) the outer boundary of birefringence decrease, and the depths of 5) the outer boundary of birefringence decrease, 6) the outer boundary of vascular thrombosis as well as 6) the outer boundary of perivascular inflammation and

edema as defined in Table 6.2. The histological lesion sizes in Figure 6.5 were the average of 3 measurements in the histological section located at the center of the lesion.

6.4.4. Model Predictions of Lesion Dimensions

The widths and depths of damage measured experimentally were compared to predicted values from our optical-thermal-damage model which contained a rate-process, light propagation, and heat transfer model. Temperature and damage as a function of time was computed for each spatial grid point in the model. Predicted surface temperatures were validated by thermal camera measurements (Chen, Thomsen et al. 2006). Final values of $\Omega(r,z)$ that were equal to 1.0 defined the predicted boundaries of damage. The model predicted thermal lesion boundaries that were bowl-shaped. An example of predicted lesion boundaries for the 0.93 W irradiation at 2.5 s - 5 mm is shown in Figure 6.6. Figure 6.6 demonstrates an example of optical-thermal-damage model prediction with various lesion boundaries by choosing the Gaylor coefficients for thrombosis as well as epidermal necrosis and the Pearce coefficients for birefringence decrease. Within these boundaries, Ω was greater than 1.

Besides rate coefficients from Gaylor and Pearce, seven sets of rate process coefficients found in literature for skin damage (listed in Table 6.1) were tested by using our optical-thermal-damage model. The predictions of lesion depths and widths using these coefficients are compared with experimental data in Tables 6.3 and 6.4, respectively. The model using coefficients proposed by Fugitt predicted no damage at most of the laser conditions, and the model with Wu's coefficients gave much larger lesions than the experimental data. Model results using these two sets of coefficients were not listed in the Tables 6.3 and 6.4.

Another thermal damage marker, decrease of birefringence intensity, was examined for a 5-mm spot size and 2.5-s exposure duration. Rate process coefficients, $A = 1.606\times10^{45}$ [1/s] and $E_0 = 3.06\times10^{5}$ [J/mole], proposed by Pearce *et al.* for birefringence loss in rat skin heated *in vitro* (Pearce, Thomsen et al. 1993; Pearce and Thomsen 2003), were used to predict the extent of birefringence change in the pig skin. The model prediction was compared with the experimental measurements in Table 6.5.

Table 6.3. The maximum depths of thrombosis of gross threshold lesions: Comparison of histological measurements with damage model predictions using various rate process coefficients.

Laser condition	Depth of thrombosis (mm) [1]	Model_T (mm) [2]	Model_H (mm) [3]	Model_W (mm) [4]	Model_G (mm) [5]
5mm - 0.25s	0.00	0.28	0.24	0.21	0.19
5mm – 0.5s	0.16	0.47	0.39	0.31	0.29
5mm – 1.0s	0.27	0.36	0.29	0.30	0.27
5mm – 2.5s	0.15	0.25	0.24	0.25	0.23
10mm–0.25s	0.09	0.13	0.12	0.07	0.00
10mm – 0.5s	0.04	0.13	0.12	0.08	0.00
10mm – 1.0s	0.20	0.21	0.21	0.19	0.16
10mm – 2.5s	0.14	0.27	0.27	0.28	0.26
15mm – 0.25s	0.06	0.15	0.15	0.12	0.08
15mm -0.5s	0.17	0.15	0.15	0.12	0.07
15mm – 1.0s	0.08	0.17	0.17	0.15	0.10
15mm – 2.5s	0.00	0.06	0.07	0.06	0.00

[1]: Depth of thrombosis as defined in Table 6.2.
[2]: Prediction using rate process coefficients proposed by Takata.
[3]: Prediction using rate process coefficients proposed by Henriques.
[4]: Prediction using rate process coefficients proposed by Weaver and Stoll.
[5]: Prediction using rate process coefficients proposed by Gaylor.

Table 6.4. Comparisons of the damage widths of the histological measurements with damage model predictions using various rate process coefficients.

Laser condition	Width of epidermal necrosis [1]	Width of thrombosis[2]	Model_ T [3]	Model_ H [4]	Model_ W [5]	Model_ G [6]
5mm - 0.25s	1.35	0.00	2.32	2.30	2.05	1.81
5mm – 0.5s	2.28	1.88	2.68	2.64	2.50	2.30
5mm – 1.0s	2.26	2.07	2.23	2.18	2.07	1.90
5mm – 2.5s	1.32	1.08	1.44	1.41	1.43	1.29
10mm–0.25s	0.92	0.88	2.70	2.54	1.50	0.00
10mm – 0.5s	0.63	0.60	2.44	2.32	1.45	0.00
10mm – 1.0s	1.88	1.80	3.20	3.10	2.75	2.18
10mm – 2.5s	2.16	2.00	2.90	2.84	2.88	2.64
15mm–0.25s	1.60	1.49	4.53	4.39	3.27	1.89
15mm -0.5s	1.56	1.48	3.82	3.62	2.73	0.80
15mm – 1.0s	2.18	1.89	3.35	3.22	2.59	1.28
15mm – 2.5s	1.40	0.00	1.02	1.16	1.00	0.00

[1,2]: the widths as defined in Table 6.2.
[3,4,5,6]: prediction using various rate process coefficients as defined in Table 6.3.

Table 6.5. Comparisons of birefringence change by histology measurement and computer modeling (laser condition: 2.5 s exposure duration, 5mm spot size).

Power	Lesion	Histology[1]	Model[2]
0.93 W	Width	1.82 mm	2.06 mm
	Depth	0.318 mm	0.375 mm
0.56W	Width/Depth	No birefringence change	No birefringence change

[1]: The width and maximum depth of the outer boundary of birefringence decrease. (n=2 for each tested laser condition)
[2]: Prediction using rate process coefficients proposed by Pearce (Pearce, Thomsen et al. 1993).

6.5. DISCUSSION

6.5.1. Histological Damage

A critical safety concern is the indication of damage in histological sections associated with transient threshold radiant exposures. Figure 6.1 showed that the threshold radiant exposure for transient exposures were smaller than those for persistent

redness. Twelve selected skin samples, where redness appeared acutely but disappeared 48 hours later, were examined for evidence of any microscopic injury in the epidermis or dermis at power levels below persistent redness thresholds. No injury specifically attributed to thermal injury could be seen in the epidermis. All of these samples displayed mild, diffuse perivascular edema and some infiltrates of inflammatory cells in the superficial (papillary) dermis extending beyond the laser irradiation site (Figure 6.2a(H)). As power was increased but still below persistent redness thresholds, more perivascular inflammatory cells infiltrated into the papillary dermis. Moreover, the more severe perivascular inflammation and edema were more likely present in the irradiation center and associated with laser irradiation. Hyperhemia (redness) is a physiological vascular response to tissue heating associated with increased blood flow marked by dilation of the blood vessels and increased numbers of open vessels in the dermis. This non-lethal thermal effect is reversible and does not leave any permanent damage in the skin. The blood vessels as well as blood perfusion reverted to their normal states after a few hours, resulting the disappearance of the acute redness.

We did not find any lethal thermal damage in histological sections associated with irradiations below thresholds; however, the number of samples was limited and the microscopic observations of persistent redness lesions suggested that lethal thermal injury occurred in the epidermis before the dermis. Epidermal necrosis without any intravascular thrombosis or other severe dermal vascular damage in the dermis, was found in four selected lesion samples with threshold irradiation (at 5 mm - 0.25 s and 15 mm- 2.5 s). It indicated that: as power increased, epidermal cells were damaged before any lethal injury extended to the dermal vessels. Therefore, we believed the microscopically minimal lesion for 2.0 μm laser irradiation was intraepidermal necrosis without any lethal thermal damage in the dermis. Since most of the persistent redness

lesions contained relatively more severe thermal damage including coagulative necrosis of the epidermis and dermis in varying depths, we postulate that the threshold powers for persistent redness were slightly higher than those for microscopically minimal lesions which only contained necrosis of the superficial epidermal cells.

Determination of threshold damage is a function of the method of observation and the observer's ability to see a thermally induced change in natural skin. Due to the diversity of each mini-pig and large uncertainty in identification of the red lesion on the brown pigmented skin surface, for each grossly observable threshold lesion, there was a multitude of histologic events, including: 1) trans-epidermal necrosis with scattered area of epidermolysis, which were observed consistently in all of the processed threshold lesions, 2) vascular thrombosis predominately in papillary layer, occurring within less than 0.3 mm in depth. and was not present in four selected threshold lesions (at 5 mm – 0.25 s and 15 mm – 2.5 s), 3) intravascular epithelial detachment and vascular endothelium loss in the papillary layer, which were found in 10 processed threshold lesions. In the total of 24 representative threshold lesions, epithelial detachment and endothelium loss were relatively more severe thermal damage and only present in the lesions where vascular thrombosis was deeper than 0.15 mm.

Compared to the dermal vessels, the collagen bundles in the dermis had less thermal sensitivity. At the persistent redness threshold, the collagen bundles just below the necrotic epidermis were slightly swollen and glassy but there was no change of birefringence. Roughly, 80% of the collagen birefringence is form birefringence due to the crystalline array of the macromolecules while the rest is the intrinsic molecular birefringence. Thermal denaturation of the collagen proteins disrupts their crystalline arrays and tertiary molecular structures leading to a loss of their birefringent properties. Depending on the temperature and time of heating, different zones of partial and

complete birefringence loss of collagen can been seen and their boundaries measured (Thomsen 2000). No birefringence change was observed until the irradiated power increased by 1.5-2.5 times beyond threshold (Figure 6.4c). With this power, the peak temperatures at the irradiation center reached about 100 ^{o}C. The underlying collagen fibers of the papillary and upper reticular dermis were swollen and hyalinized (Figure 6.2d(H)). The laser induced temperature rise was directly proportional to input power, thus the critical temperature rise to induce collagen birefringence change was about 1.5-2.5 times higher than that for thrombosis in the superficial dermal region. At much higher powers, such as 4.83 W for 2.5 s exposure duration and 5 mm spot size, an audible pop accompanied with an abrupt temperature drop was noticed, and total birefringence loss of dermal collagen was found (Figure 6.4d).

Cell death and subsequent necrosis are direct responses to laser irradiation and resulted when (1) the damage is sufficiently severe that the vital, energy producing mitochondrial enzymes and membrane apparatus are disrupted and when (2) other repair mechanisms such as the mediators of the repair mechanisms (DNA and RNA transcription enzymes and protein synthesis enzymes) are thermally destroyed (Welch and vanGemert 1995). Cellular necrosis, the “gold standard” marker of death, which is easily recognized at 24 to 72 hours depending on the tissues, was evident at 48 hrs in the skin samples. Cell necrosis particularly in the epidermis was found to have relatively clear and smooth boundary in light microscopic sections of lesions 48 hours after irradiation. The width of epidermal necrosis was strongly dependent on the irradiation power. Vascular thrombosis and perivascular inflammation were secondary responses to the heat damage in dermal vessels particularly to endothelial cells. The boundaries of these damage zones were measurable but relatively irregular. The extent of these injuries depended on the input power (Figure 6.5). Besides these quantitative parameters, the

birefringence intensity change was another measurable parameter which had a relatively sharp boundary in the dermis and was easier to observe than the boundaries of mild hyalinization and fiber swelling.

In conclusion, there was a sequence of microscopic damage endpoints defined in the skin as power increased. Beginning at the lowest and going to the highest power (super-threshold), these measurable endpoints included: 1) perivascular inflammation and edema , which occurred at power levels less than those for persistent redness threshold, 2) epidermal necrosis, which was contained in all the processed persistent redness lesions and defined as microscopically minimal thermal damage in the skin to 2.0 μm wavelength laser irradiation, 3) dermal vascular thrombosis, which was present in most of the selected persistent redness lesions and 4) decrease of dermal collagen birefringence, which happened in the skin with irradiation 1.5-2.5 times beyond persistent redness threshold. Figure 6.5 illustrated the sequence of power levels and sizes of damage zones associated with these endpoints for 5-mm spot size and 2.5-s exposure duration. The central damage became more severe and the concentric damage zones extended deeper and wider than those of the threshold lesions. Beyond this zone of severe damage was a zone of perivascular inflammation with infiltrates of inflammatory cells and varying degrees of edema. The depths of lesion zone boundaries formed by mechanisms of thermal vascular damage, that was, the thrombosis and perivascular inflammation with edema roughly parallel each other once threshold has been reached.

6.5.2. Optical-Thermal-Damage Model

Rate process coefficients listed in Table 6.1 were tested using our optical-thermal-damage model to estimate the extent of damage. The widths of damage predicted by the model were compared with histological measurements of the widths of epidermal

necrosis as well as dermal thrombosis in Table 6.3. The comparison of the depths of predicted damage and the outer boundary of dermal thrombosis was listed in Table 6.4. No prediction was made for perivascular inflammation and edema due to the lack of associated rate process coefficients. Moreover, the inflammatory response of the skin to laser irradiation was a complex matter, intimately linked to the biological response of the skin subsequent to laser irradiation, and not simply a result of laser irradiation alone. Therefore, it may be not feasible to use standard rate process model to predict edema and perivascular inflammation.

It was found in Tables 6.3 and 6.4 that the widths and depths of thermal damage predicted with Gaylor coefficients were similar to histological measurements. The variation between the model prediction with Gaylor coefficients and histological measurement can be attributed to the diversity of optical and thermal properties in different mini-pigs, the variation in processing histological sections, and pathophysiological differences of endpoint defined in Gaylor's and our experiments. On the other hand, the models with other rate process coefficients gave slightly higher predictions than experimental data. Wilcoxon signed ranks tests were conducted to test the similarity between the model predictions and experimental data (Table 6.6). The p value indicated: At the 0.05 level, neither the lesion widths nor depths predicted with Gaylor coefficients were significantly different from histological data. The model using the coefficients other than Gaylor coefficients gave predictions that were significantly different from histological measurements. Gaylor et al. measured the change in cell membrane permeability which was observed as a decrease in cell fluorescence of a carboxyfluorescein diacetate dye in cells. In terms of determining of thermal damage by short time heating, this method had much higher sensitivity than the gross determination of bulk tissue death used in Takata's, Henriques's or Weaver's experiments. Moreover,

Takata, Henriques or Weaver defined the damage endpoint as trans-epidermal necrosis, which was a different damage endpoint from dermal thrombosis. Thus, the lesion depths predicted using their rate process coefficients cannot be related to the histological measurements of dermal vascular thrombosis. Cell membrane lysis was probably the initial destructive event of thermal damage, and rate process of cell membrane rupture was a fairly good model in predicting not only epidermal cell death but also dermal thrombosis which was induced by vascular endothelial cell coagulation. The similarity between histological measurements and model predictions with Gaylor's coefficients indicated that our optical-thermal-damage model was valid for predicting transient laser-induced epidermal necrosis and dermal vascular thrombosis.

Table 6.6. Wilcoxon signed ranks test to compare histological measurements of lesion depths [1] and widths [2] with model predictions.

Test result	Histology – Model_T		Histology – Model_H		Histology – Model_W		Histology – Model_G	
	Depth [1]	Width [2]	Depth	Width	Depth	Width	Depth	Width
P values	0.004	0.006	0.004	0.006	0.015	0.010	0.444	0.158

[1]: Depth of thrombosis as defined in Table 6.2.
[2]: surface width of epidermal necrosis as defined in Table 6.2.

Predictions of lesion size beyond threshold power were computed for 5-mm spot sizes and 2.5-s exposure duration (Figure 6.7). Predicted lesion widths and depths increased with laser power. The differences between predictions and histological data, especially for lesion depth, became larger as power increased. At powers beyond threshold, skin was coagulated and experienced a notable change of optical and thermal properties which were not addressed in our damage model. Changes in optical and thermal properties would influence predictions of lesion depth measured at the irradiation center more than that of lesion width obtained on the surface at the boundary of damaged and normal skin. Besides, vascular thrombosis was a dynamic process triggered by

endothelial injury and related to release of tissue factors, adherence of platelets, endothelial damage with exposure of sub-endothelial collagen (and other platelet activators), and thus may not closely follow the first order rate process model, especially when more severe damage beyond damage threshold was present in vessels.

Histologically, birefringence intensity change indicated coagulation of collagen bundles. Rate process coefficients proposed by Pearce (Pearce, Thomsen et al. 1993) (Table 6.1), were used in the model to predict the boundary of birefringence change defined as the outer boundary where change of polarization image intensity started to be notable through TPM. The comparison between limited experimental data and model prediction is listed in Table 6.5. The model gave close prediction to the experimental measurements. It indicated the capability of the model to predict decrease of birefringence due to thermal collagen coagulation in dermis.

We are aware that the rate process coefficients retrieved from literature do not exactly correlate to the end points defined in our skin injury study. All rate process coefficients were based to some degree on specific experimental protocols and definitions of damage endpoint. For example, the rate process coefficients derived for birefringence loss in the skin were based on different species (rat rather than pig used in our experiments) and under *in vitro* experimental conditions (Pearce, Thomsen et al. 1993). The damage experiments by Gaylor were performed on the membrane of isolated mammalian skeletal muscle cells in cell culture rather than *in situ* and *in vivo* epidermal cells or dermal vascular endothelium. However, the closeness between the model predictions and microscopic measurements on the extent of thermal injuries, defined as epidermal necrosis, vascular thrombosis, or birefringence change, demonstrates the feasibility of using models to predict various types of thermal injuries by adjusting the corresponding rate process coefficients.

6.6. CONCLUSION

There was a sequence of microscopic damage endpoints defined in the skin as power increased. Beginning at the lowest and going to the highest power, these separated measurable endpoints included: 1) perivascular inflammation and edema, which occurred at sub-threshold power, 2) epidermal necrosis, which was defined as microscopically minimal thermal damage to 2.0 μm wavelength laser irradiation, 3) dermal vascular thrombosis, and 4) decrease of dermal collagen birefringence, which happened at irradiation 1.5-2.5 times beyond persistent redness threshold.

We have shown a relation between the degree of histological damage and irradiance, and the rate coefficients that approximate the rate process of damage for each histological endpoint.

The optical-thermal-damage model was indicated to be valid for predicting transient laser-induced epidermal necrosis and dermal thrombosis, with the rate process coefficients proposed by Gaylor indicating better agreement with experimental data than the commonly used bulk skin coefficients proposed by Henriques. The latest version of our optical-thermal-damage model, supported by experimental validation, provided a system for predicting the thermal response of skin to laser irradiation and damage size caused by such irradiation. By adjusting the rate process coefficients, the optical-thermal-damage model was capable of predicting various types of thermal injury in the skin, such as epidermal necrosis, vascular thrombosis, and dermal collagen coagulation.

6.7. ACKNOWLEDGMENT

Opinions, interpretations, conclusions, and recommendations are those of the authors and are not necessarily endorsed by the University of Texas, the United States Air Force or the Department of Defense.

The authors wish to thank the Air Force Research Laboratory as well as Dr Randolph D. Glickman and Peggy Miller, Lions Eye Pathology Laboratory, UTHSCSA for their preparation of histological tissue sections.

6.8. REFERENCES

ANSI (2007). ANSI Z136.1-2007, American National Standard for Safe Use of Lasers. Orlando, FL, Laser Institute of America, American National Standards Institute.

Chen, B., D. C. O'Dell, et al. (2005). "Porcine skin ED50 damage thresholds for 2,000 nm laser irradiation." Lasers Surg Med **37**(5): 373-81.

Chen, B., S. L. Thomsen, et al. (2006). "Modeling thermal damage in skin from 2000-nm laser irradiation." J Biomed Opt **11**(6): 064028.

Diller, K. R. (1994). "The mechanisms and kinetics of heat injury accumulation." Ann N Y Acad Sci **720**: 38-55.

Diller, K. R., L. J. Hayes, et al. (1991). "Analysis of alternate models for simulating thermal burns." J Burn Care Rehabil **12**(2): 177-89.

Fried, N. M. (2005). "High-power laser vaporization of the canine prostate using a 110 W thulium fiber laser at 1.91 mu m." Lasers in Surgery and Medicine **36**(1): 52-56.

Fried, N. M. (2005). "Thulium fiber laser lithotripsy: An in vitro analysis of stone fragmentation using a modulated 110-watt thulium fiber laser at 1.94 mu m." Lasers in Surgery and Medicine **37**(1): 53-58.

Fried, N. M. and K. E. Murray (2005). "New technologies in endourology - High-power thulium fiber laser ablation of urinary tissues at 1.94 mu m." Journal of Endourology **19**(1): 25-31.

Fugitt, C. E. (1955). A rate process of thermal injury. Armed Forces Special Weapons Project No. AFSWP-606.

Gaylor, D. C. (1989). Physical mechanism of celluar injury in electrical trauma Massachusetts Institute of Technology. **Ph. D.**

Gowrishankar, T. R., D. A. Stewart, et al. (2004). "Transport lattice models of heat transport in skin with spatially heterogeneous, temperature-dependent perfusion." Biomed Eng Online **3**(1): 42.

Henriques, F. F. (1947). "Studies of thermal injury V " Arch. of Pathol. **43**: 489-502.

Jackson, S. D. and A. Lauto (2002). "Diode-pumped fiber lasers: A new clinical tool?" Lasers in Surgery and Medicine **30**(3): 184-190.

Jackson, S. D., A. Sabella, et al. (2007). "Application and development of high-power and highly efficient silica-based fiber lasers operating at 2 mu m." Ieee Journal of Selected Topics in Quantum Electronics **13**(3): 567-572.

Jacques, S. L. (1993). "Role of tissue optics and pulse duration on tissue effects during high-power laser irradiation." Applied Optics **32**(13): 2447-2454.

Li, H. J., X. X. Zhang, et al. (2002). "Measurement of blood perfusion using the temperature response to constant surface flux heating." International Journal of Thermophysics **23**(6): 1631-1644.

Maher, E. J. (1978). Transmission and absorption coefficients for ocular media of the rhesus monkey. Report SAM-TR-78-32. San Antonio, Texas, Brooks Air Force Base.

McCally, R. L., R. A. Farrell, et al. (1992). "Cornea epithelial damage thresholds in rabbits exposed to Tm:YAG laser radiation at 2.02 microns." Lasers Surg Med **12**(6): 598-603.

Moritz, A. R. and F. C. Henriques, Jr. (1947). "Studies of thermal injury: II. The relative importance of time and surface temperature in the causation of cutaneous burns." Am J Pathol **23**: 695-720.

Niemz, M. H. (1996). Laser-Tissue Interactions. Berlin, Germany, Springer-Verlag Berlin Heidelberg.

Pearce, J. A., S. Thomsen, et al. (1993). Kinetics for birefringence changes in thermally coagulated rat skin collagen, Proc. SPIE 1876:180-185.

Pearce, J. A. and S. L. Thomsen (2003). Thermal damage parameters from laser coagulation experiments, San Jose, California, USA, Progress in Biomedical Optics and Imaging(SPIE) 4954:58-63.

Pennes, H. H. (1948). "Analysis of tissue and arterial blood temperatures in resting human forearm." J. Appl. Physiol. **1**: 93-122.

Rendell, M. S., S. T. Kelly, et al. (1993). "The effect of increasing temperature on skin blood flow and red cell deformability." Clin Physiol **13**(3): 235-45.

Sorokina, I. T. and K. L. Vodopyanov, Eds. (2007). Solid-State Mid-Infrared Laser Sources (Topics in Applied Physics Vol. 89) Springer Verlag GmbH.

Takata, A. N. (1974). "Development of criterion for skin burns." Aerosp. Med. **45**: 634-637.

Thomsen, S. L. (2000). "Qualitative and quantitative pathology of clinically relevant thermal lesions " Crit. Rev. Opt. Sci. Technol. **75** 425-58.

Torres, J. H. and M. Motamedi (1993). "Experimental evaluation of mathematical-models for predicting the thermal response of tissue to laser irradiation " Appl. Opt **32**(4): 597-606.

Tropea, B. I. and R. C. Lee (1992). "Thermal injury kinetics in electrical trauma." J Biomech Eng **114**(2): 241-50.

Weaver, J. A. and A. M. Stoll (1967). NADC Memo Report 6708. Johnsville, Pennsylvania, United Stated Naval Air Development Center.

Welch, A. J. and M. J. C. vanGemert (1995). Optical-thermal response of laser-irradiated tissue. Chapter 17: Rate processs analysis of thermal damage. New York and London, Plenum Press.

Wu, Y. C. (1982). A Modified Criterion for predicting thermal injury. Nat. Bur. Stand. Washington, District of Columbia.

Zuclich, J. A., D. J. Lund, et al. (2007). "Wavelength dependence of ocular damage thresholds in the near-ir to far-ir transition region: Proposed revisions to MPEs." Health Physics **92**(1): 15-23.

Chapter 7. Porcine Skin ED50 Damage Thresholds for 1214 nm Laser Irradiation

7.1. ABSTRACT

A series of experiments were conducted *in vivo* on porcine skin to determine the ED50 damage thresholds for 1214 nm continuous wave laser irradiation. These results provide new information for refinement of Maximum Permissible Exposure (MPE). The study employed exposure durations of 1 sec, 3 sec, and 10 seconds with nominal spot diameters of 6 mm, 8 mm and 10 mm and as a function of laser power. The effect of each irradiation was evaluated acutely, one hour after exposure, and 24 hours post exposure. Probit analysis was conducted to estimate the dose for 50% probability of laser-induced damage (ED50); Damage was defined as persistent redness at the site of irradiation for the pig skin after 24 hours. The results indicated that Maximum Permissible Exposure (MPE) limits should be lowered for the laser beam diameters larger than 6 mm.

7.2. INTRODUCTION

The weak absorption of near infrared (NIR) radiation by skin tissues between 700 and 1400 nm offers an important window for optical diagnosis and laser therapy. Unlike visible light, NIR penetrates deeply into skin; it therefore offers a potential spectral window for functional imaging and medical monitoring without the hazards of ionizing radiation (Welch and vanGemert 1995). Another application for these wavelengths region is selective photothermolysis which is a widely used treatment approach that preferentially heats tissue targets, that absorb a pulse of optical radiation more strongly than surrounding tissues (Anderson, Beck et al. 1989; Altshuler, Anderson et al. 2001). The near-infrared spectral region of 700-1400 nm includes the most tissue-penetrating optical wavelengths. In this spectral region, absorption is low because the photon quantum energy is less than the electronic transition energy in most organic molecules. In

2006, Anderson *et al*. investigated the selective photothermolysis potential of lipid-rich tissues. Their study suggested that selective photothermal targeting of fatty tissues is feasible using infrared lipid absorption bands centered at 1200 nm (Anderson, Beck et al. 1989).

The potential wide spread interest in CW lasers wavelengths around 1.2 μm and large spot sizes requires a reevaluation of the current safety limits for the maximum permissible exposure (MPE) at 1.2 μm. The ANSI MPE value (see Table 7.1) for skin at this wavelength is based on sparse experimental data that was obtained with an aperture diameter less than 3.5 mm (ANSI 2007). However, at 1.2 μm wavelength, large beam spot sizes (from 5 to 25 mm) are being employed for cellulite reduction. This chapter describes an *in vivo* experiment to determine ED50 threshold at 1.2 μm for large spot sizes and long exposure durations.

Table 7.1. Maximum permissible exposure (MPE) for skin exposure to a laser beam (ANSI 2007)

Wavelength(μm)	Exposure Duration, *t* (s)	MPE (J cm^{-2})	Limiting Aperture Diameter (mm)
0.400 to 1.400	10^{-7} to 10	$1.1C_A t^{0.25} = 5.5\ t^{0.25}$	3.5

where *t* is the laser exposure duration.

7.3. MATERIAL AND METHODS

7.3.1. Animal Preparation

The animal use protocol was approved by the Institutional Animal Care and Use Committee at the University of Texas at Austin. Two Sinclair pig weighting 14.1 and 22.2 kg and one Hanford pig weighting 27.2 kg, were used in this study. Before beginning each of the experiments, the pig was anesthetized initially with IM Telazol-Ketamine-Xylazine(TKX) and intubated. Isoflurane (1~3%) was administered for

anesthesia maintenance throughout the procedure by a certified registered laboratory animal technologist. Heart rate, SpO_2 and respiration were monitored throughout the experiment. In addition, Rimadyl (Carprofen) was given at the end of the procedure to alleviate possible post surgical pain. After the pig was anesthetized, its hair was removed with an electric razor and then Nair® depilatory was applied. Nair® was removed five minutes after application and the pig skin was bathed with water. The pig was marked with a metallic-black permanent marker to make grids for identification and location of the numerous irradiation sites. The dimensions of the grids depended upon the laser spot size. A cross pattern was drawn around each irradiated location to locate the center of irradiation after each laser exposure.

7.3.2. Experimental Setup

A CW diode laser (Candela Inc.) with a maximum 58 W output at a nominal wavelength 1214 nm was used to create an array of irradiations. Output power was adjusted on the front panel, and a power meter (Molectron Detector, Inc.; Portland, OR; Model: PM-3) with air-cooled power meter probes PM30 (Molectron Detector, Inc.) measured the output power at each power setting before each *in vivo* experiments. Power measurements were also made after some selective laser exposure settings to confirm the stability of the laser system. The laser light was transmitted through an optical fiber to a handpiece attached to the distal end of the fiber. Various spot sizes were achieved by adjusting the calibrated distance of the fiber end to a optical lens in the handpiece and confirmed with a thermal paper. During the laser exposure, the handpiece was placed perpendicularly against the skin surface.

7.3.3. Experimental Procedures

Radiant exposures were made at specified exposure durations of 1 sec, 3 sec, and 10 seconds for nominal spot diameters of 6 mm, 8 mm, and 10 mm. The laser condition of 3 seconds and an 8 mm spot size was not tested due to the limited available animals. The nominal exposure durations of 1, 3 and 10 seconds were actually 0.981, 3.05 and 9.81 seconds, respectively. The number of irradiations for each of the 8 spot size-exposure conditions was 52 - 163 with an average of 85 per condition. Variation in laser power provided sufficient data points for probit analysis of damage/no damage response as a function of power. The size and type of lesions were evaluated acutely, 1 hour and 24 hours after exposure. After each laser exposure the test location was examined with the aid of an overhead surgical light to evaluate the presence or absence of skin lesions. A lesion was recorded as a "yes" if both readers identified it as positive. The consensus "yes" or "no" response of the observers was recorded on the data sheet. If consensus of the two observers could not be reached on damage a note of "questionable" was recorded on the data sheet and a third reader was used to make the final decision. This align-expose-examine procedure was repeated until all accessible skin locations were exhausted. The same evaluation procedures were repeated 1 hour and 24 hours after laser exposure. Based on visible skin damage/no damage, probit analysis was used to determine the ED50 damage threshold. Probit analysis provided a statistically-estimated dose for 50% probability of minimal visual laser-induced damage (ED50) for the pig skin (Finney 1971). Data points (damage/no damage for each condition) were entered into a probit statistical analysis package (Lund, B., Probit Fit Dose-Response Data Analysis Program, Version 1.02, U.S. Army Medical Research and Material Command, Hazards Research Branch) and a ED50 value was calculated along with fiducial limits at the 95% confidence level.

7.4. RESULTS

The effect of each irradiation was evaluated acutely, 1 hour and 24 hours after exposure. The gross apparent minimal visible lesion was defined as the presence of superficial redness on skin surface. For the safety concern, threshold lesion evaluated at 24 hours post exposure was defined as persistent redness and represented the permanent damage by 1.214 μm laser irradiation. The data discussed in this chapter were from 24-hrs observation. A gross picture of threshold persistent redness is shown in Figure 7.1.

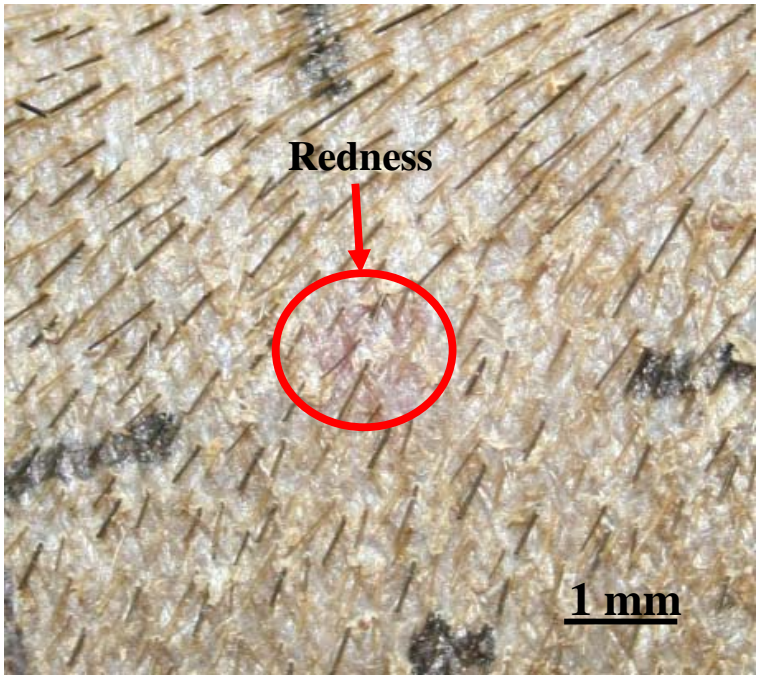

Figure 7.1. A gross image of thermal lesion at the threshold 24-hrs post exposure. Exposure condition: beam diameter 6 mm, exposure duration 1 s, laser power 8.6 W.

The ED50 threshold powers for 24-hour post exposure are listed in Table 7.2 along with their 95% fiducial limits.

Table 7.2. ED50 power for minimal visible lesion threshold at 1.214 μm along with their 95% fiducial limits [W].

Diameter (mm) / Duration (s)	6	8	10
1	8.6 (7.84-9.36*)	14.1 (13.2-15.0)	23 (21.9-23.9)
3	3.66 (3.25-4.10)	N/A	7 (6.36-7.53)
10	1.3 (1.30-1.30)	1.76 (1.64-2.04)	2.67 (2.56-2.80)

*: 95% lower-upper fiducial limits.

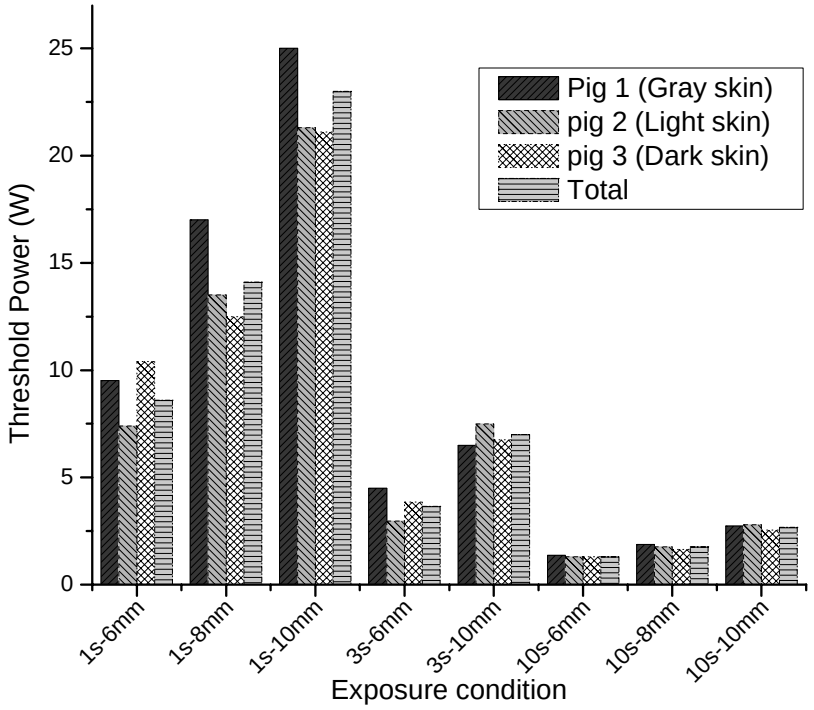

Figure 7.2. Comparison of ED50 powers obtained from pigs with various skin color Skin pigmentation density from lowest to highest: pig 2 (light skin), pig 1 (gray skin), pig 3(dark skin). ED50 powers obtained based on results from all 3 pigs are represented as "total" in the figure.

Three pigs with noticeable skin color variation were tested in this study to examine the possible melanin effect in determination of skin damage threshold. The same laser conditions were repeated on each pig. Figure 7.2 compares ED50 threshold powers

estimated using experimental data from each pig for all tested exposure conditions. The ED50 powers using data from 3 pigs are also included in Figure 7.2. Skin pigmentation density from lowest to highest: pig 2 (light skin), pig 1 (gray skin), pig 3(dark skin).

7.5. DISCUSSION

Most of the one hour threshold lesions were still visible at 24 hours. However, some barely visible superficial lesions disappeared. No new lesions were observed at 24 hours. Therefore, damage threshold evaluated at one hour give a slightly more conservative threshold values than at 24 hours. Since three pigs with noticeable skin color variation were tested in this study, a Friedman test (Friedman 1940) was conducted to detect the differences in ED50 threshold powers obtained from each pig skin with various pigmentations (see Figure 7.2). P value of this test was 0.159. Therefore, for a confidence level at 0.05, there was no significant difference in ED50 threshold powers for various pigmentations. That is to say, none of the threshold results from each pig skin showed any overall statistical evidence that the density of melanin affected threshold results beyond experimental uncertainties. However, there was insufficient detail to determine the effect of exposure duration and pigmentation upon the results.

The experimental results of average radiant exposures for threshold irradiations are compared with the ANSI MPE standard at each exposure duration in Table 7.3. The safety factor is defined as experimental threshold radiant exposure divided by the corresponding MPE value at same laser condition. Since the MPE level is defined for a limit aperture of 3.5 mm, the large spot sizes tested in our experiment provide additional data for the specification of safety standards for large spots. MPE values have usually been assumed to be a factor of 10 below the radiant exposures at damage thresholds, although a factor of less than ten is “safe” when experimental uncertainty is small

(Sliney, Mellerio et al. 2002). In our experiments, the experimental safety factors for all tested laser conditions are smaller than this commonly used value. Therefore, for large spot size (larger than 6 mm), it may be necessary to reevaluate the current MPE standards and consider refinement for large spot sizes.

Table 7.3. Average radiant exposure for minimal visible lesion threshold at 1.214 μm along with their 95% fiducial limits compared with MPE values calculated at the same exposure durations. [J/cm^2]

Diameter(mm) / Duration (s)	6	8	10	MPE$^{\$}$ (safety factor$^{\&}$)
1	29.8 (27.7-33.1*)	27.5(25.8-29.3)	28.7 (27.4-29.9)	5.5 (5.4-5.2$^{\%}$)
3	39.5 (35.1-44.2)	N/A	27.2 (24.7-29.2)	7.3 (5.4-3.7)
10	45.1 (45.1-45.1)	34.3 (32.0-39.8)	33.3 (32.0-35.0)	9.8 (4.6-3.4)

*: 95% lower-upper fiducial limits.
$: calculated based on ANSI136.1-2000. See Table 7.1.
&: safety factor = Minimal visible lesion threshold/MPE value

The average radiant exposures for minimal visible lesion thresholds at 1.214 μm are compared in Figure 7.2 with threshold values at 2.0 μm that was obtained from previous experiments (detailed in chapter 3). Based on our experimental data at 2.0 μm wavelength, we proposed a power-law relation between the exposure duration (t) and average radiant exposure (H) for ED50 damage threshold, an empirical equation was obtained by fitting the experimental data (Chen, O'Dell et al. 2005):

$$H = \mathrm{a} \times t^{b} \tag{7.1}$$

where a and b are two positive coefficients. The least square fit of 2.0 μm threshold data showed that coefficient a was spot size dependent but b was approximately constant with a value of 0.206 at all tested spot sizes (5, 10, and 15 mm). We tried to fit threshold data at 1.214 μm by using this proposed power law relation. Both coefficient a and b are spot

size dependent. The values of a and b noted as (a, b) are approximately (0.17, 31.1), (0.10, 27.6) and (0.07, 27.4) for spot diameter 6, 8 and 10 mm, respectively.

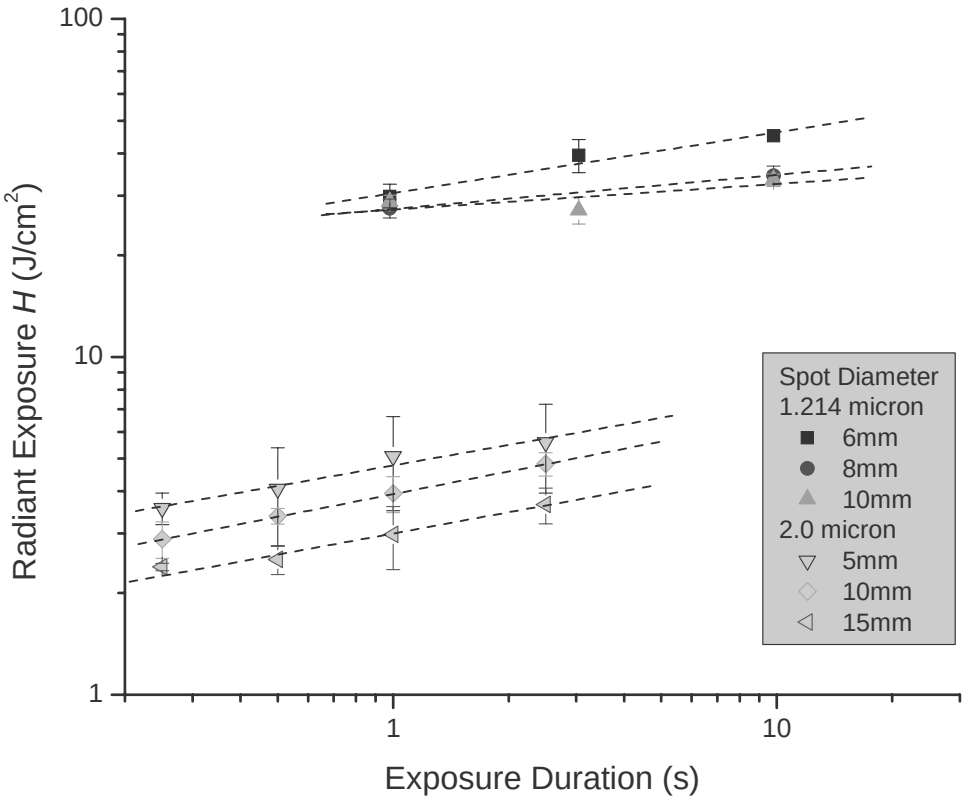

Figure 7.3. Comparison of threshold average radiant exposures for 2.0 and 1.214 μm laser irradiations. Dash lines represent power law fitting curve for each spot diameter.

Figure 7.2 shows that threshold radiant exposures at 1.214 μm are approximately 7 times larger than values at 2.0 μm with the same laser exposure duration and spot size. The thermal damage was estimated using a rate process model which is a integral of a temperature function. The damage parameter Ω, which indicates the level of damage, was computed using:

$$\Omega(r,z) = A\int_0^{\infty} e^{-\frac{E_0}{RT(r,z,t)}} dt\,, \tag{7.2}$$

where A is the molecular collision frequency factor, E_0 is denaturation activation energy, and R is the universal gas constant (Henriques 1947). Therefore, theoretically, the thermal-induce injury in skin could be predicted if skin thermal and optical properties are known. Table 7.4 lists the major absorbers in skin at 1.214 and 2.0 μm. Apparently, the absorption coefficient of skin at 1.214 μm is much smaller than it at 2.0 μm. However, on the other hand, at 1.214 μm, there is significant scattering ($\mu'_s \approx 27$ cm^{-1}) (Du, Hu et al. 2001). Because of the scattering, the fluence rate just under the surface is greatly increased and thus results a higher temperature rise than the value calculated based on Beer's law (Welch and vanGemert 1995).

Table 7.4. Absorption coefficients of various constitutes in skin at 1.214 and 2.0 μm. [cm^{-1}]

Wavelength (μm) / constitutes in skin	1.214	2.0
Water	1.0	69.1
Fat	2.0	2.2
Melanin*	31.4	5.5

*: Absorption coefficients estimated based on an empirical equation $\mu_a = 1.7 \times 10^{12} \times \lambda[\text{nm}]^{-3.48}$ (Jacques, Newman et al. 1991).

In 2001, Y Du et al. measured the collimated/diffuse transmittance and diffuse reflectance of *in vitro* porcine skin dermis samples and used Monte Carlo simulations to inversely determine the absorption coefficient, scattering coefficient and anisotropy factor of the dermis samples in the spectral range from 900 to 1500 nm (Du, Hu et al. 2001). Their data shows that: At 1.214 μm wavelength, the dermal absorption coefficient (μ_a) is about 2 cm^{-1}, and scattering coefficient is (μ_s) 270 cm^{-1} with an

anisotropy factor (g) 0.9. In contrast, the dermal optical properties at 2.0 μm have been discussed in chapter 5: dermal absorption coefficient is about 58 cm^{-1}, while scattering is neglectable (Chen, Thomsen et al. 2006).

Diffusion theory for a semi-infinite slab with mismatched refractive indices and collimated incidence shows that the normalized fluence rate $\bar{\phi}_t$ (fluence rate ϕ_t / input irradiance $(1\text{-}r_{ce})E_0$) can be calculated by:

$$\bar{\phi}_t(z) = \frac{5-r_{21}}{1-r_{21}+2\left(\frac{\mu_a}{\mu_{eff}}\right)(1+r_{21})}\exp(-\mu_{eff}z) - 2\exp(-\mu_t z) \quad (7.3)$$

where $\mu_{eff} = \{3\mu_a[\mu_a + (1-g)\mu_s]\}^{1/2}$ and r_{21} is a reflection factor at the interface of two media (Welch and vanGemert 1995). Figure 7.3 compares the normalized fluence rate $\bar{\phi}_t$ at 1.214 and 2.0 μm. At 2.0 μm, since scattering is neglectable, $\bar{\phi}_t$ is described simply by using Beer's law:

$$\bar{\phi}_t(z) = \exp(-\mu_t z) = \exp(-\mu_a z) \quad (7.4)$$

However, due to the strong scattering at 1.214 μm, the maximum $\bar{\phi}_t$ could be four times bigger than it at 2.0 μm.

To simplify the analysis, we ignore heat diffusion in the following discussion. Therefore, the temperature rise by laser irradiation is estimated by:

$$\Delta T = \frac{(1-r_{ce})E_0\,\bar{\phi}_t\mu_a}{\rho C}\,t \quad (7.5)$$

where μ_a (@2.0 μm) ≈ 58 cm^{-1} ; μ_a (@1.214 μm) ≈ 2 cm^{-1} , and $(\bar{\phi}_t)_{max}$ @1.214 μm ≈ 4 × $(\bar{\phi}_t)_{max}$ @2.0 μm

Therefore, the ratio of temperature rise by 2.0 and 1.214 μm irradiations with the same irradiance (E_0) estimated using the above equation is:

$$\Delta T\,(@2.0\ \mu m) \approx 7.25 \times \Delta T\,(@1.214\ \mu m) \quad (7.6)$$

That is to say, in order to generate the same temperature rise to induce injury in skin, radiant exposure at 1.214 μm needs to be 7.25 times larger than it at 2.0 μm. This

value is close to the ratio of threshold average radiant exposures at these two wavelengths.

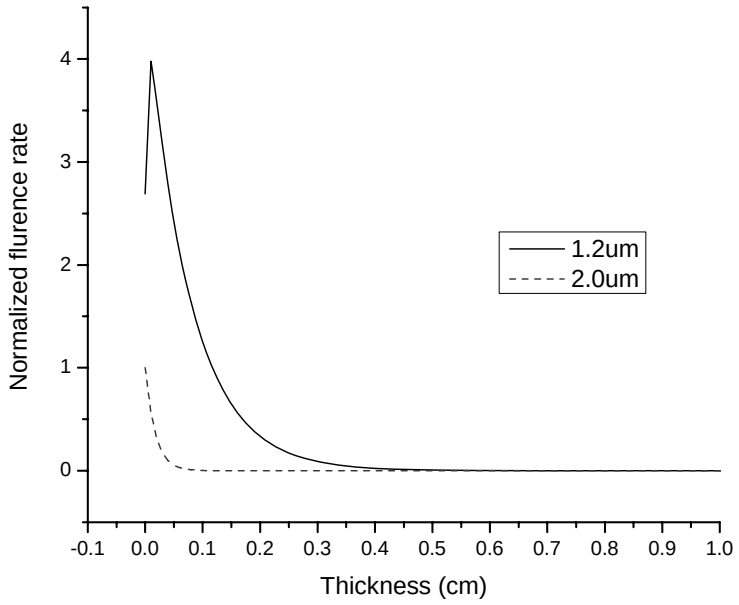

Figure 7.4. Comparison of normalized fluence rates at two wavelengths. 1.214 μm curve is calculated based on diffuse theory, 2.0 μm curve is based on Beer's law.

7.6. CONCLUSION

Experiments were conducted to measure the threshold powers for minimal visible lesion at three large spot sizes (6, 8, and 10 mm diameters) and three exposure durations (1, 3, 10 seconds) by 1.214 μm wavelength laser irradiation. We calculated the MPE from ANSI standards for this wavelength at the exposure duration used in the experiments and concluded that the safety factors are from 3.4 to 5.4 for all test conditions, which are about 2-3 times smaller than the traditional value of 10 in MPE determination. Therefore, decreased MPE values should be considered for spot sizes larger than 3.5 mm.

Three pigs with noticeable skin color differences were tested with same exposure conditions to examine the possible melanin effect in determination of skin damage threshold. None of the threshold results from each pig skin showed any evidence that the density of melanin affected threshold results beyond experimental uncertainties.

The 1.214 μm thresholds were compared with results at 2.0 μm. The data indicated that threshold radiant exposure at 1.214 μm were about 7 times larger than it at 2.0 μm with the same spot size and exposure duration. The difference was explained by the much larger absorption but smaller scattering at 2.0 μm than those at 1.214 μm.

7.7. REFERENCES

Altshuler, G. B., R. R. Anderson, et al. (2001). "Extended theory of selective photothermolysis." Lasers in Surgery and Medicine **29**(5): 416-432.

Anderson, R. R., W. Farinelli, et al. (2006). "Selective photothermolysis of lipid-rich tissues: A free electron laser study." Lasers in Surgery and Medicine **38**(10): 913-919.

Anderson, R. R. and J. A. Parrish (1983). "Selective Photothermolysis - Precise Microsurgery by Selective Absorption of Pulsed Radiation." Science **220**(4596): 524-527.

ANSI (2000). ANSI Z136.1-2000, American National Standard for Safe Use of Lasers. Orlando, FL, Laser Institute of America, American National Standards Institute.

Chen, B., D. C. O'Dell, et al. (2005). "Porcine skin ED50 damage thresholds for 2,000 nm laser irradiation." Lasers Surg Med **37**(5): 373-81.

Chen, B., S. L. Thomsen, et al. (2006). "Modeling thermal damage in skin from 2000-nm laser irradiation." J Biomed Opt **11**(6): 064028.

Du, Y., X. H. Hu, et al. (2001). "Optical properties of porcine skin dermis between 900 nm and 1500 nm." Physics in Medicine and Biology **46**(1): 167-181.

Finney, D. J. (1971). Probit Analysis 3rd ed. New York, Cambridge University Press.

Friedman, M. (1940). "A comparison of alternative tests of significance for the problem of m rankings." The Annals of Mathematical Statistics **11**(1): 86-92.

Henriques, F. F. (1947). "Studies of thermal injury V: The predictability and the significance of thermally induced rate processes leading to irreversible epidermal injury." Arch. of Pathol. **43**: 489-502.

Jacques, S. L. and D. J. Mcauliffe (1991). "The Melanosome - Threshold Temperature for Explosive Vaporization and Internal Absorption-Coefficient during Pulsed Laser Irradiation." Photochemistry and Photobiology **53**(6): 769-775.

Sliney, D. H., J. Mellerio, et al. (2002). "What is the meaning of threshold in laser injury experiments? Implications for human exposure limits." Health Physics **82**(3): 335-347.

Welch, A. J. and M. J. C. vanGemert (1995). Optical-thermal response of laser-irradiated tissue. Chapter 17: Rate processs analysis of thermal damage. New York and London, Plenum Press.

Chapter 8. Corneal Minimal Visible Lesion Thresholds for 2.0 μm Laser Radiation

8.1. ABSTRACT

To support refinement of the Maximum Permissible Exposure safety limits, a series of experiments were conducted *in vivo* on Dutch Belted rabbit corneas to determine corneal minimum visible lesion thresholds for 2.0 μm continuous-wave laser irradiation. Single pulse radiant exposures were made at specified pulse durations of 0.1, 0.25, 0.5, 1.0, 2.0 and 4.0 seconds for spot $1/e^2$ diameters of 1.17 mm and 4.02 mm. Threshold lesions were defined as the presence of a superficial surface whitening one hour after irradiation. Temperature measurements indicated that threshold peak temperatures were dependent upon spot size and exposure duration. The exposure duration dependence of threshold average radiant exposure was described by an empirical power law equation: Threshold radiant exposure[J/cm^2] = a × exposure duration[s] ^{b}.

8.2. INTRODUCTION

The eye and skin are the most susceptible parts of the body to accidental laser irradiation and due to the importance of vision to the quality of life, eye hazards are by far the more important consideration for safety. Wavelengths greater than 1.4 μm are primarily absorbed in the cornea and aqueous humor with insignificant energy reaching the retina. Since the absorption coefficient of cornea at 2.0 μm has been reported to be 45.9 cm^{-1} (Maher 1978), approximately 90% of the irradiation delivered to the anterior surface of the human cornea is absorbed within an average central thickness of 520 μm.

Early safety studies for wavelengths beyond 1.4 μm investigated CO_2 laser radiation of the cornea at 10.6 μm (Peabody, Zweng et al. 1969; McCally, Bargeron et al. 1983; Zuclich, Blankenstein et al. 1984; Bargeron, Deters et al. 1989; McCally and Bargeron 2001), where the 1/e penetration depth was approximately 10 μm (Maher

1978). Bargeron et al. found that most of the CO_2 radiation was absorbed with in the 50 μm thick human corneal epithelium (Bargeron, Deters et al. 1989). In 1992, McCally et al. reported corneal damage thresholds for Tm:YAG laser radiation (2.02 μm) on New Zealand white rabbits (McCally, Farrell et al. 1992). The laser spot diameter was approximately 1 mm and exposure durations were 0.082 sec, 0.235 sec and 4.28 seconds. Based on the very little experimental data and mainly on the extrapolation of CO_2 threshold data, the American National Standard for Safe Use of Lasers (ANSI Z136.1-2007 (ANSI 2007)) defined the Maximum Permissible Exposure (MPE) for the eye at wavelengths between 1.8 μm and 2.6 μm and laser exposures from 1.0 ms to 10.0 s (listed in Table 8.1):

Table 8.1. Maximum permissible exposure (MPE) for corneal exposure to a laser beam (From ANSI Z136.1-2000).

Wavelength(μm)	Exposure Duration, t (s)	MPE (J cm^{-2})	Limit Aperture Diameter (mm)
1.800 to 2.600	10^{-3} to 0.3	0.56 $t^{0.25}$	1.0
	0.3 to 10	0.56 $t^{0.25}$	1.5 $t^{0.375}$

A recent threshold damage study of skin to 2.0 μm laser irradiation suggested that the current laser safety standard may need to be adjusted for spot diameters larger than 3.5 mm (Chen, O'Dell et al. 2005). Therefore, this study was conducted to provide large spot size thresholds for the cornea to 2.0 μm laser irradiation.

Safety standards are specified in terms of the MPE which is typically defined as a factor of ten below the ED50 damage threshold for retinal hazards(Sliney, Mellerio et al. 2002). The largest safety factors of an order of magnitude were intended for small retinal exposures where there was an enormous level of uncertainty. Since irradiation of the skin or eye to levels at the published MPE values may be “uncomfortable”, it is good practice to maintain exposure levels sufficiently below the MPE(ANSI 2007). In this paper, we

report the corneal minimal visible damage thresholds for two spot diameters and exposure duration from 0.1 sec to 4 seconds and describe the thermal response of the cornea to laser irradiation. These results may help refine current ANSI MPE values.

8.3. MATERIAL AND METHODS

8.3.1. Experimental Setup

A rack mountable thulium fiber optic CW laser (IPG Photonics Corporation; Oxford, MA; Model: TLR-20-2000-LP) with a maximum 20 W output at a wavelength 2.0 μm provided the source of CW irradiation. A small fraction of the incident laser power was reflected onto a powermeter (Molectron Detector, Inc.; Portland, OR; Model: EPM2000 with an air-cooled powermeter probe PM30) using a beam splitter. Telescopes were employed to generate collimated laser beams with desired spot diameters. A low power alignment beam (fiber optic stable source 600nm-700nm; OZ optics, Ltd; Canada) was injected into the 2.0 μm beam path using a beam combining cube. Co-alignment of the two laser beams was accomplished at the cornea plane and at an intermediate aperture by adjustment of the position of the alignment laser fiber mount with respect to the combining cube. An iris shutter system (Uniblitz, Inc.; Rochester, NY; Model VMM-T1) was used to control exposure duration. Laser power was controlled by adjusting the current setting on the control panel of the laser. After energizing the laser, a settling time prior to corneal exposure was allowed until a stable power meter reading was obtained. A pulse generator (Stanford Research Systems. Inc; Sunnyvale, CA; Model DG535) was used to trigger the iris shutter system as well as a function generator (Hewlett-Packard, Ltd; Model HP 33120A), which controlled the imaging rate of an IR array detector thermal camera (Phoenix^{TM} DAS camera system, Indigo, CA). The IR camera employed a 320 x 256 InSb array which detected wavelengths between 3 μm and 5 μm. The IR

camera began capturing infrared images 0.1 second before laser irradiation, and continued recording for about 7 seconds after the laser was turned off. The imaging rate of IR camera was set at 100 Hz. The measurement system was arranged as depicted in Figure 8.1. The telescope, IR mirror and the IR camera were mounted together to ensure all burn sites were located at a fixed distance from the laser for the same spot size. Temperature calibration for the IR camera was done by using a blackbody radiator before laser irradiations. Power calibration of the reference was accomplished prior to and following each day in which laser exposures were delivered. The power meter used for calibration (Molectron Detector, Inc.; Portland, OR; Model: PM-3) was placed in the plane of the cornea and at least fifteen measurements, spanning the operational range used in testing for that day, were collected prior to corneal exposure. Normal incidence to the cornea for the 2.0 μm laser was assured by incorporating a video camera, co-imaged with the IR camera at the corneal plane. First (anterior cornea) and second surface (posterior cornea) specular reflections from the visible alignment laser were imaged on a video monitor using the video camera. When first and second surface reflections overlapped at the detector plane of the video camera, constructive interference was observed on the monitor and the incident beam was deemed normal to the corneal surface. To facilitate this alignment, fine positioning of the cornea was accomplished with the use of a goniometric animal stage which had 5-1/2 axes of adjustment.

Two different laser spot sizes were employed. The laser beam profiles were measured using a beam profiler (Pyrocam I; Spiricon, Inc; Logan, UT) and were confirmed by a measurement of temperature distribution on a plastic plate prior to heat conduction (Chen, O'Dell et al. 2005). Moreover, beam diameters were checked with the knife-edge method (Siegman, Sasnett et al. 1991). All measurements indicated that the

laser beam profiles were nominally Gaussian with 1/e2 diameters of 1.17 mm and 4.02 mm for the two telescope settings.

Average radiant exposure [J/cm2] reported in this paper was calculated as the applied laser energy divided by the $1/e^2$ spot area rather than 1/e spot area used in some laser safety classifications. The peak radiant exposure for our near Gaussian profile was twice the average value.

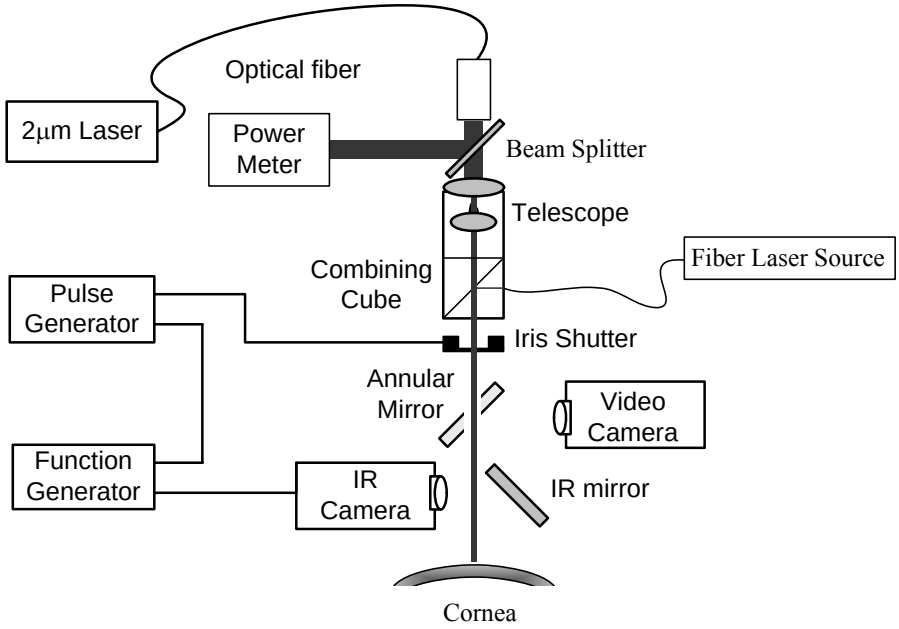

Figure 8.1. Experimental configuration for corneal damage study.

8.3.2. Animal

Rabbit cornea is an established animal model for determining laser damage thresholds with infrared radiation. Seventeen Dutch Belted rabbits of either sex weighting 2.14-2.36 kg were used in this study. The animal use protocol was approved by the Institutional Animal Care and Use Committee at the University of Texas at Austin. The rabbits were chemically restrained using 20-40 mg/kg ketamine and 3-5 mg/kg xylazine ,

intramuscularly (IM). Two drops each of 0.5% proparacaine hydrochloride (Bausch and Lomb) and 5% homatropine hydrobromide (Alcon), were administered to both eyes for analgesia, cycloplegia and pupillary dilation. Anesthesia was maintained with isoflurane (1.5-3%) inhalant anesthesia. Isoflurane was supplemented by acepromazine (0.5-1.0 mg/kg) administered intramuscularly as needed for individual rabbits demonstrating a high intolerance to isoflurane. Prior to corneal laser exposures and once again after the completion of corneal irradiations, the animal was transported to a surgical table for slit lamp (Topcon; Paramus, New Jersey; Model: SL6E) examination. Once inhalant anesthesia was induced, the animal was physically secured in the sternal position on a specially designed adjustable animal stage to facilitate precise laser exposure. One hour prior to termination of isoflurane, buprenorphine 0.01-0.05 mg/kg was administered IM. Oxygen saturation and pulse, heart and respiration rate were continuously monitored throughout the study.

Eyelids of the rabbits were held open with a wire-lid speculum, and moisture of the cornea was maintained by frequent irrigation with 0.9% buffered saline solution at room temperature. In order to create a reproducible tear film, the irrigation was stopped 1 minute prior to laser exposure and the excess fluid was blotted at the limbus. Thermal measurement showed that the corneal surface returned to its normal temperature before the time of exposure.

On several animals, fluorescein sodium drops (0.25%) and benoxinate HCl (0.4%) ophthalmic solution (Alcon Laboratories, Ft. Worth, TX) were applied topically to the cornea to enhance lesion visibility during the slit lamp examination. Excess dye was flushed using buffered saline solution. A blue-wavelength pass filter was used with the slit lamp to enhance visibility of epithelial damage sites which were stained by the fluorescent dye.

After completion of the final examination, the subject was euthanized and the eyes were enucleated. Sutures were placed in the nasal and superior aspects of the enucleated eye to mark orientation for histological sectioning. Enucleated eyes were stored in formalin (10% buffered) and preserved for histology.

8.3.3. Damage Determination

At least two examiners evaluated all exposure locations acutely and approximately one-hour post irradiation. In addition, twenty-four hour examinations were conducted for selected laser conditions. A grade of "yes" or "no" was recorded acutely and a numerical grade as described below was assigned at the one and twenty-four hour examinations.

Grade 0, no visible damage;

Grade 1, superficial damage minimally visible without magnification;

Grade 2, readily apparent lesion on surface with some circular symmetry;

Grade 3, severe lesion, circular symmetric opacity with shrinking of epithelium at the center.

Digitized video and still frame photography was used to document the exposure of the cornea and post exposure slit-lamp examination respectively. Probit analysis (Finney 1971) was conducted to estimate ED50 damage thresholds. Data points (damage/no damage for each condition) were entered into the probit statistical analysis package (Lund, B., Probit Fit Dose-Response Data Analysis Program, Version 1.02, U.S. Army Medical Research and Material Command, Hazards Research Branch) to calculate the ED50 values.

8.3.4. Experimental Procedures

After anesthetized rabbits were secured upon the animal stage, reflections from the cornea surface were observed on the video camera and the rabbit's position was adjusted within the FOV of the video camera until the angle of incidence of the co-aligned laser beams at the cornea was determined to be zero (i.e., normal approach). Constructive interference observed at the video monitor between first surface and second surface corneal reflections was used as an indication of "good alignment". Once alignment was established, the eye was irrigated with saline solution and one minute passed before laser irradiation. Power readings from the reference power meter were obtained at the time of corneal exposure. Thermal imagery was automatically recorded for each exposure. The thermal video was observed after each exposure to verify stability of the eye. Radiant exposures were made at specified exposure durations of 0.1 sec, 0.25 sec, 0.5 sec, 1 sec, 2 sec and 4 seconds for spot diameters of 1.17 mm and 4.02 mm. The number of irradiations for each of the 12 spot size-exposure duration conditions was 8 - 33 with an average of 20 per condition. The variation in laser power provided sufficient data points for probit analysis of damage/no damage response as a function of power. After each laser exposure the test location was examined to evaluate the presence or absence of corneal lesions with the aid of an overhead surgical light. A lesion was recorded as a "yes" if both readers identified it as positive. The consensus "yes" or "no" response of the observers was recorded on the data sheet. If consensus of the two observers could not be reached on damage a note of "questionable" was recorded on the data sheet and a third reader was used to give final decision based on slit lamp observation 1 hour later. This align-expose-examine procedure was repeated until all accessible corneal locations using the adjustable animal platform were exhausted. Nominally nine exposure locations were tested on each cornea with the 1.17 mm

diameter beam and five were tested with the 4.02 mm beam. Practically the number of accessible corneal locations was limited by eye movement during testing which led to a disorganized grid pattern thus limiting the available corneal area for testing.

8.3.5. Corneal Emissivity Measurement

The IR images taken by the IR camera during laser irradiation were converted to temperature reading on the corneal surface. In order to obtain precise temperature readings, it was necessary to measure the emissivity of cornea within the camera's 3-5 μm sensitivity bandwidth. It was assumed that the IR camera reading (N) was directly proportional to the received radiation power (P). The total received radiation power (P) originated from three source terms:

1) Emission from the object = $\varepsilon TRP(\mathrm{T_{obj}})$, where ε was the emissivity of the object, T was the transmittance of the atmosphere, R was the reflectance of the IR mirror, $P(\mathrm{T_{obj}})$ was the radiation power of an ideal black body at object temperature $\mathrm{T_{obj}}$. T and R are constant through all the temperature measurements.

2) Reflected emission from ambient source = $(1\text{-}\varepsilon)TRP_{\mathrm{refl}}$, where $(1\text{-}\varepsilon)$ was the reflectance of the object. P_{refl} was the total radiation power from surrounding environment.

3) Emission from the surroundings, such as atmosphere, IR mirror, and etc. These out-of-focus signals were insignificant and ignored in this measurement.

Therefore, the total received radiation power was:

$$P_{tot} = \varepsilon TRP(\mathrm{T_{obj}}) + (1-\varepsilon)TRP_{refl}\,. \qquad [\mathrm{W}] \tag{8.1}$$

Since the IR camera reading N was directly proportional to the received radiation power, the IR camera reading N_{tot} was described as:

$$N_{tot} = \varepsilon N(\mathrm{T_{obj}}) + (1-\varepsilon)N_{refl}\,, \tag{8.2}$$

where $N(T_{obj})$ represented the camera reading of an ideal black body at object temperature T_{obj}, and N_{refl} was the camera reading of an ideal reflector.

Electrical tape (3M Scotch® 33+ electrical tape) with a known emissivity of 0.95 was placed on the corneal surface. Pressure was applied around the tape to ensure good thermal contact at the corneal surface. At least 10 minutes were given for the tape to reach temperature equilibrium with the cornea. Before taking IR images, warm saline irrigation ensured that both the corneal and tape surfaces reached the same temperature. When irrigation was stopped, fluid was blotted at the limbus and several IR images of the cornea including the tape were taken by the IR camera. The IR camera reading N_{cor} (corneal image reading) and N_{tape} (tape image reading) were described as:

$$\begin{aligned} N_{tape} &= 0.95N(T_{tape}) + (1-0.95)N_{refl} \\ N_{cor} &= \varepsilon N(T_{cor}) + (1-\varepsilon)N_{refl} \end{aligned}, \tag{8.3}$$

where $N(T_{tape})$ and $N(T_{cor})$ represented the camera reading of an ideal black body at the temperature of the tape and cornea respectively. Since $T_{tape} = T_{cor}$, $N(T_{tape}) = N(T_{cor})$ and the emissivity of cornea was calculated by:

$$\varepsilon = 0.95\frac{N_{cor} - N_{refl}}{N_{tape} - N_{refl}}. \tag{8.4}$$

An ideal reflection (N_{refl}) estimate was obtained from the IR image of a crumpled aluminum foil ($\varepsilon<0.1$) placed in the plane of the cornea . The camera reading of N_{foil} was set equal to N_{refl}.

8.4. RESULTS

8.4.1. Corneal Emissivity

In order to measure the corneal emissivity, IR images were taken on two rabbit corneas on which Scotch™ 33 electrical tape was attached. Ten *in vivo* measurements

were conducted for each eye. One cornea (cornea 1) was at a room temperature of 25 ^{o}C. Corneal surface temperature was controlled by warm saline irrigation, varying from 30^{o}C to 38^{o}C. The same procedure was conducted on another corneal surface (cornea 2) at a room temperature of 19 ^{o}C and corneal surface temperatures varying from 27^{o}C to 33^{o}C. Measurements gave consistent emissivity values of 0.83±0.02 and 0.82±0.02 for cornea 1 and cornea 2 respectively. Therefore, 0.83 was selected as the corneal emissivity in temperature conversion from IR images.

8.4.2. ED50 Damage Threshold Power

The effect of each irradiation was evaluated acutely by visual observation of the eye and the final determination of lesion formation was made using a slit lamp at 1 hour post exposure. For some selected laser conditions, twenty-four hour evaluations were conducted to examine the damage at post exposure interval longer than 1 hour. The grossly apparent minimal visible lesion was defined as the presence of a superficial surface whitening at 1 hour after irradiation (see figure 8.2a)). At the threshold level, the barely visible opaque lesions were smaller than the Gaussian beam diameter. The threshold lesion sizes were measured roughly using slit lamp images. These diameters ranged from 0.3 mm - 0.6 mm (0.4 ± 0.12 mm) and 0.8 mm - 1.1 mm (1.0 ± 0.12 mm) for the 1.17 mm and 4.02 mm spot sizes respectively.

The ED50 threshold powers and standard deviations for 1-hour post exposure are listed in Table 8.2 along with their fiducial limits and slopes of the probit curves. The "standard deviation" (σ) was derived from the probit fit curve using the definition:

$$\sigma = (ED_{84} - ED_{16})/2, \tag{8.5}$$

where ED_{84} represented the dose for 84% probability of laser-induced damage, and similarly for ED_{16}. Fiducial limits were calculated at the 95% confidence level. Slope of the probit curve was defined as:

$$\text{Slope} = \frac{\delta p}{\delta d}, \tag{8.6}$$

where δp was the probability change and δd was the dose change (Finney 1971).

Table 8.2. The ED50 threshold power [mw] and standard deviation associated with their fiducial limits and probit curve slopes.

t (s) / D(mm)	4	2	1	0.5	0.25	0.1
1.17	73.2 ± 0.8* (73.2–73.2)** slope 217.7 #	87.6 ± 1.9 (87.6–87.6) slope 211.2	114.9 ± 5.1 (114.9-114.9) slope 52.4	116.5 ± 1.1 (116.5-116.5) slope 250.1	154.1 ± 3.6 (154.1-154.1) slope 200.8	236.1 ± 2.7 (236.1-236.1) Slope 200.3
4.02	303.6 ± 3.5 (303.6-303.6) slope 207.6	402.4 ± 48.6 (402.4-402.4) slope 19.0	538.2 ± 60.8 (446.0-585.9) slope 20.3	788.1 ± 5.5 (788.1-788.1) slope 328.7	1209.0 ± 23.1 (1153.3-1251.0) slope 120.3	2272.8 ± 45.2 (2272.8-2272.8) slope 115.1

*: ED50 threshold power [mw] ± standard deviation.

**: fiducial limits at the 95% confidence level.

#: the slope of probit curve.

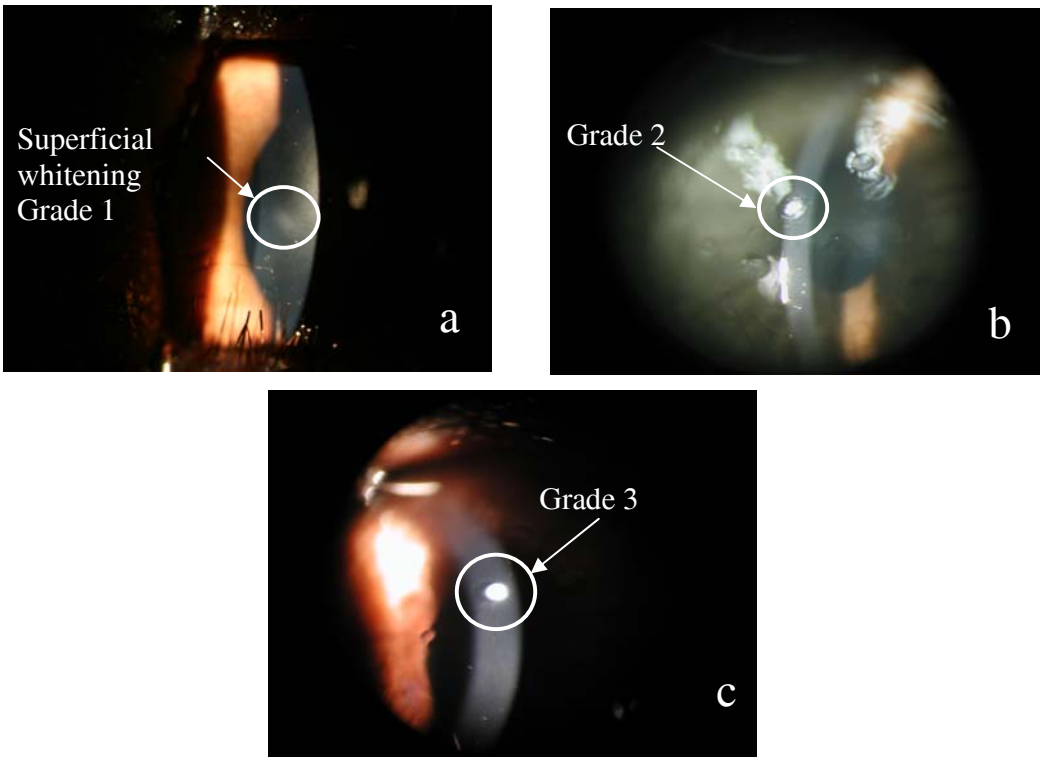

Figure 8.2. Slit lamp images of thermal damage at 1 hour post exposure. a) spot diameter 4.02 mm, exposure duration 0.5 s, power 789.7 mW (approximately equals threshold power). Grade 1 was assigned as the severity of the lesion. This superficial surface whitening was defined as threshold lesion. b) spot diameter 1.17 mm, exposure duration 0.25 s, power 181 mW (approximately 1.2 times threshold power). Grade 2 was assigned. c) spot diameter 1.17 mm, exposure duration 0.25 s, power 231.2 mW (approximately 1.5 times threshold power). Grade 3 was assigned.

8.4.3. Peak Temperature Response

An example of the linear fit of peak temperature rise as a function of laser power is presented in Figure 8.3. Base line temperatures were approximately 32 $^{\circ}C$. Peak temperature rise is defined as the maximum temperature rise at the irradiation center on the cornea relative to the initial cornea temperature at the start of radiation. Because of the Gaussian shape of the laser beam, peak temperature represents the temperature at the irradiation center. Table 8.3 lists the slopes of linear fits of peak temperature rise with respect to power for all the laser spot size-exposure duration combinations. Examples of

transient peak temperature response for a 2.0 seconds irradiation duration at 1.17 mm and 4.02 mm spot diameters are compared in Figure 8.4. The respective powers were 93.2 mw (threshold power:87.6 mW) and 412.4 mw (threshold power:402.4 mW). These powers correspond to the first experimental points above the respective ED50 damage thresholds of Table 8.2.

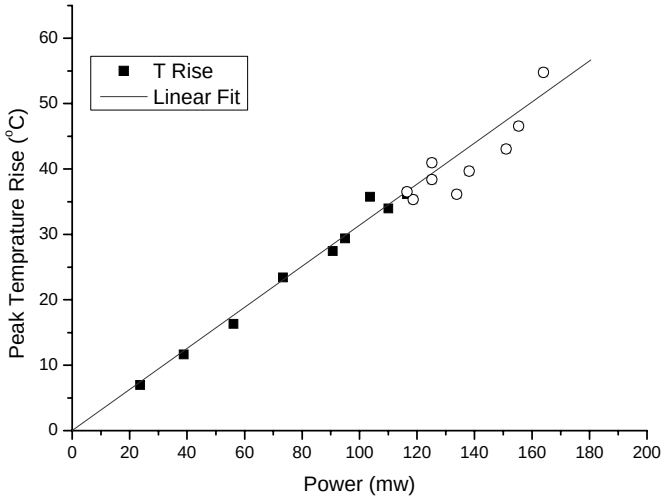

Figure 8.3. An example of the linear fit of peak temperature rise versus power. Laser condition: 1.17 mm spot diameter, 0.5 s exposure duration. Circles represent damage observed on cornea after laser irradiation.

8.4.4. Peak Temperature at the Spot Center for Threshold Irradiation

A range of peak temperatures at the spot center associated with threshold thermal damage was found. The range for peak temperatures at the center associated with threshold damage was determined from the maximum temperature at which no damage was observed compared to the minimum temperature at which damage was consistently observed. Ranges of peak temperatures at the center for various threshold laser conditions are compared in Table 8.4. Due to the non-uniform laser beam profile (i.e. Gaussian profile) on cornea, the peak temperature at the spot center does not represent the actual

threshold temperature that is associated with the boundary between normal and significant thermal damaged cornea.

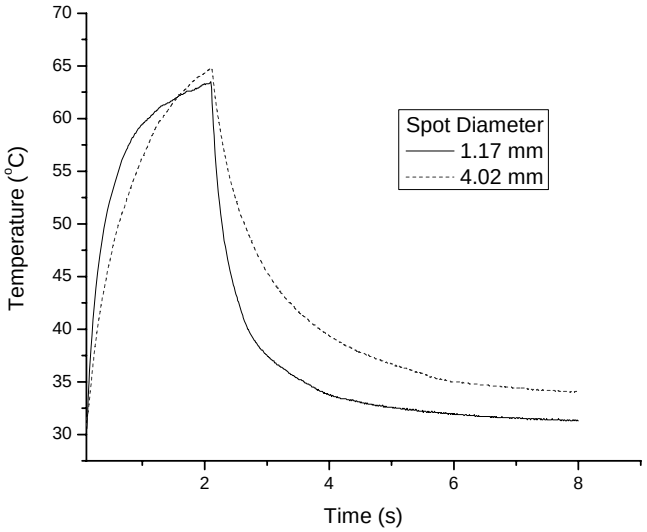

Figure 8.4. Comparison of transient peak temperature responses by threshold power irradiation at 1.17 mm and 4.02 mm spot diameters. Solid line: 2.0 s exposure duration, 93.2 mW power (threshold power:87.6 mW); Dash line: 2.0 s exposure duration, 412.4 mW power (threshold power:402.4 mW).

Table 8.3. The Slopes of the linear fits of peak temperature rise with respect to power. (i.e., Peak temperature rise [^{0}C] = Slope * Irradiated power [mw])

t (s) / D (mm)	4	2	1	0.5	0.25	0.1
1.17 mm	0.418	0.382	0.338	0.303	0.235	0.157
4.02 mm	0.102	0.087	0.075	0.049	0.029	0.016

Table 8.4. Peak temperature at the spot center for threshold irradiation: (^{0}C)

t (s) / D (mm)	4	2	1	0.5	0.25	0.1
1.17	54.2-57.0*	62.7-63.5	63.5-70.0	65.0-69.2	65.4 - 71.7	69.0-74.1
4.02	60.5-61.0	62.5-66.2	66.0-72.4	67.1-69.5	64.6-68.9	71.4-72.4

*: Ranges of peak temperatures at the spot center for threshold irradiation is defined as: Maximum peak temperature with consistent absence of damage - Minimum peak temperature with consistent presence of damage.

8.5. DISCUSSION

Most of the one hour threshold lesions were still visible 24 hours after exposure. However, some barely visible superficial lesions disappeared. No new lesions were observed at 24 hours. All one hour threshold lesions were included in our evaluation of threshold. Damage threshold evaluated at one hour may give slightly more conservative threshold values than at 24 hours. As laser power was increased beyond threshold, readily apparent surface lesions with somewhat circular symmetry were seen. More severe lesions with circular symmetric opacity and shrinking of epithelium at the center were observed at powers around 1.5 times threshold. In this case, dehydration and coagulation of corneal epithelium as well as denaturization of corneal stroma occurred (see figure 8.2). In 1992, McCally *et al.* studied the corneal damage thresholds for Tm:YAG laser radiation (2.02 μm) on new Zealand white rabbits (McCally, Farrell et al. 1992). Based on their histopathlogic study of corneal threshold lesions, McCally *et al* claimed that the threshold damage was confined to the epithelium and no obvious stromal abnormalities were present (McCally and Bargeron 2003; McCally, Bargeron et al. 2005). Our observation of 2.0 μm threshold lesions using a slit lamp also suggested that the corneal opacity was present in a very thin layer, most probably only in the epithelium. Qualitative and quantitative histopathologic study of corneal damage will be performed to determine the mechanisms of laser induced damage and map the extent and severity of the lesions to confirm this conclusion.

Generally, the small standard deviations of threshold powers, closeness of lower and upper fiducial limits and sharp slopes of the probit curves indicated that the damage thresholds were well defined with a little overlap between exposures that produce damage and those that do not. The larger spot size (4.02 mm) had more uncertainty in damage thresholds than 1.17 mm spot at most of the exposure durations. The observational

uncertainties of barely visible whitening on the corneal surface was more notable for the larger spot size (4.02 mm diameter). These threshold lesions appeared much more superficial and fainter than threshold lesions associated with the 1.17 mm spot size.

Typically, non uniform beam profiles are specified as 1/e diameter rather than $1/e^2$ to give more conservative radiant exposures to compare to published MPE values in the laser safety classification. The radiant exposures based on 1/e diameter are twice as large as the $1/e^2$ diameter radiant exposure for a Gaussian beam. Although 1/e diameter is a conservative estimation of the laser hazard classification, $1/e^2$ diameters must be used to truly evaluate laser damage thresholds which require average irradiance. All calculations in this paper are based on the $1/e^2$ definition of spot size. The average radiant exposure (H) is calculated as:

$$H = \frac{J}{\pi r^2}, \qquad [\mathrm{J/cm^2}] \tag{8.7}$$

where J is the threshold energy and r is the $1/e^2$ radius of the laser spot.

In Figure 8.5, the 2.0 μm threshold radiant exposures are compared with the single-pulse damage thresholds that were determined for Tm:YAG laser (2.02 μm wavelength) radiation by McCally *et al* (McCally, Farrell et al. 1992). McCally *et al.* studied the corneal damage thresholds for Tm:YAG laser radiation (2.02 μm) on new Zealand white rabbits. Threshold average radiant exposures were determined as 4.23 $\mathrm{J/cm^2}$ and 29.6 $\mathrm{J/cm^2}$ for 1.33 mm $1/e^2$ spot diameter and exposure durations of 0.235 sec and 4.28 seconds respectively (McCally, Farrell et al. 1992; McCally, Bargeron et al. 2005). The slightly higher threshold values at 2.02 μm wavelength than our experimental results for 2.0 μm laser at 1.17 mm spot size are mainly due to the smaller absorption coefficient of cornea at 2.02 μm. Water is the primary absorber around the 2-μm

wavelength, the absorption coefficient of cornea can be estimated by the product of absorption coefficient of water and the water content of cornea:

$$\mu_a = \mu_{water} \times w, \quad [1/\text{cm}] \tag{8.8}$$

where μ_{water} is the absorption coefficient of water, which is 69.12 cm^{-1} at 2.0 μm and 55.99 cm^{-1} at 2.02 μm wavelength (Hale and Querry 1973), and *w* is the water content of the cornea, approximately equals 0.78 for the rabbit (Maurice 1984). Therefore, corneal absorption coefficients are estimated to be 53.91 cm^{-1} and 43.67 cm^{-1} at 2.0 μm and 2.02 μm wavelengths respectively. Consequently, for 2.02 μm laser radiation, more input energy is needed to achieve the same temperature rise resulting from radiant exposure at 2.0 μm. Comparing McCally's threshold results (1.33 mm spot size) at exposure duration 0.235 sec and 4.28 seconds with our corresponding results (1.17 mm spot size) at 0.25 s and 4 seconds respectively, the relative differences of threshold radiant exposures are close to 20 %, which corresponds to the percent difference in corneal absorption coefficients at these two wavelengths. A more precise analysis should consider the transient temperature profiles and the temperature dependent changes in the absorption coefficients at the water absorption peak.

An empirical power law relation of threshold radiant exposure and exposure duration was proposed by McCally *et al.* (McCally, Bargeron et al. 2005). They investigated single-pulse threshold damage on cornea at three different wavelengths (10.6 μm CO_2 laser, 2.02 μm Tm:YAG laser and 1.54 μm Er fiber laser), and suggested that the threshold radiant exposure followed an empirical power law relationship:

$$H = at^b \quad , \qquad [\text{J/cm}^2] \tag{8.9}$$

where *H* is the threshold radiant exposure, *t* is the exposure duration, *a* and *b* are two positive coefficients selected to fit the experimental data. Although the absorption coefficients for these wavelengths span nearly 2 orders of magnitude, McCally found that

the coefficient *b*'s were nearly identical at all three wavelengths. Our results confirmed the general hypothesis of equation 8.9. However when spot size was considered (see Figure 8.5) different coefficients for *a* and *b* were determined. Our power law fitting results are listed in Table 8.5.

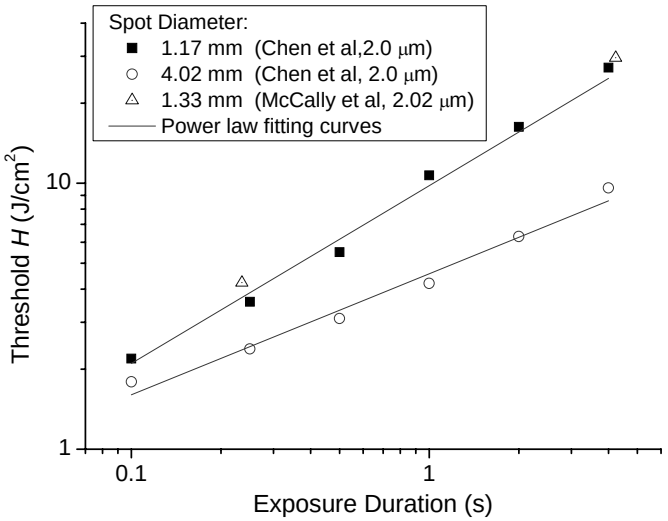

Figure 8.5. Comparison of threshold average radiant exposures along with the power law fitting curves for 1.17 mm and 4.02 mm spot sizes.

Table 8.5. The results of power-law fitting of threshold radiant exposure. ($H = at^b$)

Spot size [mm]	a [J/cm^2]	b	R (correlation coefficient)
1.17	9.79	0.669	0.98
4.02	4.57	0.456	0.97
MPE*	0.56	0.25	N/A

*: ANSI MPE definition for corneal exposure at 2.0 μm. See Table 8.1.

The light 1/e penetration depth ($\delta = 1/\mu_a$) in the cornea at 2.0 μm is approximately 180 μm and the associated characteristic thermal diffusion time for spot

diameters much larger than δ is about 250 ms (Jacques 1993). The power law relation is not valid when the exposure duration is much less than the characteristic diffusion time such that heat conduction during the laser pulse is negligible and the impulse response is a function of pulse energy and independent of pulse duration. Threshold peak temperature predicted by the damage rate process integral is only a function of the temperature decay transient at the end of the short laser pulse (Priebe and Welch 1978).

In the IR wavelength range of 1.800 to 2.600 μm, the ANSI Z136.1-2000 defined MPE as follows:

$$H_{\max} = 0.56\, t^{0.25}, \qquad [\mathrm{J/cm^2}] \tag{8.10}$$

where $H_{\max}$ is the maximum allowed radiant exposure and t is exposure duration. The ANSI standard of MPE for eye exposure to 2.0 μm laser and the experimental results of threshold average radiant exposure at various durations and spot sizes are compared in Table 8.6. A safety factor is defined as the threshold radiant exposure divided by MPE value. The safety factors calculated from experimental radiant exposures are listed in Table 8.6 as well. Dividing the empirical threshold power law equation 8.9 by MPE definition (equation 8.10), the safety factor is predicted by following equation:

$$k = \frac{a}{0.56} t^{(b-0.25)}, \tag{8.11}$$

where k is the safety factor and a and b are the power law coefficients in equation 8.11. The safety factor monotonically decreases as exposure duration decreases, and reaches 7.1 for 1.17 mm and 5.8 for 4.02 mm spot sizes at 100 ms. If equation 8.11 is extrapolated to 30 ms, the predicted safety factor is about 4 for both spot sizes. Although the safety factor is smaller than the typical choice of 10 for MPE definition, more careful consideration should be given due to the very sharp boundary and small uncertainties of damage threshold determination. The concept of a safety factor must consider the overall level of uncertainty in the threshold data, experimental detail, sources

of potential error, differences between animal and humans, and knowledge of the injury mechanisms and the biological sequelae. Although the typical safety factor is set as 10 in most cases for retinal thresholds, a smaller safety factor may be adequate for corneal MPE determination due to the small uncertainty of cornea damage (Sliney, Mellerio et al. 2002).

Table 8.6. Experimental threshold average radiant exposures [J/cm^2] and ANSI MPE values along with their safety factors.

t (s) / D (mm)	4	2	1	0.5	0.25	0.1
1.17	27.2	16.3	10.7	5.5	3.58	2.19
4.02	9.6	6.3	4.2	3.1	2.38	1.79
MPE	0.79	0.67	0.56	0.47	0.40	0.31
Safety factor, *k*	34.4(12.2)*	24.3(9.4)	19.1(7.5)	11.7(6.6)	9.0(6.0)	7.1(5.8)

*: safety factor calculated based on: 1.17 mm data (4.02 mm data)

For exposure durations shorter than 30 ms at 2 μm, absorbed energy is confined and for any spot size there is a constant threshold radiant exposure until non-thermal damage mechanisms begin to play a role.

Temperature measurements show that the corneal temperature response is proportional to the radiant energy; In other words, the energy absorbed and converted to heat in the cornea is directly proportional to the radiant energy. Table 8.6 indicates that more energy is required to induce a visible lesion as laser exposure duration is increased as a result of heat transfer from hot to cool regions during irradiation. As exposure duration is increased, a greater percent of the absorbed energy is transferred to the surrounding area. Although a decreased continuous laser power results in thermal damage, more total energy is needed to raise the cornea temperature to the critical level that induces injury. Temperature measurements show that the slope of peak temperature

rise with respect to radiant energy is smaller for longer exposure durations (calculated based on the slopes listed in Table 8.3 divided by corresponding exposure durations.).

Another feature evident from Table 8.6 is that the threshold radiant exposure decreases with increasing the spot size because of spot diameter dependent heat conduction. Theoretically, if there is no heat transfer during laser irradiation, the temperature rise on the cornea is linearly proportional to the local radiant exposure. However, heat conduction cannot be ignored for durations longer than the characteristic thermal diffusion time, which is applicable for these experiments. The light 1/e penetration depth (δ) is approximately 180 μm and the associated characteristic thermal diffusion time for spot diameters much larger than δ is about 250 ms (Jacques 1993). The radial distribution of the 4.02 mm spot diameter radiant exposure is much flatter than that of 1.17 mm spot size. For 4.02 mm spot irradiation, heat energy is primarily conducted along axial direction rather than radial direction. However, since the 0.585 mm spot radius is comparable with the light 1/e penetration depth (0.18 mm), heat flow along axial and radial directions are both significant for the 1.17 mm spot size. Therefore, less heat energy is confined within the radiated area compared to the 4.02 mm spot size, consequently a higher radiant energy is needed to induce injury.

Thermal injury is considered to depend upon time and temperature. A standard rate process model is typically used to predicted tissue thermal damage:

$$\Omega(x,y,z,t) = \int_0^t A e^{-\left[\frac{E_0}{RT(x,y,z,t')}\right]} dt', \tag{8.12}$$

where Ω is a dimensionless damage parameter, t is time, A is the pre-exponential frequency factor, E_0 [J/mol] is an energy barrier molecules surmount in changing from a native state to denatured, R [J/mol K] is the gas constant and T [K] is the temperature (Moritz and Henriques 1947). The damage parameter Ω indicates the level of thermal

injury. Although more energy is required to generate a lesion on cornea for longer laser exposure durations, the peak temperature at the spot center for threshold irradiations in inverse proportion to exposure duration (see Table 8.4). According to the rate process model (see Equation 8.12), a longer exposure duration is associated with a lower temperature rise which requires a lower irradiance. Table 8.4 indicates that the peak temperatures at the spot center for threshold irradiation at 4.02 mm spot size are higher than 1.17 mm spot size, especially for longer exposure durations (i.e. 2.0 seconds and 4.0 seconds). In this case, not only the peak temperature but also the transient profile of the temperature response are important factors in the damage rate process model (Equation 8.12). Figure 8.4 illustrates two transient temperature curves at the spot center resulting from slightly above ED50 threshold irradiations for 1.17 mm and 4.02 mm spot sizes. The associated irradiances are 8.67 W/cm^2 and 3.25 W/cm^2 respectively. Because of the much larger irradiance of the small spot, the initial slope of the center temperature is much larger (~2.7). However the diffusion time is smaller for the small spot relative to the large spot, which rapidly decreases the slope of the temperature transient. For a continuous irradiation, the large spot would have a higher steady state temperature (see trend in Figure 8.4).

Although the peak temperature provides an important aspect of the temperature trait on the cornea, it does not necessarily represent the actual threshold temperature that is associated with the boundary between normal and significant thermally-damaged tissue. Therefore, the real threshold temperature should be measured at the boundary of normal and abnormal cornea surface. Threshold lesions induced by the 4.02 mm irradiation were about 1.0 mm in diameter which is larger than the 0.4 mm lesions produced with the 1.17 mm spot size. Unfortunately, the gross measurement of the lesion size on cornea surface was too rough to be used for retrieving accurate temperature

profile at damage boundary. To achieve precise lesion size, quantitative histopathologic study of corneal damage will be performed to map the extent and severity of the lesions. The corresponding temperature at the lesion boundary may help to find the threshold temperature associated with threshold damage for the cornea.

In addition to observational uncertainty, experimental uncertainties included measurement error in spot diameter and laser power as well as exposure duration. Laser beam spatial profiles measured by a beam profiler were elliptical rather than circular, with the major axis about 10 % longer than the minor axis. To simplify calculations, spot diameters were estimated by arithmetically averaging the major and minor diameters. Uncertainties in calculated radiant exposure was magnified by uncertainties in spot diameter. The air-cooled power meter probe PM30 had 3% uncertainty, and the power meter EPM2000 had 1% read-out error. The iris shutter system with shutter LS6Z (Uniblitz, Inc.; Rochester, NY) used to control exposure duration at 1.17 mm spot size radiation has a 0.7 ms opening time, while VS25 shutter (Uniblitz, Inc.; Rochester, NY) used for 4.02 mm spot size setting had a 3 ms opening time. In conclusion, there was about 4% uncertainty in power measurements and 14% uncertainty in calculated radiant exposure.

8.6. CONCLUSION

We have defined and determined the *in-vivo* minimal visible threshold lesions on Dutch Belted rabbit corneas to 2.0 μm continuous-wave laser irradiation at six specified exposure durations (0.1 s - 4.0 s) and two spot sizes (1.17 mm and 4.02 mm in diameter). Threshold lesions were defined as the presence of superficial surface whitening one hour post irradiation. A power law relation between threshold radiant exposure and exposure duration was evaluated for different spot diameters: *Threshold radiant exposure*[J/cm^2] =

$a \times exposure\ duration[\text{s}]^{b}$. Coefficient a was 9.79 and b was 0.669 for the 1.17 mm spot diameter; values of a and b were 4.57 and 0.456 respectively for the 4.02 spot diameter. Based on the empirical power laws, safety factors at 2.0 μm compared to the ANSI standard were predicted to have a minimum limit of four for both 4.02 mm and 1.17 mm spot diameters. Due to the very sharp boundary and small uncertainties of damage threshold determination, it is suggesting that a factor of 4 "padding" is adequate and the safety standard may not need to be changed.

Temperature measurements indicated that peak temperature at spot center for threshold irradiation were dependent upon spot size and exposure duration. Peak temperature at spot center for threshold irradiation was lower for longer exposure durations. Radiation with 4.02 mm spot diameter had slightly higher threshold peak temperature than 1.17 mm spot diameter.

8.7. ACKNOWLEDGMENT

Opinions, interpretations, conclusions, and recommendations are those of the authors and are not necessarily endorsed by the University of Texas, the United States Air Force or the Department of Defense.

The authors wish to thank Dr. Robert J. Thomas, Andrew Cummins, Victor Villavicencio, Kathyrn Starr and Jennifer Cassaday for their kind help.

8.8. REFERENCES

ANSI (2007). ANSI Z136.1-2007, American National Standard for Safe Use of Lasers, Laser Institute of America, Orlando, FL American National Standards Institute.

Bargeron, C. B., O. J. Deters, et al. (1989). "Epithelial damage in rabbit corneas exposed to CO2 laser radiation." Health Phys **56**(1): 85-95.

Chen, B., D. C. O'Dell, et al. (2005). "Porcine skin ED50 damage thresholds for 2,000 nm laser irradiation." Lasers Surg Med **37**(5): 373-81.

Finney, D. J. (1971). Probit Analysis, Cambridge University Press, New York

Hale, G. M. and M. R. Querry (1973). "Optical constants of water in the 200nm to 200µm wavelength region." Appl. Opt. **12**: 555--563.

Jacques, S. L. (1993). "Role of Tissue Optics and Pulse Duration on Tissue Effects during High-Power Laser Irradiation." Applied Optics **32**(13): 2447-2454.

Maher, E. J. (1978). Transmission and absorption coefficients for ocular media of the rhesus monkey. Report SAM-TR-78-32. San Antonio, Texas, Brooks Air Force Base.

Maurice, D. M. (1984). The cornea and sclera. In The Eye.3rd ed., Davson H, editor. Orlando, Florida, Academic Press.

McCally, R. L. and C. B. Bargeron (2001). "Epithelial damage thresholds for multiple-pulse exposures to 80 ns pulses of CO2 laser radiation." Health Phys **80**(1): 41-6.

McCally, R. L. and C. B. Bargeron (2003). "Corneal epithelial injury thresholds for multiple-pulse exposures to Tm : YAG laser radiation at 2.02 mu m." Health Physics **85**(4): 420-427.

McCally, R. L., C. B. Bargeron, et al. (2005). "Laser eye safety research at APL." Johns Hopkins Apl Technical Digest **26**(1): 46-55.

McCally, R. L., C. B. Bargeron, et al. (1983). "Stromal damage in rabbit corneas exposed to CO2 laser radiation." Exp Eye Res **37**(6): 543-50.

McCally, R. L., R. A. Farrell, et al. (1992). "Cornea epithelial damage thresholds in rabbits exposed to Tm:YAG laser radiation at 2.02 microns." Lasers Surg Med **12**(6): 598-603.

Moritz, A. R. and F. C. Henriques, Jr. (1947). "Studies of thermal injury: II. The relative importance of time and surface temperature in the causation of cutaneous burns." Am J Pathol **23**: 695-720.

Peabody, R. R., C. Zweng, et al. (1969). "Threshold damage from CO2 lasers." Arch Ophthalmol **82**(1): 105-7.

Priebe, L. A. and A. J. Welch (1978). "Asymptotic Rate Process Calculations of Thermal Injury to Retina Following Laser Irradiation." Mechanical Engineering **100**(5): 100-100.

Siegman, A. E., M. W. Sasnett, et al. (1991). "Choice of Clip Levels for Beam Width Measurements Using Knife-Edge Techniques." Ieee Journal of Quantum Electronics **27**(4): 1098-1104.

Sliney, D. H., J. Mellerio, et al. (2002). "What is the meaning of threshold in laser injury experiments? Implications for human exposure limits." Health Phys **82**(3): 335-47.

Zuclich, J. A., M. F. Blankenstein, et al. (1984). "Corneal damage induced by pulsed CO2 laser radiation." Health Phys **47**(6): 829-35.

Chapter 9. *In Vivo* Optical Properties Measurement Using Photothermal Radiometry and Diffuse Reflectance

9.1. ABSTRACT

An experimental setup combining pulse photothermal radiometry (PPTR), an IR detector and diffuse reflectance measurement (DR) with an integrating sphere provided a system for simultaneously estimating absorption and reduced scattering of *in vivo* tissues. Purely absorbing phantoms with no scattering and turbid phantoms with both absorption and scattering were used to validate the system. Tests were conducted on *in vivo* human skin with various pigmentation. The skin absorption coefficient measured at 585 nm wavelength was strongly dependent on melanin density. The absorption and reduce scattering coefficients for human skin determined from PPTR and DR measurements were comparable to *in vitro* results from literature.

9.2. INTRODUCTION

Determination of tissue optical properties is fundamental for application of light in either therapeutic or diagnostic procedures. measurements of optical properties can lead to optical diagnostic tools (Peters, Wyman et al. 1990), improvements in laser surgery (Jacques 1992), quantitative determination of chromophore(Patterson, Schwartz et al. 1989) and fluorophore concentration (Gardner, Jacques et al. 1996), drug pharmacokinetics (Braichotte, Wagnieres et al. 1995), and improvements in photodynamic therapy (PDT) dosimetry (Jacques 1989).

Laser propagation in a turbid tissue is governed by scattering (scattering coefficient μ_s, anisotropy factor g) and absorption (absorption coefficient μ_a). Experimental determination of these optical properties has been proposed using different methodologies, such as integrating sphere (Prahl, Vangemert et al. 1993), frequency-domain diffuse reflectance (Sevick, Chance et al. 1991), time-domain diffuse reflectance

(Patterson, Chance et al. 1989), optoacoustics (Oraevsky, Jacques et al. 1997), and spatially resolved steady-state diffuse reflectance (Farrell, Patterson et al. 1992).

A method using the thermal response was employed in this research to measure the absorption coefficient of *in vivo* skin at 2.0 μm where scattering was neglectable (see Chapter 5). However, at laser wavelengths below 1.4 μm where scattering cannot be ignored, this method must be adjusted to include diffuse scattering inside the tissue.

An method is explored for measuring *in vivo* optical properties by combining pulse photothermal radiometry (PPTR) and diffuse reflectance (DR) measurements. Under conditions of insignificant heat conduction (exposure duration, t_0 << diffusion time (τ)) the peak temperature for very short pulses or the slope of temperature *vs*. time provides a fluence rate dependent measure of the absorption coefficient, μ_a

$$\Delta T(r, z=0, t) = \frac{\phi(z=0^+)\mu_a t}{\rho C} \tag{9.1}$$

where ϕ is the fluence rate just below the surface. ϕ is approximately equal to the fluence $E_0(1\text{-}r_{ce})$ when light scattering is insignificant. E_0 is the irradiance on the surface and r_{ce} is specular reflectance. Using $E_0(1\text{-}r_{ce})$ for ϕ defines an upper bound for the absorption coefficient. The diffuse reflectance measurement provides a method for correcting μ_a and estimating μ_s', the reduced scattering coefficient [$\mu_s' = \mu_s(1-g)$]. The total diffuse reflectance, R_d, is the fraction of the incident flux which is remitted through the irradiated surface. For an optically homogenous, semi-infinite tissue volume irradiated by a collimated beam, R_d is a function of μ_a, μ_s and g, and surface refractive mismatch, n_{rel}. For high reduced albedo (a' >0.5), the value of R_d depends only on the reduced albedo, a', and n_{rel}. Diffusion theory shows that (Flock, Patterson et al. 1989; Flock, Wilson et al. 1989):

$$R_d = \frac{a'}{\{1+2k(1-a')+(1+\frac{2k}{3})\sqrt{3(1-a')}\}} \tag{9.2}$$

where a', the transport albedo, is given by:

$$a' = \frac{\mu_s'}{\mu_s' + \mu_a} \tag{9.3}$$

and:

$$k = \frac{1+r_d}{1-r_d} \tag{9.4}$$

where r_d is the internal reflection coefficient for diffuse light. For index mismatching at the surface, empirical relations between r_d and the relative index of refraction n_{rel} have been derived by Groenhuis *et al* (Groenhuis, Ferwerda et al. 1983; Groenhuis, Tenbosch et al. 1983)

$$n_{rel} = \frac{n_{tissue}}{n_{exterior\ medium}} \tag{9.5}$$

$$r_d = -1.440 n_{rel}^{-2} + 0.710 n_{rel}^{-1} + 0.668 + 0.0636 n_{rel} \tag{9.6}$$

In 1989, Anderson et al. used a heuristic argument based on the internal reflection of backscattered photons at the surface boundary to relate the surface fluence rate with the diffuse reflectance, their result was (Anderson, Beck et al. 1989):

$$\phi(z=0^+) = E_0(1-r_{ce})(1+2kR_d) \tag{9.7}$$

for wide area irradiation.

In this chapter, An experimental setup was designed with a combination of PPTR and DR measurements. It provided a system for simultaneously measuring temperature and diffuse reflectance which yielded absorption and reduced scattering coefficients. Furthermore, since both the PPTR and DR measurements were conducted on sample surfaces, it was feasible to apply this technique for non-invasive *in vivo* tissue properties measurement. A simple test was conducted on human skin and discussed in this chapter.

9.3. MATERIAL AND METHODS

9.3.1. Experimental Setup:

A lens coupled fiber optics dye pulse laser (Candela SPTL-1) with adjustable output energy and a maximum 10 J output at a wavelength 585 nm was used to irradiate sample surfaces. The pulse duration was approximately 450 microseconds at FWHM. A small fraction of the incident laser energy was reflected using a beam splitter onto an energy-meter (Molectron Detector, Inc.; Portland, OR; Model: EPM2000 with an air-cooled energy-meter probe J25). The first several pulses were blocked until stable energy meter readings were obtained. A two inches diameter lens was used to project a collimated 6-mm diameter laser spot on the sample surface. In front of the input-port of a integrating sphere (Labsphere, Inc) was a dichroic mirror which transmitted visible light and reflected most of MIR and FIR wavelengths radiation. The sample-port of the integrating sphere was placed on top of the sample surface. An air-cooled energy-meter probe was tightly attached at the signal-port of the integrating sphere to record energy of diffuse reflected light (air-cooled energy-meter probe J25; with EPM2000 energy-meter; Molectron Detector, Inc.; Portland, OR). Infrared radiation was detected by a liquid-nitrogen cooled HgCdTe detector (Fermionics Corp. Model: PV-11-1) which detected wavelengths between 2 and 11 μm with peak sensitivity at 10 μm. A low noise current preamplifer (Standard research system. Model SR570) was used to amplify the signal from HgCdTe detector and output to a 500MHz digitizing oscilloscope (Tektronix. Model TDS640A). The field of view of the detector was defined by 1 inch diameter CaF_2 lens with a germanium filter (long-pass filter with cut-on wavelength of 1800nm) in front to eliminate the interface of scattered input light. The experimental setup was arranged as depicted in Figure 9.1.

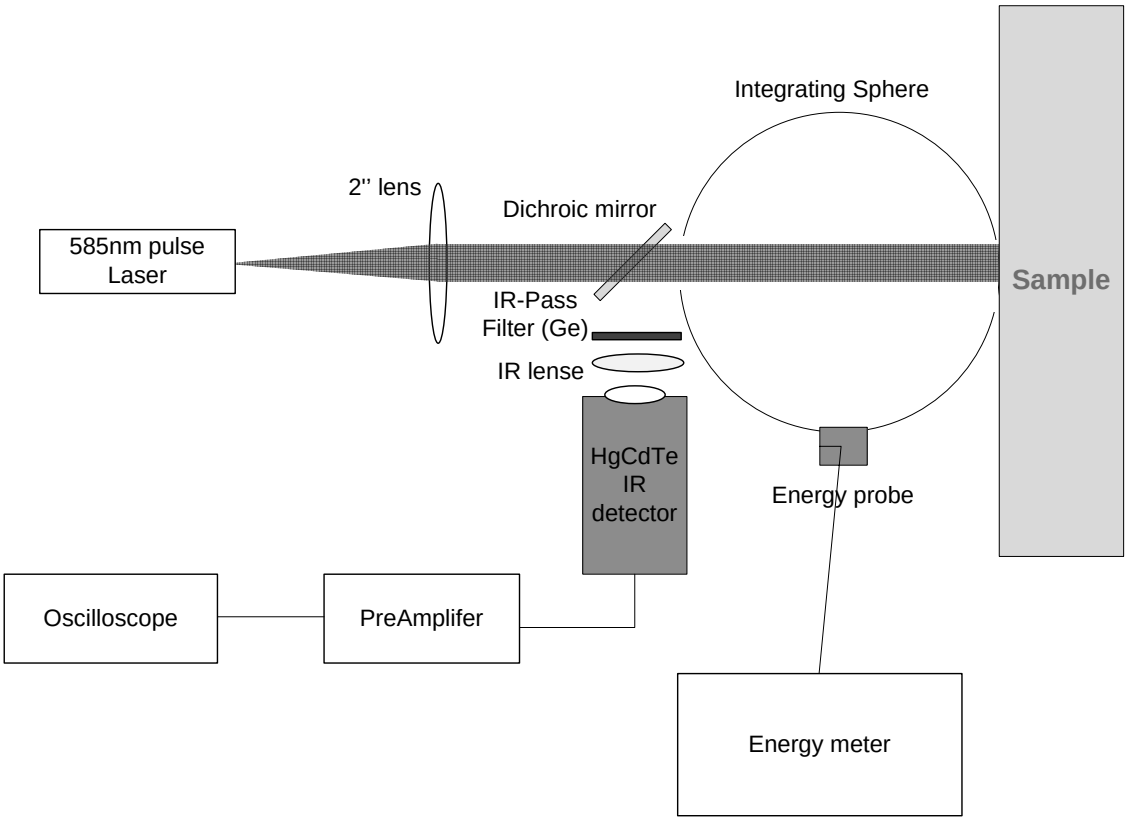

Figure 9.1. Schematic of experimental setup.

9.3.2. Sample Preparation

Aqueous 3% gelatin phantoms with about 8-mm thickness were made in 35-mm diameter petri dishes and used in experiments within 2 hours after solidification. Systematically varying amounts of an absorbing dye (Blue food color, Crown Colony Corp.) and/or scattering particles (1-μm Latex microsphere, Duke scientific Corp.) were added into the phantom to produce purely absorbing or turbid tissue phantoms. Quantitative dilution was made to provide absorption coefficients in the phantoms ranging from 0.2 cm^{-1} to 60 cm^{-1} at 585 nm. The absorption coefficients at 585 nm were obtained by using a spectrophotometer. Due to the sensitivity of the spectroscopy, concentrated dye phantom solutions with absorption coefficients beyond 10 cm^{-1} were

quantitatively diluted into a volume of water before measurement. A series of turbid phantoms were made by quantitatively adding various amount of scattering particles with a constant absorption coefficient.

9.3.3. Experimental Procedure

A series of tissue phantoms were used to test the system. Fresh phantoms made within 2 hours were placed against the 2-cm diameter sample-port of a integrating sphere. At least five measurements were made for each phantom. The infrared signal remitted at the sample surface was detected using a HgTdTe detector and recorded on an oscilloscope. At the same time, reflected light from the sample was measured by a energy probe at a signal-port of the integrating sphere. The specular component of the reflectance projected out of the input-port and thus was eliminated from the diffuse reflectance measurement. A series of reflectance standards (Labsphere Inc.) with diffuse reflectance values ranging from 2% to 99% were used for calibration. Laser energy was adjusted below 1 J to prevent melting tissue phantoms. No change was observed on phantom surface after experiments.

Once phantom measurements were completed, the system was used to measure temperature and diffuse reflectance *in vivo* using four subjects. A simple test was conducted on *in vivo* human skin using this system. Four human subjects with noticeable skin color difference (shown in Figure 9.5) were measured. The subjects were comfortably seated during the measurements. The back of hand was placed against the sample-port of the integrating sphere. Five measurements were conducted on each hand. Time intervals between each measurement were large enough to make sure the skin temperature went back to normal before each irradiation.

9.4. RESULTS

9.4.1. Temperature Calibration

Temperature calibration for the HgCdTe detector was done by using a blackbody radiator at the sample-port of the integrating sphere before laser irradiations (Figure 9.2). The calibration was done over the temperature range from 28 to 43 ^{o}C which covers the range of temperatures tested in the experiments. The main goal was to determine the slope of the detector output versus temperature to convert measured transient signal induced by optical excitation of the samples to temperature reading on surface. As indicated in Figure 9.2, the slope was nearly constant, at 0.147 V/^{o}C within temperature range 28-43 ^{o}C.

9.4.2. Absorbing Tissue Phantom Measurement

A series of phantoms with absorption coefficients ranging from approximately 0.2 cm^{-1} to 60 cm^{-1} at 585 nm were used to test the system. The homogenous phantoms were made by adding quantitatively diluted dye without any scattering particles. Diffuse reflectance from these absorbing phantoms was less than 3%. Absorption coefficients were confirmed by spectrophotometer measurements. The linear fit of absorption coefficients versus temperature rise is demonstrated in Figure 9.3. The linear fit of experimental results gives:

$$\text{Temperature jump } (T) \approx 0.22 \times \text{absorption coefficient} \tag{9.8}$$

The value of ρC for the phantoms was 4.2 [J/cm^3 ^{o}C].

9.4.3. Turbid Tissue Phantom Measurement

A series of turbid tissue phantoms with constant absorption coefficient were made by adding various amount of scattering particles in tissue phantoms with same concentration of absorbing dye. For samples with a given concentration of absorbing

dye, increasing amounts of scattering particles results in a proportionate increase of both diffuse reflectance and temperature jump on the surface. the relative temperature jumps (T/T_0) versus diffuse reflectance from a series of turbid phantoms with constant absorption and various scattering is illustrated in Figure 9.4. A linear fit was attempted to give a relation between temperature rise and diffuse reflectance:

$$T / T_0 = 1.09 + 6.36 \times R_{\mathrm{d}} \tag{9.9}$$

where T is the measured temperature jump in turbid phantoms, T_0 is the measured temperature jump in a absorbing phantom with same absorption coefficient but no scattering. R_{d} is the measured diffuse reflectance.

The differences of specular reflectance, emissivity, refractive index between skin and tissue phantom were smaller than 5%, to simplify the analysis, these difference were neglected for the following discussion. Therefore,

$$\mu_a = \frac{T_0}{[\frac{\phi(z=0^+)t}{(\rho C)_{skin}}]} = \frac{T}{[\frac{E_0(1-r_{ce})t}{(\rho C)_{skin}}](1+2kR_d)} \tag{9.10}$$

Considering the slope of a linear fit to the phantom data in figure 9.3 by $\frac{E_0(1-r_{ce})t}{(\rho C)_{phantom}} = 0.22$ and using the theoretical values of 2.85 for k. $(\rho C)_{phantom}/(\rho C)_{skin} \approx 1.08$, based on a value of $(\rho C)_{skin} \approx 3.89$ [J/cm^3 ^{o}C] for human skin. Therefore,

$$\mu_a = \frac{4.21T}{(1+5.7R_d)} \tag{9.11}$$

The reduced scattering coefficient was derived from the absorption coefficient and the transport albedo *a*' which was obtained from equation 2 based on the diffuse reflectance value. The measured diffuse reflectance and temperature jump for each subject is shown in Table 9.1. The calculated skin optical properties (absorption coefficient and reduced scattering coefficient) are listed in Table 9.1 as well. Published

values of human absorption and reduce scattering coefficients at 585 nm are shown in Table 9.2.

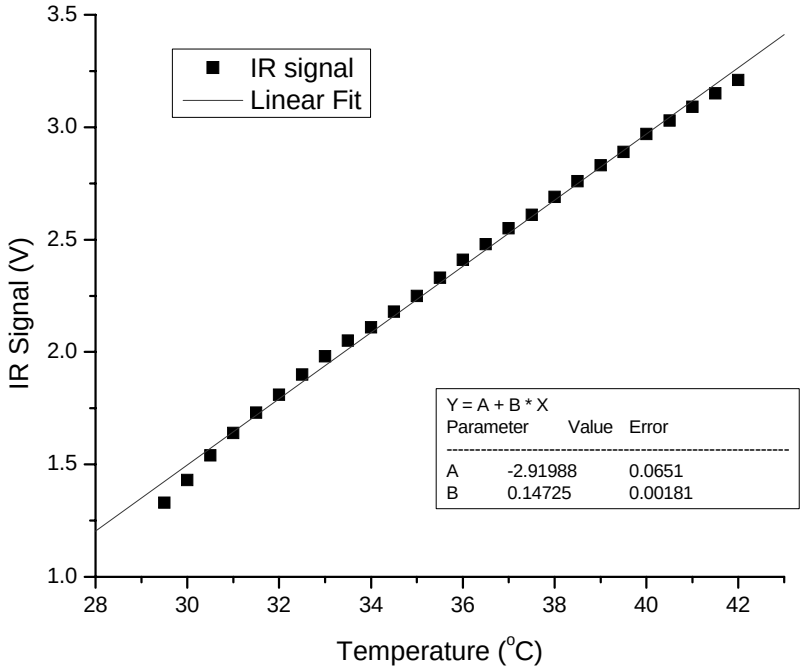

Figure 9.2. HgCdTe detector calibration curve by using a blackbody radiator.

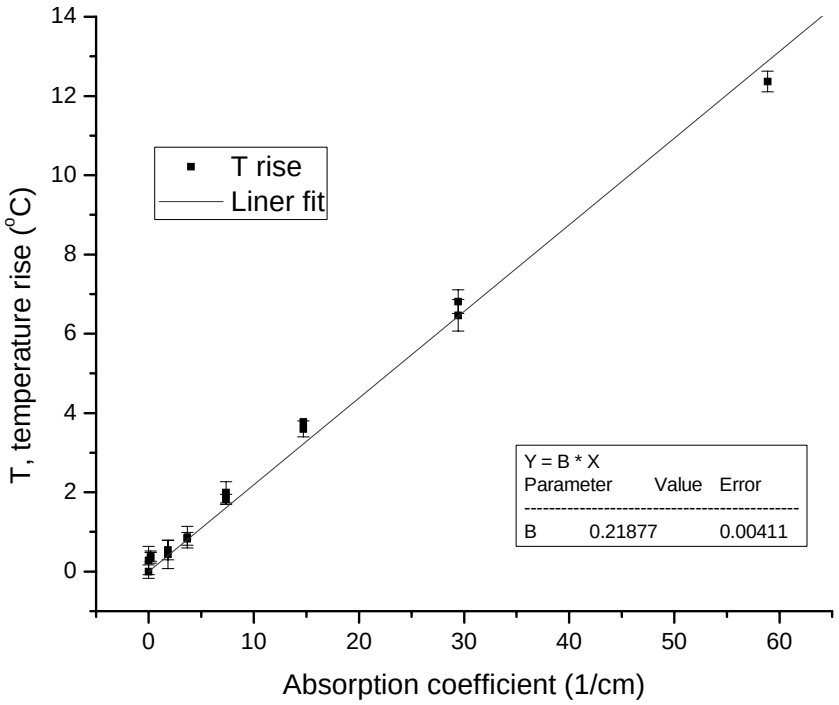

Figure 9.3.Temperature jump for homogeneous absorbing gels with various absorption coefficients. Linear fit $T = 0.22 \times \mu_a$ (absorption coefficient).

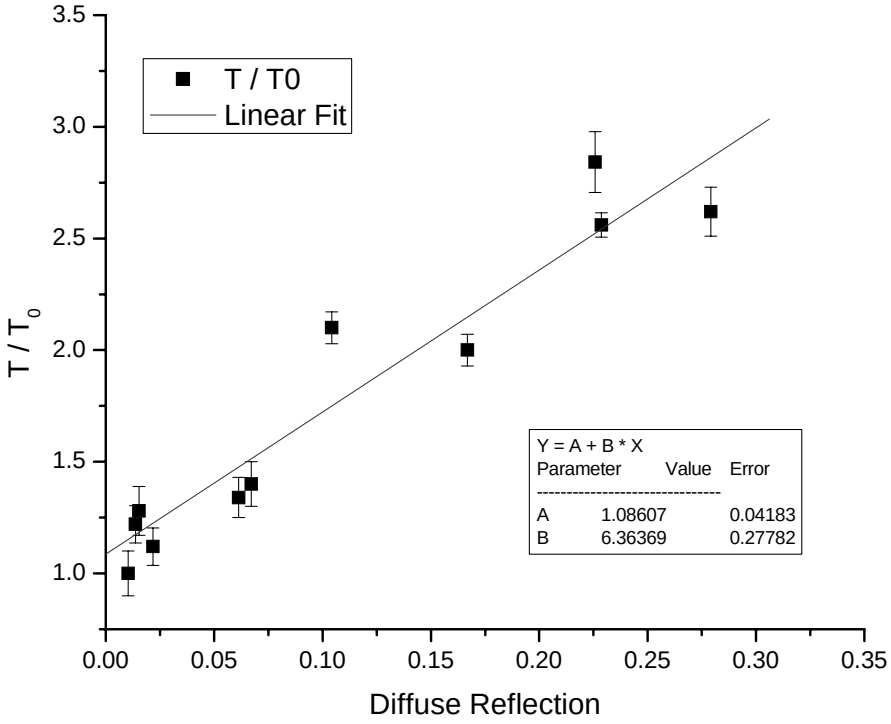

Figure 9.4. Increase in temperature rise measured by HgCdTe detector in turbid gels as a function of diffuse reflectance R_d at a laser wavelength of 585 nm. T: measured temperature jump in turbid gels. T_0: measured temperature jump in a absorbing gel with same absorption coefficients but no scattering. The linear fit shows that: $T/T_0 = 1.09 + 6.36 \times R_d$

9.5. DISCUSSION

In theory, for a laser pulse much shorter than the thermal confinement time, the temperature jump produced by the laser pulse in a homogeneous absorber is:

$$T = [\frac{\phi(z = 0^+)t}{\rho C}]\mu_a \tag{9.12}$$

where ϕ is approximately equal to the fluence $E_0(1\text{-}r_{ce})$ when light scattering is insignificant. E_0 is the irradiance on the surface and r_{ce} is specular reflectance. Physically, an IR detector (i.e. a HgCdTe detector in this experiment) measures infrared radiation

emitted from within the sample at depths comparable to $1/\bar{\delta}$, where $\bar{\delta}$ is an average absorption coefficient of the sample over the wavelengths of the IR detection band. Therefore, the measured temperature jump in photothermal radiometry is reduced by a factor of ($\bar{\delta}$ /($\bar{\delta}$ + μ_a)), where μ_a is the absorption coefficient for the sample at the irradiation wavelength. The value of μ_a' for the tissue phantom was about 850 cm^{-1} by weighted integration of the absorption coefficient for water over the spectral response of the HgCdTe detector used in the experiment. For small value of μ_a (less than 85 cm^{-1}) , this effect is negligible. Figure 9.3 shows a linear fit of temperature rise measured from IR detector versus absorption coefficients of tissue phantoms with absorption coefficients less than 60 cm^{-1}. The correlation coefficient of the linear fit is 0.998. Moreover, the slope of the linear fit curve gives a systematical coefficient which is a function of irradiance E_0 and exposure duration t:

$$slope = [\frac{\phi(z=0^+)t}{\rho C}] = [\frac{E_0(1-r)t}{\rho C}] \tag{9.13}$$

The photothermal radiometry of turbid phantoms clearly shows that scattering strongly increases the fluence rate just below the surface and thus results a higher temperature jump in the sample of a given absorption coefficient. Anderson et al. proposed a relation between the surface fluence rate and the diffuse reflectance, their result was:

$$\phi(z=0^+) = (1-r_{ce})E_0(1+2kR_d) \tag{9.14}$$

Therefore, the temperature jump was noted to vary with diffuse reflectance as follows:

$$\frac{T}{T_0} = (1+2kR_d) \tag{9.15}$$

where T is the temperature jump measured in a turbid phantom with diffuse reflectance R_d at 585 nm. T_0 is the temperature jump in a phantom with the same absorption

coefficient but no scattering, k is a constant coefficient which depends on refractive index difference of the sample and external medium. For tissue phantom with refractive index of 1.34 and air as the external medium, k equals 2.85 calculated from equations 9.4, 9.5, and 9.6. Figure 9.4 shows the measured temperature jumps versus diffuse reflectance from a series of turbid phantom with a given absorption and various scattering. The linear fit shows that:

$$T/T_0 = 1.09 + 6.36 \times R_d . \tag{9.16}$$

The slope of the linear fit curve is 6.36, which is close to the theoretical value 5.7. The slightly larger value of slope may due to the absorption contributed from scattering particles added in the phantom.

Since the absorption coefficient of skin ($\bar{\delta}$) at IR detector spectra (2 -11 micron) is very large, the infrared radiation signal for PPTR measurement is obtained from a superficial layer in skin. The PPTR theory assumes skin as a homogenous tissue with uniform absorption coefficient. Therefore, the absorption coefficient derived from PPTR experiment is close to the literature value of epidermis which is on top of the skin and contributes most of the IR signal. Melanin in the epidermis and epidermis/dermal junction may contribute some IR radiation signal to the detector. The data shows that the density of melanin affects temperature jump measurement significantly and results a large increase of "absorption coefficient" derived from PPTR measurements. In contrast, the measured "scattering coefficient" only increased a little for dark skin. Back-scattered photons were from both epidermis and dermis, while melanin granules only contributed a small portion to scattering events. Therefore, the calculated "scattering coefficient" from dark skin was slightly larger than for light skin.

Table 9.1. Comparison of measured absorption and reduce scattering coefficients on human subjects with various pigmentation.

	Light skin				Dark skin			
	Subject 1		Subject 2		Subject 3		Subject 4	
	Right hand	Left hand	Right hand	Left hand	Right hand	Left hand	Right hand	Left hand
Reflection [%]	24.5 ± 0.6	23.3 ± 1.0	22.4 ± 0.7	23.0 ± 0.9	16.8 ± 0.6	15.6 ± 0.2	17.1 ± 0.1	17.9 ± 0.2
ΔT [^oC]	7.61 ± 0.37	7.44 ± 0.42	9.28 ± 0.63	9.95 ± 0.39	12.26 ± 1.02	12.17 ± 1.98	17.31 ± 1.46	17.69 ± 0.27
μ_a [cm^{-1}]	14.44 ± 0.69	14.54 ± 0.82	18.52 ± 1.25	19.54 ± 0.74	28.43 ± 2.36	29.26 ± 4.77	39.81 ± 3.33	39.81 ± 0.59
μ_s' [cm^{-1}]	96.94 ± 8.98	88.70 ± 12.59	105.46 ± 12.96	116.85 ± 13.43	99.81 ± 14.35	91.57 ± 17.04	143.98 ± 13.52	154.81 ± 5.81

Table 9.2. Absorption and reduce scattering coefficients published in literature.

Constitutes	Absorption coefficient (μ_a) [1/cm]	Reduce scattering coefficient (μ_s') [1/cm]
Epidermis [$]	18	98.7
Dermis [$]	0.24	27.1
Melanin[*]	399	N/A
Blood [$]	191	2.3

[*]: Estimated based on an empirical equation $\mu_a = 1.70 \times 10^{12}\ \lambda[\text{nm}]^{-3.48}$ (Jacques and Prahl 1987)

[$:] Data from (vanGemert, Welch et al. 1995).

We are aware of that the turbid medium PPTR and DR analysis depend on the applicability of the diffuse approximation to the material under study. The analysis discussed in this paper is just a simplified case assuming one homogenous layer. However, skin has multiply layers, consisting epidermis, dermis and hypodermis. Each layer has various optical and thermal properties. Therefore, the contribution from different layers should be considered to improve the feasibility and accuracy of this technique.

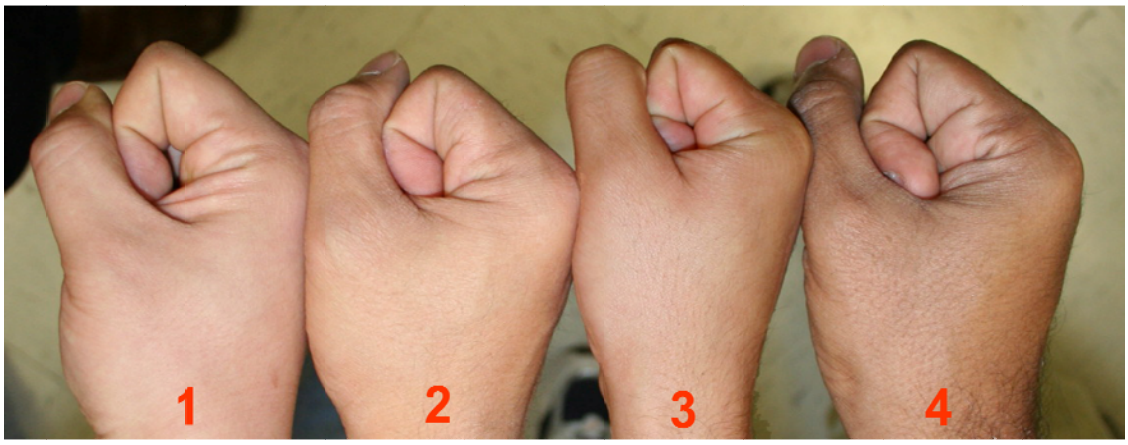

Figure 9.5. Back of hand of four human subjects with noticeable skin color difference. Subject 1 to 4: skin color from lightest to darkest.

9.6. CONCLUSION

A system combining PPTR and DR measurements was designed for non-invasive measurement of optical properties (absorption and reduced scattering coefficients) in *in vivo* tissues. A series of tissue phantoms were used to test the system. Temperature rise measured with an IR detector was linear proportional to phantom absorption coefficient when absorption coefficient was less than 60 cm^{-1}. The PPTR of turbid phantoms clearly demonstrated that scattering strongly increased the fluence rate just below the surface and thus results a higher temperature jump in the sample of a given absorption coefficient. The temperature jump was noted to vary with diffuse reflectance as follows:

$$\frac{T}{T_0} = (1 + 2kR_d)$$

where T is the temperature jump measured in a turbid phantom with diffuse reflectance R_d at 585 nm. T_0 is the temperature jump in a phantom with the same absorption coefficient but no scattering, k is a coefficient which depends on refractive index difference of the sample and external medium. The linear fitting of temperature jump

from various turbid tissue phantoms gave a *k* value of 3.18, as compared to the theoretical *k* value of 2.85 for a tissue phantom with air as external medium.

Simple tests using PPTR-DR system were conducted on *in vivo* human skin with various pigmentation. The measured *in vivo* skin absorption coefficient was strongly dependent on the melanin density. Both absorption and reduce scattering coefficients were comparable to optical properties measured *in vitro* from literature. Once the system was calibrated, μ_a and μ_s' were directly computed from values of temperature and diffuse reflectance.

9.7. REFERENCES

Anderson, R. R., H. Beck, et al. (1989). "Pulsed Photothermal Radiometry in Turbid Media - Internal-Reflection of Backscattered Radiation Strongly Influences Optical Dosimetry." Applied Optics **28**(12): 2256-2261.

Braichotte, D. R., G. A. Wagnieres, et al. (1995). "Clinical pharmacokinetic studies of photofrin by fluorescence spectroscopy in the oral cavity, the esophagus, and the bronchi." Cancer **75**(11): 2768-78.

Chen, B., S. L. Thomsen, et al. (2006). "Modeling thermal damage in skin from 2000-nm laser irradiation." J Biomed Opt **11**(6): 064028.

Farrell, T. J., M. S. Patterson, et al. (1992). "A Diffusion-Theory Model of Spatially Resolved, Steady-State Diffuse Reflectance for the Noninvasive Determination of Tissue Optical-Properties Invivo." Medical Physics **19**(4): 879-888.

Flock, S. T., M. S. Patterson, et al. (1989). "Monte-Carlo Modeling of Light-Propagation in Highly Scattering Tissues .1. Model Predictions and Comparison with Diffusion-Theory." Ieee Transactions on Biomedical Engineering **36**(12): 1162-1168.

Flock, S. T., B. C. Wilson, et al. (1989). "Monte-Carlo Modeling of Light-Propagation in Highly Scattering Tissues .2. Comparison with Measurements in Phantoms." Ieee Transactions on Biomedical Engineering **36**(12): 1169-1173.

Gardner, C. M., S. L. Jacques, et al. (1996). "Fluorescence spectroscopy of tissue: Recovery of intrinsic fluorescence from measured fluorescence." Applied Optics **35**(10): 1780-1792.

Groenhuis, R. A. J., H. A. Ferwerda, et al. (1983). "Scattering and Absorption of Turbid Materials Determined from Reflection Measurements .1. Theory." Applied Optics **22**(16): 2456-2462.

Groenhuis, R. A. J., J. J. Tenbosch, et al. (1983). "Scattering and Absorption of Turbid Materials Determined from Reflection Measurements .2. Measuring Method and Calibration." Applied Optics **22**(16): 2463-2467.

Jacques, S. L. (1989). Simple theory, measurements, and rules of thumb for dosimetry during photodynamic therapy. Photodynamic Therapy:Mechanisms, T. J. Dougherty, Ed. Proc. SPIE 1065: 100-108.

Jacques, S. L. (1992). "Laser-tissue interactions. Photochemical, photothermal, and photomechanical." Surg Clin North Am **72**(3): 531-58.

Jacques, S. L. and S. A. Prahl (1987). "Modeling optical and thermal distributions in tissue during laser irradiation." Lasers Surg Med **6**(6): 494-503.

Oraevsky, A. A., S. L. Jacques, et al. (1997). "Measurement of tissue optical properties by time-resolved detection of laser-induced transient stress." Applied Optics **36**(1): 402-415.

Patterson, M. S., B. Chance, et al. (1989). "Time Resolved Reflectance and Transmittance for the Noninvasive Measurement of Tissue Optical-Properties." Applied Optics **28**(12): 2331-2336.

Patterson, M. S., E. Schwartz, et al. (1989). Quantitative reflectance spectrophotometry for the noninvasive measurement of photosensitizer concentration in tissue during photodynamic therapy. Photodynamic Therapy: Mechanisms, Dougherty, T J Ed. Proc SPIE 1065:115-122.

Peters, V. G., D. R. Wyman, et al. (1990). "Optical properties of normal and diseased human breast tissues in the visible and near infrared." Phys Med Biol **35**(9): 1317-34.

Prahl, S. A., M. J. C. Vangemert, et al. (1993). "Determining the Optical-Properties of Turbid Media by Using the Adding-Doubling Method." Applied Optics **32**(4): 559-568.

Sevick, E. M., B. Chance, et al. (1991). "Quantitation of Time-Resolved and Frequency-Resolved Optical-Spectra for the Determination of Tissue Oxygenation." Analytical Biochemistry **195**(2): 330-351.

vanGemert, M. J. C., A. J. Welch, et al. (1995). Optical-thermal response of laser-irradiated tissue. Chapter 23: Laser Treatment of Port Wine Stains. New York and London, Plenum Press.

Chapter 10. Conclusion and Future Studies

10.1. CONCLUSION

This research is related to the study of maximum permissible exposure (MPE) limits for class IV lasers at wavelengths 1.2 and 2.0 μm. The exposure duration and spot size were larger than typical work. ANSI Z136.1 2007 defined MPE standards for skin at wavelengths below 100 μm with a limiting aperture of 3.5 mm. The MPE values in the whole spectra are not defined as functions of spot size. However, it is more realistic to consider spot size-effects for large beam exposure on human body. From a laser safety perspective, exposure limits must be based on a clear understanding of both the thermal response to, and the minimum damage threshold endpoint for a given laser. The measurement of a small-beam threshold, regardless of the endpoint, does not necessarily constitute a "minimal" threshold. Radial diffusion effects will play a role even for strongly-absorbed wavelengths, at longer exposure durations (100s ms to seconds). The correlations between threshold radiant exposures and spot size/exposure duration were investigated thoroughly on *in vivo* skin and cornea for 2.0 μm laser irradiation (in Chapters 3, 4 and 8). Similar study was also conducted using 1.214 μm laser on *in vivo* skin and compared with 2.0 μm results (in Chapter 7).

This PhD study has, for the first time, linked temperature response, histopathology, and the more common "minimal visible lesion" endpoint into what can be a meaningful comparison of rate process models for injury. Based on experimental data, a finite-element optical-thermal-damage model was developed. The model simulated light propagation, heat generation, transient temperature response, and thermal damage produced by a radially symmetric laser beam of normal incidence. With that in hand, the model ensured that rate process models are used correctly in the prediction of "MVL" thresholds which seem to be based upon a finite damage extent and not necessarily

central surface layer damage. Moreover, this optical-thermal-damage model, supported by experimental validation, provided a system for predicting the thermal response of skin to laser irradiation and the damage caused by various MIR wavelengths laser irradiations (in chapter 5).

Although many studies have been conducted over a 30 years period to measure and model thermal damage in skin, there are few examples that compare multiple histological end points with corresponding measurements of laser induced transient temperatures. Histological damage is measured and modeled using sub-threshold, threshold, and super-threshold 2.0 μm laser powers. The data provides experimental evidence of the correlation of sub-threshold histological change to visible threshold lesion for the irradiation condition of this study (in Chapter 6).

Thermal image method was employed in this research to measure the absorption coefficient of *in vivo* skin at 2.0 μm (in Chapter 5). Scattering is neglectable at this wavelength. However, at laser wavelengths below 1.4 μm where scattering cannot be ignored, this method must be adjusted to include diffuse scattering inside the tissue. An ameliorative method was explored for measuring *in vivo* optical properties by combining pulse photothermal radiometry (PPTR) and diffuse reflectance (DR) measurements. Purely absorbing phantoms with no scattering and turbid phantoms with both absorption and scattering were used to validate the system. Tests were conducted on *in vivo* human skin with various pigmentation. The skin absorption coefficient measured at 585 nm wavelength was strongly dependent on melanin density. The measured absorption and reduce scattering coefficients were comparable to *in vitro* results from literature (in Chapter 9).

10.2. FUTURE STUDIES

10.2.1. Polarization Analysis of Cornea Lesions

Gross observation and histological study are the most widely used methods to evaluate the extent of lesions of thermal damage to laser irradiation. However, both methods have apparent disadvantage. Gross observation cannot provide either precise or subsurface information of lesions in the biological tissue, and histological study can give details of injury insides, but is expensive and time-consuming. One possible technique to map the extent of lesions on i*n vivo* tissue is optical coherence tomography (OCT). Furthermore, a Polarization Sensitive - OCT system provides extra functional information for determination of normal and damaged tissue and evaluation of the extent of thermal lesions. Another possible application of PS-OCT system is related to the study of damage rate process model. Successful use of kinetic models of thermal damage processes depends critically upon the identification of a quantitative measure of thermal damage. However, the surface gross observations to evaluate thermal damage are qualitative in nature and are not easily studied by the standard Arrhenius formulation. The loss of birefringence provides a quantitative way to measure thermal alteration in tissue. The corneal stroma is the central and thickest layer of the cornea. It consists of great number of stacked lamellae. Each lamella has the form of a thin ribbon which is mainly composed of collagen fibrils. The fibrils are oriented parallel to the surfaces of the lamellae. Due to this particular structure, a lamella can be compared to a linear retarder in which slow and fast axes lie, respectively, parallel and perpendicular to the fibril direction. The local phase retardation and optic axis of light transmitted through the whole cornea can be measured by a polarization microscope with cross polarizers and a compensator plate. Moreover, using PS-OCT we can measure the change in polarization state of light at a given position while cornea remains *in situ*. Furthermore, PS-OCT

could present depth resolved polarization images which is useful to observe thermal damage regions in cornea. Since the damaged cornea may give different polarized and phase information compared to normal cornea due to the change in birefringence, it is promising to image clear lesion boundary based on polarization differences. The extent of thermal damage and the associated transient temperature is necessary for the thermal analysis.

10.2.2. Fiber-based *in vivo* Optical Properties Measurement

An experimental setup combining pulse photothermal radiometry (PPTR) using an IR detector and diffuse reflectance measurement (DR) with an integrating sphere provided a system for simultaneously measuring absorption and reduced scattering of *in vivo* tissues. The measured absorption and reduce scattering coefficients were comparable to *in vitro* results from literature. With the recent development of MIR transmitting optical fiber, it is possible to conduct PPTR measurement based on fiber-design. A design of multiple probes bundle should include illumination fibers (transmit input light), VIS-NIR fibers (collect light from diffuse reflection), and MIR fibers (use for measure transient temperature response). This endoscopic design has great advantage in its flexibility and could be used *in vivo* in many applications, such as cancer detection. Since many kind of tumor is original developed from epithelium layer, it is possible to differentiate tumor cell from normal cells based on their absorption and scattering differences.

BIBLIOGRAPHY

Agah, R. (1988). Quantitative characterization of arterial tissue thermal damage (MSE Thesis). Austin, The University of Texas at Ausin.

Agah, R., J. A. Pearce, et al. (1994). "Rate process model for arterial tissue thermal damage: implications on vessel photocoagulation." Lasers Surg Med **15**(2): 176-84.

Ali, S., I. U. Haq, et al. (2005). "Double mutant of Aspergillus oryzae for improved production of L-dopa (3,4-dihydroxyphenyl-L-alanine) from L-tyrosine." Biotechnol Appl Biochem **42**(Pt 2): 143-9.

Anderson, R. R., H. Beck, et al. (1989). "Pulsed Photothermal Radiometry in Turbid Media - Internal-Reflection of Backscattered Radiation Strongly Influences Optical Dosimetry." Applied Optics **28**(12): 2256-2261.

ANSI (2007). ANSI Z136.1-2007, American National Standard for Safe Use of Lasers, Laser Institute of America, Orlando, FL American National Standards Institute.

Bargeron, C. B., O. J. Deters, et al. (1989). "Epithelial damage in rabbit corneas exposed to CO2 laser radiation." Health Phys **56**(1): 85-95.

Beckham, J. T., M. A. Mackanos, et al. (2004). "Assessment of cellular response to thermal laser injury through bioluminescence imaging of heat shock protein 70." Photochem Photobiol **79**(1): 76-85.

Bhowmick, P., J. E. Coad, et al. (2004). "In vitro assessment of the efficacy of thermal therapy in human benign prostatic hyperplasia." Int J Hyperthermia **20**(4): 421-39.

Birngruber, R., F. Hillenkamp, et al. (1985). "Theoretical Investigations of Laser Thermal Retinal Injury." Health Physics **48**(6): 781-796.

Bischof, J. C., J. Padanilam, et al. (1995). "Dynamics of Cell-Membrane Permeability Changes at Supraphysiological Temperatures." Biophysical Journal **68**(6): 2608-2614.

Borrelli, M. J., L. L. Thompson, et al. (1990). "Time-Temperature Analysis of Cell Killing of Bhk Cells Heated at Temperatures in the Range of 43.5-Degrees-C to 57.0-Degrees-C." International Journal of Radiation Oncology Biology Physics **19**(2): 389-399.

Braichotte, D. R., G. A. Wagnieres, et al. (1995). "Clinical pharmacokinetic studies of photofrin by fluorescence spectroscopy in the oral cavity, the esophagus, and the bronchi." Cancer **75**(11): 2768-78.

Brown, S. L., J. W. Hunt, et al. (1992). "Differential Thermal Sensitivity of Tumor and Normal Tissue Microvascular Response during Hyperthermia." International Journal of Hyperthermia **8**(4): 501-514.

Cain, C. P. and G. D. Noojin (1996). A Comparison of Various Probit Methods for Analyzing Yes/No Data on a Log Scale, Brooks AFB, TX: USAF Armstrong Laboratory; AL/OE-TR-1996-0102.

Canizares, P., I. Gracia, et al. (2004). "Thermal degradation of allicin in garlic extracts and its implication on the inhibition of the in-vitro growth of Helicobacter pylori." Biotechnol Prog **20**(1): 32-7.

Chen, B., D. C. O'Dell, et al. (2005). "Porcine skin ED50 damage thresholds for 2,000 nm laser irradiation." Lasers Surg Med **37**(5): 373-81.

Chen, B., S. L. Thomsen, et al. (2006). "Modeling thermal damage in skin from 2000-nm laser irradiation." J Biomed Opt **11**(6): 064028.

Clark, A. W., H. I. Robins, et al. (1983). "Structural-Changes in Murine Cancer Associated with Hyperthermia and Lidocaine." Cancer Research **43**(4): 1716-1723.

Cohen, I. K., R. F. Diegelmann, et al. (1992). Wound Healing: Biochemical and Clinical Aspects. Philadelphia, W.B.Saunders, Co.

Cress, A. E. and E. W. Gerner (1980). "Cholesterol Levels Inversely Reflect the Thermal Sensitivity of Mammalian-Cells in Culture." Nature **283**(5748): 677-679.

Dewey, W. C. (1989). "Failla memorial lecture. The search for critical cellular targets damaged by heat." Radiat Res **120**(2): 191-204.

Diller, K. R. (1994). "The mechanisms and kinetics of heat injury accumulation." Ann N Y Acad Sci **720**: 38-55.

Diller, K. R., L. J. Hayes, et al. (1991). "Analysis of alternate models for simulating thermal burns." J Burn Care Rehabil **12**(2): 177-89.

Eggleston, T. A., W. P. Roach, et al. (2000). "Comparison of two porcine (Sus scrofa domestica) skin models for in vivo near-infrared laser exposure." Comp Med **50**(4): 391-7.

Farrell, T. J., M. S. Patterson, et al. (1992). "A Diffusion-Theory Model of Spatially Resolved, Steady-State Diffuse Reflectance for the Noninvasive Determination of Tissue Optical-Properties Invivo." Medical Physics **19**(4): 879-888.

Finney, D. J. (1971). Probit Analysis 3rd ed. New York, Cambridge University Press.

Flock, S., L. Smith, et al. (1993). Quantifying the effects on blood of irradiation with four different vascular-lesion lasers, Proceedings of SPIE 1882: 237-242

Flock, S. T., M. S. Patterson, et al. (1989). "Monte-Carlo Modeling of Light-Propagation in Highly Scattering Tissues .1. Model Predictions and Comparison with Diffusion-Theory." Ieee Transactions on Biomedical Engineering **36**(12): 1162-1168.

Flock, S. T., B. C. Wilson, et al. (1989). "Monte-Carlo Modeling of Light-Propagation in Highly Scattering Tissues .2. Comparison with Measurements in Phantoms." Ieee Transactions on Biomedical Engineering **36**(12): 1169-1173.

Foster, K. R., J. A. D'Andrea, et al. (2003). "Thermal modeling of millimeter wave damage to the primate cornea at 35 GHz and 94 GHz." Health Phys **84**(6): 764-9.

Freeman, M. L., M. J. Borrelli, et al. (1995). "Characterization of a Signal Generated by Oxidation of Protein Thiols That Activates the Heat-Shock Transcription Factor." Journal of Cellular Physiology **164**(2): 356-366.

Fugitt, C. E. (1955). A rate process of thermal injury. Armed Forces Special Weapons Project No. AFSWP-606.

Gardner, C. M., S. L. Jacques, et al. (1996). "Fluorescence spectroscopy of tissue: Recovery of intrinsic fluorescence from measured fluorescence." Applied Optics **35**(10): 1780-1792.

Gaylor, D. C. (1989). Physical mechanism of celluar injury in electrical trauma Massachusetts Institute of Technology. **Ph. D. Dissertation**.

Gowrishankar, T. R., D. A. Stewart, et al. (2004). "Transport lattice models of heat transport in skin with spatially heterogeneous, temperature-dependent perfusion." Biomed Eng Online **3**(1): 42.

Groenhuis, R. A. J., H. A. Ferwerda, et al. (1983). "Scattering and Absorption of Turbid Materials Determined from Reflection Measurements .1. Theory." Applied Optics **22**(16): 2456-2462.

Groenhuis, R. A. J., J. J. Tenbosch, et al. (1983). "Scattering and Absorption of Turbid Materials Determined from Reflection Measurements .2. Measuring Method and Calibration." Applied Optics **22**(16): 2463-2467.

Hale, G. M. and M. R. Querry (1973). "Optical constants of water in the 200nm to 200μm wavelength region." Appl. Opt. **12**: 555--563.

He, X., S. McGee, et al. (2004). "Investigation of the thermal and tissue injury behaviour in microwave thermal therapy using a porcine kidney model." Int J Hyperthermia **20**(6): 567-93.

Henriques, F. F. (1947). "Studies of thermal injury V: The predictability and the significance of thermally induced rate processes leading to irreversible epidermal injury." Arch. of Pathol. **43**: 489-502.

Hornback, N. B. (1989). "Historical aspects of hyperthermia in cancer therapy." Radiol Clin North Am **27**(3): 481-8.

Jackson, S. D. and A. Lauto (2002). "Diode-pumped fiber lasers: A new clinical tool?" Lasers in Surgery and Medicine **30**(3): 184-190.

Jackson, S. D., A. Sabella, et al. (2007). "Application and development of high-power and highly efficient silica-based fiber lasers operating at 2 mu m." Ieee Journal of Selected Topics in Quantum Electronics **13**(3): 567-572.

Jacques, S. L. (1989). Simple theory, measurements, and rules of thumb for dosimetry during photodynamic therapy. Photodynamic Therapy:Mechanisms, T. J. Dougherty, Ed. Proc. SPIE 1065: 100-108.

Jacques, S. L. (1992). "Laser-tissue interactions. Photochemical, photothermal, and photomechanical." Surg Clin North Am **72**(3): 531-58.

Jacques, S. L. (1993). "Role of tissue optics and pulse duration on tissue effects during high-power laser irradiation." Applied Optics **32**(13): 2447-2454.

Jacques, S. L. and M. O. Gaeeni (1989). "Thermally induced changes in optical properties of heart." IEEE Eng. Med. Biol. Mag. **11(Part 4/6)**: 1199-1200.

Jacques, S. L., M. Motamedi, et al. (1993). Computer simulation of laser coagulation of prostate: a guide to dosimetry. American Society for Lasers in Medicine and Surgery Lasers Surg. Med. Suppl 5, abstract 311, New Orleans.

Jacques, S. L., C. Newman, et al. (1991). Thermal coagulation of tissues: Liver studies indicate a distribution of rate parameters not a single rate parameter describes the coagulation process. Proc. Annual Winter Meeting of the American Society of Mechanical Engineers, Atlanta, GA.

Jacques, S. L. and S. A. Prahl (1987). "Modeling optical and thermal distributions in tissue during laser irradiation." Lasers Surg Med **6**(6): 494-503.

Jacquez, J. A., J. Huss, et al. (1955). "Spectral reflectance of human skin in the region 0.7-2.6mu." J Appl Physiol **8**(3): 297-9.

Kampmeier, J., B. Radt, et al. (2000). "Thermal and biomechanical parameters of porcine cornea." Cornea **19**(3): 355-363.

Kang, M. S., C. W. Song, et al. (1980). "Role of Vascular Function in Response of Tumors Invivo to Hyperthermia." Cancer Research **40**(4): 1130-1135.

Keijzer, M., J. W. Pickering, et al. (1991). "Laser beam diameter for port wine stain treatment." Lasers Surg Med **11**(6): 601-5.

Lepock, J. R. (2003). "Cellular effects of hyperthermia: relevance to the minimum dose for thermal damage." Int J Hyperthermia **19**(3): 252-66.

Lepock, J. R., H. E. Frey, et al. (1989). "Relationship of hyperthermia-induced hemolysis of human erythrocytes to the thermal denaturation of membrane proteins." Biochim Biophys Acta **980**(2): 191-201.

Li, H. J., X. X. Zhang, et al. (2002). "Measurement of blood perfusion using the temperature response to constant surface flux heating." International Journal of Thermophysics **23**(6): 1631-1644.

Lund, D. J., E. S. Beatrice, et al. (1981). Biological Research in Support of Project MILES, Letterman Army Institute of Research Report- Institute Report No. 96.

Maher, E. J. (1978). Transmission and absorption coefficients for ocular media of the rhesus monkey. Report SAM-TR-78-32. San Antonio, Texas, Brooks Air Force Base.

Maitland, D. J. and J. T. Walsh, Jr. (1997). "Quantitative measurements of linear birefringence during heating of native collagen." Lasers Surg Med **20**(3): 310-8.

Majno, G. (1975). The healing hand. Cambridge, MA, Harvard University Press.

Matthewson, K., P. Coleridge-Smith, et al. (1987). "Biological effects of intrahepatic neodymium:yttrium-aluminum-garnet laser photocoagulation in rats." Gastroenterology **93**(3): 550-7.

Maurice, D. M. (1984). The cornea and sclera. In The Eye.3rd ed., Davson H, editor. Orlando, Florida, Academic Press.

McCally, R. L. and C. B. Bargeron (2001). "Epithelial damage thresholds for multiple-pulse exposures to 80 ns pulses of CO2 laser radiation." Health Phys **80**(1): 41-6.

McCally, R. L. and C. B. Bargeron (2003). "Corneal epithelial injury thresholds for multiple-pulse exposures to Tm : YAG laser radiation at 2.02 mu m." Health Physics **85**(4): 420-427.

McCally, R. L., C. B. Bargeron, et al. (2005). "Laser eye safety research at APL." Johns Hopkins Apl Technical Digest **26**(1): 46-55.

McCally, R. L., C. B. Bargeron, et al. (1983). "Stromal damage in rabbit corneas exposed to CO2 laser radiation." Exp Eye Res **37**(6): 543-50.

McCally, R. L., R. A. Farrell, et al. (1992). "Cornea epithelial damage thresholds in rabbits exposed to Tm:YAG laser radiation at 2.02 microns." Lasers Surg Med **12**(6): 598-603.

Miles, C. A. (1993). "Kinetics of collagen denaturation in mammalian lens capsules studied by differential scanning calorimetry." Int J Biol Macromol **15**(5): 265-71.

Min, K., H. Leu, et al. (1996). "Quantitative determination of ablation in weight of lumbar intervertebral discs with holmium: YAG laser." Lasers Surg Med **18**(2): 187-90.

Moritz, A. R. and F. C. Henriques, Jr. (1947). "Studies of thermal injury: II. The relative importance of time and surface temperature in the causation of cutaneous burns." Am J Pathol **23**: 695-720.

Moussa, N. A., E. N. Tell, et al. (1979). "Time progression of hemolysis of erythrocyte populations exposed to supraphysiological temperatures." ASME J. Biomech. Eng, **101**: 176-184.

Niemz, M. H. (1996). Laser-Tissue Interactions. Berlin, Germany, Springer-Verlag Berlin Heidelberg.

Oraevsky, A. A., S. L. Jacques, et al. (1997). "Measurement of tissue optical properties by time-resolved detection of laser-induced transient stress." Applied Optics **36**(1): 402-415.

Oswal, V. H. and B. J. Bingham (1992). "A pilot study of the holmium YAG laser in nasal turbinate and tonsil surgery." J Clin Laser Med Surg **10**(3): 211-6.

Patterson, M. S., B. Chance, et al. (1989). "Time Resolved Reflectance and Transmittance for the Noninvasive Measurement of Tissue Optical-Properties." Applied Optics **28**(12): 2331-2336.

Patterson, M. S., E. Schwartz, et al. (1989). Quantitative reflectance spectrophotometry for the noninvasive measurement of photosensitizer concentration in tissue during photodynamic therapy. Photodynamic Therapy: Mechanisms, Dougherty, T J Ed. Proc SPIE 1065:115-122.

Peabody, R. R., C. Zweng, et al. (1969). "Threshold damage from CO2 lasers." Arch Ophthalmol **82**(1): 105-7.

Pearce, J. A., S. Thomsen, et al. (1993). Kinetics for birefringence changes in thermally coagulated rat skin collagen, Proc. SPIE 1876:180-185.

Pearce, J. A. and S. L. Thomsen (2003). Thermal damage parameters from laser coagulation experiments, San Jose, California, USA, Progress in Biomedical Optics and Imaging(SPIE) 4954:58-63.

Pearce, J. A., S. L. Thomsen, et al. (1993). Kinetics for birefringence changes in thermally coagulated rat skin collagen, Proc. SPIE 1876.

Pennes, H. H. (1948). "Analysis of tissue and arterial blood temperatures in resting human forearm." J. Appl. Physiol. **1**: 93-122.

Peters, V. G., D. R. Wyman, et al. (1990). "Optical properties of normal and diseased human breast tissues in the visible and near infrared." Phys Med Biol **35**(9): 1317-34.

Pfefer, T. J., B. Choi, et al. (2000). "Pulsed laser-induced thermal damage in whole blood." J Biomech Eng **122**(2): 196-202.

Pop, M., A. Molckovsky, et al. (2003). "Changes in dielectric properties at 460 kHz of kidney and fat during heating: importance for radio-frequency thermal therapy." Phys Med Biol **48**(15): 2509-25.

Prahl, S. A., M. J. C. Vangemert, et al. (1993). "Determining the Optical-Properties of Turbid Media by Using the Adding-Doubling Method." Applied Optics **32**(4): 559-568.

Priebe, L. A. and A. J. Welch (1978). "Asymptotic Rate Process Calculations of Thermal Injury to Retina Following Laser Irradiation." Mechanical Engineering **100**(5): 100-100.

Quinn, P. J. (1989). "Principles of Membrane Stability and Phase-Behavior under Extreme Conditions." Journal of Bioenergetics and Biomembranes **21**(1): 3-19.

Rakow, A. L. and R. M. Hochmuth (1975). "Effect of Heat-Treatment on Elasticity of Human Erythrocyte-Membrane." Biophysical Journal **15**(11): 1095-1100.

Razvi, H. A., J. D. Denstedt, et al. (1997). "Intracorporeal lithotripsy with the holmium:YAG laser - Reply." Journal of Urology **158**(1): 187-187.

Rendell, M. S., S. T. Kelly, et al. (1993). "The effect of increasing temperature on skin blood flow and red cell deformability." Clin Physiol **13**(3): 235-45.

Rockwell, R. J., Jr and L. Goldman (1974). Research on human skin laser damage threshold. Final report, Conract F41609-72-C-0007. Brooks Air Force Base, TX., USAF School of Aerospace medicine.

Rothman, L. S., R. R. Gamache, et al. (1992). "The Hitran Molecular Database - Editions of 1991 and 1992." Journal of Quantitative Spectroscopy & Radiative Transfer **48**(5-6): 469-507.

Ryan, T. P. and T. Z. Wong (1999). Thermal Treatment of Tissue with Image Guidance. Proc. SPIE 3594:1-234.

Schober, R., F. Ulrich, et al. (1986). "Laser-induced alteration of collagen substructure allows microsurgical tissue welding." Science **232**(4756): 1421-2.

Sevick, E. M., B. Chance, et al. (1991). "Quantitation of Time-Resolved and Frequency-Resolved Optical-Spectra for the Determination of Tissue Oxygenation." Analytical Biochemistry **195**(2): 330-351.

Shapshay, S. M., E. E. Rebeiz, et al. (1991). "Holmium: yttrium aluminum garnet laser-assisted endoscopic sinus surgery: laboratory experience." Laryngoscope **101**(2): 142-9.

Shapshay, S. M., E. E. Rebeiz, et al. (1992). "Holmium:yttrium aluminum garnet laser-assisted endoscopic sinus surgery: clinical experience." Laryngoscope **102**(10): 1177-80.

Siegman, A. E., M. W. Sasnett, et al. (1991). "Choice of Clip Levels for Beam Width Measurements Using Knife-Edge Techniques." Ieee Journal of Quantum Electronics **27**(4): 1098-1104.

Skinner, M. G., S. Everts, et al. (2000). "Changes in optical properties of ex vivo rat prostate due to heating." Phys Med Biol **45**(5): 1375-86.

Sliney, D. H., J. Mellerio, et al. (2002). "What is the meaning of threshold in laser injury experiments? Implications for human exposure limits." Health Phys **82**(3): 335-47.

Song, C. W. (1984). "Effect of Local Hyperthermia on Blood-Flow and Microenvironment - a Review." Cancer Research **44**(10): 4721-4730.

Sorokina, I. T. and K. L. Vodopyanov, Eds. (2007). Solid-State Mid-Infrared Laser Sources (Topics in Applied Physics Vol. 89) Springer Verlag GmbH.

Stoll, A. M. and L. C. Greene (1959). "Relationship between pain and tissue damage due to thermal irradiation." J App. Physiology **14**(3): 372-382.

Takata, A. N. (1974). "Development of criterion for skin burns." Aerosp. Med. **45**: 634-637.

Takata, A. N. (1977). Laser-induced thermal damage of skin. USAF School of Aerospace Medicine. Brooks Air Force Base, TX.

Takata, A. N., L. Goldfinch, et al. (1974). Thermal Model of Laser-Induced Eye Damage. USAF School of Aerospace Medicine Report IITRI J-TR-74-6324.

Takema, Y., A. Nishijima, et al. (1997). "Skin morphology at the time of UV irradiation is important for wrinkle formation." Journal of the Society of Cosmetic Chemists **48**(6): 297-306.

Tan, O. T., M. Motemedi, et al. (1988). "Spotsize effects on guinea pig skin following pulsed irradiation." J Invest Dermatol **90**(6): 877-81.

Tandori, J., Z. Tokaji, et al. (2005). "Thermodynamics of light-induced and thermal degradation of bacteriochlorins in reaction center protein of photosynthetic bacteria." Photochem Photobiol **81**(6): 1518-25.

Thomsen, S. (1991). "Pathologic analysis of photothermal and photomechanical effects of laser-tissue interactions." Photochem Photobiol **53**(6): 825-35.

Thomsen, S. L. (2000). "Qualitative and quantitative pathology of clinically relevant thermal lesions " Crit. Rev. Opt. Sci. Technol. **75** 425-58.

Thomsen, S. L. and J. E. Coad (2007). Developing clinically successful biomedical devices by understanding the pathophysiology of the target tissue: insights from over 25 years at the microscope. Proceedings of SPIE 6440

Torres, J. H. and M. Motamedi (1993). "Experimental evaluation of mathematical-models for predicting the thermal response of tissue to laser irradiation " Appl. Opt **32**(4): 597-606.

Trauner, K., N. Nishioka, et al. (1990). "Pulsed holmium:yttrium-aluminum-garnet (Ho:YAG) laser ablation of fibrocartilage and articular cartilage." Am J Sports Med **18**(3): 316-20.

Trauner, K. B., N. S. Nishioka, et al. (1995). "Acute and chronic response of articular cartilage to holmium:YAG laser irradiation." Clin Orthop Relat Res(310): 52-7.

Tropea, B. I. and R. C. Lee (1992). "Thermal injury kinetics in electrical trauma." J Biomech Eng **114**(2): 241-50.

vanGemert, M. J. C., A. J. Welch, et al. (1995). Optical-thermal response of laser-irradiated tissue. Chapter 23: Laser Treatment of Port Wine Stains. New York and London, Plenum Press.

Vassiliadis, A., H. C. Christian, et al. (1971). Ocular laser threshold investigations. Aerosp. Med. Report F41609-70-0002.

Weaver, J. A. and A. M. Stoll (1967). NADC Memo Report 6708. Johnsville, Pennsylvania, United Stated Naval Air Development Center.

Weijers, M., P. A. Barneveld, et al. (2003). "Heat-induced denaturation and aggregation of ovalbumin at neutral pH described by irreversible first-order kinetics." Protein Sci **12**(12): 2693-703.

Welch, A. J. and G. D. Polhamus (1984). "Measurement and prediction of thermal injury in the retina of the rhesus monkey." IEEE Trans Biomed Eng **31**(10): 633-43.

Welch, A. J. and M. J. C. vanGemert (1995). Optical-thermal response of laser-irradiated tissue. Chapter 17: Rate processs analysis of thermal damage. New York and London, Plenum Press.

Wimberly, B. T., D. E. Brodersen, et al. (2000). "Structure of the 30S ribosomal subunit." Nature **407**(6802): 327-39.

Wu, Y. C. (1982). A Modified Criterion for predicting thermal injury. Nat. Bur. Stand. Washington, District of Columbia.

Yang, Y., A. J. Welch, et al. (1991). "Rate process parameters of albumen." Lasers Surg Med **11**(2): 188-90.

Yatvin, M. B. and W. A. Cramp (1993). "Role of Cellular Membranes in Hyperthermia - Some Observations and Theories Reviewed." International Journal of Hyperthermia **9**(2): 165-185.

Zuclich, J. A., M. F. Blankenstein, et al. (1984). "Corneal damage induced by pulsed CO2 laser radiation." Health Phys **47**(6): 829-35.

Zuclich, J. A., D. J. Lund, et al. (2007). "Wavelength dependence of ocular damage thresholds in the near-ir to far-ir transition region: Proposed revisions to MPEs." Health Physics **92**(1): 15-23.

VITA

Bo Chen was born in Hefei, Anhui province, China on Nov 24, 1978, the second son of Suwei Chen and Yuexia Zhang. He received his B.S. and M.S. degrees in physics from Tsinghua University, China in 2000 and 2003 respectively. As a graduate student, Bo worked under the supervision of Dr. Hui Ma to investigate fluorescence correlation spectroscopy and photon counting histogram.

In September 2003, he entered a PhD program in physics department at the University of Texas at Austin, Texas and transferred to biomedical engineering department in spring, 2005. He expects to complete his Doctor of Philosophy in Biomedical Engineering in December, 2007.

Permanent Address: Room 601, Building 34, 28 South Huancheng Road
Heifei, Anhui, 230061, China

This dissertation was typed by the author.